METHODOLOGICAL ADVANCES OF MALDI MASS SPECTROMETRY-BASED TECHNIQUES IN ORGANIC AND BIOMEDICAL ANALYSIS

EDITED BY: Cheng Guo, Gerard Bolbach, Lucrece Matheron, Kezhi Jiang, Lei Yue and Lin Wang

PUBLISHED IN: Frontiers in Chemistry

frontiers Research Topics

ISSN 1664-8714
ISBN 978-2-88976-436-5
DOI 10.3389/978-2-88976-436-5

About Frontiers

Frontiers is more than just an open-access publisher of scholarly articles: it is a pioneering approach to the world of academia, radically improving the way scholarly research is managed. The grand vision of Frontiers is a world where all people have an equal opportunity to seek, share and generate knowledge. Frontiers provides immediate and permanent online open access to all its publications, but this alone is not enough to realize our grand goals.

Frontiers Journal Series

The Frontiers Journal Series is a multi-tier and interdisciplinary set of open-access, online journals, promising a paradigm shift from the current review, selection and dissemination processes in academic publishing. All Frontiers journals are driven by researchers for researchers; therefore, they constitute a service to the scholarly community. At the same time, the Frontiers Journal Series operates on a revolutionary invention, the tiered publishing system, initially addressing specific communities of scholars, and gradually climbing up to broader public understanding, thus serving the interests of the lay society, too.

Dedication to Quality

Each Frontiers article is a landmark of the highest quality, thanks to genuinely collaborative interactions between authors and review editors, who include some of the world's best academicians. Research must be certified by peers before entering a stream of knowledge that may eventually reach the public - and shape society; therefore, Frontiers only applies the most rigorous and unbiased reviews.
Frontiers revolutionizes research publishing by freely delivering the most outstanding research, evaluated with no bias from both the academic and social point of view. By applying the most advanced information technologies, Frontiers is catapulting scholarly publishing into a new generation.

What are Frontiers Research Topics?

Frontiers Research Topics are very popular trademarks of the Frontiers Journals Series: they are collections of at least ten articles, all centered on a particular subject. With their unique mix of varied contributions from Original Research to Review Articles, Frontiers Research Topics unify the most influential researchers, the latest key findings and historical advances in a hot research area! Find out more on how to host your own Frontiers Research Topic or contribute to one as an author by contacting the Frontiers Editorial Office: frontiersin.org/about/contact

METHODOLOGICAL ADVANCES OF MALDI MASS SPECTROMETRY-BASED TECHNIQUES IN ORGANIC AND BIOMEDICAL ANALYSIS

Topic Editors:
Cheng Guo, Zhejiang University, China
Gerard Bolbach, Sorbonne Universités, France
Lucrece Matheron, Sorbonne Universités, France
Kezhi Jiang, Hangzhou Normal University, China
Lei Yue, Hunan University, China
Lin Wang, Chinese Academy of Medical Sciences and Peking Union Medical College, China

Citation: Guo, C., Bolbach, G., Matheron, L., Jiang, K., Yue, L., Wang, L., eds. (2022). Methodological Advances of MALDI Mass Spectrometry-Based Techniques in Organic and Biomedical Analysis. Lausanne: Frontiers Media SA.
doi: 10.3389/978-2-88976-436-5

Table of Contents

04 ***Application of MALDI-TOF MS Profiling Coupled With Functionalized Magnetic Enrichment for Rapid Identification of Pathogens in a Patient With Open Fracture***
Jichong Ying, Wenjing Gao, Dichao Huang, Chuanfan Ding, Ling Ling, Tao Pan and Shaoning Yu

11 ***Optimized MALDI-TOF MS Strategy for Characterizing Polymers***
Zhenxin Wang, Quanqing Zhang, Huali Shen, Pengyuan Yang and Xinwen Zhou

21 ***An Improved Method for Rapid Detection of* Mycobacterium abscessus *Complex Based on Species-Specific Lipid Fingerprint by Routine MALDI-TOF***
Min Jia Khor, Agnieszka Broda, Markus Kostrzewa, Francis Drobniewski and Gerald Larrouy-Maumus

28 ***Design of Experiments for Matrix-Assisted Laser Desorption/Ionization of Amphiphilic Poly(Ethylene Oxide)-b-Polystyrene Block Copolymers***
Hélène Pizzala, Magalie Claeys-Bruno, Valérie Monnier, Michelle Sergent and Laurence Charles

39 ***Characterizing Oligomeric Hydroxyl Silicon Oils by MALDI-TOF MS With the Pyridine-Modified Matrix***
Xiaoxiao Zhang, Yan Wang, Yiqiu Hu, Cheng Guo, Chenghua Li and Kezhi Jiang

47 ***Quantifying the Matrix Metalloproteinase 2 (MMP2) Spatially in Tissues by Probe via MALDI Imaging Mass Spectrometry***
Daojiang Yu, Peng Lai, Tao Yan, Kai Fang, Lei Chen and Shuyu Zhang

54 ***Recent Advances in Combinations of TLC With MALDI and Other Desorption/Ionization Mass-Spectrometry Techniques***
Roman Borisov, Anastasiia Kanateva and Dmitry Zhilyaev

66 ***MALDI-TOF MS Based Bacterial Antibiotics Resistance Finger Print for Diabetic Pedopathy***
Haojie Sun, Peng Lai, Wei Wu, Hao Heng, Shanwen Si, Yan Ye, Jiayi Li, Hehe Lyu, Caiyan Zou, Mengzhe Guo, Yu Wang, Houfa Geng and Jun Liang

77 ***Advances in MALDI Mass Spectrometry Imaging Single Cell and Tissues***
Xiaoping Zhu, Tianyi Xu, Chen Peng and Shihua Wu

104 ***Lipid Analysis of Fracture Hematoma With MALDI-MSI: Specific Lipids are Associated to Bone Fracture Healing Over Time***
Rald V. M. Groven, Sylvia P. Nauta, Jane Gruisen, Britt S. R. Claes, Johannes Greven, Martijn van Griensven, Martijn Poeze, Ron M. A. Heeren, Tiffany Porta Siegel, Berta Cillero-Pastor and Taco J. Blokhuis

frontiers in Chemistry

ORIGINAL RESEARCH
published: 30 April 2021
doi: 10.3389/fchem.2021.672744

Application of MALDI-TOF MS Profiling Coupled With Functionalized Magnetic Enrichment for Rapid Identification of Pathogens in a Patient With Open Fracture

Jichong Ying[1†], Wenjing Gao[2†], Dichao Huang[1], Chuanfan Ding[2], Ling Ling[2], Tao Pan[3*] and Shaoning Yu[2*]*

[1]Ningbo No. 6 Hospital, Ningbo, China, [2]Key Laboratory of Advanced Mass Spectrometry and Molecular Analysis of Zhejiang Province, Institute of Mass Spectrometry, School of Material Science and Chemical Engineering, Ningbo University, Ningbo, China, [3]Department of Breast Surgery and Oncology, The Second Affiliated Hospital, Zhejiang University School of Medicine, Hangzhou, China

OPEN ACCESS

Edited by:
Cheng Guo,
Zhejiang University, China

Reviewed by:
Quanqing Zhang,
University of California, United States
Ge Ma,
Sinopec Research Institute of Safety Engineering, China

***Correspondence:**
Ling Ling
lingling@nbu.edu.cn
Shaoning Yu
yushaoning@nbu.edu.cn
Tao Pan
2311318@zju.edu.cn

[†]*These authors contributed equally to this work*

Specialty section:
This article was submitted to Analytical Chemistry, a section of the journal Frontiers in Chemistry

Received: *26 February 2021*
Accepted: *19 April 2021*
Published: *30 April 2021*

Citation:
Ying J, Gao W, Huang D, Ding C, Ling L, Pan T and Yu S (2021) Application of MALDI-TOF MS Profiling Coupled With Functionalized Magnetic Enrichment for Rapid Identification of Pathogens in a Patient With Open Fracture. Front. Chem. 9:672744. doi: 10.3389/fchem.2021.672744

Posttraumatic infections can occur in orthopedic trauma patients, especially in open fractures. Rapid and accurate identification of pathogens in orthopedic trauma is important for clinical diagnosis and antimicrobial treatment. Matrix-assisted laser desorption/ionization time-of-flight mass spectrometry (MALDI-TOF MS) has been successfully used for first-line identification of pathogens grown on culture plates. However, for direct analysis of liquid clinical specimens, pre-purification of the sample is necessary. Herein, we investigated the feasibility of coupling Fc-MBL@Fe_3O_4 enrichment with MALDI-TOF MS profiling in the identification of pathogens in liquid-cultured samples. This method is successfully used for the identification of pathogens in a patient with an open-leg fracture obtained at sea. Pathogens were enriched by Fc-MBL@Fe_3O_4 from briefly pre-cultured liquid media and identified by MALDI-TOF MS. We identified an opportunistic pathogen, *Vibrio alginolyticus*, which is uncommon in clinical orthopedic trauma infection but exists widely in the sea. Therefore, combining Fc-MBL@Fe_3O_4 enrichment and MALDI-TOF MS profiling has great potential for direct identification of microbes in clinical samples.

Keywords: MALDI-TOF MS, orthopedic trauma infection, magnetic enrichment, pathogen identification, *Vibrio alginolyticus*

INTRODUCTION

Orthopedic traumas are complex and diverse. Serious wounds are always difficult to debride; especially, when complicated fractures are combined, the surgical treatment is often required (Morgenstern et al., 2018; Tuon et al., 2019). Posttraumatic infections can occur in orthopedic trauma patients when it is not treated in a timely manner or after surgical treatment (Arnold et al., 2013; Yun et al., 2016; Backes et al., 2018). Rapid identification of pathogenic bacteria in orthopedic trauma, especially open fractures, guides the clinical diagnosis and antimicrobial treatment (Yun et al., 2016; Patrulea et al., 2020). Thus, superficial wound swabs or deep fluid samples are always sent to the clinical microbiology lab for bacterial identification.

The current standard of bacterial identification in hospitals continues to rely on culture-based biochemical testing, which may take days to complete (Varadi et al., 2017; Backes et al., 2018). Moreover, culture-based methods suffer increasing skepticism about their sensitivity and accuracy (Rhoads et al., 2012; Firoozabadi et al., 2015). Molecular methods that rely on the analysis of genomic markers, such as ribosomal RNA sequencing, have better sensitivity and accuracy for pathogen identification (Rhoads et al., 2012). However, molecular diagnostic methods have high cost and require sophisticated expertise (Woo et al., 2008; Segawa et al., 2014). In recent years, matrix-assisted laser desorption/ionization time-of-flight mass spectrometry (MALDI-TOF MS) has been introduced into clinical microbiology laboratories. Due to the specificity, speed of analysis, and low cost of consumables, MALDI-TOF MS has been widely acclaimed for clinical bacterial identification (Welker et al., 2019; Feng et al., 2020; Nomura et al., 2020; Papagiannopoulou et al., 2020). MALDI-TOF MS identification is mainly based on the MS fingerprint pattern of bacterial ribosomal proteins in the *m/z* range of 2–20 kDa, which can be compared to the MS database to identify the bacterial genus and species (Singhal et al., 2015). MALDI-TOF MS databases with more than 4000 strains have been set up and are widely used in the identification of clinical bacteria, fungi, mycobacteria, and *Nocardia* (Feng et al., 2020). Nevertheless, the single colonies are always needed for this method. Clinical samples or liquid cultured samples are inoculated on solid culture plate to grow single colonies for identification by MALDI-TOF MS. For direct analysis of bacteria in liquid clinical samples, the pre-purification steps are mandatory. Since approximately 10^5 CFU of bacteria are needed for successful identification, direct analysis of bacteria in clinical samples seems only possible for urine samples (Zboromyrska et al., 2016). Utilizing of liquid cultures has increased the sensitivity and decreased the turn-around time of bacterial culture, especially for samples with low bacterial loads. Hence, development of pre-purification methods for liquid-cultured bacterial sample is sorely needed.

Functionalized magnetic nanoparticles (MNPs) have been developed to capture bacteria and simplify the purification processes due to its large ratio of surface area to volume, ease of operation, and good biocompatibility (Liébana et al., 2009; Cheng et al., 2016; Zhu et al., 2016; Yi et al., 2018; Nemr et al., 2019). Specific aptamers and antibodies were conjugated with MNPs to enrich certain bacteria or part of microbes from suspension (Liébana et al., 2009; Cheng et al., 2016; Zhu et al., 2016; Yi et al., 2018; Nemr et al., 2019). Mannose-binding lectin (MBL) is an important opsonin component of the lectin pathway associated with innate immunity, which can recognize and bind carbohydrates on the surfaces of different bacteria, fungi, and viruses in a calcium-dependent manner (Takahashi and Ezekowitz, 2005). Ingber et al. genetically engineered a new version of MBL by fusing the carbohydrate recognition region of MBL to the flexible neck of the Fc portion of IgG1, which conjugated with MNPs and was used to cleanse septic blood or enrich bacteria in clinical samples (Kang et al., 2014; Bicart-See et al., 2016). These studies indicated that Fc-MBL has binding capability for a wide range of microbes, which prompted us to utilize Fc-MBL@Fe_3O_4 to enrich bacteria and combine with the MALDI-TOF MS identification.

Herein, we investigated the feasibility of the MALDI-TOF MS profiling coupled with Fc-MBL@Fe_3O_4 enrichment for identification of bacteria in liquid culture media (**Scheme 1**). After the verification, the application of this method in real case was explored. A patient obtained an open fracture at sea and did not acquire treatment for more than 20 h due to diagnostic limitations. Considering that the patient was injured at sea, uncommon species of bacteria may have adhered to the wound; we attempt to use Fc-MBL@Fe_3O_4 enrichment coupled with MALDI-TOF MS identification. A wound swab and fluid were short-term cultured on liquid media and analyzed by the proposed method, wherein *Vibrio alginolyticus* was identified. These results show that these pathogen identification procedures are more rapid than traditional methods and beneficial for clinical treatment of patients.

MATERIAL AND METHODS

Patient

A 56-year-old male patient was crushed while working on the boats, and his right calf was stressed, accompanied by skin lacerations and bleeding. He had an open wound approximately 6 × 15 cm in the lower part of the right calf, and the fractured end was exposed. Because the patient was unable to acquire clinical treatment at sea, the wound was simply bandaged to stop the bleeding. After more than 20 h, the patient was sent to the hospital and diagnosed with open comminuted fracture of the lower right tibia and fibula. This study was approved by the Ethics Committee of Ningbo No. 6 Hospital.

Chemicals and Instruments

α-Cyano-4-hydroxycinnamic acid (CHCA), formic acid, and acetonitrile (ACN) were purchased from Merck (Darmstadt, Germany). Trifluoroacetic acid (TFA) was obtained from Shanghai Macklin Biochemical Technology Co., Ltd. (Shanghai, China). Tryptone soybean agar (TSA) and Luria–Bertani (LB) broth were purchased from Beijing Land Bridge Technology Co., Ltd (Beijing, China). The functionalized MNPs (Fc-MBL@Fe_3O_4) were synthesized as in our previous study (Sun et al., 2021). The detailed synthesis procedures and characterization results are presented in the Supporting Information.

The mass spectra for the verification of method were obtained by Autoflex max TOF/TOF mass spectrometer (Bruker Daltonics, Germany) with a pulsed Nd:YAG laser (355 nm) in a linear positive mode. The acceleration voltage was set at 20 kV, each spectrum was acquired by 1000 laser shots, and the laser intensity was regulated to ensure a good signal-to-noise ratio. MALDI-TOF MS identification was carried out using an M-Discover 100 mass spectrometer (Zhuhai Meihua Medical Technology Co., Ltd. China) in a linear positive mode with the *m/z* range 2–20 KDa. The mass spectra were calibrated by *Escherichia coli* (ATCC 8739) according to the manufacturer's

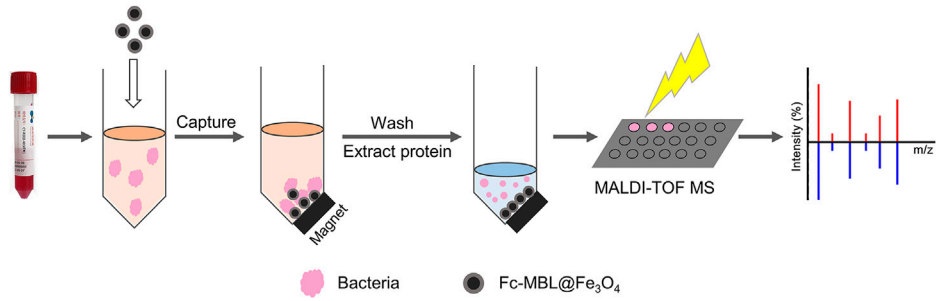

SCHEME 1 | Workflow for the identification of pathogens from the clinical liquid sample.

instructions. MicroCtrl 1.0 software was used to acquire the spectra and for real-time interpretation and identification; the raw spectra were processed by smoothing, baseline removal, and peak-picking, and the processed spectra were compared with the reference spectra in the database by using the pattern-matching algorithm of the software. The scores that ranged from 0.00 to 3.00 were calculated based on the correlation between the two spectra. According to the manufacturer, a score >2.0 is considered reliable in the species level, a score 1.7–2.0 indicates identification in the genus level, and a score <1.7 indicates unreliable result. Transmission electron microscopy (TEM) images were obtained by microscope JEOL JEM 2100 (Japan) at 200 kV.

Sample Preparation and MNP Enrichment

For verification of the method, the standard bacteria strains (*S. aureus*, ATCC 25923; *K. pneumoniae*, CICC 21519) were inoculated on the TSA solid plate, and the single colonies were adjusted to certain concentrations by measuring the absorbance at 600 nm using UV–vis absorption spectroscopy. For the enrichment efficiency of Fc-MBL@Fe_3O_4, 1000 or 100 CFUs of *S. aureus* and 10 μl of Fc-MBL@Fe_3O_4 solution (10 mg/ml) were added in 30 μl Tris-HCl buffer (0.1 mM, pH 7.4) containing 10 mM $CaCl_2$ and 0.05% Tween-20 and incubated at 37°C for 15 min with shaking. After magnetic enrichment, the pellets were washed twice with 30 μl of water. The supernatant was collected and cultured on the TSA solid media for 13 h, together with the original solution and pellets. For the *S. aureus* assay, different amounts (10^8, 10^7, 10^6, and 10^5 CFU) of bacteria in 1 ml of buffer solution were enriched by the similar method, wherein the pellets were washed with 100 μl of water. The *S. aureus* and *K. pneumoniae* in LB liquid media at the concentration of 10^8 CFU/ml were carried out as follows; 300 μl of buffer solution and 10 μl of Fc-MBL@Fe_3O_4 solution were added subsequently in 100 μl of bacteria suspension, and the mixture was incubated at 37°C for 15 min with shaking. The pellets were washed twice with 100 μl of water. The bacterial proteins were extracted from the Fc-MBL@Fe_3O_4 by use of 5 μl of 70% formic acid and 5 μl of ACN, and the extracted solution was subjected to MALDI-TOF MS analysis.

For the real case, a wound swab and 1 ml of trauma fluid from the patient were collected in sterile containers and subjected to magnetic enrichment and MALDI-TOF MS profiling. The wound swab and fluid were both subcultured in 5 ml of liquid LB medium at 37°C for 8 h. For enrichment, 1 ml of buffer solution was added to 300 μl of subcultured liquid, and then, 20 μl of Fc-MBL@Fe_3O_4 solution was added. The obtained solution was incubated at 37°C for 15 min with shaking. After magnetic enrichment, the pellets were washed twice with 100 μl of water. The bacterial proteins were extracted as above description. For the verification, the subcultured liquid samples were grown on the TSA solid medium for 24 h, and the bacterial colonies were identified by MALDI-TOF MS.

MALDI-TOF MS Analysis

The bacterial protein solution (1 μl) extracted from MNPs was deposited on a MALDI target plate. Then, CHCA matrix (10 mg/ml in ACN/H_2O (v/v = 1/1) containing 2% TFA) was deposited on the sample spot after drying. For analysis of bacteria grown on the solid TSA medium, the standard extraction method was used (Matsuda et al., 2012). Briefly, a 1-μl loop of bacteria was suspended in 300 μl H_2O, and 900 μl ethanol was added. After vigorous vortex, the mixture was centrifuged at 12,000 rpm for 5 min. The supernatant was discarded, and 30 μl of 70% formic acid was added to the pellets and thoroughly mixed. Next, 30 μl of ACN was added, and the resulting solution was centrifuged again at 12,000 rpm for 5 min. One microliter of supernatant was deposited on the MALDI target plate and dried at room temperature. Finally, 1 μl of CHCA matrix was placed on the sample spots and left to dry.

Clinical Routine Pathogen Identification

The clinical samples were inoculated on the Columbia blood agar, Sabourand's fungus agar, and anaerobic medium plate in a sterile manner and incubated in 35 ± 2°C for 24–48 h in clinical microbiology laboratory. The bacteria grown on the solid media were subjected to Gram staining, and the isolates were identified using a VITEK2-Compact automatic bacterial identification instrument (Biomérieux) in accordance with the manufacturer's instructions.

RESULTS AND DISCUSSION

Feasibility of the Proposed Method

The workflow of the proposed method was illustrated in **Scheme 1**. The pathogens in liquid clinical samples or short-term–cultured liquid samples were captured by Fc-MBL@

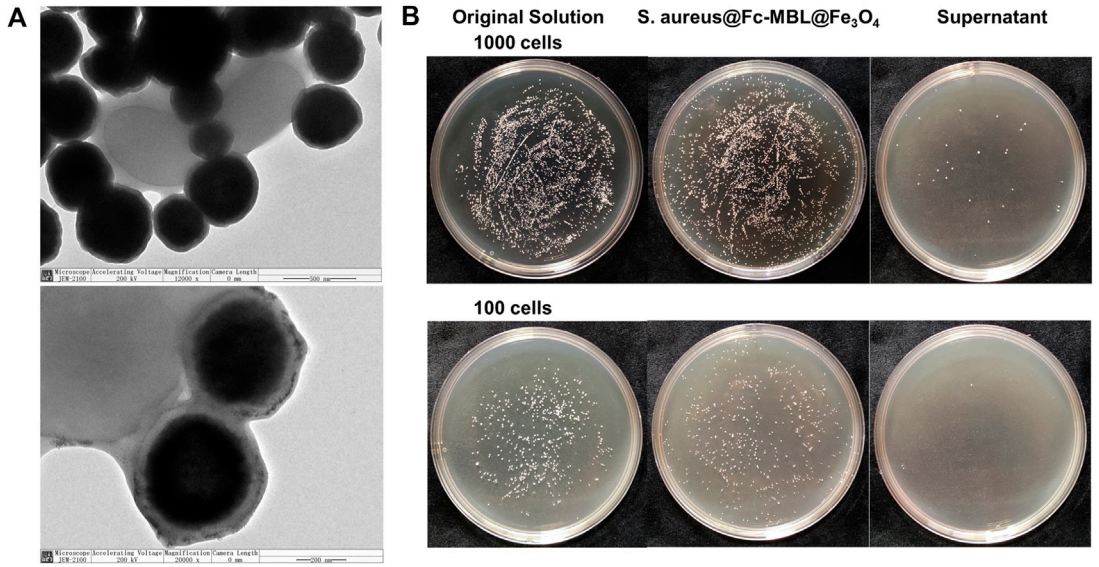

FIGURE 1 | (A) TEM images of *S. aureus* conjugated with Fc-MBL@Fe_3O_4. **(B)** Photographs of cultured plate of original solution, enriched pellets, and supernatant.

Fe_3O_4; the enriched bacteria were extracted by formic acid from Fc-MBL@Fe_3O_4 and subjected to MALDI-TOF MS identification. Before application in real case, we investigated the feasibility of the method. A common pathogen in orthopedic infection, *Staphylococcus aureus* (*S. aureus*), was selected as model to verify the method. The synthesis and characterization of Fc-MBL@Fe_3O_4 were presented in supporting information. The TEM images of Fc-MBL@Fe_3O_4 binding to *S. aureus* are shown in **Figure 1A**, which indicated the binding capability of Fc-MBL@Fe_3O_4 to *S. aureus*. Next, the capture efficiency of Fc-MBL@Fe_3O_4 was evaluated by the plate-counting method. Briefly, the different amounts of *S. aureus* suspension were enriched by Fc-MBL@Fe_3O_4; the bacteria in original solution, captured by Fc-MBL@Fe_3O_4, and the supernatant were inoculated on the TSA plate in parallel, and the results are shown in **Figure 1B**. It can be seen that bacteria were almost captured completely by Fc-MBL@Fe_3O_4. Then, the different amounts (10^8/10^7/10^6/10^5 CFU) of *S. aureus* in 1 ml buffer solution were enriched by Fc-MBL@Fe_3O_4 and identified by MALDI-TOF MS. As shown in **Figure 2**, the spectra of $\geq 10^6$ CFU of bacteria in buffer enriched by Fc-MBL@Fe_3O_4 show similar profiles with the standard spectrum of pure bacteria. It is should be noted that approximately ~10^5 CFU are needed on the target plate for successful bacteria identification with MALDI-TOF MS (Segawa et al., 2014), which means the concentration of 10^8 CFU/ml is needed, wherein 1 µl of bacteria suspension is deposited on the target plate. In this method, the enriched pellets were eluted by 10 µl solution (5 µl 70% formic acid +5 µl ACN), and the 1 µl of solution is deposited on the target plate. Thus, the results are rational that 10^6 CFU of bacteria in 1 ml buffer solution could be detected successfully by the proposed method.

Furthermore, *S. aureus* and another bacteria *Klebsiella pneumoniae* (*K. pneumoniae*) were spiked in LB liquid media at 10^8 CFU/ml (the concentration of clinical positive cultures is ~10^8 CFU/ml). The 100 µl of liquid bacterial cultures were enriched by Fc-MBL@Fe_3O_4 and analyzed by MALDI-TOF MS. The pure bacteria were tested by MALDI-TOF MS, and the obtained spectra were compared with those captured by Fc-MBL@Fe_3O_4 from LB media. As shown in **Figure 3**, the spectra of captured bacteria (*S. aureus* and *K. pneumoniae*) from LB media show similar profiles to pure bacteria. For evaluation of reproducibility, the sample of *S. aureus* in LB broth was carried out in triplicate, and each sample was deposited at three spots; the obtained spectra all show matched profiles (**Supplementary Figure S5**). These results indicated the feasibility of the proposed method for rapid identification of bacteria in clinical bacterial liquid cultures.

Identification of Bacteria in a Patient With Open Fracture

Rapid and accurate identification of progressive bacteria colonizing orthopedic trauma, especially open fracture, is important for clinical diagnosis and treatment to avoid posttraumatic or postoperative infections. In the case presented here, the patient's leg suffered an open fracture on the coastal sea of China. Fc-MBL@Fe_3O_4 possesses a universal enrichment capacity for different pathogens, and MALDI-TOF MS can identify a wide range of pathogens, including bacteria and fungi, with high accuracy at both the genus and species level (97–99% and 85–97%, respectively) (Patel, 2013). Considering the special of this case, we attempt to use MALDI-TOF MS in coupling with Fc-MBL@Fe_3O_4 enrichment for the identification of probable pathogens in this case. For analysis of clinical bacterial samples, a short-term subculture step is always needed since the amount of ~10^5 CFU is requisite for MALDI-TOF MS identification. Herein, the wound swab and fluid were short-term cultured in liquid LB media, and the liquid samples were analyzed by the proposed method. As a control, a sterile swab was

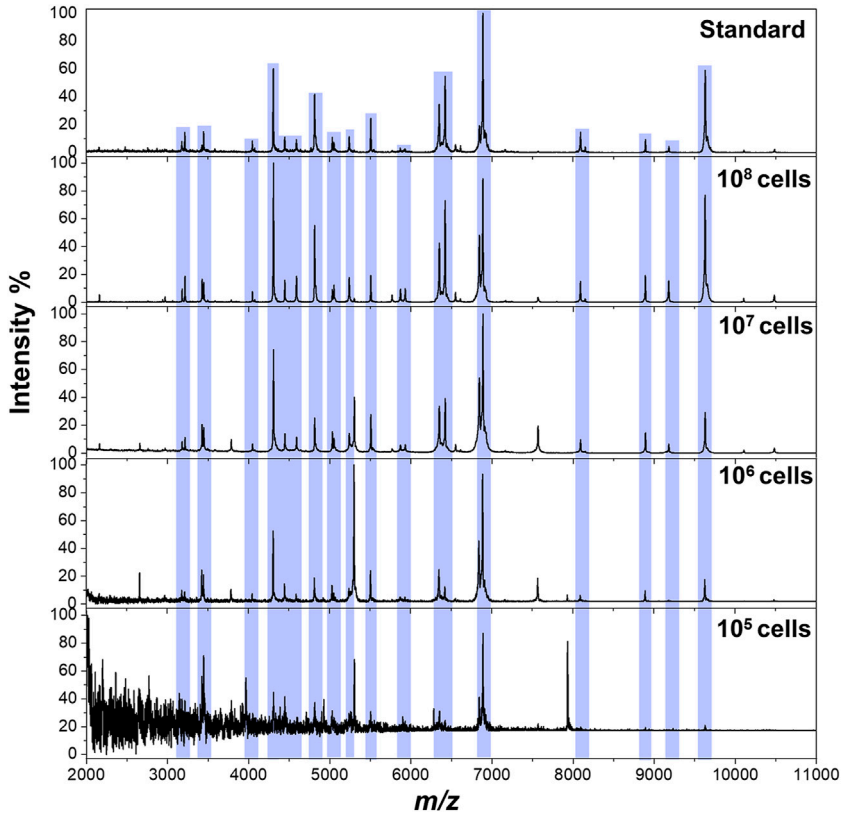

FIGURE 2 | MALDI-TOF MS spectra of *S. aureus* obtained from pure solution **(top)** and enriched by Fc-MBL@Fe_3O_4 from 1 ml buffer solution at different amounts.

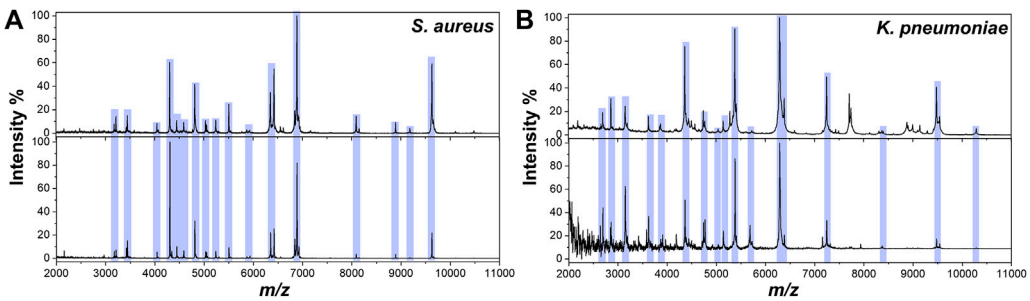

FIGURE 3 | MALDI-TOF MS spectra of **(A)** *S. aureus* and **(B)** *K. pneumoniae* obtained from pure solution **(top)** and enriched by Fc-MBL@Fe_3O_4 from LB liquid media **(bottom)**.

cultured in liquid LB media in parallel. Four sample spots were tested in parallel, and the representative mass spectrum is shown in **Figure 4**. The mass spectra of the bacteria in the wound swab matched *Vibrio alginolyticus* (*V. alginolyticus*), a common pathogenic bacteria of numerous aquatic animals that is widely present in the sea, with an average score of 2.15 (**Table 1**). The fluid sample was also identified as *V. alginolyticus*, with an average score of 2.31 (**Table 1**). Thus, these scores indicated that the identification results were reliable at the species level. The LB media of the control group keep the clear liquid phase, and the identification results by the proposed method were unreliable (score <1.7), indicating that the control group is negative for bacteria.

Verification of the Results

To verify the results, short-term–cultured liquid samples continue to grow on a solid medium, and the isolates were analyzed by MALDI-TOF MS. The results were consistent with those obtained by magnetic enrichment coupled with MALDI-TOF MS (**Table 1** and **Supplementary Figure S6**).

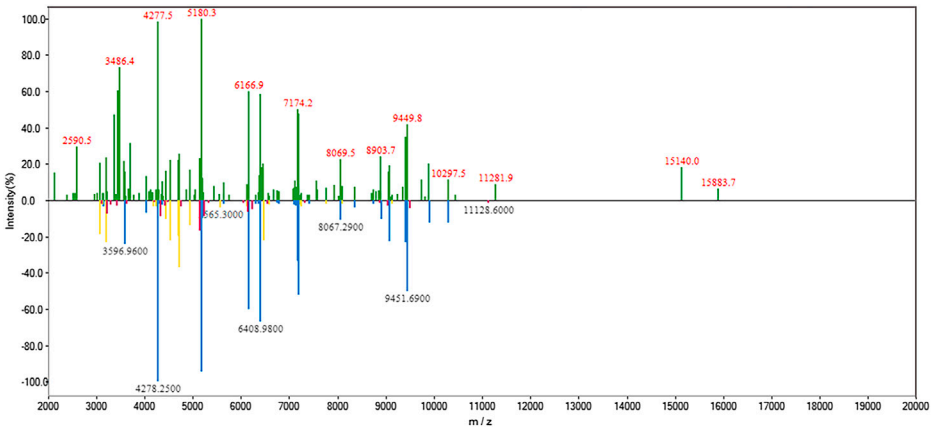

FIGURE 4 | MALDI-TOF MS spectrum of bacteria enriched by Fc-MBL@Fe_3O_4 **(top)** and matched spectrum of *V. alginolyticus* in the database **(bottom)**. In the lower spectrum, the blue peaks represent matched peaks with high similarity, red peaks represent low similarity, and yellow peaks represent intermediate similarity.

TABLE 1 | MALDI-TOF MS identification of bacteria in a real case.

Sample	The proposed method			Solid culture-based method		
	Genus	Species	Score	Genus	Species	Score
Swab	*Vibrio*	*alginolyticus*	2.14	*Vibrio*	*alginolyticus*	2.41
Swab	*Vibrio*	*alginolyticus*	2.14	*Vibrio*	*alginolyticus*	2.39
Swab	*Vibrio*	*alginolyticus*	2.12	*Vibrio*	*alginolyticus*	2.27
Swab	*Vibrio*	*alginolyticus*	2.21	*Vibrio*	*alginolyticus*	2.35
Fluid	*Vibrio*	*alginolyticus*	2.29	*Vibrio*	*alginolyticus*	2.28
Fluid	*Vibrio*	*alginolyticus*	2.26	*Vibrio*	*alginolyticus*	2.29
Fluid	*Vibrio*	*alginolyticus*	2.33	*Vibrio*	*alginolyticus*	2.35
Fluid	*Vibrio*	*alginolyticus*	2.35	*Vibrio*	*alginolyticus*	2.30

Furthermore, Gram staining showed that the bacteria were Gram-negative rods (**Supplementary Figure S7**), and the pathogen was identified as *V. alginolyticus* by the VITEK2-Compact automatic bacterial identification system. *V. alginolyticus*, a type of Gram-negative opportunistic bacteria, infects both humans and aquatic animals (Xie et al., 2020). This infection is one of the main causes of aquaculture disease resulting in economic losses in mariculture in South China (Xie et al., 2005; Yu et al., 2018; Yu et al., 2019). Therefore, it was not surprising that *V. alginolyticus* was identified in this case. The whole process of the routine method required >24 h. The identification results from MALDI-TOF MS coupled with Fc-MBL@Fe_3O_4 enrichment were in agreement with the conventional method and required only ~9 h.

CONCLUSION

In conclusion, direct pathogen identification from liquid-cultured clinical samples can be achieved by MALDI-TOF MS identification and appropriate pre-purification. Fc-MBL@Fe_3O_4 could recognize and capture broad-spectrum microbes, and therefore, it is adaptable to combine with MALDI-TOF MS. In this study, we identified *V. alginolyticus* in a patient with an open fracture using MALDI-TOF MS profiling coupled with Fc-MBL@Fe_3O_4 enrichment. With extension of the MALDI microbial database, particularly for bacterial mixtures, magnetic enrichment coupled with MALDI-TOF MS has great potential for more clinical samples.

DATA AVAILABILITY STATEMENT

The original contributions presented in the study are included in the article/**Supplementary Material**, further inquiries can be directed to the corresponding authors.

AUTHOR CONTRIBUTIONS

JY: conceptualization, methodology, resources, and validation; WG: investigation, visualization, data curation, and validation; DH: resources, investigation, and validation; CD: investigation and conceptualization; LL: investigation, writing—original draft, and writing—reviewing and editing; TP: conceptualization and supervision; SY: conceptualization, supervision, funding acquisition, and project administration.

FUNDING

National Key Research and Development Program of China (No. 2018YFF0212501) and National Natural Science Foundation of China (No. 31470786). These two funds can pay for open-access publication fees.

SUPPLEMENTARY MATERIAL

The Supplementary Material for this article can be found online at: https://www.frontiersin.org/articles/10.3389/fchem.2021.672744/full#supplementary-material

REFERENCES

Arnold, W. V., Shirtliff, M. E., and Stoodley, P. (2013). Bacterial Biofilms and Periprosthetic Infections. *J. Bone Jt. Surg. Am.* 95 (24), 2223–2229. doi:10.2106/jbjs.m.00261

Backes, M., Spijkerman, I. J., de Muinck-Keizer, R.-J. O., Goslings, J. C., and Schepers, T. (2018). Determination of Pathogens in Postoperative Wound Infection after Surgically Reduced Calcaneal Fractures and Implications for Prophylaxis and Treatment. *J. Foot Ankle Surg.* 57 (1), 100–103. doi:10.1053/j.jfas.2017.08.016

Bicart-See, A., Rottman, M., Cartwright, M., Seiler, B., Gamini, N., Rodas, M., et al. (2016). Rapid Isolation of *Staphylococcus aureus* Pathogens from Infected Clinical Samples Using Magnetic Beads Coated with Fc-Mannose Binding Lectin. *PLoS One* 11 (6), e0156287. doi:10.1371/journal.pone.0156287

Cheng, D., Yu, M., Fu, F., Han, W., Li, G., Xie, J., et al. (2016). Dual Recognition Strategy for Specific and Sensitive Detection of Bacteria Using Aptamer-Coated Magnetic Beads and Antibiotic-Capped Gold Nanoclusters. *Anal. Chem.* 88 (1), 820–825. doi:10.1021/acs.analchem.5b03320

Feng, B., Shi, H., Xu, F., Hu, F., He, J., Yang, H., et al. (2020). FTIR-assisted MALDI-TOF MS for the Identification and Typing of Bacteria. *Analytica Chim. Acta* 1111, 75–82. doi:10.1016/j.aca.2020.03.037

Firoozabadi, R., Alton, T., and Wenke, J. (2015). Novel Strategies for the Diagnosis of Posttraumatic Infections in Orthopaedic Trauma Patients. *J. Am. Acad. Orthopaedic Surgeons* 23 (7), 443–451. doi:10.5435/JAAOS-D-14-00174

Kang, J. H., Super, M., Yung, C. W., Cooper, R. M., Domansky, K., Graveline, A. R., et al. (2014). An Extracorporeal Blood-Cleansing Device for Sepsis Therapy. *Nat. Med.* 20 (10), 1211–1216. doi:10.1038/nm.3640

Liébana, S., Lermo, A., Campoy, S., Cortés, M. P., Alegret, S., and Pividori, M. I. (2009). Rapid Detection of Salmonella in Milk by Electrochemical Magneto-Immunosensing. *Biosens. Bioelectron.* 25 (2), 510–513. doi:10.1016/j.bios.2009.07.022

Matsuda, N., Matsuda, M., Notake, S., Yokokawa, H., Kawamura, Y., Hiramatsu, K., et al. (2012). Evaluation of a Simple Protein Extraction Method for Species Identification of Clinically Relevant Staphylococci by Matrix-Assisted Laser Desorption Ionization-Time of Flight Mass Spectrometry. *J. Clin. Microbiol.* 50 (12), 3862–3866. doi:10.1128/JCM.01512-12

Morgenstern, M., Kühl, R., Eckardt, H., Acklin, Y., Stanic, B., Garcia, M., et al. (2018). Diagnostic Challenges and Future Perspectives in Fracture-Related Infection. *Injury* 49, S83–S90. doi:10.1016/S0020-1383(18)30310-3

Nemr, C. R., Smith, S. J., Liu, W., Mepham, A. H., Mohamadi, R. M., Labib, M., et al. (2019). Nanoparticle-Mediated Capture and Electrochemical Detection of Methicillin-ResistantStaphylococcus Aureus. *Anal. Chem.* 91 (4), 2847–2853. doi:10.1021/acs.analchem.8b04792

Nomura, F., Tsuchida, S., Murata, S., Satoh, M., and Matsushita, K. (2020). Mass Spectrometry-Based Microbiological Testing for Blood Stream Infection. *Clin. Proteom* 17, 14. doi:10.1186/s12014-020-09278-7

Papagiannopoulou, C., Parchen, R., Rubbens, P., and Waegeman, W. (2020). Fast Pathogen Identification Using Single-Cell Matrix-Assisted Laser Desorption/Ionization-Aerosol Time-Of-Flight Mass Spectrometry Data and Deep Learning Methods. *Anal. Chem.* 92 (11), 7523–7531. doi:10.1021/acs.analchem.9b05806

Patel, R. (2013). MALDI-TOF Mass Spectrometry: Transformative Proteomics for Clinical Microbiology. *Clin. Chem.* 59 (2), 340–342. doi:10.1373/clinchem.2012.183558

Patrulea, V., Borchard, G., and Jordan, O. (2020). An Update on Antimicrobial Peptides (AMPs) and Their Delivery Strategies for Wound Infections. *Pharmaceutics* 12 (9), 840. doi:10.3390/pharmaceutics12090840

Rhoads, D. D., Wolcott, R. D., Sun, Y., and Dowd, S. E. (2012). Comparison of Culture and Molecular Identification of Bacteria in Chronic Wounds. *Ijms* 13 (3), 2535–2550. doi:10.3390/ijms13032535

Segawa, S., Sawai, S., Murata, S., Nishimura, M., Beppu, M., Sogawa, K., et al. (2014). Direct Application of MALDI-TOF Mass Spectrometry to Cerebrospinal Fluid for Rapid Pathogen Identification in a Patient with Bacterial Meningitis. *Clinica Chim. Acta* 435, 59–61. doi:10.1016/j.cca.2014.04.024

Singhal, N., Kumar, M., Kanaujia, P. K., and Virdi, J. S. (2015). MALDI-TOF Mass Spectrometry: an Emerging Technology for Microbial Identification and Diagnosis. *Front. Microbiol.* 6, 791. doi:10.3389/fmicb.2015.00791

Sun, J., Shi, H., Xue, Y., Cheng, W., Yu, M., Ding, C., et al. (2021). Releasing Bacteria from Functional Magnetic Beads Is Beneficial to MALDI-TOF MS Based Identification. *Talanta* 225, 121968. doi:10.1016/j.talanta.2020.121968

Takahashi, K., and Ezekowitz, R. A. B. (2005). The Role of the Mannose-Binding Lectin in Innate Immunity. *Clin. Infect. Dis.* 41 (Suppl. 7), S440–S444. doi:10.1086/431987

Tuon, F. F., Cieslinski, J., Ono, A. F. M., Goto, F. L., Machinski, J. M., Mantovani, L. K., et al. (2019). Microbiological Profile and Susceptibility Pattern of Surgical Site Infections Related to Orthopaedic Trauma. *Int. Orthopaedics (Sicot)* 43 (6), 1309–1313. doi:10.1007/s00264-018-4076-7

Váradi, L., Luo, J. L., Hibbs, D. E., Perry, J. D., Anderson, R. J., Orenga, S., et al. (2017). Methods for the Detection and Identification of Pathogenic Bacteria: Past, Present, and Future. *Chem. Soc. Rev.* 46 (16), 4818–4832. doi:10.1039/c6cs00693k

Welker, M., Van Belkum, A., Girard, V., Charrier, J.-P., and Pincus, D. (2019). An Update on the Routine Application of MALDI-TOF MS in Clinical Microbiology. *Expert Rev. Proteomics* 16 (8), 695–710. doi:10.1080/14789450.2019.1645603

Woo, P. C. Y., Lau, S. K. P., Teng, J. L. L., Tse, H., and Yuen, K.-Y. (2008). Then and Now: Use of 16S rDNA Gene Sequencing for Bacterial Identification and Discovery of Novel Bacteria in Clinical Microbiology Laboratories. *Clin. Microbiol. Infect.* 14 (10), 908–934. doi:10.1111/j.1469-0691.2008.02070.x

Xie, Z.-Y., Hu, C.-Q., Chen, C., Zhang, L.-P., and Ren, C.-H. (2005). Investigation of Seven Vibrio Virulence Genes Among Vibrio Alginolyticus and Vibrio Parahaemolyticus Strains from the Coastal Mariculture Systems in Guangdong, China. *Lett. Appl. Microbiol.* 41 (2), 202–207. doi:10.1111/j.1472-765X.2005.01688.x

Xie, Z. Y., Gong, X. X., Xu, X. D., Mei, B., Xuan, X. Z., Long, H., et al. (2020). Identification of Vibrio Alginolyticus Virulent Strain-specific DNA Regions by Suppression Subtractive Hybridization and PCR. *J. Appl. Microbiol.* 129 (6), 1472–1485. doi:10.1111/jam.14739

Yi, J., Qin, Q., Wang, Y., Zhang, R., Bi, H., Yu, S., et al. (2018). Identification of Pathogenic Bacteria in Human Blood Using IgG-Modified Fe3O4 Magnetic Beads as a Sorbent and MALDI-TOF MS for Profiling. *Microchim Acta* 185 (12), 542. doi:10.1007/s00604-018-3074-1

Yu, Q., Li, F., Wang, Y., Qin, X., Chen, X., Wu, L., et al. (2018). Isolation, Identification and Pathogenicity of Vibrio Alginolyticus from Marine Cultured Trachinotus Ovatus in Beibu Gulf,Guang Xi. *Guangxi Sci.* 25, 68–73. doi:10.13656/j.cnki.gxkx.20180208.001

Yu, Q., Liu, M., Xiao, H., Wu, S., Qin, X., Ke, K., et al. (2019). Development of Novel Aptamer-based Enzyme-linked Apta-sorbent Assay (ELASA) for Rapid Detection of Mariculture Pathogen Vibrio Alginolyticus. *J. Fish. Dis.* 42 (11), 1523–1529. doi:10.1111/jfd.13066

Yun, H. C., Murray, C. K., Nelson, K. J., and Bosse, M. J. (2016). Infection after Orthopaedic Trauma: Prevention and Treatment. *J. Orthop.* 30, S21–S26. doi:10.1097/bot.0000000000000667

Zboromyrska, Y., Rubio, E., Alejo, I., Vergara, A., Mons, A., Campo, I., et al. (2016). Development of a New Protocol for Rapid Bacterial Identification and Susceptibility Testing Directly from Urine Samples. *Clin. Microbiol. Infect.* 22, e1–561.e1–6. doi:10.1016/j.cmi.2016.01.025

Zhu, Y., Qiao, L., Prudent, M., Bondarenko, A., Gasilova, N., Möller, S. B., et al. (2016). Sensitive and Fast Identification of Bacteria in Blood Samples by Immunoaffinity Mass Spectrometry for Quick BSI Diagnosis. *Chem. Sci.* 7 (5), 2987–2995. doi:10.1039/c5sc04919a

Conflict of Interest: The authors declare that the research was conducted in the absence of any commercial or financial relationships that could be construed as a potential conflict of interest.

frontiers in Chemistry

ORIGINAL RESEARCH
published: 24 June 2021
doi: 10.3389/fchem.2021.698297

Optimized MALDI-TOF MS Strategy for Characterizing Polymers

Zhenxin Wang[1†], *Quanqing Zhang*[2†], *Huali Shen*[3], *Pengyuan Yang*[4*] *and Xinwen Zhou*[5*]

[1]*Institutes of Biomedical Sciences of Shanghai Medical School and Laboratory Medicine of Zhongshan Hospital, Fudan University, Shanghai, China,* [2]*Department of Chemistry, University of California, Riverside, CA, United States,* [3]*Institutes of Biomedical Sciences of Shanghai Medical School and Minhang Hospital, Fudan University, Shanghai, China,* [4]*Institutes of Biomedical Sciences of Shanghai Medical School and Department of Chemistry, Fudan University, Shanghai, China,* [5]*Institutes of Biomedical Sciences of Shanghai Medical School, Fudan University, Shanghai, China*

In recent years, matrix-assisted laser desorption/ionization time-of-flight mass spectrometry (MALDI-TOF MS) plays an essential role in the analysis of polymers. To acquire a more reliable strategy for polymer profiling, we characterized four representative polymers including polyethylene glycol 6000, polyvinylpyrrolidone K12, polymer polyol KPOP-5040, and polyether polyol DL-4000. The preparation methods of these four polymer samples have been optimized from six aspects, including matrix, cationization reagent, solvent, mixing ratio of cationization reagent to polymer, mixing ratio of matrix to polymer, and laser intensity. After investigating the effects of seven commonly used matrices on the ionization efficiency of four polymers, *trans*-2-[3-(4-tert-butylphenyl)-2-methyl-2-propenylidene] malononitrile (DCTB) was found to be the only matrix suitable for the analysis of all the four polymers. Our experimental results suggested that different polymers showed a certain preference for different cationization reagents. For example, the polymer polyol KPOP-5040 was suitable for sodium iodide as the cationization reagent, while polyvinylpyrrolidone K12 was more suitable for silver trifluoroacetate (AgTFA). For the choice of solvent, tetrahydrofuran is a reagent with rapid evaporation and a wide range of dissolution which can achieve the best results for the analysis of four polymers. The optimized method was successfully applied to the identification of DSPE-PEG-NH_2 with different polymerized degrees. This MALDI-TOF strategy potentially provided the supplementary function through the polymer's application in biomedical and visible probing.

Keywords: MALDI-TOF MS, polymer, polyvinylpyrrolidone K12, polymer polyol KPOP-5040, polyether polyol DL-4000, polyethylene glycol 6000

OPEN ACCESS

Edited by:
Cheng Guo,
Zhejiang University, China

Reviewed by:
Kezhi Jiang,
Hangzhou Normal University, China
Mengzhe Guo,
Xuzhou Medical University, China

***Correspondence:**
Pengyuan Yang
pyyang@fudan.edu.cn
Xinwen Zhou
zhouxinwen@fudan.edu.cn

[†]*These authors have contributed equally to this work*

Specialty section:
This article was submitted to Analytical Chemistry, a section of the journal Frontiers in Chemistry

Received: *21 April 2021*
Accepted: *04 June 2021*
Published: *24 June 2021*

Citation:
Wang Z, Zhang Q, Shen H, Yang P and Zhou X (2021) Optimized MALDI-TOF MS Strategy for Characterizing Polymers. Front. Chem. 9:698297. doi: 10.3389/fchem.2021.698297

INTRODUCTION

Compared with electrospray mass spectrometry (MS), matrix-assisted laser desorption/ionization time-of-flight mass spectrometry (MALDI-TOF MS) has the characteristics of high sensitivity, easy operation, and wide application (Danis et al., 1992; Roy et al., 1995; Nielen, 1999; Falkenhagen and Weidner, 2010; Peng and Kinsel, 2010). With the development of MALDI-TOF MS, it is increasingly used in the research of polymer structure analysis, including the number of repeating polymer units, molecular weight distribution, terminal structure, and other information, which could perfectly complement the other traditional techniques such as NMR and XRD. Sample preparation is one of the most critical steps for MALDI-TOF MS (Michael et al., 1985; Zhang and

Kinsel, 2002) analysis. Since polymers have the characteristics of large molecular weight range and limited solubility, optimization for the polymer preparation method is significant (Hanton and Parees, 2005).

The molecular weight ranges from several hundreds to a few millions in different polymers. In the meantime, the structure of polymers is also complex and diverse. Therefore, a suitable polymer sample solvent, matrix, cationization reagent, instrument parameter, and spotting method, etc., are the key conditions for the sample preparation method of MS-based polymer characterization (Juhasz et al., 1993; Dai et al., 1996; Bauer et al., 2010; Skelton et al., 2013). Six aspects need to be considered when performing polymer MALDI-TOF MS analysis, including the compatibility of different polymers and matrices, the compatibility of different polymers and cationization reagent solvents, with the best selection of matrices and cationization reagents, taking into account the proportional relation between different polymers and the matrix, the proportional relation between different polymers and the cationization agent, the volatilization of mixed solvents, and the uniform cocrystallization. In this study, MALDI-TOF MS was used to characterize four representative polymers including polyethylene glycol 6000(PEG-6000), polyvinylpyrrolidone K12 (PVPK12), polymer polyol KPOP-5040 (KPOP-5040), and polyether polyol DL-4000 (DL-4000). At the same time, the preparation methods of these four polymer samples had also been further optimized in this study.

To determine the molecular weight of polymers by MS is important to illustrate their structure and function. PEG is widely used in industrial and consumer products. During biochemical assays, PEG is always employed to partition proteins in aqueous two-phase systems (Singh and Tavana, 2018). Recently, PEG was described as a high-risk hidden allergen in drug and food items that can induce allergic reactions and diseases (Przepiorka et al., 1980). A research suggested that PEG may have a potential role in the allergic reactions to the COVID-19 vaccine, and for patients testing positive, avoidance of PEG and PEG analogues is strictly recommended (Cabanillas et al., 2020). PVP is widely used in automobile, furniture, and petroleum industries and as the main raw materials of curing waterproof coating; furthermore, it was also found to be better formulations to achieve introducing a clinically relevant hydrophobic anticancer drug into self-assembled nanoparticles successfully (Chowdhury et al., 2018; Schupp et al., 2018). The use of the polyether polyol enables the production of a low-density, low-hardness flexible urethane foam using a small amount of water, without requiring any environment-unfriendly chlorofluorocarbon and without being accompanied by deterioration of humid age compression set and other characteristics. Therefore, it is essential to generate a widespread method for polymer detection. We took a comparative work on the selection of matrix, solvent, and different proportions of polymer detection conditions, aiming at the promotion of polymer ionization efficiency and mass spectrum signal.

EXPERIMENT

Reagents and Materials

PEG-6000 and PVPK12 were purchased from Sigma-Aldrich (St. Louis, MO, United States). KPOP-5040 was purchased from Guodu Chemical Company (Kunshan, Jiangsu, China). DL-4000 was purchased from Bluestar Dongda Chemical Company (Zibo, Shandong, China). 2,5-Dihydroxybenzoic acid (DHB), *trans*-2-[3-(4-tert-butylphenyl)-2-methyl-2-propenylidene] malononitrile (DCTB), dithranol, 2,3,4-trihydroxyacetophenone (2,3,4-THAP), 2,4,6-trihydroxyacetophenone (2,4,6-THAP), a-cyano-4-hydroxycinnamic acid (CHCA), 9-aminoacridines (9AA), silver trifluoroacetate (AgTFA),sodium iodide, and sodium trifluoroacetate (NaFTA) were purchased from Sigma-Aldrich (St. Louis, MO, United States). High-performance liquid chromatography (HPLC)-grade chloroform, acetonitrile, tetrahydrofuran, methanol, acetone, and trifluoroacetic acid were purchased from Merck Millipore (Billerica, MA, United States). The water used in all experiments was prepared in a Milli-Q water purification system and displayed a resistivity of $\geq$18.2 MΩ cm^{-1}.

Instruments

The centrifugal dryer (Concentrator plus), high-speed centrifuge (Centrifuge, 5417R), and thermomixer comfort were produced by Eppendorf (Germany). The BS110S precision balance was produced by Sartorius (Germany). The MALDI-T0F/TOF 5800 system was produced by SCIEX (United States).

Experimental Procedure

Effects of Matrix

Seven commonly used matrices (CHCA, DHB, DCTB, dithranol, 9AA, 2,3,4-THAP, and 2,4,6-THAP) were weighted separately and dissolved in tetrahydrofuran to prepare a 20 mg/ml solution. Three cationization reagents (silver trifluoroacetate, sodium iodide, and sodium trifluoroacetate) were weighted separately and dissolved in tetrahydrofuran to prepare a 5 mg/ml solution. Two solid particle polymers (PEG-6000 and PVPK12) were weighted separately and dissolved in tetrahydrofuran to prepare a 10 mg/ml solution. 10 μL of two solution polymers (KPOP-5040 and DL-4000) was transferred into the tube separately with a sample gun and diluted to 1 ml with tetrahydrofuran. Ultrasound was used to assist in dissolving all of the above solutions and mixing according to polymer/matrix/cationization agent = 5/15/1 (v/v/v). The cationization reagent was fixed as silver trifluoroacetate.

Cationization Reagent Application Optimization

According to the method described in Effects of Matrix, the matrix, cationization reagent, and polymer were taken in the corresponding amount, dissolved, and diluted with 1 ml of tetrahydrofuran, respectively. Then, according to the best matrix for each polymer, polymer/matrix/cationization agent = 5/15/1 (v/v/v) was mixed with silver trifluoroacetate, sodium iodide, and sodium trifluoroacetate chosen as cationization reagents.

According to the best matrix and cationization reagent for each polymer, polymer/matrix = 5/15 μL (v/v) was mixed. Different amounts of cationization reagents (0, 1, 2, 4, 6, 8, and 10 μL) were set for mixing with the polymer and matrix with a fixed volume ratio.

Effects of the Matrix Solution Composition

According to the method described in Effects of Matrix, the matrix, cationization reagent, and polymer were taken in the corresponding amount, dissolved, and diluted with 1 ml of tetrahydrofuran, 1 ml methanol, and 1 ml acetone, respectively. Then, according to the best matrix and cationization reagent for each polymer, polymer/matrix/cationization agent = 5/15/1 (v/v/v) was mixed.

Matrix and Cationization Reagent Mixing Ratio Optimization

According to the method described in Effects of Matrix, the corresponding amount of matrix, cationization agent, and polymer were taken, respectively, dissolved, and diluted with 1 ml of tetrahydrofuran. Then, the volume of each polymer was fixed at 5 μL with the best matrix and cationization reagent. According to the selected optimal cationization reagent amount, different amounts of the matrix solution (1, 5, 15, 25, 35, 50, and 100 μL) were set for mixing.

Laser Intensity Optimization

The optimized matrix, cationization reagents, and their ratio of each polymer selected according to the previous experiment were applied for sample preparation; different laser energies for MALDI-TOF MS analysis are used to screen out the optimal laser energy conditions.

MALDI-TOF MS-Based Sample Analytical Procedure

MALDI-TOF/TOF MS analysis was performed with the SCIEX ® 5800 system. To reduce the operational error and systematic error, enzymatically hydrolyzed peptide of myoglobin from the horse was used for each sample group before analysis, as an external sample for external instrument calibration. The MS parameter was set as follows. An Nd: YAG laser at 335 nm was used with a pulse frequency of 40 Hz and acceleration voltage was set as 20 kV. The reflected positive ion mode was selected and the data are acquired as the automatic acquisition mode. The best scanning mass-to-charge ratio (m/z) range for MALDI-TOF MS was 600–12,000. Each scan accumulated 500 mass spectrum signals, and each sample accumulated 2,000 signals. Peak identifications were performed using Data Explorer software (version 4.5).

RESULTS AND DISCUSSION

Effect of Matrix on Polymer Ionization Efficiency

As a small molecule compound, the matrix has the function of absorbing laser energy and transferring protons in the MALDI process. Generally, the compatibility of the matrix and the polymer is the first thing to be considered when choosing the matrix for polymer analysis (Dwyer, 1996). Only by choosing a matrix that is relatively close to the hydrophilicity/hydrophobicity of the polymer can the uniformity of the two mixtures be ensured, including the uniformity of the solution and the uniformity of the crystals on the target after cocrystallization (Tummala and Limbach, 2010). In this study, MALDI-TOF MS was used to characterize four representative polymers including PEG-6000, PVPK12, KPOP-5040, and DL-4000. The preparation methods of these four polymer samples have been optimized from six aspects, including matrix, cationization reagent, solvent, mixing ratio of cationization reagent to polymer, mixing ratio of matrix to polymer, and laser intensity (**Figure 1**).

Firstly, we mixed the fixed volume ratio of polymer, matrix, and cationization reagent to 5/15/1(v/v/v) based on experience. Silver trifluoroacetate was used as a fixed cationization reagent for all polymers, in order to examine the effects of different matrices on the ionization efficiency of the four polymers separately. **Figure 2** shows the results of PEG-6000 detection on seven matrices, including CHCA, DHB, DCTB, dithranol, 9AA, 2,3,4-THAP, and 2,4,6-THAP (**Figures 2A–G**). It was suggested that different polymers have preferences for different matrices (**Figure 2H**). In our experiments, DCTB, DHB, dithranol, and CHCA were considered to have better ionization effects than the other three matrices. Interestingly, DCTB was the only matrix that had good effects for all four polymers. This result suggested that DCTB was a good matrix for polymers with different structures or molecular weights. It was shown that 2,3,4-THAP and 2,4,6-THAP as the matrix have the most unsatisfactory results, indicating that these two matrices with similar structures were not suitable for analysis. Since the use of DHB required a stronger laser, a large number of fragment ion peaks were generated in the low molecular weight region. However, DHB required a higher energy laser, and the uniformity of the crystal was not as effective as DCTB.

Effect of Cationization Reagent on Polymer Ionization Efficiency

Analytes with strong proton affinity (containing amino groups) were easily ionized by most matrices. However, for polymers, it is difficult for conventional acidic matrices to provide a suitable ionization strategy (Biemann, 1994; Otto et al., 2010). For these special analytes, it is very necessary to choose a suitable cationization reagent (Brandt et al., 2010). The correct choice of the cationization reagent depends on the chemical properties of the analyte. The addition of alkaline ions is considered to be the best way to help polymers without containing amino groups to be ionized. Considering that most polymers were dissolved in

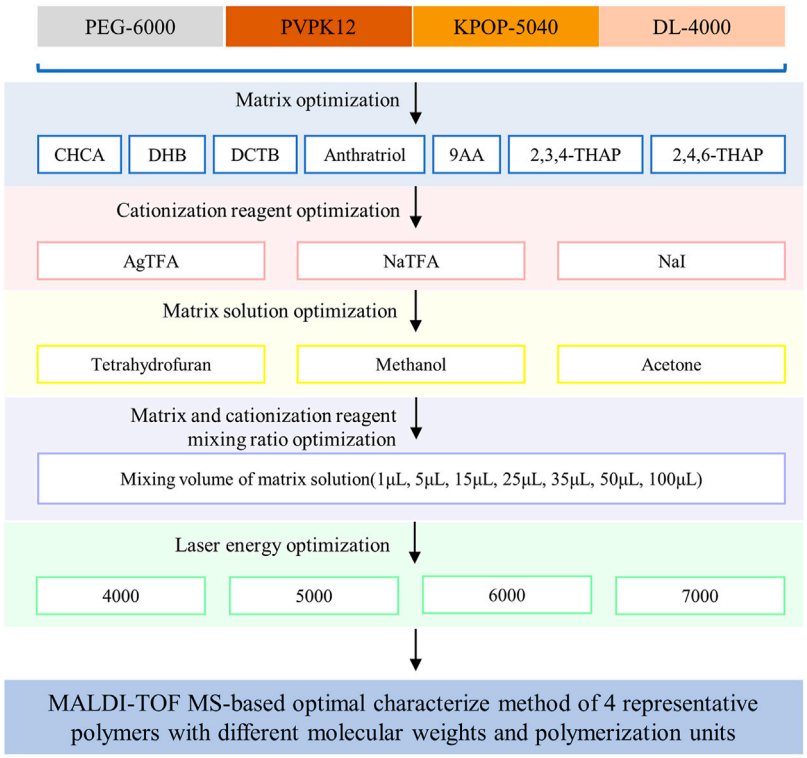

FIGURE 1 | Experiment scheme. Workflow of the study.

organic solvents with higher volatility before MALDI-TOF MS analysis, basic salts with better compatibility with organic solvents, such as trifluoroacetate (Evason et al., 2000), are selected. It is valuable to consider the affinities of different polymers with basic ions, especially those polymers whose functional group charge properties differ from those of basic ions.

Among the four polymers selected in this experiment, except PVPK12 which selected DHB as the matrix, DCTB was selected as the matrix of the other three polymers. Then, according to the best matrix for each polymer, polymer/matrix/cationization agent = 5/15/1 (v/v/v) was mixed. The silver trifluoroacetate, sodium iodide, and sodium trifluoroacetate were the cationization reagents we chose. We explored the effects of three different cationization reagents on the ionization effect of PEG-6000 (**Figures 3A–C**) and recommended sodium iodide as the more appropriate one. Our research has found that different polymers have a preference for cationization reagents (**Figure 3D**). For example, the KPOP-5040 was suitable for sodium iodide as the cationization reagent, while AgTFA was more suitable for PVPK12. In addition, the DL-4000 prefers NaTFA.

Effect of Solvents on Polymer Ionization Efficiency

For MALDI mass spectrometry analysis based on solution drying, the first consideration for sample preparation is to completely dissolve the analyte, matrix, and cationization reagent (Marie et al., 2000). The solubility of different analytes themselves, as well as their solubility with the matrix and cationization reagents, should be taken into consideration at the same time. The ideal situation is to choose only one solvent during the entire experiment to avoid precipitation that might be caused by multiple solvents not evaporating at the same time. In addition, to avoid matrix recrystallization over the solvent evaporation process, it is better to choose a solvent that evaporates very quickly (Schwarzinger et al., 2012). Thus, solvents with a wide range of dissolution and rapid evaporation were ideal for polymer sample preparation.

In this study, three common solvents (methanol, tetrahydrofuran, and acetone) with a wide range of dissolution and rapid evaporation were selected for comparison and optimization. Our experimental results suggested that only tetrahydrofuran had the ability to be compatible with all nine substances, in the process of dissolving four polymers, two substrates, and three cationization reagents. DCTB and PEG-6000 showed relatively poor solubility in methanol, while PEG-6000 and PVPK12 exhibited poor solubility in acetone. PEG-6000 dissolved in tetrahydrofuran showed the best ionization efficiency (**Supplementary Figures S1A–C**). We deduced that the most likely reason was the different polarities of the three solvents. The polarity of these three solvents is methanol > acetone > tetrahydrofuran in descending order. Since PEG-6000 is a nonpolar polymer, it has better compatibility with tetrahydrofuran, which is relatively smaller polarity. The experimental result indicated that, when tetrahydrofuran was

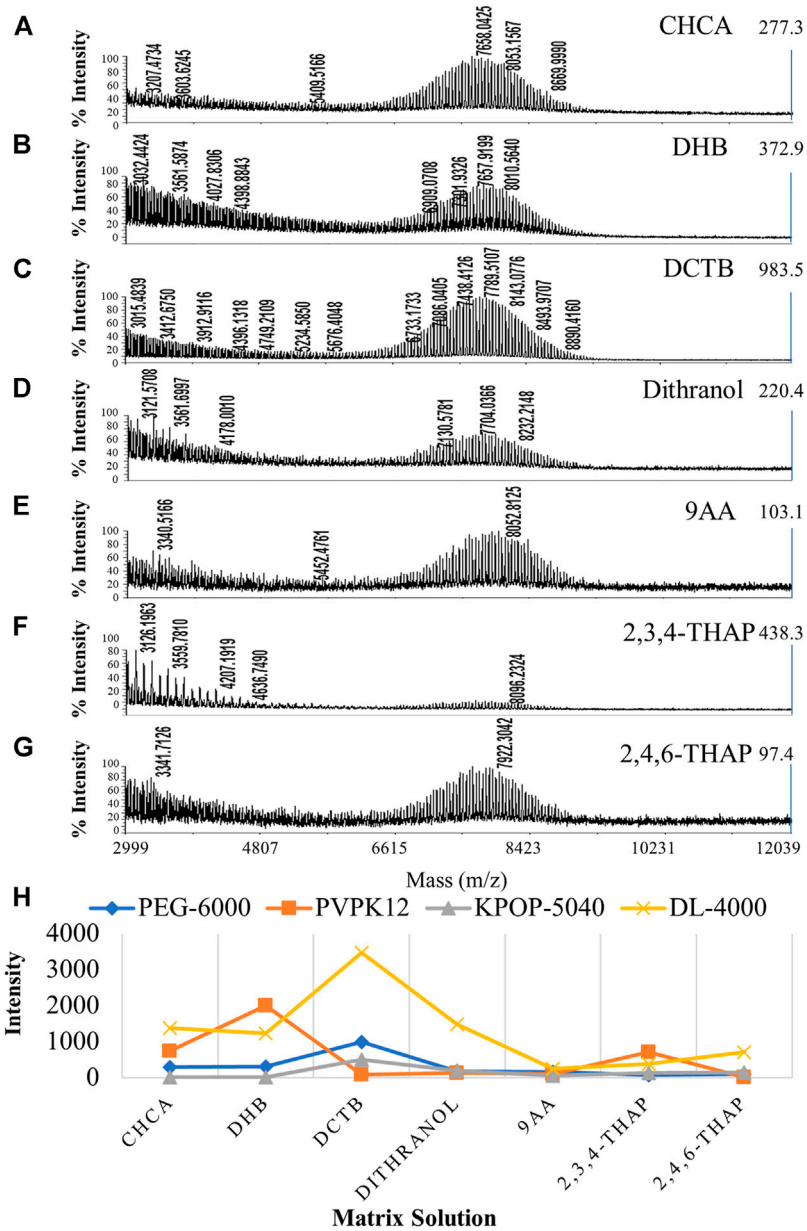

FIGURE 2 | MALDI-TOF MS spectrums of PEG-6000 with different matrices including CHCA **(A)**, DHB **(B)**, DCTB **(C)**, dithranol **(D)**, 9AA **(E)**, 2,3,4-THAP **(F),** and 2,4,6-THAP **(G)**. Effect of the matrix on polymer ionization efficiency **(H)**. Blue, orange, gray, and yellow colors indicate the peak intensity of PEG-6000, PVPK12, KPOP-5040, and DL-4000, respectively.

used as the solvent, the MS spectra of the four polymers had the best quality (**Figure 3E**). At the same time, no obvious signal was detected when PVPK12 was dissolved in methanol and acetone, which was consistent with the poor solubility of PVPK12 over the sample dissolution process. It can be proved that the successful screening of a solvent which simultaneously dissolves the polymer, matrix, and cationization agent is essential and a success factor for the MALDI-TOF MS analysis of molecular polymers.

Effect of Different Mixing Ratios on the Polymer Ionization Efficiency

After selecting the matrix, cationization agent, and solvent corresponding to each polymer, the mixing ratio among them also had a great effect on the ionization efficiency of the polymer. First of all, the sample, matrix, and cationization reagent should be dissolved in a reasonable concentration. When the mixture was volatilizing, precipitation would occur if the sample was the earliest one that reached the dissolution limit, and the effect of

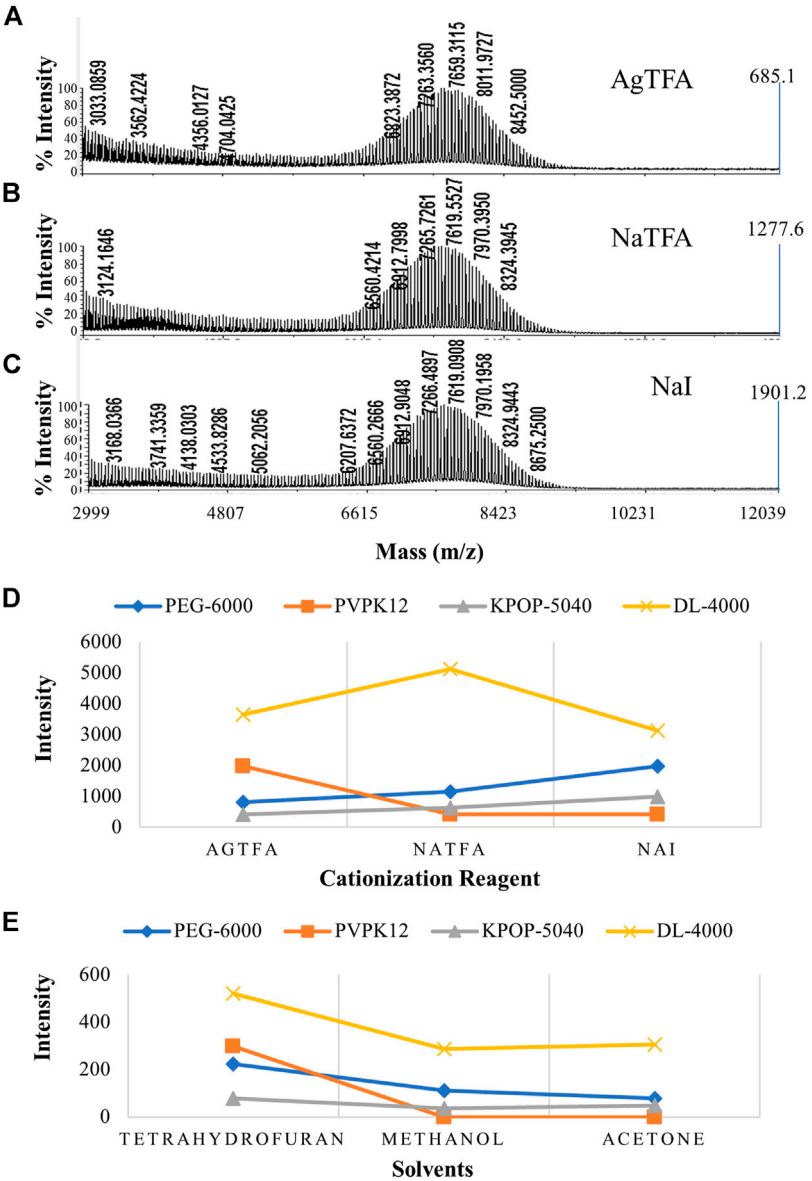

FIGURE 3 | MALDI-TOF MS spectrums of PEG-6000 with different cationization reagents including AgTFA **(A)**, NaTFA **(B)**, and NaI **(C)**. Intensities of four polymers with different cationization reagents **(D)**. Effect of solvent on the polymer ionization efficiency **(E)**. Blue, orange, gray, and yellow colors indicate the peak intensity of PEG-6000, PVPK12, KPOP-5040, and DL-4000, respectively.

forming cocrystal crystals would be poor (Schriemer and Liang, 1997).

The first step is to take into account the mixing ratio between the cationization reagent and the polymer. Under the condition of a fixed amount of matrix, the polymer peak was very weak, when the amount of cationization reagent is 0 μL, which suggested that the cationization reagent was really able to increase the intensity of the polymer signal (**Figures 4A,B**). However, when the amount of cationization reagent was gradually increased from 1 to 10 μL, there was no obvious difference in the effect of the four polymers, which suggested that excessive cationization reagent had no obvious effect on the improvement of the polymer signal (**Figure 4C**). Interestingly, the cationization reagent was found to not only increase the signal strength of the polymer, but also interfere with the analysis of MALDI-TOF MS. For example, in the analysis of PVPK12, with the increase of AgTFA concentration, the silver-added cluster peaks formed by the polymer became more and more obvious.

The second step is to take into account the mixing ratio between the matrix and the polymer. Since the selection of a suitable matrix plays a very important role in polymer analysis, a suitable mixing ratio of the matrix and polymer also has a great effect on the analysis signal (Macha et al., 2001). Generally, the

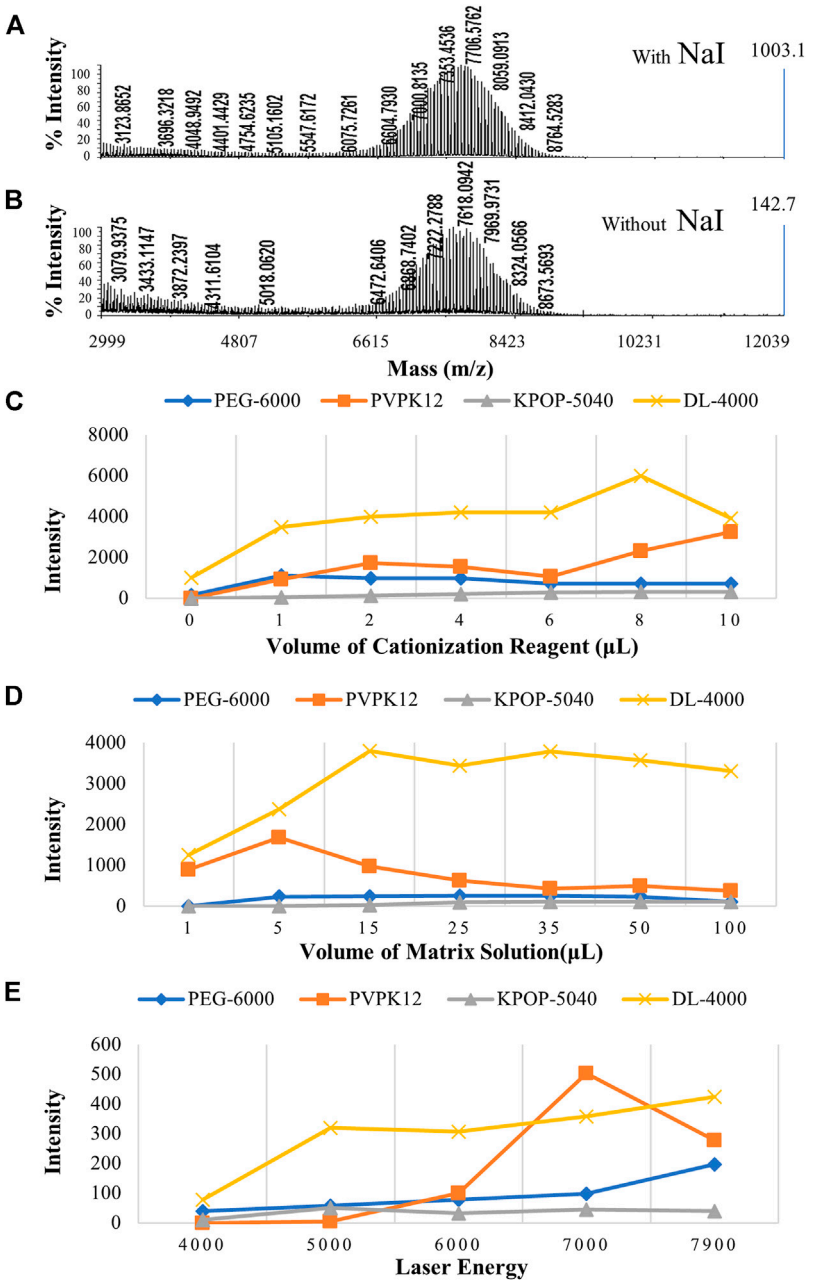

FIGURE 4 | MALDI-TOF MS spectrums of polymers with the cationization reagent **(A)** and without the cationization reagent **(B)**. The effect of different ratios of the cationization reagent **(C)**, different ratios of the matrix **(D)**, and laser energy **(E)** on the polymer ionization efficiency. Blue, orange, gray, and yellow colors indicate the peak intensity of PEG-6000, PVPK12, KPOP-5040, and DL-4000, respectively.

matrix/polymer whose molar ratio was in the range of 100/1 to 100,000/1 was able to get good detection results (**Figure 4D**). However, when the polymer itself could not be ionized, such as when the amount of matrix was quite low, the peaking effect would become very poor. In this experiment, the signal strength of the four polymers was very weak when the molar ratio of the matrix to polymer was at a low level (the matrix volume was set as 1 and 5 μL). On the contrary, while the molar ratio of the matrix to the polymer was gradually increased (the matrix volume was set from 15 to 100 μL), the four polymers could obtain sufficiently strong signal intensities.

Effect of Laser Energy on the Polymer Ionization Efficiency

For MALDI-TOF MS, in addition to the sample preparation that determines whether the analyte can be ionized under the optimal conditions, the laser energy also affects the peaking of the analyte

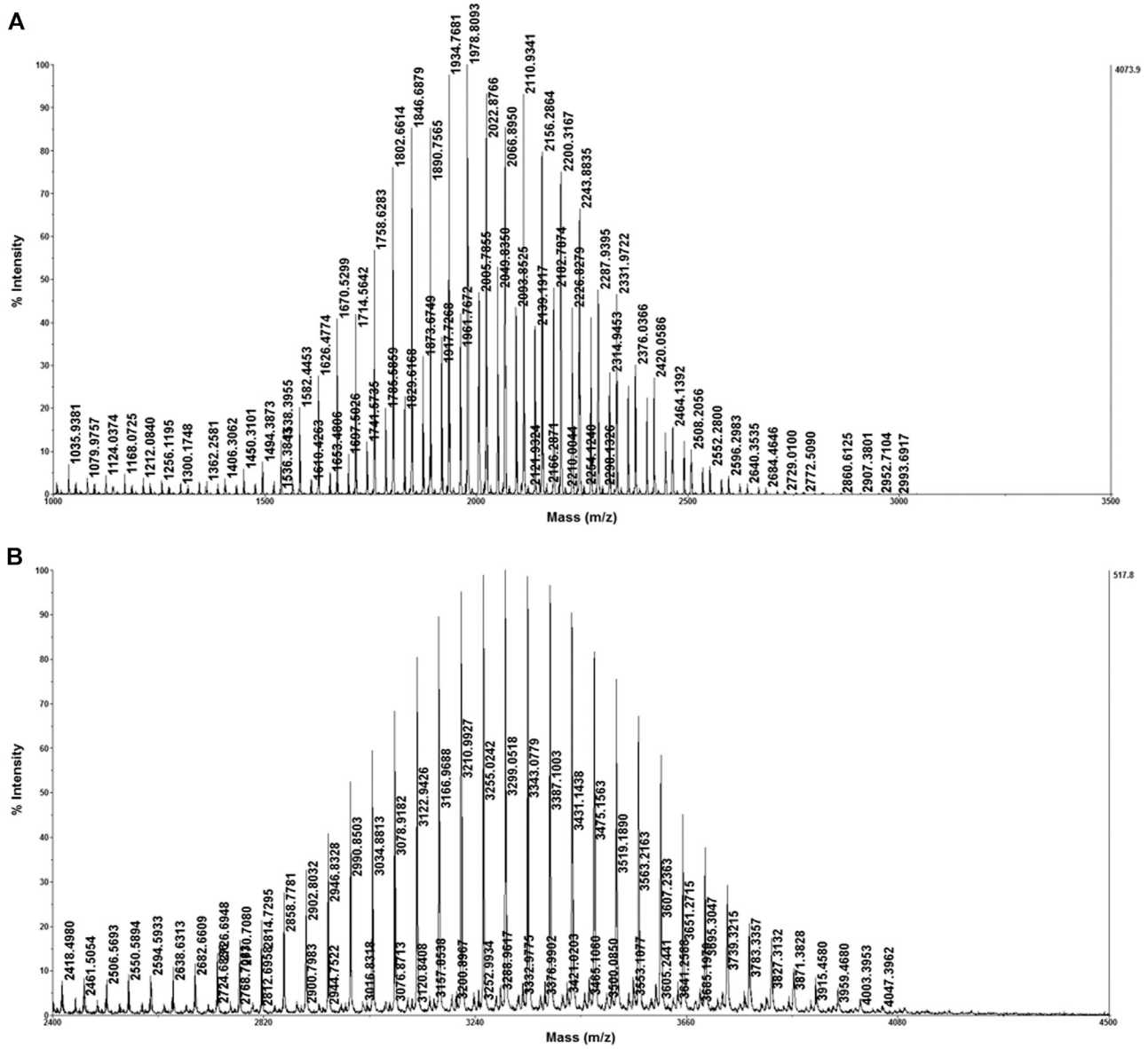

FIGURE 5 | Identification of DSPE-PEG-NH2-2000 **(A)** and DSPE-PEG-NH2-3400 **(B)** with the optimized strategy.

(Cohen and Chait, 1996). In the process of MALDI source ionization, the laser plays two important roles, including providing energy for the matrix and analyte and ionizing the matrix to generate ion current (Wang et al., 1996). The sample cannot be ionized at low laser energy. Properly increasing the laser energy can significantly increase the signal of the analyte (Montaudo et al., 1995). The prerequisite is that the laser energy must be higher than the minimum energy required for sample ionization. In this study, the signals of the four polymers have been observed to be significantly improved when the laser energy was gradually increased from 4000 to about 7000 (**Figure 4E** and **Supplementary Figures 2A–D**). However, when the laser energy reached 7900, the signal of the polymer was not significantly improved as wished, but the resolution of the peak was reduced. This result might suggest that, when the laser energy was too high, it would produce negative effects. This would affect the analysis of the polymer structure from two aspects, including the reduction of resolution due to the saturation of the detector signal and fragments formed due to the fracture of the polymer.

DSPE-PEG-NH_2 Identification

As a significant linker for liposomal nanocarrier, different degrees of polymerized DSPE-PEG-NH_2 were widely used in biomedical and visible probing (Kang and Ko, 2019; Rodrigues et al., 2019). We further applied the optimized method to identify DSPE-PEG-NH_2 with different polymerized degrees. DSPE-PEG-NH_2-2000 and DSPE-PEG-NH_2-3400 were first dissolved in tetrahydrofuran in order to get better ionization efficiency.

DCTB was chosen as the matrix due to the better compatibility for polymers. Sodium iodide was employed as the cationization reagent to achieve better ionization efficiency. As shown in **Figure 5**, both DSPE-PEG-NH_2-2000 and DSPE-PEG-NH_2-3400 were identified with excellent intensity even when the concentration was only 0.5 mg/ml.

CONCLUSION

In this study, MALDI-TOF MS was used to characterize four representative polymers including PEG-6000, PVPK12, KPOP-5040, and DL-4000. The preparation methods of these four polymer samples have been optimized from six aspects, including matrix, cationization reagent, solvent, mixing ratio of cationization reagent to polymer, mixing ratio of matrix to polymer, and laser intensity. After investigating the effects of seven commonly used matrices on the ionization efficiency of four polymers, DCTB was found to be the only matrix suitable for the analysis of all the four polymers. For PVPK12, DHB was also a suitable matrix, which was helpful for improving sensitivity. Our experimental results suggested that sufficient strong signal intensities were obtained only when the molar ratio of matrix to polymer was at a certain high level. Otherwise, the effect of forming cocrystal crystals would be poor while the molar ratio of matrix to polymer was at a low level. The polymer peak was very weak without the cationization reagent. We found that it was really able to increase the intensity of the polymer signal when the amount of cationization reagent was gradually increased. However, different polymers showed a certain preference for different cationization reagents. For example, the KPOP-5040 was suitable for sodium iodide as the cationization reagent, while PVPK12 was more suitable for AgTFA. In addition, the DL-4000 prefers NaTFA. For the choice of solvent, tetrahydrofuran is a reagent with rapid evaporation and a wide range of dissolution which can achieve the best results for the analysis of four polymers. Finally, the optimization of laser energy was also crucial. The appropriate laser energy we chose was able to achieve the best ionization effect without breaking the polymer. The optimized method was successfully applied to the identification of DSPE-PEG-NH_2 with different polymerized degrees. We have systematically analyzed the relevant factors for the high molecular polymer MALDI-MS assay and thus optimized the MALDI-MS strategy. This work provides an effective method for the fast characterization of polymers with MALDI-MS.

DATA AVAILABILITY STATEMENT

The raw data supporting the conclusion of this article will be made available by the authors, without undue reservation.

AUTHOR CONTRIBUTIONS

XW, PY, and QZ initiated the study, supervised the study, and discussed the results. XW, HS, and ZW contributed to method development and performed the experiment. ZW contributed to data acquisition and performed the analysis. QZ and HS contributed to analysis and interpretation of the data. ZW and XW contributed to the drafting of the manuscript. All the authors have accepted responsibility for the entire content of this submitted manuscript and approved submission.

FUNDING

The study was funded by the National Key Research and Development Program of China (Grants 2018YFA0507501, 2017YFA0505001), 973A Program (Grant 2014CBA02003), and Zhongshan Hospital Fudan University Youth Foundation (Grant 2020ZSQN30).

SUPPLEMENTARY MATERIAL

The Supplementary Material for this article can be found online at https://www.frontiersin.org/articles/10.3389/fchem.2021.698297/full#supplementary-material

REFERENCES

Bauer, B. J., Byrd, H. C., and Guttman, C. M. (2010). Small Angle Neutron Scattering Measurements of Synthetic Polymer Dispersions in Matrix-Assisted Laser Desorption/ionization Matrixes. *Rapid Commun. Mass. Spectrom.* 16, 1494–1500. doi:10.1002/rcm.737

Biemann, J. K. (1994). Mass Spectrometric Molecular-Weight Determination of Highly Acidic Compounds of Biological Significance via Their Complexes with Basic Polypeptides. *Proc. Natl. Acad. Sci. United States America* 91, 4333–4337.

Brandt, H., Ehmann, T., and Otto, M. (2010). Solvent Selection for Matrix-Assisted Laser Desorption/ionization Time-Of-Flight Mass Spectrometric Analysis of Synthetic Polymers Employing Solubility Parameters. *Rapid Commun. Mass. Spectrom.* 24, 2439–2444. doi:10.1002/rcm.4668

Cabanillas, B., Akdis, C., and Novak, N. (2020). Allergic Reactions to the First COVID-19 Vaccine: a Potential Role of Polyethylene Glycol? *Allergy* 76 (6), 1617–1618. doi:10.1111/all.14711

Chowdhury, P., Nagesh, P. K. B., Khan, S., Hafeez, B. B., Chauhan, S. C., Jaggi, M., et al. (2018). Development of Polyvinylpyrrolidone/paclitaxel Self-Assemblies for Breast Cancer. *Acta Pharmaceutica Sinica B* 8, 602–614. doi:10.1016/j.apsb.2017.10.004

Cohen, S. L., and Chait, B. T. (1996). Influence of Matrix Solution Conditions on the MALDI-MS Analysis of Peptides and Proteins. *Anal. Chem.* 68, 31–37. doi:10.1021/ac9507956

Dai, Y., Whittal, R. M., and Li, L. (1996). Confocal Fluorescence Microscopic Imaging for Investigating the Analyte Distribution in MALDI Matrices. *Anal. Chem.* 68, 2494–2500. doi:10.1021/ac960238z

Danis, P. O., Karr, D. E., Mayer, F., Holle, A., and Watson, C. H. (1992). The Analysis of Water-Soluble Polymers by Matrix-Assisted Laser Desorption Time-Of-Flight Mass Spectrometry. *Org. Mass Spectrom.* 27, 843-846. doi:10.1002/oms.1210270717

Dwyer, J. (1996). A Novel Sample Preparation Device for MALDI-MS. *Am. Lab.* 28, 51–54. doi:10.1016/s0022-3182(96)70055-9

Evason, D. J., Claydon, M. A., and Gordon, D. B. (2000). Effects of Ion Mode and Matrix Additives in the Identification of Bacteria by Intact Cell Mass

Spectrometry. *Rapid Commun. Mass. Spectrom.* 14, 669–672. doi:10.1002/(sici)1097-0231(20000430)14:8<669::aid-rcm932>3.0.co;2-7

Falkenhagen, J., and Weidner, S. M. (2010). Detection Limits of Matrix-Assisted Laser Desorption/ionisation Mass Spectrometry Coupled to Chromatography-Aa New Application of Solvent-free Sample Preparation. *Rapid Commun. Mass. Spectrom.* 19, 3724–3730. doi:10.1002/rcm.2256

Hanton, S. D., and Parees, D. M. (2005). Extending the Solvent-free MALDI Sample Preparation Method. *J. Am. Soc. Mass. Spectrom.* 16, 90–93. doi:10.1016/j.jasms.2004.09.019

Juhasz, P., Costello, C. E., and Biemann, K. (1993). Matrix-assisted Laser Desorption Ionization Mass Spectrometry with 2-(4-hydroxyphenylazo) benzoic Acid Matrix. *J. Am. Soc. Mass Spectrom.* 4, 399–409. doi:10.1016/1044-0305(93)85005-i

Kang, J. H., and Ko, Y. T. (2019). Enhanced Subcellular Trafficking of Resveratrol Using Mitochondriotropic Liposomes in Cancer Cells. *Pharmaceutics* 11, 423. doi:10.3390/pharmaceutics11080423

Macha, S. F., Limbach, P. A., Hanton, S. D., and Owens, K. G. (2001). Silver Cluster Interferences in Matrix-Assisted Laser Desorption/ionization (MALDI) Mass Spectrometry of Nonpolar Polymers. *J. Am. Soc. Mass. Spectrom.* 12, 732–743. doi:10.1016/s1044-0305(01)00225-2

Marie, A., Fournier, F., and Tabet, J. C. (2000). Characterization of Synthetic Polymers by MALDI-TOF/MS: Investigation into New Methods of Sample Target Preparation and Consequence on Mass Spectrum finger Print. *Anal. Chem.* 72, 5106–5114. doi:10.1021/ac000124u

Michael, K., Doris, B., and Hillenkamp, F. (1985). Influence of the Wavelength in High-Irradiance Ultraviolet Laser Desorption Mass Spectrometry of Organic Molecules. *Anal. Chem.* 57, 2935–2939. doi:10.1021/ac00291a042

Montaudo, G., Montaudo, M. S., Puglisi, C., and Samperi, F. (1995). Molecular Weight Distribution of Poly(dimethylsiloxane) by Combining Matrix-assisted Laser Desorption/ionization Time-of-flight Mass Spectrometry with Gel-permeation Chromatography Fractionation. *Rapid Commun. Mass Spectrom.* 9, 1158-1163. doi:10.1002/rcm.1290091215

Nielen, M. (1999). Maldi Time-Of-Flight Mass Spectrometry of Synthetic Polymers. *Mass Spectrom. Rev.* 18, 309-344. doi:10.1002/(SICI)1098-2787(1999)18:5<309::AID-MAS2>3.0.CO;2-L

Otto, M., Brandt, H., and Ehmann, T. (2010). Toward Prediction: Using Chemometrics for the Optimization of Sample Preparation in MALDI-TOF MS of Synthetic Polymers. *Anal. Chem.* 82**,** 8169–8175, .doi:10.1021/ac101526w

Peng, L., and Kinsel, G. R. (2010). Improving the Sensitivity of Matrix-Assisted Laser Desorption/ionization (MALDI) Mass Spectrometry by Using Polyethylene Glycol Modified Polyurethane MALDI Target. *Anal. Biochem.* 400, 56–60. doi:10.1016/j.ab.2010.01.009

Przepiorka, D., Mokyr, M. B., and Dray, S. (1980). Effect of Polyethylene Glycol 6000 on the Generation of Antitumor Cytotoxicity in MOPC-315 Tumor Bearer Spleen Cells Cultured in the Presence or Absence of Inactivated Stimulator Tumor Cells. *Cancer Res.* 40, 4565–4570.

Rodrigues, B. S., Lakkadwala, S., Kanekiyo, T., and Singh, J. (2019). Development and Screening of Brain-Targeted Lipid-Based Nanoparticles with Enhanced Cell Penetration and Gene Delivery Properties. *Int. J. Nanomedicine* 14, 6497–6517. doi:10.2147/IJN.S215941

Roy, S. L., and Deborah, S. S. (1995). Polymer Molecular Weight Distribution: Results from Matrix-Assisted Laser Desorption Ionization Compared with Those from Gel-Permeation Chromatography. *Rapid Commun. Mass Spectrom.* 9, 91-92. 10.1002/rcm.1290090119.

Schriemer, D. C., and Li, L. (1997). Mass Discrimination in the Analysis of Polydisperse Polymers by MALDI Time-Of-Flight Mass Spectrometry. 1. Sample Preparation and Desorption/Ionization Issues. *Anal. Chem.* 69, 4169–4175. doi:10.1021/ac9702610

Schupp, T., Austin, T., Eadsforth, C. V., Bossuyt, B., Shen, S. M., and West, R. J. (2018). A Review of the Environmental Degradation, Ecotoxicity, and Bioaccumulation Potential of the Low Molecular Weight Polyether Polyol Substances. *Rev. Environ. Contam. Toxicol.* 244, 53–111. doi:10.1007/398_2017_2

Schwarzinger, C., Gabriel, S., Beißmann, S., and Buchberger, W. (2012). Bei?Mann, S., andQuantitative Analysis of Polymer Additives with MALDI-TOF MS Using an Internal Standard Approach. *J. Am. Soc. Mass. Spectrom.* 23, 1120–1125. doi:10.1007/s13361-012-0367-1

Singh, S., and Tavana, H. (2018). Collagen Partition in Polymeric Aqueous Two-phase Systems for Tissue Engineering. *Front. Chem.* 6, 379. doi:10.3389/fchem.2018.00379

Skelton, R., Dubois, F., and Zenobi, R. (2013). A MALDI Sample Preparation Method Suitable for Insoluble Polymers. *Anal. Chem.* 72, 1707–1710. doi:10.1021/ac991181u

Tummala, R., and Limbach, P. A. (2010). Effect of Sodium Dodecyl Sulfate Micelles on Peptide Mass Fingerprinting by Matrix-Assisted Laser Desorption/ionization Mass Spectrometry. *Rapid Commun. Mass. Spectrom.* 18, 2031–2035. doi:10.1002/rcm.1588

Wang, L., May, S. W., Browner, R. F., and Pollock, S. H. (1996). Low-flow Interface for Liquid Chromatography–Inductively Coupled Plasma Mass Spectrometry Speciation Using an Oscillating Capillary Nebulizer. *J. Anal. At. Spectrom.* 11, 1137-1146. doi:10.1039/JA9961101137

Zhang, J., and Kinsel, G. R. (2002). Quantification of Protein-Polymer Interactions by Matrix-Assisted Laser Desorption/Ionization Mass Spectrometry. *Langmuir* 18, 4444–4448. doi:10.1021/la015594d

Conflict of Interest: The authors declare that the research was conducted in the absence of any commercial or financial relationships that could be construed as a potential conflict of interest.

frontiers in Chemistry

ORIGINAL RESEARCH
published: 27 July 2021
doi: 10.3389/fchem.2021.715890

An Improved Method for Rapid Detection of *Mycobacterium abscessus* Complex Based on Species-Specific Lipid Fingerprint by Routine MALDI-TOF

Min Jia Khor[1], *Agnieszka Broda*[2], *Markus Kostrzewa*[3], *Francis Drobniewski*[2] *and Gerald Larrouy-Maumus*[1]*

[1]MRC Centre for Molecular Bacteriology and Infection, Department of Life Sciences, Faculty of Natural Sciences, Imperial College London, London, United Kingdom, [2]Department of Infectious Diseases, Faculty of Medicine, Imperial College London, London, United Kingdom, [3]Bruker Daltonics GmbH & Co. KG, Bremen, Germany

OPEN ACCESS

Edited by:
Gerard Bolbach,
Sorbonne Universités, France

Reviewed by:
Tao Yu,
North Carolina State University, United States
Adrian Arendowski,
University of Rzeszow, Poland

***Correspondence:**
Gerald Larrouy-Maumus
g.larrouy-maumus@imperial.ac.uk

Specialty section:
This article was submitted to Analytical Chemistry, a section of the journal Frontiers in Chemistry

Received: 27 May 2021
Accepted: 28 June 2021
Published: 27 July 2021

Citation:
Jia Khor M, Broda A, Kostrzewa M, Drobniewski F and Larrouy-Maumus G (2021) An Improved Method for Rapid Detection of Mycobacterium abscessus Complex Based on Species-Specific Lipid Fingerprint by Routine MALDI-TOF. Front. Chem. 9:715890. doi: 10.3389/fchem.2021.715890

Rapid diagnostics of bacterial infection is the key to successful recovery and eradication of the disease. Currently, identification of bacteria is based on the detection of highly abundant proteins, mainly ribosomal proteins, by routine MALDI-TOF mass spectrometry. However, relying solely on proteins is limited in subspecies typing for some pathogens. This is the case for, for example, the mycobacteria belonging to the *Mycobacterium abscessus* (MABS) complex, which is classified into three subspecies, namely, *M. abscessus* subsp. *abscessus*, *M. abscessus* subsp. *bolletii*, and *M. abscessus* subsp. *massiliense*. Being able to detect bacteria accurately and rapidly at the subspecies level could not only reliably identify the pathogen causing the disease but also enable better antibiotic stewardship. For instance, *M. abscessus* subsp. *abscessus* and *M. abscessus* subsp. *bolletii* possess a functional erm41 (erythromycin ribosomal methylation gene 41) gene, whilst *M. abscessus* subsp. *massiliense* does not, resulting in differences in macrolide antibiotic (e.g., clarithromycin and azithromycin) susceptibilities. This presents a challenge for physicians when designing an appropriate treatment regimen. To address this challenge, in addition to proteins, species-specific lipids have now been considered as a game changer in clinical microbiology diagnostics. However, their extraction can be time-consuming, and analysis requires the use of apolar toxic organic solvents (e.g., chloroform). Here, we present a new method to accurately detect species and subspecies, allowing the discrimination of the mycobacteria within the MABS complex and relying on the use of ethanol. We found that a combination of the matrix named super-DHB with 25% ethanol with a bacterial suspension at McFarland 20 gave robust and reproducible data, allowing the discrimination of the bacteria within the MABS complex strains tested in this study (n = 9). Further investigations have to be conducted to validate the method on a larger panel of strains for its use in diagnostic laboratories.

Keywords: MALDI, lipids, diagnostics, mycobacteria, solvent

INTRODUCTION

Matrix-assisted laser desorption ionization/time-of-flight (MALDI-TOF) mass spectrometry (MS), a cost-effective, rapid, and accurate method for microbial identification based on protein signatures, has revolutionized microbiological diagnostics (Croxatto et al., 2012; Clark et al., 2013; Singhal et al., 2015). However, protein profiling by MALDI-TOF MS possesses some limitations when it comes to an efficient typing for some closely related species and subspecies (Kostrzewa et al., 2019; Welker et al., 2019).

That is the case for the bacterium named *Mycobacterium abscessus*, which is part of a complex of very similar organisms. The *M. abscessus* complex (MABS complex) is classified into three subspecies, namely, *M. abscessus* subsp. *abscessus*, *M. abscessus* subsp. *bolletii*, and *M. abscessus* subsp. *massiliense*. *M. abscessus* is found to be present within 80% of the respiratory isolates of rapidly growing mycobacteria and demonstrates resistance to many antibiotic classes like aminoglycosides, β-lactams, and macrolides (Johansen et al., 2020). For example, *M. abscessus* subsp. *abscessus* and *M. abscessus* subsp. *bolletii* possess a functional erm41 (erythromycin ribosomal methylation gene 41) gene, whilst *M. abscessus* subsp. *massiliense* does not (Kim et al., 2010; Ryu et al., 2016; Ryan and Byrd, 2018). This results in different macrolide antibiotic (i.e., clarithromycin and azithromycin) susceptibilities. Therefore, identification of the different subspecies is important in the clinical environment. As mentioned earlier, clarithromycin is more effective against *M. abscessus* subsp. *massiliense* lung infections, while resistance is commonly observed in *M. abscessus* subsp. *abscessus* and *M. abscessus* subsp. *bolletii* isolates (Adekambi et al., 2006; Esther et al., 2010; Kim et al., 2010; Koh et al., 2011; Harada et al., 2012). This presents a challenge for physicians when designing an appropriate treatment regimen (Koh et al., 2011; Brown-Elliott et al., 2012; Harada et al., 2012; Kothavade et al., 2013).

Current available tools, such as PCR, sequencing of multiple genes, and whole genome sequencing, are time-consuming, relatively expensive, and require experts for the sample preparation and data analysis, which is not ideal for routine clinical use despite offering excellent subspecies identification (Nash et al., 2009; Kim et al., 2010; Koh et al., 2011). That is why having a diagnostic tool that allows early MABS complex identification would be ideal for subspecies identification and therefore guiding drug prescription (Ryu et al., 2016). In order to introduce this tool across clinical laboratories worldwide, it needs to be simple, rapid, inexpensive, and highly specific. Therefore, the continuous development of laboratory techniques for subspecies-level discrimination between bacterial species alongside the identification of their antibiotic-resistant counterparts is of utmost importance to best assist physicians in the administration of an appropriate drug regimen.

MALDI-TOF MS offers an alternative to the methods cited earlier. Indeed, several studies report on the use of MALDI-TOF MS to detect bacteria within the MABS complex (Tseng et al., 2013; Fangous et al., 2014; Panagea et al., 2015; Kehrmann et al., 2016; Luo et al., 2016). Those approaches rely on a multistep sample preparation consisting of the inactivation of the bacteria, followed by mechanical lysis in order to have access to intracellular proteins that serve as markers. However, the multistep strategy combined with extensive data analysis used to detect the MABS complex can be improved in order to ease routine microbiology laboratory practice.

In terms of addressing this unmet need, species-specific lipid fingerprints could represent an attractive approach when it comes to microbial identification by MALDI-ToF MS. Lipids are highly abundant in bacteria and structurally diverse. Several studies have reported successfully on the use of microbial lipidomics by MALDI-ToF MS and their uses in academic laboratories and diagnostic laboratories for accurate microbial identification, making lipid fingerprinting a complementary approach to protein-based fingerprinting in order to tackle the challenge of microbial differentiation by MALDI-ToF MS (Shu. et al., 2012; Voorhees et al., 2013; Cox et al., 2015; Larrouy-Maumus and Puzo, 2015; Leung et al., 2017; Gonzalo et al., 2020; Lellman and Cramer, 2020).

Nevertheless, those methods, based on lipid fingerprints (cited earlier), rely on the use of highly toxic organic solvents (e.g., $CHCl_3$, CH_3OH, or a mixture of $CHCl_3$ and CH_3OH), hampering an easy implementation of the method in routine clinical laboratories due to safety concerns. Also, those solvents have a relative polarity ranging from 0.259 to 0.762, which could have an impact on the selectivity of the species-specific lipids to be extracted and detected by MALDI-TOF MS, influencing the outcome of bacterial identification. To address this challenge, we investigated the use of ethanol (CH_3CH_2OH, relative polarity 0.654) as a commonly used organic solvent widely used in routine clinical microbiology laboratories worldwide as an alternative to chloroform and methanol to extract species-specific lipids for the rapid identification of bacteria belonging to the MABS complex.

MATERIALS AND METHODS

Bacterial Strains and Growth Conditions

M. abscessus subsp. *abscessus* ATCC 19977, *M. abscessus* subsp. *abscessus* M02004436, *M. abscessus* subsp. *abscessus* M07001466, *M. abscessus* subsp. *bolletii* M09013950, *M. abscessus* subsp. *bolletii* M04009973, *M. abscessus* subsp. *bolletii* H123680049, *M. abscessus* subsp. *massiliense* M10010169, *M. abscessus* subsp. *massiliense* M07012434, and *M. abscessus* subsp. *massiliense* H120280022 obtained from the National Mycobacterium Reference-NMRS-South (United Kingdom) were cultured in Middlebrook 7H9 broth liquid medium supplemented with 0.5 g/L Fraction V (bovine serum albumin), 0.05% tyloxapol, 0.2% dextrose, 0.2% glycerol, and 10 mM NaCl. The inoculated cultures were then incubated at 37°C for 2 days. Bacterial pellets were heat-killed at 95°C for 30 min before leaving the BSL3 containment area.

Sample Preparation

100 µl of bacterial suspension (from liquid- or agar-based media) was placed into 1.5 ml microtubes that contain 200 µl of double-distilled water. The bacteria were then washed twice with 200 µl of

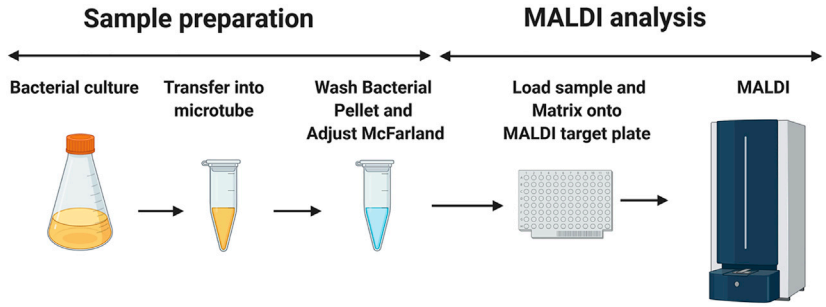

FIGURE 1 | Schematic diagram of the sample preparation before the MALDI mass spectrometry measurement. 1.5 ml of mycobacterial culture is aliquoted in a microtube. The mycobacterial suspension is then washed twice with double-distilled water and adjusted to the desired McFarland suspension. 0.5 µL of this preparation is loaded into the MALDI target plate, followed by the addition of 1.2 µl of the matrix (super-DHB solubilized at 10 mg/ml in ethanol) and mixing on the MALDI MBT 96 Biotarget plate. Once dried, the mass spectra are acquired in the linear positive ion mode. The image has been created using BioRender.

double-distilled water and suspended at various McFarland standards ranging from 5 to 40 using a McFarland tube densitometer (Grant-Bio®). Then, 0.5 µl of the resuspended pellet was pipetted onto the MALDI target plate and mixed with 1.2 µl of the MALDI matrix (**Figure 1**). The matrix used consisted of a 9:1 mixture of 2,5-dihydroxybenzoic acid and 2-hydroxy-5-methoxybenzoic acid (super-DHB, Sigma-Aldrich) at a concentration of 10 mg/ml in ethanol at various percentages ranging from 0 to 100%. Additionally, for external calibration, 0.5 µl of calibration peptide mixture was loaded along with 0.5 µl of the given calibration matrix (peptide calibration standard II, Bruker Daltonics, Germany). The samples were loaded onto a disposable MBT 96 Biotarget plate (Bruker Part-No. 1840375).

Mass Spectrometry Analysis

MS analyses were performed on an MALDI Biotyper Sirius system (Bruker Daltonics, Germany). The mass spectra were scanned in the range of m/z 1,100–1,600. The mass profiles were acquired using FlexControl 3.4 software (Bruker Daltonics, Germany). The spectra were recorded in the linear positive ion mode (laser intensity 95%, ion source 1 = 10.00 kV, ion source 2 = 8.98 kV, lens = 3.00 kV, detector voltage = 2652 V, pulsed ion extraction = 150 ns). Each spectrum corresponded to an ion accumulation of 5,000 laser shots randomly distributed on the spot. The spectra obtained were processed with default parameters using FlexAnalysis v.3.4 software (Bruker Daltonics, Germany).

RESULTS AND DISCUSSION

In this study, we optimized the number of bacteria loaded onto the MALDI target plate and the solvent to solubilize the matrix prior to MS analyses in the positive ion mode to address the major challenge in subspecies typing by MALDI-TOF MS inside the MABS complex.

By using the reference strain *M. abscessus* subsp. *abscessus* ATCC 19977, we found that a suspension of bacteria at McFarland 20 combined with the matrix super-DHB solubilized in 25% ethanol at a final concentration of 10 mg/ml was most appropriate for our experiments. We chose to use super-DHB as a matrix due to its versatility for the analysis of lipids and glycolipids (Schiller et al., 2007). This was decided following observation of the raw mass spectra obtained across 5 McFarland dilutions (5, 10, 20, 30, and 50) and 5 percentages of ethanol used to solubilize the matrix (10, 25, 50, 70, and 100%). Regardless of the McFarland dilution and percentage of ethanol used in the study, the positive ion mass spectra of *M. abscessus* subsp. *abscessus* ATCC 19977 showed two sets of peaks starting at *m/z* 1201.8 up to *m/z* 1299.9 and starting at *m/z* 1375.9 up to *m/z* 1445.9, distant of 14 mass units with the most intense peaks at *m/z* 1259.9 and *m/z* 1405.9 assigned to potassium cationized–diglycosylated glycopeptidolipids ($[M + K]^+$ *m/z* 1259.9) and triglycosylated glycopeptidolipids ($[M + K]^+$ *m/z* 1405.9) (**Figure 2A**), which are known to make up more than 70% of the surface-exposed mycobacterial lipids. Glycopeptidolipids have been demonstrated to play a key role in mycobacterial physiology and pathogenicity (Byrd and Lyons, 1999; Howard et al., 2006; Catherinot et al., 2007; Ripoll et al., 2007; Whang et al., 2017; Gutierrez et al., 2018; Tran et al., 2019; Kurz and Rivas-Santiago, 2020; Jackson et al., 2021). Such lipid profiles are similar in terms of lipid species detected to the ones that have been obtained in the literature using conventional methods (Ripoll et al., 2007; Gonzalo et al., 2020); this indicates that as a solvent (to solubilize the matrix), ethanol produces efficient extraction and co-crystallization, and thereby desorption and ionization of surface lipids on the MALDI target plate. A possible mechanism is that ethanol could act as an eraser enabling the selective on-target extraction of the surface-exposed di- and triglycosylated glycopeptidolipids and their co-crystallization with the matrix, allowing their desorption and ionization.

In addition, here, we aimed to have the highest quality signal in order to enhance reproducible and robust data. To decide which bacterial suspension and percentage of ethanol were appropriate for performing the analysis, we recorded the signal-to-noise (S/N), resolution, and intensity of the dominant peak at *m/z* 1259.9. First, regarding the S/N, as seen in **Figure 2B**, at McFarland 5, the S/N is ~10 across all percentages of ethanol tested. Interestingly, when using a bacterial suspension of McFarland 10, the S/N

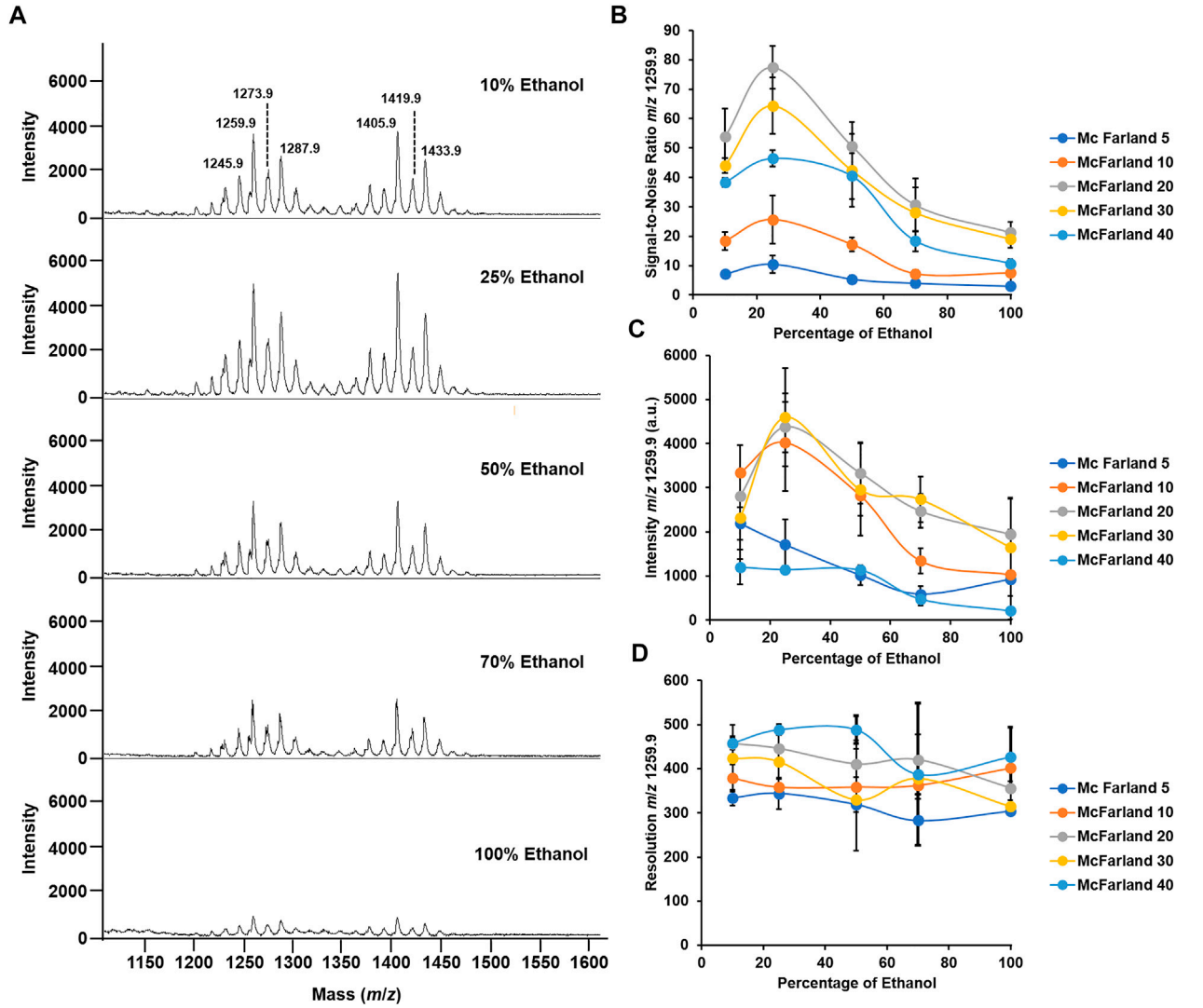

FIGURE 2 | Optimization of McFarland and percentage of ethanol for the optimal mass spectrum signal. **(A)** Mass spectra acquired in the positive ion mode of *M. abscessus* subsp. *abscessus* ATCC 19977 set at McFarland 20 and for a percentage of ethanol to solubilize the matrix ranging from 10 to 100%. (**B**) Graph depicting the changes in the S/N ratio in the function of the percentage of ethanol across 5 McFarland dilutions. (**C**) Graph depicting the changes in the intensity of the peak at *m/z* 1259.9 in the function of the percentage of ethanol across 5 McFarland dilutions. (**D**) Graph depicting the changes in the resolution of the peak at *m/z* 1259.9 in the function of the percentage of ethanol across 5 McFarland dilutions. Experiments have been performed in biological and technical triplicates. Error bars indicate the standard deviation.

increases when passing from 10 to 25% ethanol, going from S/N 18 to 25, and then decreases and plateaus at S/N 7.5 for a percentage of ethanol of 100%. A similar pattern is observed when using higher McFarland values. Indeed, for a bacterial suspension set at McFarland 20, at 10% ethanol, the S/N is ~50, which is almost 3 times higher than it is when using McFarland 10, and it even increases up to S/N ~80 for a value of 25% ethanol before decreasing gradually to S/N ~20 for 100% ethanol. However, when using higher bacterial suspension, for example, McFarland 30 or 40, the S/N tends to decrease across all percentages of ethanol tested compared to the S/N observed for McFarland 20, going for S/N to at 25% ethanol to S/N ~60 and S/N ~40 for the same percentage of ethanol. Such observations could be explained by the ratio of the matrix to the sample required for the optimal co-crystallization of the molecules of interest with the matrix on the MALDI target plate and allowing their optimal desorption and ionization (Smolira and Wessely-Szponder, 2015; Wiangnon and Cramer, 2015; Wang et al., 2016; Boesl, 2017). In other words, the fact that higher McFarland or higher percentage of ethanol did not generate good quality spectra could be explained by the poor co-crystallization with the matrix. That could lead to a nonhomogeneous spot on the MALDI target plate, precluding any transfer of the energy provided by the laser to the matrix in allowing the desorption of the molecules of interest (Dreisewerd, 2003; Wang et al., 2016).

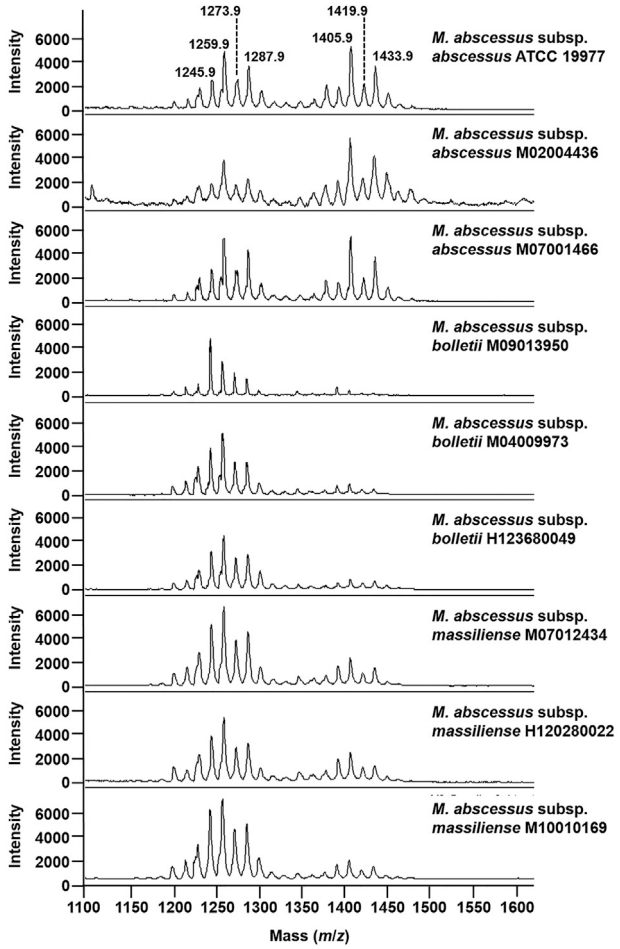

FIGURE 3 | Mass spectra of mycobacteria belonging to the *M. abscessus* complex. Mass spectra were acquired in the positive ion mode with a bacterial suspension set at McFarland 20 and using the super-DHB as a matrix solubilized at 10 mg/ml in 25% ethanol.

A similar conclusion can be drawn for the intensity of the signal. As seen in **Figure 2C**, for both McFarland 5 and McFarland 40, the signal intensity remains low across all the percentages of ethanol tested, with an intensity of ~1,000 a.u. However, for intermediate McFarland values, when going from 10% ethanol to 25% ethanol, the intensity of the signal increases from ~2,000 a.u. to 5,000 a.u. and then decreases gradually when reaching 100% ethanol. That agrees with the S/N data where McFarland 20 and 25% ethanol are the parameters required for the optimal quality signal.

Regarding the resolution, neither McFarland nor the percentage of ethanol seems to influence that parameter which has its range from 300 to 500 with no significative differences (**Figure 2D**).

Taken together, a bacterial suspension set at McFarland 20 and the use of the super-DHB solubilized at 10 mg/ml in 25% ethanol gave the most appropriate quality data for bacterial species identification by routine MALDI-TOF MS.

To test if that optimized methodological approach has the potential to address the challenge of subspecies typing in the MABS complex, we applied the developed method to *M. abscessus* subsp. *abscessus* ATCC 19977, *M. abscessus* subsp. *abscessus* M02004436, *M. abscessus* subsp. *abscessus* M07001466, *M. abscessus* subsp. *bolletii* M09013950, *M. abscessus* subsp. *bolletii* M04009973, *M. abscessus* subsp. *bolletii* H123680049, *M. abscessus* subsp. *massiliense* M10010169, *M. abscessus* subsp. *massiliense* M07012434, and *M. abscessus* subsp. *massiliense* H120280022. . As seen in **Figure 3** for the mass spectra for the *M. abscessus* subsp. *abscessus* strains, the mass spectra for the *M. abscessus* subsp. *bolletii* strains and *M. abscessus* subsp. *massiliense* strains are composed of two sets of peaks starting at *m*/*z* 1201.8 up to *m*/*z* 1299.9 and starting at *m*/*z* 1375.9 up to *m*/*z* 1445.9, distant of 14 mass units with the most intense peaks assigned to potassium cationized–diglycosylated glycopeptidolipids and triglycosylated glycopeptidolipids. However, as opposed to the mass spectrum of *M. abscessus* subsp. *abscessus* strains, where the ratio of diglycosylated glycopeptidolipids/triglycosylated glycopeptidolipids is ~1:1, in the mass spectra of *M. abscessus* subsp. *bolletii* strains, the ratio of diglycosylated glycopeptidolipids/triglycosylated glycopeptidolipids is ~1:0.2 and for *M. abscessus* subsp. *massiliense* strains, the ratio of diglycosylated glycopeptidolipids/triglycosylated glycopeptidolipids is ~1:0.5 (**Figure 3**). Taken together, those data suggest that the lipid fingerprint has the potential to discriminate between mycobacteria within the MABS complex.

CONCLUSION

Here, we provide a new and simple method for the detection of subspecies-specific lipids, applied to the MABS complex. The method is easy to put in place, requires a minimal number of steps, and is performed on a routine MALDI mass spectrometer in the positive ion mode. One of the limitations of the study resides in the use of a very limited amount of strains (n = 9). Further studies are now required to test and validate that new approach in the rapid detection of the mycobacteria belonging to the MABS complex, using characterized clinical isolates and other bacterial species and subspecies.

DATA AVAILABILITY STATEMENT

The original contributions presented in the study are included in the article/Supplementary Material; further inquiries can be directed to the corresponding author.

AUTHOR CONTRIBUTIONS

GL-M and MJK conceived the study, participated in its design, and performed the experiments. AB and FD provided bacterial strains. All authors discussed, reviewed, and approved the final manuscript.

FUNDING

This study was supported by the MRC Confidence in Concept Fund and the ISSF Wellcome Trust Grant 105603/Z/14/Z (GL-M).

REFERENCES

Adekambi, T., Berger, P., Raoult, D., and Drancourt, M. (2006). rpoB Gene Sequence-Based Characterization of Emerging Non-tuberculous Mycobacteria with Descriptions of Mycobacterium Bolletii Sp. Nov., Mycobacterium Phocaicum Sp. Nov. And Mycobacterium Aubagnense Sp. Nov. *Int. J. Syst. Evol. Microbiol.* 56 (Pt 1), 133–143. doi:10.1099/ijs.0.63969-0

Boesl, U. (2017). Time-of-flight Mass Spectrometry: Introduction to the Basics. *Mass. Spec. Rev.* 36 (1), 86–109. doi:10.1002/mas.21520

Brown-Elliott, B. A., Nash, K. A., and Wallace, R. J., Jr. (2012). Antimicrobial Susceptibility Testing, Drug Resistance Mechanisms, and Therapy of Infections with Nontuberculous Mycobacteria. *Clin. Microbiol. Rev.* 25 (3), 545–582. doi:10.1128/CMR.05030-11

Byrd, T. F., and Lyons, C. R. (1999). Preliminary Characterization of a Mycobacterium Abscessus Mutant in Human and Murine Models of Infection. *Infect. Immun.* 67 (9), 4700–4707. doi:10.1128/IAI.67.9.4700-4707.1999

Catherinot, E., Clarissou, J., Etienne, G., Ripoll, F., Emile, J.-F., Daffé, M., et al. (2007). Hypervirulence of a Rough Variant of the Mycobacterium Abscessus Type Strain. *Infect. Immun.* 75 (2), 1055–1058. doi:10.1128/IAI.00835-06

Clark, A. E., Kaleta, E. J., Arora, A., and Wolk, D. M. (2013). Matrix-Assisted Laser Desorption Ionization-Time of Flight Mass Spectrometry: a Fundamental Shift in the Routine Practice of Clinical Microbiology. *Clin. Microbiol. Rev.* 26 (3), 547–603. doi:10.1128/CMR.00072-12

Cox, C. R., Jensen, K. R., Saichek, N. R., and Voorhees, K. J. (2015). Strain-Level Bacterial Identification by CeO2-Catalyzed MALDI-TOF MS Fatty Acid Analysis and Comparison to Commercial Protein-Based Methods. *Sci. Rep.* 5, 10470. doi:10.1038/srep10470

Croxatto, A., Prod'hom, G., and Greub, G. (2012). Applications of MALDI-TOF Mass Spectrometry in Clinical Diagnostic Microbiology. *FEMS Microbiol. Rev.* 36 (2), 380–407. doi:10.1111/j.1574-6976.2011.00298.x

Dreisewerd, K. (2003). The Desorption Process in MALDI. *Chem. Rev.* 103 (2), 395–426. doi:10.1021/cr010375i

Esther, C. R., Jr., Esserman, D. A., Gilligan, P., Kerr, A., and Noone, P. G. (2010). Chronic Mycobacterium Abscessus Infection and Lung Function Decline in Cystic Fibrosis. *J. Cystic Fibrosis* 9 (2), 117–123. doi:10.1016/j.jcf.2009.12.001

Fangous, M.-S., Mougari, F., Gouriou, S., Calvez, E., Raskine, L., Cambau, E., et al. (2014). Classification Algorithm for Subspecies Identification within the Mycobacterium Abscessus Species, Based on Matrix-Assisted Laser Desorption Ionization-Time of Flight Mass Spectrometry. *J. Clin. Microbiol.* 52 (9), 3362–3369. doi:10.1128/JCM.00788-14

Gonzalo, X., Broda, A., Drobniewski, F., and Larrouy-Maumus, G. (2021). Performance of Lipid Fingerprint-Based MALDI-ToF for the Diagnosis of Mycobacterial Infections. *Clin. Microbiol. Infect.* 27, 912.e1–912.e2. doi:10.1016/j.cmi.2020.08.027

Gutiérrez, A. V., Viljoen, A., Ghigo, E., Herrmann, J.-L., and Kremer, L. (2018). Glycopeptidolipids, a Double-Edged Sword of the Mycobacterium Abscessus Complex. *Front. Microbiol.* 9, 1145. doi:10.3389/fmicb.2018.01145

Harada, T., Akiyama, Y., Kurashima, A., Nagai, H., Tsuyuguchi, K., Fujii, T., et al. (2012). Clinical and Microbiological Differences between Mycobacterium Abscessus and Mycobacterium Massiliense Lung Diseases. *J. Clin. Microbiol.* 50 (11), 3556–3561. doi:10.1128/JCM.01175-12

Howard, S. T., Rhoades, E., Recht, J., Pang, X., Alsup, A., Kolter, R., et al. (2006). Spontaneous Reversion of Mycobacterium Abscessus from a Smooth to a Rough Morphotype Is Associated with Reduced Expression of Glycopeptidolipid and Reacquisition of an Invasive Phenotype. *Microbiology (Reading)* 152 (Pt 6), 1581–1590. doi:10.1099/mic.0.28625-0

Jackson, M., Stevens, C. M., Zhang, L., Zgurskaya, H. I., and Niederweis, M. (2021). Transporters Involved in the Biogenesis and Functionalization of the Mycobacterial Cell Envelope. *Chem. Rev.* 121 (9), 5124–5157. doi:10.1021/acs.chemrev.0c00869

Johansen, M. D., Herrmann, J.-L., and Kremer, L. (2020). Non-tuberculous Mycobacteria and the Rise of Mycobacterium Abscessus. *Nat. Rev. Microbiol.* 18 (7), 392–407. doi:10.1038/s41579-020-0331-1

Kehrmann, J., Wessel, S., Murali, R., Hampel, A., Bange, F.-C., Buer, J., et al. (2016). Principal Component Analysis of MALDI TOF MS Mass Spectra Separates M. Abscessus (Sensu Stricto) from M. Massiliense Isolates. *BMC Microbiol.* 16, 24. doi:10.1186/s12866-016-0636-4

Kim, H.-Y., Kim, B. J., Kook, Y., Yun, Y.-J., Shin, J. H., Kim, B.-J., et al. (2010). Mycobacterium Massiliense Is Differentiated from Mycobacterium Abscessus and Mycobacterium Bolletii by Erythromycin Ribosome Methyltransferase Gene (Erm) and Clarithromycin Susceptibility Patterns. *Microbiol. Immunol.* 54 (6), 347–353. doi:10.1111/j.1348-0421.2010.00221.x

Koh, W.-J., Jeon, K., Lee, N. Y., Kim, B.-J., Kook, Y.-H., Lee, S.-H., et al. (2011). Clinical Significance of Differentiation ofMycobacterium massiliensefromMycobacterium Abscessus. *Am. J. Respir. Crit. Care Med.* 183 (3), 405–410. doi:10.1164/rccm.201003-0395OC

Kostrzewa, M., Nagy, E., Schröttner, P., and Pranada, A. B. (2019). How MALDI-TOF Mass Spectrometry Can Aid the Diagnosis of Hard-To-Identify Pathogenic Bacteria - the Rare and the Unknown. *Expert Rev. Mol. Diagn.* 19 (8), 667–682. doi:10.1080/14737159.2019.1643238

Kothavade, R. J., Dhurat, R. S., Mishra, S. N., and Kothavade, U. R. (2013). Clinical and Laboratory Aspects of the Diagnosis and Management of Cutaneous and Subcutaneous Infections Caused by Rapidly Growing Mycobacteria. *Eur. J. Clin. Microbiol. Infect. Dis.* 32 (2), 161–188. doi:10.1007/s10096-012-1766-8

Kurz, S. G., and Rivas-Santiago, B. (2020). Time to Expand the Picture of Mycobacterial Lipids: Spotlight on Nontuberculous Mycobacteria. *Am. J. Respir. Cel Mol. Biol.* 62 (3), 275–276. doi:10.1165/rcmb.2019-0324ED

Larrouy-Maumus, G., and Puzo, G. (2015). Mycobacterial Envelope Lipids Fingerprint from Direct MALDI-TOF MS Analysis of Intact Bacilli. *Tuberculosis* 95 (1), 75–85. doi:10.1016/j.tube.2014.11.001

Lellman, S. E., and Cramer, R. (2020). Bacterial Identification by Lipid Profiling Using Liquid Atmospheric Pressure Matrix-Assisted Laser Desorption/ionization Mass Spectrometry. *Clin. Chem. Lab. Med.* 58 (6), 930–938. doi:10.1515/cclm-2019-0908

Leung, L. M., Fondrie, W. E., Doi, Y., Johnson, J. K., Strickland, D. K., Ernst, R. K., et al. (2017). Identification of the ESKAPE Pathogens by Mass Spectrometric Analysis of Microbial Membrane Glycolipids. *Sci. Rep.* 7 (1), 6403. doi:10.1038/s41598-017-04793-4

Luo, L., Liu, W., Li, B., Li, M., Huang, D., Jing, L., et al. (2016). Evaluation of Matrix-Assisted Laser Desorption Ionization–Time of Flight Mass Spectrometry for Identification of Mycobacterium Abscessus Subspecies According to Whole-Genome Sequencing. *J. Clin. Microbiol.* 54 (12), 2982–2989. doi:10.1128/JCM.01151-16

Nash, K. A., Brown-Elliott, B. A., and Wallace, R. J., Jr. (2009). A Novel Gene, Erm (41), Confers Inducible Macrolide Resistance to Clinical Isolates of Mycobacterium Abscessus but Is Absent from *Mycobacterium chelonae*. *Antimicrob. Agents Chemother.* 53 (4), 1367–1376. doi:10.1128/AAC.01275-08

Panagea, T., Pincus, D. H., Grogono, D., Jones, M., Bryant, J., Parkhill, J., et al. (2015). Mycobacterium Abscessus Complex Identification with Matrix-Assisted Laser Desorption Ionization-Time of Flight Mass Spectrometry. *J. Clin. Microbiol.* 53 (7), 2355–2358. doi:10.1128/JCM.00494-15

Ripoll, F., Deshayes, C., Pasek, S., Laval, F., Beretti, J.-L., Biet, F., et al. (2007). Genomics of Glycopeptidolipid Biosynthesis in Mycobacterium Abscessus and *M. chelonae*. *BMC Genomics* 8, 114. doi:10.1186/1471-2164-8-114

Ryan, K., and Byrd, T. F. (2018). Mycobacterium Abscessus: Shapeshifter of the Mycobacterial World. *Front. Microbiol.* 9, 2642. doi:10.3389/fmicb.2018.02642

Ryu, Y. J., Koh, W.-J., and Daley, C. L. (2016). Diagnosis and Treatment of Nontuberculous Mycobacterial Lung Disease: Clinicians' Perspectives. *Tuberc. Respir. Dis.* 79 (2), 74–84. doi:10.4046/trd.2016.79.2.74

Schiller, J., Süß, R., Fuchs, B., Müller, M., Petković, M., Zschörnig, O., et al. (2007). The Suitability of Different DHB Isomers as Matrices for the MALDI-TOF MS Analysis of Phospholipids: Which Isomer for what Purpose? *Eur. Biophys. J.* 36 (4-5), 517–527. doi:10.1007/s00249-006-0090-6

Shu, X., Li, Y., Liang, M., Yang, B., Liu, C., Wang, Y., et al. (2012). Rapid Lipid Profiling of Bacteria by Online MALDI-TOF Mass Spectrometry. *Int. J. Mass Spectrom.* 321-322, 71–76. doi:10.1016/j.ijms.2012.05.016

Singhal, N., Kumar, M., Kanaujia, P. K., and Virdi, J. S. (2015). MALDI-TOF Mass Spectrometry: an Emerging Technology for Microbial Identification and Diagnosis. *Front. Microbiol.* 6, 791. doi:10.3389/fmicb.2015.00791

Smolira, A., and Wessely-Szponder, J. (2015). Importance of the Matrix and the Matrix/sample Ratio in MALDI-TOF-MS Analysis of Cathelicidins Obtained from Porcine Neutrophils. *Appl. Biochem. Biotechnol.* 175 (4), 2050–2065. doi:10.1007/s12010-014-1405-1

Tran, T., Bonham, A. J., Chan, E. D., and Honda, J. R. (2019). A Paucity of Knowledge Regarding Nontuberculous Mycobacterial Lipids Compared to the Tubercle bacillus. *Tuberculosis* 115, 96–107. doi:10.1016/j.tube.2019.02.008

Tseng, S.-P., Teng, S.-H., Lee, P.-S., Wang, C.-F., Yu, J.-S., and Lu, P.-L. (2013). Rapid Identification ofM. abscessusandM. Massilienseby MALDI-TOF Mass Spectrometry with a Comparison to Sequencing Methods and Antimicrobial Susceptibility Patterns. *Future Microbiol.* 8 (11), 1381–1389. doi:10.2217/fmb.13.115

Voorhees, K. J., Jensen, K. R., McAlpin, C. R., Rees, J. C., Cody, R., Ubukata, M., et al. (2013). Modified MALDI MS Fatty Acid Profiling for Bacterial Identification. *J. Mass. Spectrom.* 48 (7), 850–855. doi:10.1002/jms.3215

Wang, C.-C., Lai, Y.-H., Ou, Y.-M., Chang, H.-T., and Wang, Y.-S. (2016). Critical Factors Determining the Quantification Capability of Matrix-Assisted Laser Desorption/ionization- Time-Of-Flight Mass Spectrometry. *Phil. Trans. R. Soc. A.* 374 (2079), 20150371. doi:10.1098/rsta.2015.0371

Welker, M., Van Belkum, A., Girard, V., Charrier, J.-P., and Pincus, D. (2019). An Update on the Routine Application of MALDI-TOF MS in Clinical Microbiology. *Expert Rev. Proteomics* 16 (8), 695–710. doi:10.1080/14789450.2019.1645603

Whang, J., Back, Y. W., Lee, K.-I., Fujiwara, N., Paik, S., Choi, C. H., et al. (2017). Mycobacterium Abscessus Glycopeptidolipids Inhibit Macrophage Apoptosis and Bacterial Spreading by Targeting Mitochondrial Cyclophilin D. *Cell Death Dis.* 8 (8), e3012. doi:10.1038/cddis.2017.420

Wiangnon, K., and Cramer, R. (2015). Sample Preparation: a Crucial Factor for the Analytical Performance of Rationally Designed MALDI Matrices. *Anal. Chem.* 87 (3), 1485–1488. doi:10.1021/ac504412p

Conflict of Interest: GL-M and FD are coinventors of the method "Screening With Mass Spectrometry For Mycobacteria Prior To Cardiothoracic Surgery," for which a patent has been filed by Imperial Technology Transfer (International Publication Number WO2021064426A1). Author MK is employed by Bruker Daltonics GmbH & Co. KG (Bremen, Germany).

The remaining authors declare that the research was conducted in the absence of any commercial or financial relationships that could be construed as a potential conflict of interest.

Publisher's Note: All claims expressed in this article are solely those of the authors and do not necessarily represent those of their affiliated organizations, or those of the publisher, the editors and the reviewers. Any product that may be evaluated in this article, or claim that may be made by its manufacturer, is not guaranteed or endorsed by the publisher.

frontiers in Chemistry

ORIGINAL RESEARCH
published: 09 September 2021
doi: 10.3389/fchem.2021.740495

Design of Experiments for Matrix-Assisted Laser Desorption/Ionization of Amphiphilic Poly(Ethylene Oxide)-b-Polystyrene Block Copolymers

Hélène Pizzala[1], Magalie Claeys-Bruno[2], Valérie Monnier[3], Michelle Sergent[2] and Laurence Charles[1]**

[1]Aix Marseille Université, CNRS, UMR 7273, Institut de Chimie Radicalaire, Marseille, France, [2]Aix Marseille Université, UMR CNRS IRD 7263, Institut Méditerranéen de Biodiversité Marine et Continentale, Marseille, France, [3]Aix Marseille Université, CNRS, Centrale Marseille, FR 1739, Fédérations des Sciences Chimiques, Marseille, France

OPEN ACCESS

Edited by:
Gerard Bolbach, Sorbonne Universités, France

Reviewed by:
Scott Grayson, Tulane University, United States
Cosima Damiana Calvano, University of Bari Aldo Moro, Italy

***Correspondence:**
Magalie Claeys-Bruno
m.claeys-bruno@univ-amu.fr
Laurence Charles
laurence.charles@univ-amu.fr

Specialty section:
This article was submitted to Analytical Chemistry, a section of the journal Frontiers in Chemistry

Received: *13 July 2021*
Accepted: *26 August 2021*
Published: *09 September 2021*

Citation:
Pizzala H, Claeys-Bruno M, Monnier V, Sergent M and Charles L (2021) Design of Experiments for Matrix-Assisted Laser Desorption/Ionization of Amphiphilic Poly(Ethylene Oxide)-b-Polystyrene Block Copolymers. Front. Chem. 9:740495. doi: 10.3389/fchem.2021.740495

Matrix-assisted laser/desorption ionization (MALDI) has become a very popular ionization technique for mass spectrometry of synthetic polymers because it allows high throughput analysis of low amounts of sample while avoiding the complexity introduced by extensive multiple charging of electrospray ionization. Yet, fundamental mechanisms underlying this ionization process are not fully understood, so development of sample preparation methods remains empirical. Reliable prediction for the optimal matrix/analyte/salt system is indeed still not possible for homopolymers and it becomes even more challenging in the case of amphiphilic block copolymers where conditions dictated by one block are not compatible with MALDI requirements of the second block. In order to perform MALDI of copolymers composed of poly (ethylene oxide) (PEO) and polystyrene (PS) blocks, it was postulated here that experimental conditions suitable for both species would also be successful for PEO-*b*-PS. Accordingly, designs of experiments based on Quantitative Structure Activity Relationship (QSAR) analysis were first implemented, studying the influence of 19 matrices and 26 salts on the laser fluence requested for successful MALDI. This analysis first permitted to highlight correlations between the investigated 10 descriptors of matrices and salts and the analytical response, and then to construct models that permits reliable predictions of matrix/salt couples to be used for one or the other homopolymer. Selected couples were then used for MALDI of a PEO-*b*-PS copolymer but no general trend was observed: experimental conditions expected to work often failed whereas ionic adducts of the copolymer were clearly detected with some matrix/salt systems that were shown to badly perform for constituting homopolymers. Overall, this rules out the working assumption stating that the MALDI behavior of chains composed of PEO and PS segments should combine the behavior of the two polymeric species. Yet, although requiring a dedicated design of experiments, MALDI of the amphiphilic PEO-*b*-PS copolymer was achieved for the first time.

Keywords: MALDI, design of experiments, QSAR, space filling design, mass spectrometry, amphiphilic copolymers

INTRODUCTION

Matrix-assisted laser/desorption ionization (MALDI) (Karas and Hillenkamp, 1988; Tanaka et al., 1988) is a technique allowing production of gas phase ions upon laser irradiation of a solid mixture of non-volatile analytes embedded in matrix molecules. It has become a very popular ionization technique for mass spectrometry of macromolecules because it allows high throughput analysis of low amounts of sample. However, fundamental mechanisms underlying this ionization process are still not fully understood, which is particularly detrimental to the development of MS methods for analytes exhibiting a great structural variety such as synthetic polymers. Sample preparation, that is, proper matrix selection as well as solid-state organization, is known to be a key issue in the success of MALDI-MS analyses. Typically, MALDI samples are obtained after solvent evaporation of a matrix/analyte mixture, and although no longer present in the solid sample, the nature of solvents used to prepare individual solutions has critical impacts on sample homogeneity and hence on MALDI-MS data quality (Yalcin et al., 1998). The matrix should also fulfill different criteria, some of which are clearly defined (strong absorptivity at the employed laser wavelength or good vacuum stability) whereas other requirements, such as a good miscibility of the matrix with the analyte in the solid state, are not easily related to physico-chemical parameters of the matrix. In the particular case of synthetic polymers that mostly ionize *via* cation adduction, the solid mixture to be laser-irradiated should also contain a salt. Once the cation is chosen based on the nature and size of polymeric chains, the nature of the counter-anion often influences salt solubility (and hence the amount of available cations) depending on the solvent selected for sample preparation. Moreover, ionization yield of synthetic polymers subjected to MALDI is very sensitive to relative molar concentration of components in the ternary mixture. The task becomes even more challenging when dealing with copolymers composed of blocks with different chemical properties that may dictate incompatible experimental conditions for each segment. Overall, as long as the role of most influential parameters controlling the MALDI process is not clearly identified, accurate prediction for the optimal matrix/polymer/salt system is not possible and development of sample preparation methods remains empirical, either starting from published protocols that were shown to work for a given polymeric system (*NIST Synthetic Polymer MALDI Recipes Database*) or using a trial and error approach.

To gain insights in the MALDI process, morphology and molecular interactions within MALDI samples have been studied using a variety of techniques operating on solid state analytes such as scanning electron microscopy (Doktycz et al., 1991; Horneffer et al., 2003), time-of-flight secondary ion mass spectrometry (Hanton et al., 1999), crystallography (Mele and Malpezzi, 2000), MS imaging (Hanton et al., 2008) or solid state nuclear magnetic resonance (Pizzala et al., 2009; Major et al., 2012; Pizzala et al., 2021). Although providing useful new information, reported findings could not be clearly related to molecular properties of components in the solid mixture, and hence could not allow construction of predictive rules. Alternatively, more global approaches based on design of experiments (DoE) can be developed to take into account not only the variety of parameters that may actually be involved in the MALDI process but also their synergistic effects. The first step towards fundamental understanding of MALDI indeed implies to clearly identify which parameters are critical to the process, their respective influence as well as their interaction. Validation of these parameters typically consists of developing a model which predictive character can be experimentally verified. In mass spectrometry, the use of DoE is an emerging trend for simultaneous optimization of numerous factors (Hecht et al., 2016). Focusing on the field of MALDI-MS for synthetic polymers, different approaches have been reported. Wetzel et al. used fractional factorial design to study the effects of five instrumental parameters for different mixtures of polystyrene (PS) with dithranol or all-*trans*-retinoic acid as the matrix (Wetzel et al., 2006). While detector voltage and delay time were the most influential parameters for PS when mixed with all-*trans*-retinoic acid, laser energy was a supplemental factor to be considered when using dithranol as the matrix. Full factorial design was used by Brandt et al. to study effect of molar mixing ratio of several synthetic polymers [PS, poly(dimethylsiloxane), poly(ethylene glycol) and poly(methylmethacrylate)], using eight frequently employed matrices, five salts and thirteen different solvents (Brandt et al., 2010). The optimal ternary mixture composition was found to highly depend on the studied combination matrix/polymer/solvent used. The same group then focused on PS to build a predictive model based on partial least square regression that enables appropriate matrix/salt/solvent combinations to be defined from a few experiments (Brandt and Ehmann, 2010). A general linear model was successfully employed by Badia et al. to optimize MALDI conditions for poly(ethylene terephthalate) (Badia et al., 2011b) and for poly(lactide) (Badia et al., 2011a). The quality assessment method developed by Kooijman et al. for unsupervised quantitation of sample preparation quality was based on eight parameters (such as number and intensity of detected peaks, angular and radial signal distribution) to describe spots imaged by MALDI (Kooijman et al., 2016; Kooijman et al., 2017). The method permitted to select the best sample preparation parameters to be employed for MALDI of PEG, PMMA and polytetrahydrofuran, which were found to be highly polymer-dependent.

Here, we have evaluated the performance of a new approach, using space filling design (Santner et al., 2003; Fang et al., 2006), to construct predictive models aimed at identifying optimal conditions for MALDI-MS of PS and PEG, in order to find suitable conditions to be used when these polymeric species are part of amphiphilic PEO-*b*-PS macromolecules, assumed to combine the behavior of each segment in MALDI. In order to remove any contributing roles of the solvent that introduce additional complexity (Weidner et al., 2011), solvent-free sample preparation (Skelton et al., 2000; Trimpin et al., 2001) was used to investigate 19 matrices combined with 26 cationization agents, and considering that the MALDI process is most efficient when requiring the lowest laser fluence.

MATERIALS AND METHODS

Chemicals

Polystyrene (PS) sample (M_n 2,000 g mol^{-1}) was from Fluka (Buchs, Switzerland), the poly(ethylene glycol) (PEG) sample (M_n 4,000 g mol^{-1}) was from Sigma (St Louis, MO) while the PEO-*b*-PS block copolymer (M_n 1,800 g mol^{-1} for the PEO block, M_n 1,600 g mol^{-1} for the PS block) was purchased from Polymer Service GmbH (Altdorf, Germany). The following 19 matrices from Sigma were considered: 1,8,9-anthracenetriol (Dith), 2′,4′,6′-trihydroxyacetophenone (THAP), 2-(4′-hydroxybenzeneazo) benzoic acid (HABA), 3-hydroxypyridine-2-carboxylic acid (HPA), 2,3-dihydroxybenzoic acid (2,3-DHB), 2,4-dihydroxybenzoic acid (2,4-DHB), 2,5-dihydroxybenzoic acid (2,5-DHB), 2,6-dihydroxybenzoic acid (2,6-DHB), 2,5-dihydroxy-*p*-benzoquinone (DHBQ), 2-mercaptobenzothiazole (MBT), 3,5-dimethoxy-4-hydroxycinnamic acid (sinapinic acid, SA), *trans*-indoleacrylic acid (IAA), 3-methoxy-4-hydroxycinnamic acid (ferulic acid, FA), 5-chloro-2-mercaptobenzothiazole (CMBT), 5-chlorosalicylic acid (5-CSA), 9-nitroanthracene (9-NA), 9H-pyrido [3,4-b]indole (norharmane, NOR), anthracene-9-carboxylic acid (9-ACA), and α-cyano-4-hydroxycinnamic acid (HCCA). Salts used as cationizing agents were 16 alkali halides (combining lithium, sodium, potassium and rubidium to fluoride, chloride, bromide and iodide), 5 silver salts (AgF, AgCl, AgBr, AgI, and $AgNO_3$) and 5 copper salts (Cu Cl, CuI, CuBr, $CuCl_2$, and $Cu(NO_3)_2$) obtained from Sigma. Methanol used to prepare matrix solution subjected to fluorescence and UV-Vis experiments was from SDS (Peypin, France).

MALDI Mass Spectrometry

All MALDI samples were prepared in solvent-free conditions according to the vortex method (Hanton & Parees, 2005). Prior mixing, all chemicals and materials were stored in a glove box operated at 20°C and relative humidity of 65%: these specific conditions permit capture of atmospheric water molecules by all components, and not by the most hygroscopic ones only (Major et al., 2012). The three solid components (matrix, polymer, salt) were introduced in a 10 ml poly(propylene) tube containing six stainless steel balls (3 mm diameter) (VWR International, West Chester, PA). Matrix/salt molar ratio was 50:10 while the amount of polymer was calculated so as to reach matrix/monomer ratio of about 1:1. Total amount of ternary mixtures was about 20–40 mg. Once capped, the tube was taken out of the glove box and held on a vortex mixer (ThermoFisher Scientific, Waltham, MA) for grinding of the content at a 2,400 min^{-1} frequency for 16 min, as optimized from a previous study (Major et al., 2012). After mixing, a few grains of the sample were applied onto the MALDI target with a spatula to form a thin layer. MALDI-TOF MS experiments were carried out using a Bruker Autoflex instrument (Bruker Daltonics, Leipzig, Germany) equipped with a nitrogen laser emitting at 337 nm, a single-stage pulsed ion extraction source, and dual microchannel plate detectors. Data acquisition was performed in reflectron mode and, besides laser fluence, all instrumental parameters were kept constant: pulse frequency: 10 Hz; accelerating voltage: +19 kV; extraction delay time: 100 ns. Each sample was prepared twice and deposited in quadruplicate on the MALDI plate. Mass spectra were recorded from each deposit after 100 laser shots. The working laser fluence was arbitrarily defined just above (2%) the fluence threshold. FlexControl software version 2.2 (Bruker Daltonics) was used for instrument control and data acquisition, and FlexAnalysis software version 2.2 (Bruker Daltonics) for data processing.

Other Measurements

Additional experiments or calculations had to be performed to obtain matrix descriptors that were not available in the literature. Relative Fluorescence Intensity (RFI) was measured with a microplate spectrofluorimeter (Infinite 200, TECAN, Männedorf, Switzerland) from matrix solution in methanol (3.10^{-3} mol L^{-1}) with excitation at 337 nm. Molar absorption coefficients were measured at 337 nm from matrix solution in methanol (1.10^{-4} mol L^{-1}) on a Shimadzu UV-Visible spectrophotometer. Theoretical calculations were performed to determine dipole moments and ionization energies, with geometry optimization using a DFT B3LYP method (as implemented in Gaussian) (Frisch et al., 2004) adopting 6–311 g (d,p) basis set and MP2 and ROMP2 levels, respectively. Proton affinities of some matrices were obtained using a DFT PBE1PBE method with a 6–31 + g(2d,2p) basis set.

Design of Experiments

Experimental designs are mathematical and statistical techniques allowing the organization of experiments. These planned designs lead to an optimal quality of the information and also to a reduction of the number of experiments. More particularly, Space Filling Designs were considered here in order to spread experimental points evenly throughout the domain of interest described by the 10 descriptors. Designs of experiments were constructed using WSP algorithm (Santiago et al., 2012) which selects points to be tested among the set of 494 candidate points. The modeling was performed using stepwise regression (Hocking, 1976; Draper and Smith, 1981) from a full degree 2 model by selecting predictive variables. At each step of the model construction, coefficients to be included or excluded were tested with F-tests.

RESULTS AND DISCUSSION

Design of Experiments

Descriptors selected for MALDI matrices (X_1–X_7 in **Table 1**) are molecular parameters acknowledged to play effective roles in the MALDI process, such as absorption coefficient at the employed laser wavelength (ε_{337}, L mol^{-1} cm^{-1}), ionization energy (IE, eV), proton affinity (PA, kJ mol^{-1}) used instead of the less documented cation affinity, pKa and relative fluorescence intensity at 337 nm (RFI_{337}). Supplemental features such as molecular weight (MW, g mol^{-1}) or dipole moment (ρ, Debye) were also considered. The three descriptors used to characterize cationizing agents are the radius (in pm) of their constitutive cation and anion, and their bond energy (kJ mol^{-1}), respectively defined as X_8, X_9, and X_{10} in **Table 2**. Some of these descriptors,

TABLE 1 | Parameters selected as descriptors for matrices.

Matrix	X_1 MW (g mol^{-1})	X_2 pKa* or#	X_3 ρ# (Debye)	X_4 ε_{337}§ (L mol^{-1} cm^{-1})	X_5 RFI_{337}§	X_6 IE# (eV)	X_7 PA* or# (kJ mol^{-1})
2,3-DHB	154.12	2.94[a]	2.04	1,620	391	8.43	851[f]
2,4-DHB	154.12	3.29[a]	0.88	210	69	8.76	863[f]
2,5-DHB	154.12	2.97	2.78	3,990	8,008	8.23	855.78[f]
2,6-DHB	154.12	1.30[a]	1.73	1,490	236	8.35	864[f]
5-CSA	172.57	2.6	1.03	1,200	12,122	8.68	802.04
9-ACA	222.24	3.65	1.53	2,930	12,920	7.38	821.31
9-NA	223.23	43	4.01	2,950	663.36	7.64	875.32
CMBT	201.70	6.8	1.49	15,250	48	8.64	902.37
DHBQ	140.09	2.95[a]	0	410	97	9.48	791.97
Dith	226.23	7.16	4.22	6,720	312	8.22	885.51[g]
FA	194.18	4.04[b]	2.35	13,040	1,227	7.89	879[h]
HABA	242.23	3.57	4.93	17,731	31	3.82	949.98[g]
HCCA	189.17	2.6	2.65	24,730	59	8.48	841.55[g]
HPA	139.11	3.9[c]	4.55	680	3,216	9.46	898.49[g]
IAA	187.19	4.59	4.40	16,800	280	7.76	893.88[g]
MBT	167.25	6.93[d]	0.97	6,920	60	8.54	889.74[g]
NOR	168.19	6.8[e]	3.06	4,970	46,809	7.81	875.52[g]
SA	224.21	3.98[b]	4.52	14,900	2,159	7.91	875.88[g]
THAP	168.15	7.76	3.44	1,729	167	8.45	893.04[g]

**From the literature as referenced hereafter.*
#Calculated values.
§Experimental values.
[a]*(Schiller et al., 2007).*
[b]*(Remily-Wood et al., 2009).*
[c]*(Chou et al., 1999).*
[d]*(Woods et al., 2000).*
[e]*(De Andres et al., 2010).*
[f]*(Mormann et al., 2000).*
[g]*(Mirza et al., 2004).*
[h]*(Jorgensen et al., 1998).*

TABLE 2 | Parameters selected as descriptors for cationizing agents.

X_8, cation radius (pm)[a]				Li	Na	K	Rb	Cu			Ag
				128	166	203	220	132			145
X_9, anion radius (pm)[a]				F	Cl	Br	I	NO_3			
				64	99	121	140	200			
X_{10}, bond energy (kJ mol–1)[b] of cationizing agents											
LiF	1,030	NaF	910	KF	808	RbF	774	AgF	953	CuCl	992
LiCl	834	NaCl	769	KCl	701	RbCl	680	AgCl	910	CuBr	969
LiBr	788	NaBr	732	KBr	671	RbBr	651	AgBr	897	CuI	948
LiI	730	NaI	682	KI	632	RbI	617	AgI	881	$CuCl_2$	2,774
								$AgNO_3$	820	$Cu(NO_3)_2$	2,739

[a]*As referenced for covalent radii.(*Cambridge Crystallographic Data Center www.ccdc.cam.ac.uk/products/csd/radii*).*
[b]*As reported in referenced handbook (Lide, 2008).*

such as pKa (X_2), ε_{337} (X_4), RFI_{337} (X_5), ionization energy of the matrix (X_6) and bond energy of salts (X_{10}), have been modified using a Log transformation in order to obtain a more uniform variation range. The main computed Y response was the laser fluence required to obtain MALDI signals. Doing so, we consider that optimal ternary mixtures are characterized by low laser fluence. In contrast, poorly efficient sample compositions are identified by the need for high energy to be supplied to the solid substrate in order to record MALDI signals. More precisely, Y corresponds to the lowest laser fluence enabling to measure intensity of at least 50 counts for the oligomer at the maximum of the polymer distribution when recording mass spectra after 100 laser shots. This response is expressed as a percentage of the total laser power and was experimentally varied between 20 and 75%. When no signal was observed once reaching this upper 75% limit, samples were arbitrarily assigned a 100% fluence. MALDI experiments were also considered as unsuccessful (hence designated by a 100% laser fluence) when

TABLE 3 | Experimental ($^{PS}Y_{exp}$) *vs* predicted ($^{PS}Y_{calc}$) fluence values when using the model built for PS with Ag and Cu metals (**Eq. 1**), with residuals (res) reported as $^{PS}Y_{exp}$–$^{PS}Y_{calc}$.

Matrix/salt	$^{PS}Y_{exp}$	$^{PS}Y_{calc}$	Res
CMBT/$Cu(NO_3)_2$	22	21.5	+0.5
IAA/$AgNO_3$	26	27.0	–1.0
FA/$CuCl_2$	27	26.2	+0.8
FA/AgI	28	30.9	–2.9
5-CSA/AgI	29	28.6	+0.4
SA/$Cu(NO_3)_2$	31	32.0	–1.0
2,4-DHB/AgI	32	29.9	+2.1
HPA/$AgNO_3$	40	40.6	–0.6
2,4-DHB/$Cu(NO_3)_2$	41	40.5	+0.5
NOR/CuCl	42	42.0	0
9-NA/AgI	44	43.4	+0.6
DHBQ/$CuCl_2$	44	43.6	+0.4
HPA/$CuCl_2$	45	46.5	–1.5
9-ACA/$AgNO_3$	45	43.4	+1.6

displaying signals that do not correspond to the expected oligomers adducted with the cation from the supplemented salt. Indeed, sodium is a common matrix pollutant which was shown to efficiently compete for PS or PEG cationization in MALDI, even when present at concentration levels far below that of the added salt (Pizzala et al., 2021).

Combining 19 matrices with 26 salts leads to 494 matrix/salt couples characterized by 10 descriptors. Classically in QSAR study (Todeschini et al., 2020), a model is postulated and a subset of points is selected in order to calculate the estimations of the coefficients of this model. In our case, it is obvious that a degree 1 model is not sufficient (due to non-linear phenomenon) to model the behavior. Yet, a complete degree 2 model would need a very high number of experiments (at least 66 experiments). Alternatively, we propose a new approach which does not require postulation of a model but, instead, consists of selecting points according to a uniformity criterion. Among the 494 candidates, a subset of 25 points distributed as uniformly as possible in the space of the 10 descriptors was selected, using the WSP algorithm (Santiago et al., 2012) which guarantees a good uniformity of the points (Santiago et al., 2012; Beal et al., 2014). At the end of the experimentation, different statistical treatments were performed, such as stepwise regression to consider the most significant interaction terms or square terms.

QSAR Study of PS

Results obtained when testing the selected 25 matrix/salt couples for MALDI of PS are reported in **Table 3**. Before performing quantitative treatments to establish the variation of the fluence threshold as a function of the 10 descriptors, multidimensional descriptive analyses were performed to identify any general trends. Principal component analysis (PCA) was carried out for these 25 experimental points in order to highlight characteristics shared by matrix/salt couples associated with low fluence values *vs* those leading to failed experiments (100% fluence). For that purpose, experimentally determined fluence threshold was added as an 11th variable to the set of the 10 descriptors (X_1–X_{10}). The PCA plots shown in **Figure 1** reveal that the most discriminant variable accounting for failed MALDI of PS is the nature of the salt. On the one hand, the small angle formed by vectors associated to "fluence" and "cation radius" in **Figure 1A** reveals a positive correlation (r = +0.76) between these two variables. In other words, 100% fluence values are associated to experiments involving salt with high radius cation. PS adducts produced in the gas phase are usually described with the cation stacked between two adjacent phenyl groups (Gidden et al., 2002): our results suggest that such a conformation would be disfavored by large size cations. On the other hand, vectors associated to "salt bond energy" and "anion radius" form an angle close to 180° with the "fluence" vector (**Figure 1A**): these negative correlations (r = –0.50 and r = –0.64, respectively) indicate that 100% fluence values are associated to experiments involving salt with low radius anion or salt of low bond energy. These results are quite surprising since the amount of free cations available to interact with PS chains is expected to increase (and hence favor production of gas phase ions) as the bond energy of the salt decreases. Finally, with their vectors nearly orthogonal to the "fluence" vector in **Figure 1A**, any descriptors related to the matrix are poorly correlated with the fluence variable. Plotting the distribution of salts in this factorial plan (**Figure 1B**) clearly shows that rubidium and potassium salts all poorly perform (hence, in red) for MALDI of PS. A 100% fluence value is indeed assigned to all experiments conducted with KX or RbX salts (**Supplementary Table 1**), independently of the X counter-anion and of the matrix. Failure to acquire spectra of $[PS + K]^+$ or $[PS + Rb]^+$ was previously reported by Scrivens and coworkers when using dithranol as the matrix (Deery et al., 1997). In contrast, most data points associated to the use of silver or copper salts are located in the upper part of **Figure 1B**, indicating that these salts perform well for MALDI of PS. Of note, all detected ions in MALDI mass spectra were singly charged species, which means that Cu^{II} was reduced to Cu^{I} by electrons emitted from the metallic MALDI plate upon laser irradiation (Zhang et al., 2003). As detailed in **Supplementary Table 1**, fluence values below ~40% were recorded for four of the six experiments involving Cu and three of the five experiments conducted with Ag. This result is consistent with the role of pre-formed matrix/salt clusters in the formation of PS ions in MALDI, as well as with the less pronounced clustering propensity of silver compared to copper, as demonstrated with dithranol (Lehmann et al., 1997). An intermediate situation is observed for lithium and sodium salts, with the success of MALDI experiments being matrix-dependent, as also reported by others (Deery et al., 1997). From these first results, it was decided to remove rubidium and potassium salts from the list of cationizing agents for PS. This led to withdrawal of 152 points from the candidate set (now composed of 342 points) and of 8 matrix/salt couples from the 25-point subset. The newly obtained subset of 17 points was badly conditioned and did not permit to estimate coefficients of a mathematical model. The uniform matrix was hence repaired by choosing new couples among the 342 remaining candidate points. Using the WSP algorithm and protecting the points already chosen, 16 new points were selected and experimentally tested: fluence values show failure of MALDI

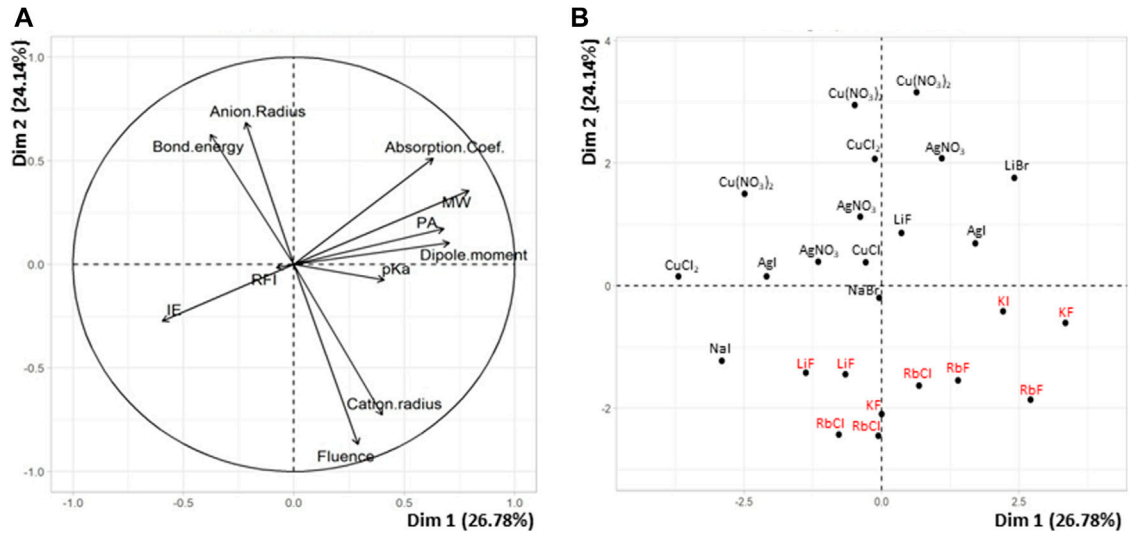

FIGURE 1 | PCA plots of **(A)** variables and **(B)** individuals for the 25 matrix/salt couples tested for MALDI of PS.

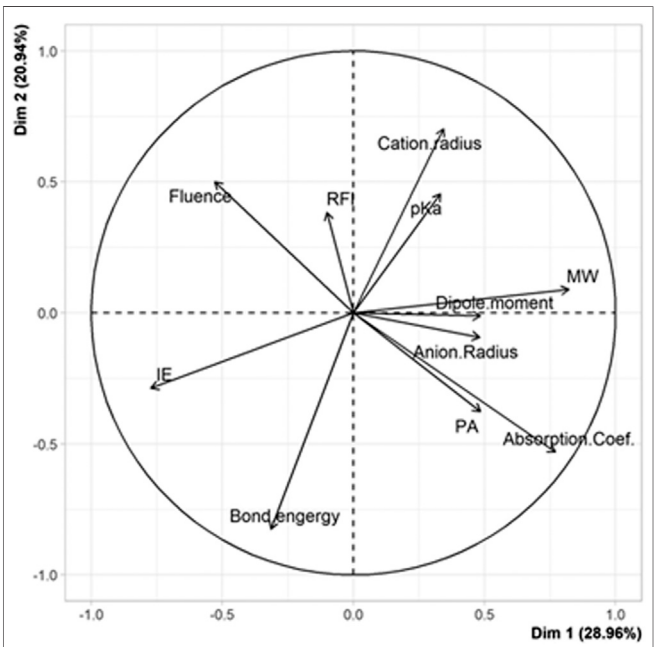

FIGURE 2 | PCA plot of variables for the 14 couples involving Ag or Cu salts tested for MALDI of PS.

experiments in six cases, five of which involve the FA matrix (**Supplementary Table 2**).

The model built when considering N = 33 points (17 remaining couples in **Supplementary Table 1** + the 16 couples of **Supplementary Table 2**) was quite bad at predicting correct fluence values and the behavior of the different couples remained very difficult to understand (data not shown). It was thus decided to split the learning set based on the nature of the cation, that is, metals such as Ag and Cu that systematically allow successful MALDI of PS *vs* alkali (Na and Li) with which production of cationized PS is matrix-dependent. The PCA plot obtained for the group of 14 couples involving either Ag or Cu salt is shown in **Figure 2**. A single positive correlation is observed between the laser fluence and matrix fluorescence: this matrix property is well-known to be detrimental to the MALDI process but the measured correlation remains quite low (r = +0.28). In contrast, a strong negative correlation (r = –0.75) is clearly revealed in **Figure 2** between the laser fluence and the absorption coefficient of the matrix (ε_{337}). Another negative correlation, yet less pronounced (r = –0.28), is found between laser fluence and proton affinity, used here to illustrate cation affinity of the matrix. This last result supports the current opinion about PS cationization occurring *via* a gas phase process (Lehmann et al., 1997): when using matrices with high cation affinity, energy input has to be increased for cations to be transferred from the matrix/salt clusters to PS chains.

The model constructed with a stepwise regression based on the subset of 14 points available for Ag and Cu salts is defined by **Eq. 1**. As reported in **Table 3**, this model allows excellent predictions of the fluence, with R^2 = 0.976 and residuals below ±3.

$$Y = 46.89 - 1.67X_1 + 5.50X_2 - 1.452X_6 + 10.75X_8 - 6.10X_9 + 11.44X_{10} + 18.45X_8X_{10} + 4.98X_1X_8 - 26.25X_2X_9 \quad (1)$$

As compared to this first model, the second model constructed for PS with the subset of 19 points related to alkali salts is slightly less efficient at predicting accurate fluence (R^2 = 0.874). It is defined by **Eq. 2** and yields $^{PS}Y_{calc}$ data with absolute value of residuals ranging from 0.5 to 22.3 (**Table 4**).

$$Y = 54.91 + 45.31X_1 - 19.00X_4 - 2.87X_6 - 23.25X_7 + 3.98X_8 + 2.56X_{10} - 108.89X_4X_6 + 53.48X_6X_{10} + 18.86X_7X_8 \quad (2)$$

However, nearly 74% of these predictions were achieved with a residual value below ±10 and, most importantly, the model allows

TABLE 4 | Experimental ($^{PS}Y_{exp}$) *vs* predicted ($^{PS}Y_{calc}$) fluence values when using the model built for PS with alkali salts (**Eq. 2**), with residuals (res) reported as $^{PS}Y_{exp}$–$^{PS}Y_{calc}$.

Matrix/salt	$^{PS}Y_{exp}$	$_{PS}$Ycalc	Res
HCCA/LiI	25	37.6	−12.6
FA/LiF	31	53.3	−22.3
CMBT/LiF	32	24.1	+7.9
2,6-DHB/NaF	34	28.7	+5.3
HABA/LiBr	42	48.8	−6.8
THAP/NaBr	43	37.9	+5.1
9-NA/LiF	46	48.5	−2.5
2,4-DHB/NaI	58	60.2	−2.2
2,4-DHB/LiI	60	62.4	−2.4
DHBQ/NaI	60	51.9	+8.1
2,4-DHB/NaCl	63	71.4	−8.4
2,4-DHB/LiF	100	107.0	−7.0
FA/LiCl	100	78.9	+21.1
FA/LiBr	100	85.8	+14.2
FA/LiI	100	95.0	+5.0
FA/NaCl	100	100.5	−0.5
FA/NaI	100	115.0	−15.0
HABA/NaF	100	92.4	+7.6
HPA/LiF	100	94.7	+5.3

unsuccessful experiments (fluence 100%) to be clearly discriminated from those yielding PS ions upon MALDI. With both models in hands, predicted fluence values were calculated for the 494 matrix/salt combinations (**Supplementary Tables 4–13**) and will be considered together with predictions obtained for PEG to rationalize the selection of matrix/salt couples for MALDI of PEO-*b*-PS block copolymer (*vide infra*).

QSAR Study of PEG

The same 25 couples as first used in the case of PS were considered in the QSAR study of PEG. However, results of MALDI experiments led us to remove some couples from this subset. The CMBT/LiF couple was no longer considered because it led to mass data strongly lacking reproducibility. Three additional couples were removed to avoid biased results due to spectral interferences between the targeted species and ionic adducts formed with residual sodium of polluted matrices. For example, safe distinction could not be achieved between $[PEG_{n-1} + Cu]^+$ and $[PEG_n + Na]^+$ ions in MALDI experiments conducted with 2,4–DBH/$Cu(NO_3)_2$ and CMBT/$Cu(NO_3)_2$. Similarly $[PEG_{n-2} + Ag]^+$ could not be resolved from $[PEG_n + Na]^+$ when using the 9-ACA/$AgNO_3$ couple. Using the WSP algorithm, addition of three new matrix/salt pairs (namely, MBT/$AgNO_3$, HPA/$Cu(NO_3)_2$ and HCCA/$CuCl_2$) was found to be sufficient to repair the matrix.

The PCA plot built with data obtained for PEG with the new 24-point subset (**Supplementary Table 3**) allows three main matrix descriptors to be identified for their influence on laser fluence (**Figure 3**). First, the positive correlation (r = +0.29) observed between laser fluence and the ionization energy of the matrix indicates that the highest fluence values are most often found for those matrix having high ionization energy (**Figure 3A**). This result is consistent with the coupled chemical and physical dynamics model proposed by Knochenmuss (Knochenmuss, 2003): formation of matrix ions is the key primary event in UV-MALDI since analyte ions observed in mass spectra are predominantly formed *via* secondary ion-molecule reactions with these matrix ions in the MALDI plume (Knochenmuss and Zenobi, 2003). Two other matrix descriptors exhibit negative correlation with the laser fluence when plotting data in a second set of dimensions (**Figure 3B**). Matrices with low ε_{337} absorption coefficient require high fluence to induce the MALDI process (r = −0.47), which is a quite obvious relationship. In contrast, the reason why matrices of low molecular weight are often found in matrix/salt associated with high fluence (r = −0.53) is more puzzling. Yet, using solid state NMR, our group has recently shown that, in the case of 2,x-DHB isomers (with x = 3–6), MALDI of PEG was influenced by matrix/polymer aggregates formed in the solid state upon grinding (Pizzala et al., 2021). A similar study should be conducted to find out whether such aggregates are also formed with alternative matrices and, if so, whether the number of molecules in such aggregates varies with the size, and hence the molecular weight, of the matrix. The PCA plot of **Figure 3A** also highlights the influence of the salt properties. The negative correlation between laser fluence and the cation radius (r = −0.43) indicates that low fluence is required to desorb PEG adducted with large cation: this is consistent with the quite long PEG chains studied here (M_n = 4 kDa) requiring rather big cation to form stable adducts in the gas phase (Jackson et al., 1997). A positive correlation is also noted between laser fluence and the anion radius (r = +0.36), although it remains hard to interpret, at least in terms of salt bond energy since the latter parameter was found to be of negligible influence (r = +0.05). Overall, unlike for PS, distribution of matrix couples in this factorial plane does not exhibit any cleavage between individuals (**Supplementary Figure 1**). Accordingly, the predictive model for PEG defined by **Eq. 3** was built using all data obtained for these 24 matrix/salt couples.

$$Y = 57.89 - 23.99X_1 - 33.30X_2 + 15.63X_3 - 4.25X_4 - 13.95X_5 - 15.565X_6 - 30.69X_8 - 1.23X_{10} + 29.42X_1X_2 - 67.97X_2X_8 + 24.715X_1X_8 + 9.38X_3X_5 \quad (3)$$

With R^2 = 0.78, this PEG model is less accurate than the two models built for PS, although 75% of predicted values have a residual value below ±15 (**Table 5**). Moreover, discrimination of unsuccessful experiments (fluence 100%) is not achieved in a few cases. For example, the fluence threshold of ~75% predicted for failed experiments conducted with $AgNO_3$ and either IAA or MBT is lower than the 83% value predicted for the THAP/NaBr couple experimentally found to produce MALDI data from 51% fluence threshold. In spite of these few limitations, this model was applied to predict fluence values in MALDI of PEG for the 494 matrix/salt combinations (**Supplementary Tables 4–13**).

MALDI of the PEO_{1800}-*b*-PS_{1600} Copolymer

As previously mentioned, the search for appropriate experimental conditions enabling successful MALDI of the targeted block copolymer relies here on the assumption that any matrix/salt couple found to properly operate (*i.e.*, with low

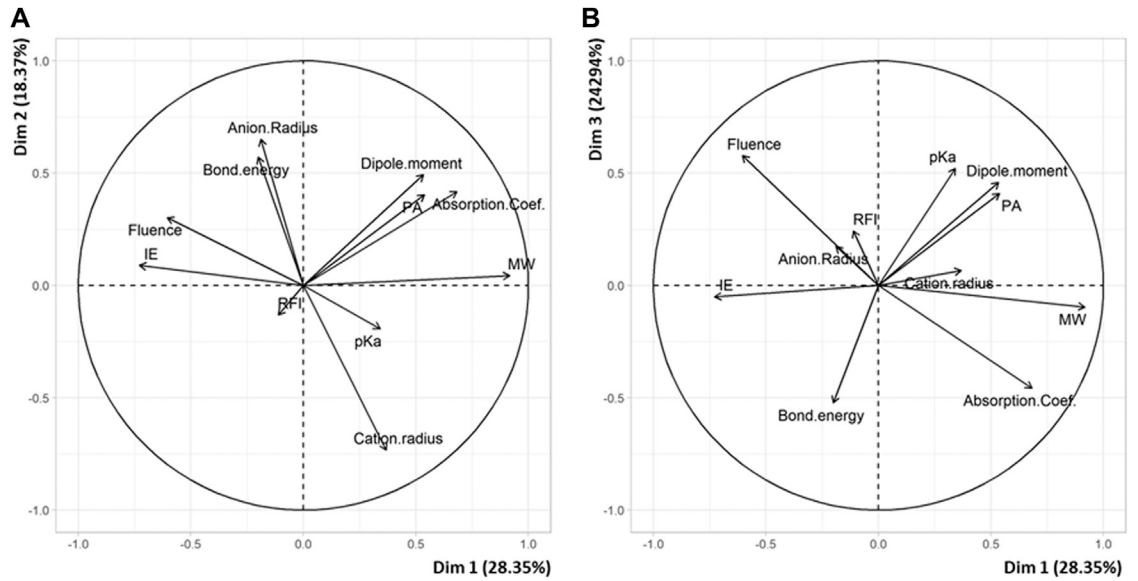

FIGURE 3 | PCA plots of variables in **(A)** dimension 2 *vs* dimension 1 and **(B)** dimension 3 *vs* dimension 1 for the 24 matrix/salt couples tested for MALDI of PEG.

TABLE 5 | Experimental ($^{PEG}Y_{exp}$) *vs* predicted ($^{PEG}Y_{calc}$) fluence values when using the model built for PEO, with residuals (res) reported as $^{PEG}Y_{exp}-^{PEG}Y_{calc}$.

Matrix/salt	$^{PEG}Y_{exp}$	$^{PEG}Y_{calc}$	Res
HABA/LiBr	24	12.7	+11.3
HCCA/$CuCl_2$	27	35.2	–8.2
CMBT/RbF	29	32.6	–3.6
5-CSA/AgI	31	29.6	+1.4
SA/$Cu(NO_3)_2$	33	31.4	+1.6
SA/KI	33	47.9	–14.9
9-NA/RbF	35	34.8	+0.2
HABA/KF	35	42.4	–7.4
FA/$CuCl_2$	39	51.8	–12.8
2,5-DHB/KF	45	57.8	–12.8
9-ACA/RbCl	48	33.4	+14.6
DHBQ/NaI	48	69.1	–21.1
HPA/RbCl	49	49.9	–0.9
THAP/NaBr	51	83.9	–32.9
2,4-DHB/RbCl	71	58.8	+12.2
2,4-DHB/LiF	73	84.2	–11.2
9-NA/AgI	100	99.3	+0.7
DHBQ/$CuCl_2$	100	84.6	+15.4
HPA/$AgNO_3$	100	82.6	+17.4
HPA/$Cu(NO_3)_2$	100	99.6	+0.4
HPA/LiF	100	97.4	+2.6
IAA/$AgNO_3$	100	74.0	+26.0
MBT/$AgNO_3$	100	75.4	+24.6
NOR/CuCl	100	103.0	–3.0

fluence threshold) for MALDI of both PEG and PS homopolymers would be relevant candidates to be tested for MALDI of PEO-*b*-PS copolymers. Accordingly, predicted $^{PEG}Y_{calc}$ and $^{PS}Y_{calc}$ values listed in **Supplementary Tables 4–13** were compared for all matrix couples, using a color code to rapidly identify which conditions were associated to low (≤50%, in green), medium (51–75%, in orange) or high (>75%, in red) laser fluence requirement. Then, selected matrix/salt couples were tested for the PEO_{1800}-*b*-PS_{1600} copolymer. Detailed analysis of these results is beyond the scope of the present study, so only typical examples are shown in **Figure 4** and **Supplementary Figure 2**. On the one hand, experimental conditions shown to work for both homopolymers often failed at producing MALDI data for the copolymer. For example, data obtained with HCCA/LiI (**Figure 4A**) revealed the presence of free PEO in the studied sample (which was confirmed by liquid chromatography analysis reported in **Supplementary Figure 3**) but no trace of the copolymeric distribution. Even worse results were obtained with the 5-CSA/AgI couple that mainly generates $[AgI]_nAg^+$ salt clusters in MALDI (**Supplementary Figure 2A**). This particular result shows that the analyte, alone or in conjunction with the matrix, actually contribute to the extent of salt dissociation upon grinding, as previously demonstrated in the case of PEG with DHB matrices (Pizzala et al., 2021). Accordingly, one way to further improve the DoE performance should be to include specific properties of the copolymer as additional variables. In contrast, employing HCCA/$CuCl_2$ permits to generate the targeted copolymeric distribution centered at the expected *m/z* ~ 3,600 (**Figure 4B**), consistent with the efficiency of this couple to promote MALDI of individual homopolymers. Detailed assignment of signals measured for co-oligomers is provided in **Supplementary Figure 4**. On the other hand, MALDI of the studied PEO-*b*-PS copolymer could also be achieved with some matrix/salt systems that were shown to badly perform for constituting segments, as depicted in **Figure 4D** with 9-NA/$CuCl_2$. Yet, again, this is not a systematic rule, as exemplified in **Figure 4C** with the MALDI mass spectrum obtained with DHBQ/NaI mainly

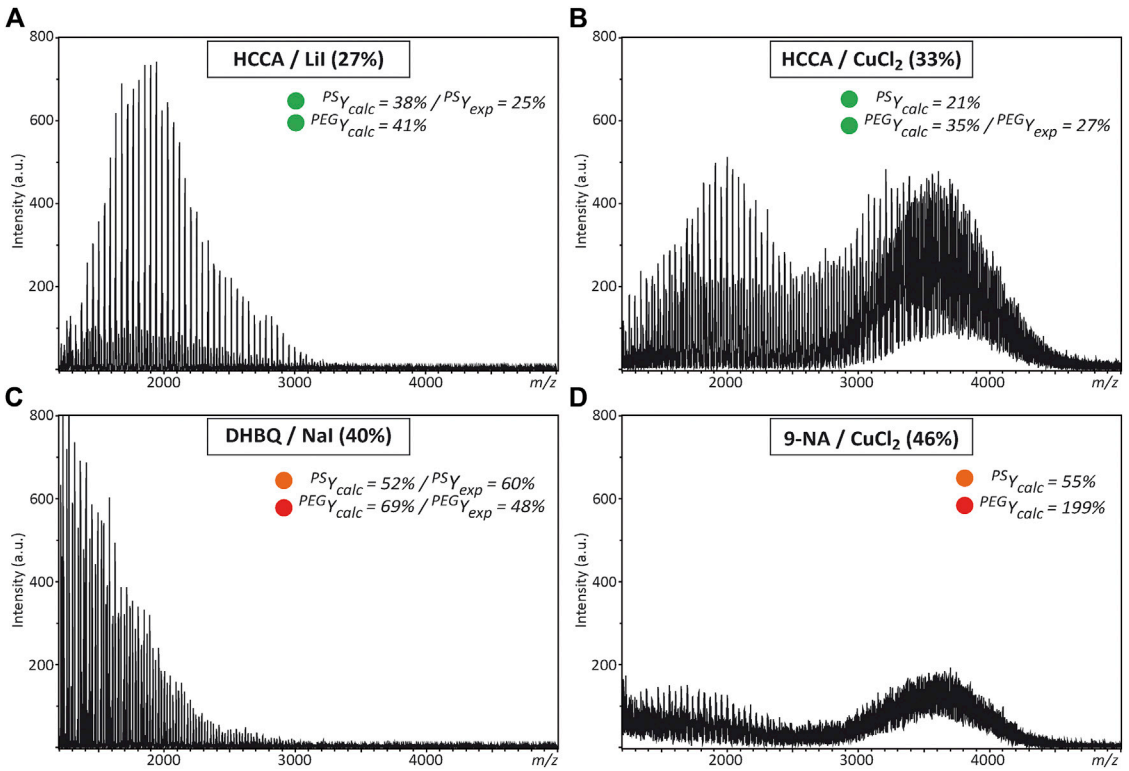

FIGURE 4 | MALDI mass spectra recorded for the PEO-*b*-PS copolymer when using **(A)** HCCA/LiI **(B)** HCCA/$CuCl_2$ **(C)** DHBQ/NaI, or (D) 9-NA/$CuCl_2$ as the matrix/salt couple, with the employed laser fluence into parenthesis. Inset: Predicted (Y_{calc}) or experimental (Y_{exp}) laser fluence when these experimental conditions are employed for PS and PEG homopolymers, using the same color code as in **Supplementary Figures 4-13** to qualify laser fluence requirement (≤50%, in green; 51–75%, in orange; > 75%, in red).

showing signals of residual PEO. Overall, these results show that chains composed of PEO and PS segments do not behave as a combination of the two polymeric species in MALDI, hence ruling out our initial assumption. Alternatively, proper modelling of the MALDI behavior of synthetic polymers would require not only matrix and salt parameters to be considered but also properties of the analyte itself. In other words, any DoE aimed at optimizing MALDI experimental conditions of amphiphilic block copolymers should be developed for the targeted copolymer itself rather than its constituting homopolymers. The approach developed here has permitted to identify some matrix/salt couples that promote ionization of the PEO-*b*-PS block copolymer, which means that the set of 19 matrices and 26 salts used in the present study can be safely used to perform a new DoE based on QSAR analysis for MALDI of PEO-*b*-PS.

CONCLUSION

In this study, 19 matrices and 26 salts were considered for a design of experiments aimed at studying the influence of 10 variables (7 for each matrix, 3 for each salt) on MALDI data of PEG and PS homopolymers, in order to further build models that can predict best experimental conditions, as measured by the lowest laser fluence threshold requested to achieve ionization. To do so, WSP algorithm was used to define reduced subsets based the uniformity of their distribution in the space of the 10 descriptors. For PS, the subset had to be split into two groups, containing 14 and 19 couples, respectively, while a single subset of 24 couples was tested for PEG. Predictive models built with QSAR were found to be quite reliable in spite of the simplicity of the singly monitored response (*i.e.*, laser fluence threshold) which enabled fast measurement while avoiding extensive mass data analysis. It should however be acknowledged that the time-limiting step was the solvent-free sample preparation, but this method was observed here to produce quite homogeneous solid mixtures while suppressing any additional (influential) factors introduced by the use of solvents. Although this was not the main goal here, this study also permitted to highlight some general correlations between individual properties of matrix and salt and the MALDI efficiency of matrix/salt combinations towards PEG and PS. For example, it was found that the nature of the salt is the key factor in MALDI of PS whereas successful MALDI of PEG is also matrix-dependent. This makes this DoE approach highly valuable in fundamental works conducted to best understand MALDI. However, some limitations were also identified, particularly in the predictive model built for PEG, which suggests that some influential parameters were

not taken into account. Most importantly, this study showed that, in terms of MALDI behavior, a block copolymer of PS and PEO is not exactly a combination of these two species, which means that DoE-based optimization of such an amphiphilic copolymer should be developed using the copolymer itself rather than its constituting blocks as models.

DATA AVAILABILITY STATEMENT

The raw data supporting the conclusion of this article will be made available by the authors, without undue reservation.

AUTHOR CONTRIBUTIONS

The manuscript was written through contribution from all authors. HP and VM performed all MALDI-MS experiments; MCB and MS conceived and performed all DoE and associated data treatments; LC conceived and supervised the study, and wrote the manuscript. All authors have given approval to the final version of the manuscript.

ACKNOWLEDGMENTS

LC acknowledges support from Spectropole, the Analytical Facility of Aix- Marseille University, by allowing a special access to the instruments purchased with European Funding (FEDER OBJ2142-3341). Warmly thanks Marion Rollet (ICR, Aix Marseille University) for liquid chromatography analysis as well as Dr Stéphane Humbel (ISM2, Aix Marseille University) for his help in theoretical calculations.

SUPPLEMENTARY MATERIAL

The Supplementary Material for this article can be found online at: https://www.frontiersin.org/articles/10.3389/fchem.2021.740495/full#supplementary-material

REFERENCES

Badía, J. D., Strömberg, E., Ribes-Greus, A., and Karlsson, S. (2011a). Assessing the MALDI-TOF MS Sample Preparation Procedure to Analyze the Influence of Thermo-Oxidative Ageing and Thermo-Mechanical Degradation on Poly (Lactide). *Eur. Polym. J.* 47 (7), 1416–1428. doi:10.1016/j.eurpolymj.2011.05.001

Badía, J. D., Strömberg, E., Ribes-Greus, A., and Karlsson, S. (2011b). A Statistical Design of Experiments for Optimizing the MALDI-TOF-MS Sample Preparation of Polymers. An Application in the Assessment of the Thermo-Mechanical Degradation Mechanisms of Poly (Ethylene Terephthalate). *Analytica Chim. Acta* 692 (1-2), 85–95. doi:10.1016/j.aca.2011.02.063

Beal, A., Claeys-Bruno, M., and Sergent, M. (2014). Constructing Space-Filling Designs Using an Adaptive WSP Algorithm for Spaces with Constraints. *Chemometrics Intell. Lab. Syst.* 133, 84–91. doi:10.1016/j.chemolab.2013.11.009

Brandt, H., Ehmann, T., and Otto, M. (2010). Investigating the Effect of Mixing Ratio on Molar Mass Distributions of Synthetic Polymers Determined by MALDI-TOF Mass Spectrometry Using Design of Experiments. *J. Am. Soc. Mass. Spectrom.* 21 (11), 1870–1875. doi:10.1016/j.jasms.2010.07.002

Brandt, H., Ehmann, T., and Otto, M. (2010). Toward Prediction: Using Chemometrics for the Optimization of Sample Preparation in MALDI-TOF MS of Synthetic Polymers. *Anal. Chem.* 82 (19), 8169–8175. doi:10.1021/ac101526w

Chou, C.-W., Williams, P., and Limbach, P. A. (1999). Matrix Influence on the Formation of Positively Charged Oligonucleotides in Matrix-Assisted Laser Desorption/ionization Mass Spectrometry. *Int. J. Mass Spectrom.* 193 (1), 15–27. doi:10.1016/s1387-3806(99)00104-9

De Andrés, F., Zougagh, M., Castañeda, G., and Ríos, A. (2010). Simultaneous Determination of Six Non-polar Heterocyclic Amines in Meat Samples by Supercritical Fluid Extraction-Capillary Electrophoresis under Fluorimetric Detection. *Electrophoresis* 31 (13), 2165–2173. doi:10.1002/elps.201000080

Deery, M. J., Jennings, K. R., Jasieczek, C. B., Haddleton, D. M., Jackson, A. T., Yates, H. T., et al. (1997). A Study of Cation Attachment to Polystyrene by Means of Matrix-Assisted Laser Desorption/ionization and Electrospray Ionization-Mass Spectrometry. *Rapid Commun. Mass. Spectrom.* 11, 57–62. doi:10.1002/(sici)1097-0231(19970115)11:1<57::Aid-rcm772>3.0.Co;2-g

Doktycz, S. J., Savickas, P. J., and Krueger, D. A. (1991). Matrix/sample Interactions in Ultraviolet Laser-Desorption of Proteins. *Rapid Commun. Mass. Spectrom.* 5 (4), 145–148. doi:10.1002/rcm.1290050402

Draper, N., and Smith, H. (1981). *Applied Regression Analysis*. 2nd Ed. John Wiley & Sons.

Fang, K. T., Runze, L., and Sudjianto, A. (2006). *Design and Modeling for Computer Experiments*. London, United Kingdom: CRC Press.

Frisch, M. J., Trucks, G. W., Schlegel, A., Scuseria, H. B., Robb, G. E., and Cheeseman, J. R. (2004). Gaussian 03, Revision C.02. Wallingford. Full List of Authors Can Be Found in Supplementary Information.

Gidden, J., Bowers, M. T., Jackson, A. T., and Scrivens, J. H. (2002). Gas-phase Conformations of Cationized Poly(styrene) Oligomers. *J. Am. Soc. Mass. Spectrom.* 13 (5), 499–505. doi:10.1016/s1044-0305(02)00367-7

Hanton, S. D., Cornelio Clark, P. A., and Owens, K. G. (1999). Investigations of Matrix-Assisted Laser Desorption/ionization Sample Preparation by Time-Of-Flight Secondary Ion Mass Spectrometry. *J. Am. Soc. Mass. Spectrom.* 10 (2), 104–111. doi:10.1016/s1044-0305(98)00135-4

Hanton, S. D., McEvoy, T. M., and Stets, J. R. (2008). Imaging the Morphology of Solvent-free Prepared MALDI Samples. *J. Am. Soc. Mass. Spectrom.* 19 (6), 874–881. doi:10.1016/j.jasms.2008.02.009

Hanton, S. D., and Parees, D. M. (2005). Extending the Solvent-free MALDI Sample Preparation Method. *J. Am. Soc. Mass. Spectrom.* 16 (1), 90–93. doi:10.1016/j.jasms.2004.09.019

Hecht, E. S., Oberg, A. L., and Muddiman, D. C. (2016). Optimizing Mass Spectrometry Analyses: A Tailored Review on the Utility of Design of Experiments. *J. Am. Soc. Mass. Spectrom.* 27 (5), 767–785. doi:10.1007/s13361-016-1344-x

Hocking, R. R. (1976). A Biometrics Invited Paper. The Analysis and Selection of Variables in Linear Regression. *Biometrics* 32 (1), 1–49. doi:10.2307/2529336

Horneffer, V., Reichelt, R., and Strupat, K. (2003). Protein Incorporation into MALDI-Matrix Crystals Investigated by High Resolution Field Emission Scanning Electron Microscopy. *Int. J. Mass Spectrom.* 226 (1), 117–131. doi:10.1016/s1387-3806(02)00979-x

Jackson, A. T., Yates, H. T., MacDonald, W. A., Scrivens, J. H., Critchley, G., Brown, J., et al. (1997). Time-lag Focusing and Cation Attachment in the Analysis of Synthetic Polymers by Matrix-Assisted Laser Desorption/ionization-Time-Of-Flight-Mass Spectrometry. *J. Am. Soc. Mass. Spectrom.* 8 (2), 132–139. doi:10.1016/s1044-0305(96)00198-5

Jørgensen, T., Bojesen, G., and Rahbek-Nielsen, H. (1998). The Proton Affinities of Seven Matrix-Assisted Laser Desorption/ionization Matrices Correlated with the Formation of Multiply Charged Ions. *Eur. J. Mass. Spectrom.* 4 (1), 39–45. doi:10.1255/ejms.189

Karas, M., and Hillenkamp, F. (1988). Laser Desorption Ionization of Proteins with Molecular Masses Exceeding 10,000 Daltons. *Anal. Chem.* 60 (20), 2299–2301. doi:10.1021/ac00171a028

Knochenmuss, R. (2003). A Quantitative Model of Ultraviolet Matrix-Assisted Laser Desorption/ionization Including Analyte Ion Generation. *Anal. Chem.* 75 (10), 2199–2207. doi:10.1021/ac034032r

Knochenmuss, R., and Zenobi, R. (2003). MALDI Ionization: The Role of In-Plume Processes. *Chem. Rev.* 103 (2), 441–452. doi:10.1021/cr0103773

Kooijman, P. C., Kok, S., and Honing, M. (2017). Independent Assessment of Matrix-Assisted Laser Desorption/ionization Mass Spectrometry (MALDI-MS) Sample Preparation Quality: Effect of Sample Preparation on MALDI-MS of Synthetic Polymers. *Rapid Commun. Mass. Spectrom.* 31 (4), 362–370. doi:10.1002/rcm.7798

Kooijman, P. C., Kok, S. J., Weusten, J. J. A. M., and Honing, M. (2016). Independent Assessment of Matrix-Assisted Laser Desorption/ionization Mass Spectrometry (MALDI-MS) Sample Preparation Quality: A Novel Statistical Approach for Quality Scoring. *Analytica Chim. Acta* 919, 1–10. doi:10.1016/j.aca.2016.03.031

Lehmann, E., Knochenmuss, R., and Zenobi, R. (1997). Ionization Mechanisms in Matrix-Assisted Laser Desorption Ionization Mass Spectrometry: Contribution of Pre-formed Ions. *Rapid Commun. Mass. Spectrom.* 11, 1483–1492. doi:10.1002/(sici)1097-0231(199709)11:14<1483::Aid-rcm982>3.0.Co;2-f

Lide, D. R. (2008). *CRC Handbook of Chemistry and Phyics*. 89th edition. Boca Raton, Florida: CRC Press.

Major, Y., Pizzala, H., Ziarelli, F., Phan, T. N. T., Mollica, G., and Charles, L. (2012). Towards the Rationalization of the MALDI Process: a Combined Mass Spectrometry/solid-State NMR Approach. *Anal. Methods* 4 (10), 3118–3126. doi:10.1039/c2ay25708d

Mele, A., and Malpezzi, L. (2000). Noncovalent Association Phenomena of 2,5-dihydroxybenzoic Acid with Cyclic and Linear Oligosaccharides. A Matrix-Assisted Laser Desorption/ionization Time-Of-Flight Mass Spectrometric and X-ray Crystallographic Study. *J. Am. Soc. Mass. Spectrom.* 11 (3), 228–236. doi:10.1016/s1044-0305(99)00143-9

Mirza, S. P., Raju, N. P., and Vairamani, M. (2004). Estimation of the Proton Affinity Values of Fifteen Matrix-Assisted Laser Desorption/ionization Matrices under Electrospray Ionization Conditions Using the Kinetic Method. *J. Am. Soc. Mass. Spectrom.* 15 (3), 431–435. doi:10.1016/j.jasms.2003.12.001

Mormann, M., Bashir, S., Derrick, P. J., and Kuck, D. (2000). Gas-phase Basicities of the Isomeric Dihydroxybenzoic Acids and Gas-phase Acidities of Their Radical Cations. *J. Am. Soc. Mass. Spectrom.* 11 (6), 544–552. doi:10.1016/s1044-0305(00)00112-4

Pizzala, H., Barrère, C., Mazarin, M., Ziarelli, F., and Charles, L. (2009). Solid State Nuclear Magnetic Resonance as a Tool to Explore Solvent-free MALDI Samples. *J. Am. Soc. Mass. Spectrom.* 20 (10), 1906–1911. doi:10.1016/j.jasms.2009.06.021

Pizzala, H., Chendo, C., and Charles, L. (2021). Using Solid-state Nuclear Magnetic Resonance to Rationalize Best Efficiency of 2,6-dihydroxybenzoic Acid over Other 2, X -dihydroxybenzoic Acid Isomers in Solvent-free Matrix-assisted Laser Desorption/ionization of Poly(ethylene Glycol). *Rapid Commun. Mass. Spectrom.* 35 (3), e8966. doi:10.1002/rcm.8966

Remily-Wood, E., Dirscherl, H., and Koomen, J. M. (2009). Acid Hydrolysis of Proteins in Matrix Assisted Laser Desorption Ionization Matrices. *J. Am. Soc. Mass. Spectrom.* 20 (11), 2106–2115. doi:10.1016/j.jasms.2009.07.007

Santiago, J., Claeys-Bruno, M., and Sergent, M. (2012). Construction of Space-Filling Designs Using WSP Algorithm for High Dimensional Spaces. *Chemometrics Intell. Lab. Syst.* 113, 26–31. doi:10.1016/j.chemolab.2011.06.003

Santner, T. J., Williams, B. J., and Notz, W. I. (2003). *The Design and Analysis of Computer Experiments*. Springer-Verlag.

Schiller, J., Süß, R., Fuchs, B., Müller, M., Petković, M., Zschörnig, O., et al. (2007). The Suitability of Different DHB Isomers as Matrices for the MALDI-TOF MS Analysis of Phospholipids: Which Isomer for what Purpose? *Eur. Biophys. J.* 36 (4-5), 517–527. doi:10.1007/s00249-006-0090-6

Skelton, R., Dubois, F., and Zenobi, R. (2000). A MALDI Sample Preparation Method Suitable for Insoluble Polymers. *Anal. Chem.* 72 (7), 1707–1710. doi:10.1021/ac991181u

Tanaka, K., Waki, H., Ido, Y., Akita, S., Yoshida, Y., Yoshida, T., et al. (1988). Protein and Polymer Analyses up Tom/z 100 000 by Laser Ionization Time-Of-Flight Mass Spectrometry. *Rapid Commun. Mass. Spectrom.* 2 (8), 151–153. doi:10.1002/rcm.1290020802

Todeschini, R., Consonni, V., Ballabio, D., and Grisoni, F. (2020). "Chemometrics for QSAR Modeling," in *Comprehensive Chemometrics*. Editors S. Brown, R. Tauler, and B. Walczak 2nd ed. (Elsevier), 599–634. doi:10.1016/b978-0-12-409547-2.14703-1

Trimpin, S., Rouhanipour, A., Az, R., Räder, H. J., and Müllen, K. (2001). New Aspects in Matrix-Assisted Laser Desorption/ionization Time-Of-Flight Mass Spectrometry: a Universal Solvent-free Sample Preparation. *Rapid Commun. Mass. Spectrom.* 15 (15), 1364–1373. doi:10.1002/rcm.372

Weidner, S., Knappe, P., and Panne, U. (2011). MALDI-TOF Imaging Mass Spectrometry of Artifacts in "dried Droplet" Polymer Samples. *Anal. Bioanal. Chem.* 401 (1), 127–134. doi:10.1007/s00216-011-4773-1

Wetzel, S. J., Guttman, C. M., Flynn, K. M., and Filliben, J. J. (2006). Significant Parameters in the Optimization of MALDI-TOF-MS for Synthetic Polymers. *J. Am. Soc. Mass. Spectrom.* 17 (2), 246–252. doi:10.1016/j.jasms.2005.11.007

Woods, R., Hope, G. A., and Watling, K. (2000). A SERS Spectroelectrochemical Investigation of the Interaction of 2-mercaptobenzothiazole with Copper, Silver and Gold Surfaces. *J. Appl. Electrochem.* 30 (11), 1209–1222. doi:10.1023/a:1026561914338

Yalcin, T., Dai, Y., and Li, L. (1998). Matrix-assisted Laser Desorption/ionization Time-Of-Flight Mass Spectrometry for Polymer Analysis: Solvent Effect in Sample Preparation. *J. Am. Soc. Mass. Spectrom.* 9 (12), 1303–1310. doi:10.1016/s1044-0305(98)00109-3

Zhang, J., Frankevich, V., Knochenmuss, R., Friess, S. D., and Zenobi, R. (2003). Reduction of Cu(II) in Matrix-Assisted Laser Desorption/ionization Mass Spectrometry. *J. Am. Soc. Mass. Spectrom.* 14 (1), 42–50. doi:10.1016/s1044-0305(02)00807-3

Conflict of Interest: The authors declare that the research was conducted in the absence of any commercial or financial relationships that could be construed as a potential conflict of interest.

Publisher's Note: All claims expressed in this article are solely those of the authors and do not necessarily represent those of their affiliated organizations, or those of the publisher, the editors and the reviewers. Any product that may be evaluated in this article, or claim that may be made by its manufacturer, is not guaranteed or endorsed by the publisher.

frontiers in Chemistry

ORIGINAL RESEARCH
published: 23 November 2021
doi: 10.3389/fchem.2021.755174

Characterizing Oligomeric Hydroxyl Silicon Oils by MALDI-TOF MS With the Pyridine-Modified Matrix

Xiaoxiao Zhang[1,2], Yan Wang[1], Yiqiu Hu[2], Cheng Guo[2], Chenghua Li[1] and Kezhi Jiang[1]**

[1]College of Material, Chemistry and Chemical Engineering, Key Laboratory of Organosilicon Chemistry and Material Technology of Ministry of Education, Hangzhou Normal University, Hangzhou, China, [2]Cancer Institute (Key Laboratory of Cancer Prevention and Intervention, China National Ministry of Education), The Second Affiliated Hospital, Zhejiang University School of Medicine, Hangzhou, China

Matrix-assisted laser desorption ionization time-of-flight mass spectrometry (MALDI-TOF) is a powerful technique for analysis of various polymers, but it is still very difficult to characterize silicone oil due to its poor ionization efficiency. In this work, oligomeric hydroxyl silicone oils were successfully characterized by MALDI-TOF, by using pyridine-modified 2,5-dihydroxylbenzoic acid (DHB) as the matrix. Furthermore, the mixed crystal of DHB and hydroxyl silicone oil was analyzed by scanning electron microscopy (SEM) and energy disperse spectroscopy (EDS), and the analytical results verified that modification with pyridine could remarkably improve the solubility of hydroxyl silicone oil in DHB, leading to the enhancement of its ionization efficiency in MALDI. The analysis of the MS spectra of a series of hydroxyl silicone oils indicated that they tended to be ionized by the attachment with Na^+, and the average molecular weight and the degree of polymerization were measured for several oligomeric hydroxyl silicon oils.

Keywords: silicon oil, MALDI-TOF, crystal structure of matrix, pyridine-modified DHB, ionization efficiency

OPEN ACCESS

Edited by:
Anna Napoli,
University of Calabria, Italy

Reviewed by:
Angela Amoresano,
Università degli Studi di Napoli Federico II, Italy
Liping Yang,
Oregon State University, United States

****Correspondence:***
Cheng Guo
cheng_guo@zju.edu.cn
Kezhi Jiang
jiangkezhi@hznu.edu.cn

Specialty section:
This article was submitted to Analytical Chemistry, a section of the journal Frontiers in Chemistry

Received: *08 August 2021*
Accepted: *04 October 2021*
Published: *23 November 2021*

Citation:
Zhang X, Wang Y, Hu Y, Guo C, Li C and Jiang K (2021) Characterizing Oligomeric Hydroxyl Silicon Oils by MALDI-TOF MS With the Pyridine-Modified Matrix. Front. Chem. 9:755174. doi: 10.3389/fchem.2021.755174

INTRODUCTION

Hydroxyl silicone oil refers to a linear polysiloxane with the Si–O–Si bond as the main chain and the silicon hydroxyl as the end group in the structure (**Figure 1**). It is usually maintained in the liquid state at ambient temperature. Owing to its plentiful merits, such as electric insulation, anti-high and -low temperatures, chemical inertia, physiological inertia, low surface tension, and water-repellent and moisture-resistant performance, silicone oil and its derivative products have been extensively applied to electricity, light industry, construction, and other fields (Chen et al., 2009; Mei et al., 2014; Aziz et al., 2018; Zhang et al., 2020). Currently, infrared (IR) spectroscopy, nuclear magnetic resonance (NMR), gel permeation chromatography (GPC), supercritical fluid chromatography (SFC), and matrix-assisted laser desorption ionization time-of-flight mass spectrometry (MALDI-TOF) are the powerful techniques to characterize silicone oil (Semchyschyn et al., 2000; Chmelik et al., 2001; Ren et al., 2019; Liu et al., 2021). GPC is a popular technique to determine the average molecular weight of polymers, but it is not suitable for the analysis of oligomeric hydroxyl silicone oils (Montaudo et al., 1995). Thus, it is essential to develop an alternative method for the characterization of the average molecular weight of oligomeric hydroxyl silicone oils.

MALDI-TOF has been widely applied for characterizing peptides, proteins, oligomers, and polymers since its invention in the 1980s, due to its high sensitivity and convenient operation (Karas et al., 1988; Tanaka et al., 1988; Li et al., 2019). The MALDI-TOF analysis can provide many

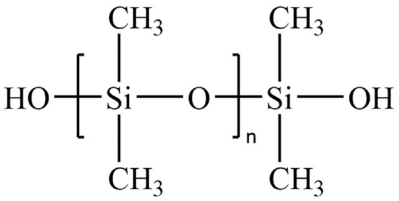

FIGURE 1 | Structure of hydroxyl silicone oil.

important information of polymers, including the repeating unit, the molecular weight distribution, and the end group (Yalcin et al., 1997; Hanton et al., 2000; Pasch et al., 2000; Bauer et al., 2002; Peacock et al., 2004). Thus, it has become an important technique to characterize oligomers or polymers (Scrivens et al., 2000; Chmelik et al., 2001; Hanton, 2001). However, silicone oil belongs to a non-polar polymer, and it is very difficult to be ionized in the MALDI source (Mautjana et al., 2012).

Interestingly, it has been reported that the addition of some organic bases could improve the homogeneous distribution of the analyte in the traditional matrix and increase the dot-to-dot reproducibility in MALDI-TOF analysis (Snovida et al., 2008). In this work, oligomeric hydroxyl silicone oils were characterized by MALDI-TOF with the pyridine-modified 2,5-dihydroxylbenzoic acid (DHB) as the matrix, and the corresponding solid crystals were analyzed by scanning electron microscopy (SEM) and energy disperse spectroscopy (EDS) in order to probe the intrinsic mechanism on the improvement of the ionization efficiency originating from the modification of the matrix with pyridine.

EXPERIMENT

Reagents and Materials

Hydroxyl silicone oils with different viscosities were purchased from Qingdao Fenghong Chemical Co., Ltd. (Shandong, China). High-performance liquid chromatography (HPLC)-grade methanol (MeOH) was purchased from Sigma-Aldrich (St. Louis, MO, United States). HPLC-grade tetrahydrofuran (THF) was purchased from Merck Millipore (Billerica, MA, United States). 2,5-Dihydroxylbenzoic acid (DHB) was purchased from Shanghai Macklin Biochemical Co., Ltd. (Shanghai, China). Sodium acetate (NaAc) and pyridine were purchased from Sinopharm (China). The water used in all experiments was prepared in a Milli-Q water purification system with a resistivity ≥18.2 MΩ cm^{-1}.

Instruments

The microflex MALDI-TOF system was produced by Bruker Corporation (Germany). The BS110S precision balance was produced by Sartorius (Germany). The YM-080S Ultrasonic Cleaner was manufactured by Fang Ao Microelectronics Co., Ltd. (Shenzhen, Guangdong, China). The Sigma 500 scanning electron microscope (SEM) was produced by Zeiss (Germany). The energy disperse spectroscopy (EDS) system was produced by EDAX (United States).

Experimental Procedure

DHB was weighted and dissolved in THF to prepare a 100 mg/mL solution. 50 μL pyridine solution was added into 1.0 mL DHB solution to prepare a solution of pyridine-modified DHB. The cationization reagent (NaAc) was weighted and dissolved in MeOH/H_2O (50:1, V:V) to prepare a 100 mM solution. Hydroxyl silicone oils were weighted separately and dissolved in THF to prepare a 1 mg/mL solution. The mixed solution was prepared by mixing the above solutions according to oligomer/matrix/NaAc (or THF) ratio (1:5:1, V/V/V), and the dissolving process was assisted by ultrasound.

In MALDI-TOF experiments, 1.0 μL mixed solution was dried on a stainless steel target at room temperature for MALDI-TOF analysis. The operating parameters of MALDI-TOF were as follows: the nitrogen laser wavelength was 337 nm and the laser pulse width was 3 ns. In the direct radiation mode, the acceleration voltage was 20.0 kV and the reflection voltage was 23.0 kV. A single scan of the mass spectrum signal was added up to 100 times.

In SEM and EDS experiments, 10.0 μL mixed solution was dropped on a tin foil to dry, and the formed dry point was sprayed with platinum to enhance its electrical conductivity. Then, the dry point was subjected to SEM and EDS analysis. The SEM analysis was carried out at the testing voltage of 3 kV under the vacuum of 5.4×10^{-8} Pa. The EDS analysis was carried out at the testing voltage of 10 kV.

RESULTS AND DISCUSSION

Effect of the Modified Matrix on the Ionization Efficiency

The 30 cP hydroxyl silicone oil was selected as a model for the MALDI-TOF analysis to investigate the effect of matrix on the ionization efficiency. As shown in **Figure 2**, the MS showed a series of equidistant peaks and an approximate *t*-distribution in the intensity of the MS signals, indicating a classical MS of the polymer. The mass gap of 74 Da for the neighboring peaks in the MS indicated the signal of silicone oil with the repeating unit of ($SiOMe_2$). With the pure DHB as the MALDI matrix (**Figure 2A**), the intensity of the silicone oil signal was about 600 at 1800 Da, while that of the corresponding noise reached 400, indicating a bad signal-to-noise ratio (S/N). At the same time, the addition of ionization agent (NaAc) into the DHB matrix could not significantly improve the ionization efficiency of the hydroxyl silicone oils in the MALDI-TOF MS (**Supplementary Figure S1**). To be interesting, the corresponding S/N increased about two times with the pyridine-modified DHB as the matrix (**Figure 2B**). What's more exciting, the noise intensity dropped to about 50, and thus, the corresponding S/N increased to 8 with the addition of some NaAc into the pyridine-modified DHB matrix. Thus, the MALDI-TOF MS was competent for structure characterization of hydroxyl silicone oils.

Similar results were obtained for MALDI-TOF analysis of the 50 cP and the 150 cP hydroxyl silicone oils (**Supplementary Figures S2 and S3**). With modification of the matrix, an enough intensive signal was produced for the MALDI-TOF MS of hydroxyl silicone oils, and thus various structural information could be obtained from the MALDI-TOF analysis.

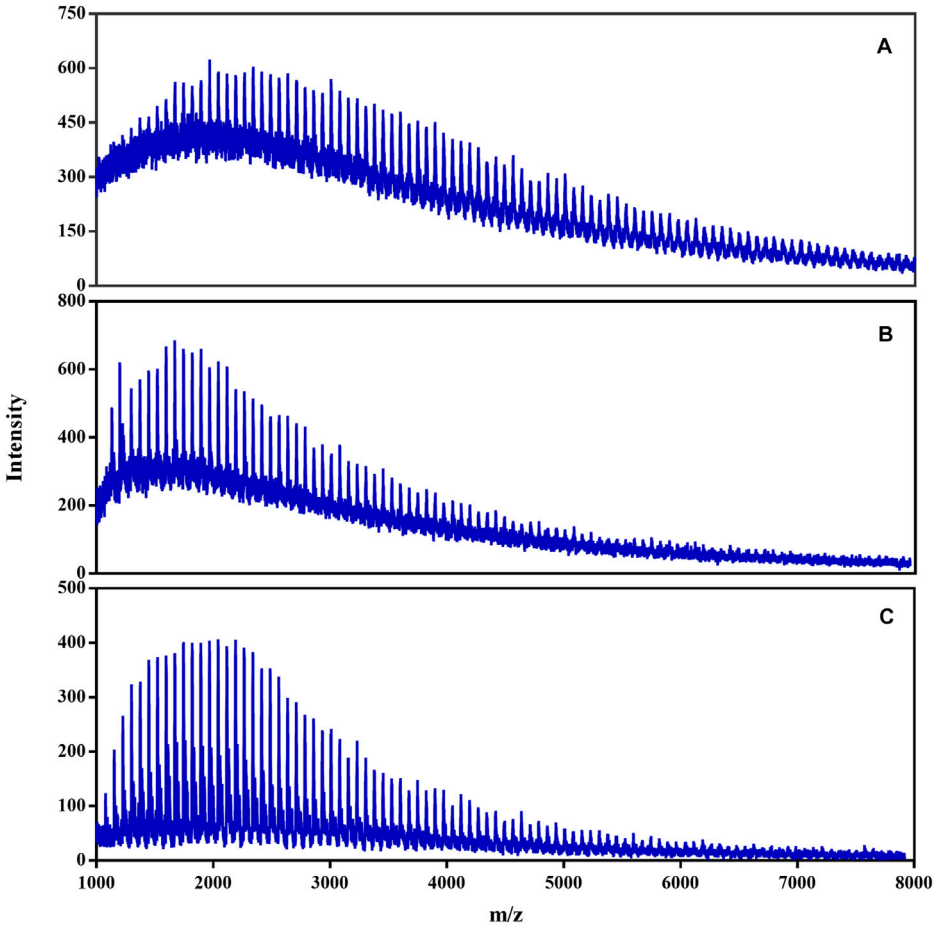

FIGURE 2 | MALDI-TOF MS of 30 cP hydroxyl silicone oil with the different matrix: A) DHB, B) pyridine-modified DHB, C) pyridine-modified DHB with the addition of NaAc.

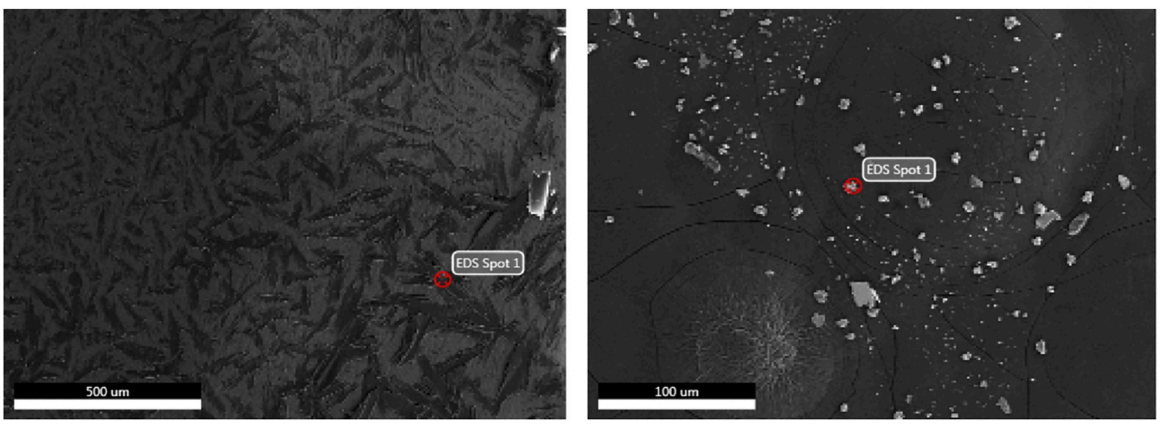

FIGURE 3 | SEM images of the schistose crystal (left) and scattered particles (right) in the mixed crystal of DHB and 30 cP hydroxyl silicone oil.

SEM and EDS Characterizing the Mixed Crystal of Matrix and Analyte

In order to further investigate the effect of matrix on the ionization efficiency, the mixed crystal of matrix and analyte was characterized by SEM and EDS. **Figure 3** shows the SEM of the mixed crystal of DHB and 30 cP hydroxyl silicone oil, in which there were full of the schistose crystal with the irregular surface and scattered particles with different diameters at the macro-scale level of 100 μm. EDS

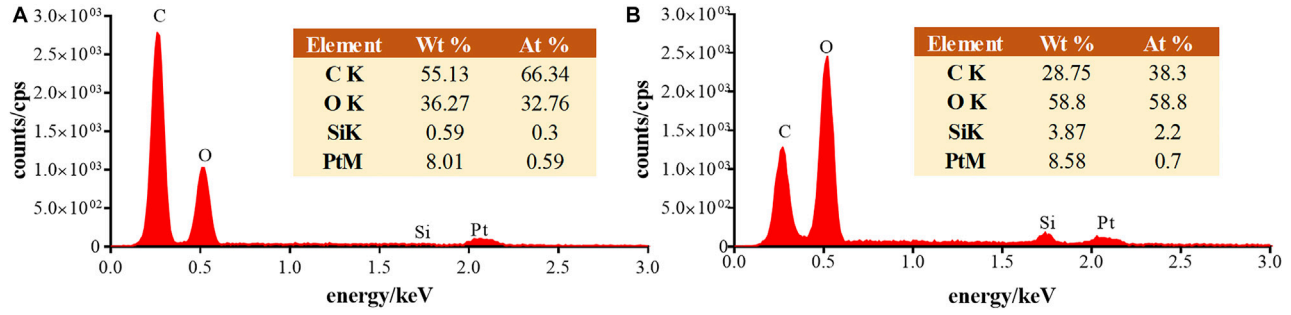

FIGURE 4 | EDS images of the schistose crystal **(A)** and the particle **(B)** in mixed crystal of DHB and 30 cP hydroxyl silicone oil.

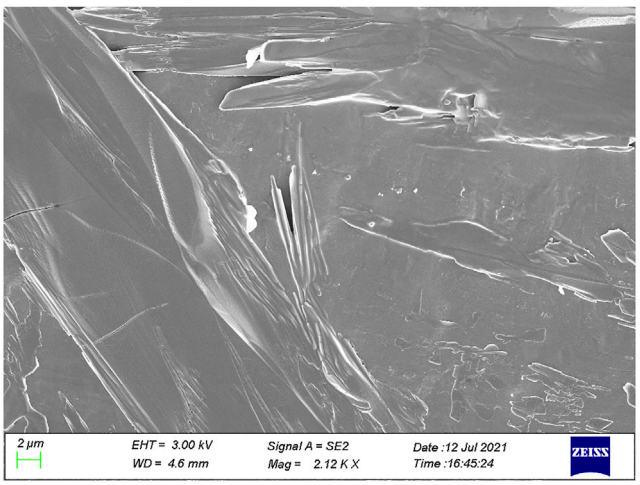

FIGURE 5 | SEM image (at the 2 µm level) of the mixed crystal of DHB and 30 cP hydroxyl silicone oil.

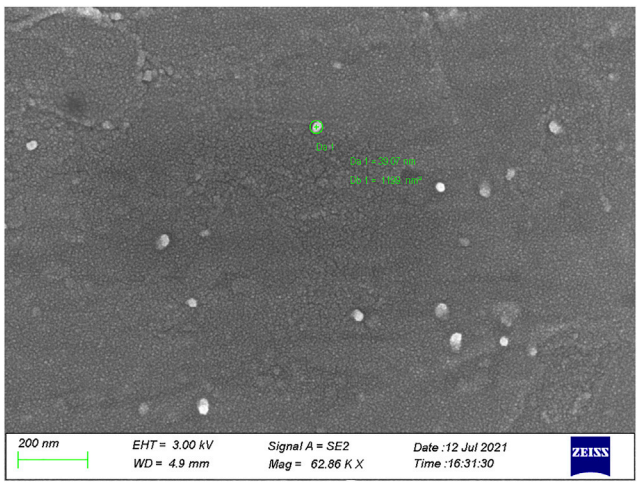

FIGURE 6 | SEM image (at the 200 nm level) of the mixed crystal of the pyridine-modified DHB and 30 cP hydroxyl silicone oil.

analysis of the schistose crystals (**Figure 4A**) showed the main elements of C and O, indicating the identity of compound DHB. In contrast, there was significantly more content of both O and Si in the EDS of the particle (**Figure 4B**), which was consistent with the identity of hydroxyl silicone oil. Thereby, the silicone oil was heterogeneously distributed in the DHB matrix.

Further magnification of the mixed crystal at a scale level of 2 µm resulted in many irregular tabular crystals with the obvious interface (**Figure 5**). The corresponding width was found at the µm-scale level. Similarly, the addition of NaAc into DHB did not significantly change the shape of the mixed crystal of matrix and analyte (**Supplementary Figure S4**). The above experimental results indicated that DHB had poor solubility with hydroxyl silicone oil, and thus, poor ionization efficiency was obtained for MALDI-TOF analysis of hydroxyl silicone oil with the pure DHB as the matrix.

On the contrary, mixing DHB with pyridine obviously changed the shape of the mixed crystal of matrix and analyte. As shown in **Figure 6**, the crystal structure almost disappeared, and the image was filled with kinds of crystal particles. The large particles had the diameters of only 39 nm. In addition, there were much more particles with the diameters less than 10 nm, which is almost near the size of a molecule. Similarly, the addition of NaAc also did not obviously change the shape of the mixed crystal of matrix and analyte, in which many scattered crystal particles had diameters of 38 nm and much more particles showed diameters less than 10 nm (**Supplementary Figure S5**). The above experimental results showed that the mixture of hydroxyl silicone oil in the pyridine-modified DHB matrix was more uniform, in which the crystal cluster diameters decreased and the solubility increased obviously. As a result, it is much easier for the matrix to transfer the absorbed laser energy to the analyte in the process of ionization. Thereby, much better ionization efficiency was obtained for hydroxyl silicone oil, when using pyridine-modified DHB as the MALDI-TOF matrix.

Characterization of Oligomeric Hydroxyl Silicone Oils

According to the optimized experimental parameters, various oligomeric hydroxyl silicone oils were characterized by MALDI-

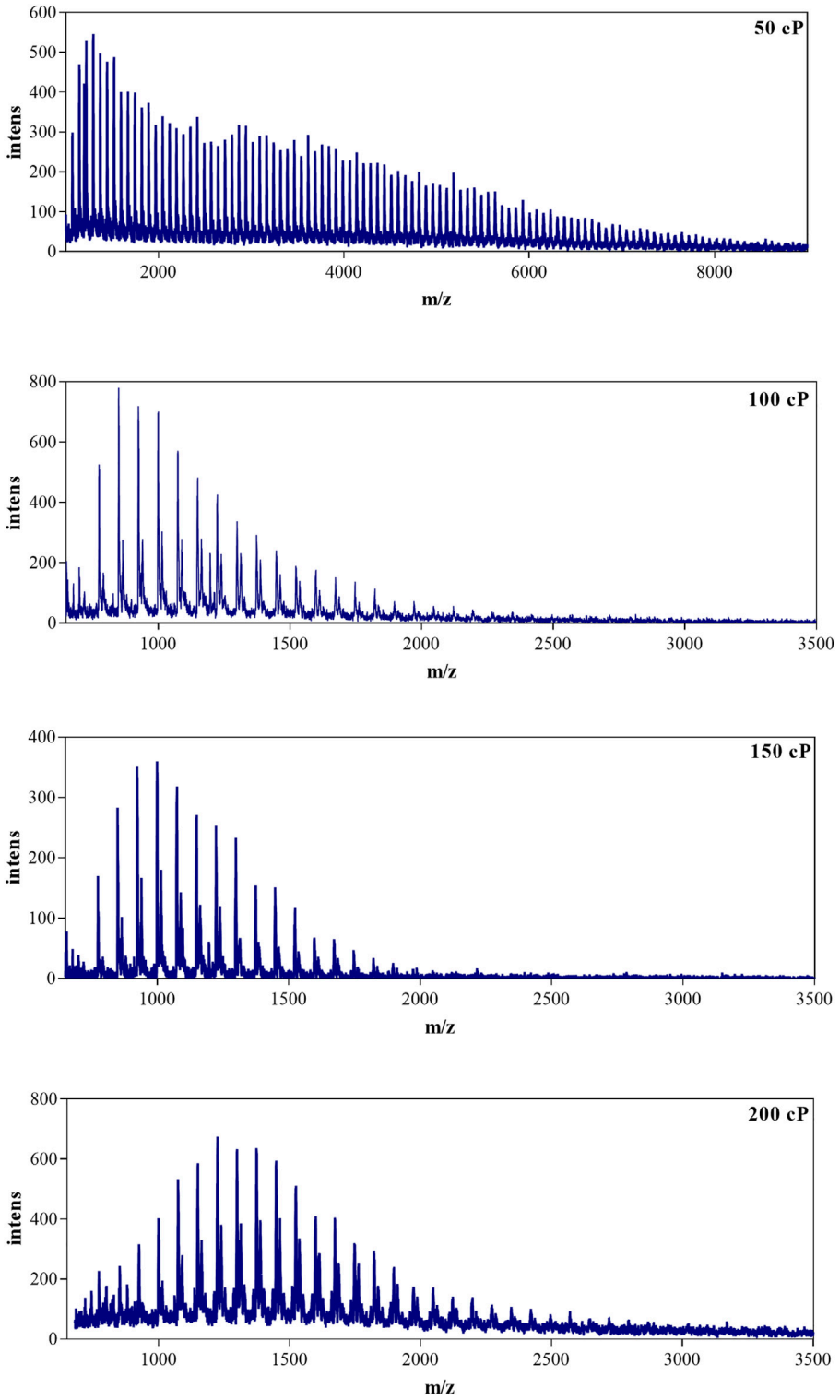

FIGURE 7 | MALDI-TOF MS of hydroxyl silicone oils (50 cP, 100cP, 150cP and 200 cP) with the matrix of DHB modified by pyridine and NaAc.

TOF (**Figure 2C** and **Figure 7**). As can be seen, the *m/z* ratio of 30 cP hydroxyl silicone oil mainly ranges from 1,000 to 7,000, and the MS data of the typical 30 cP hydroxyl silicone oil are listed in **Table 1**. The mass gap (74 Da) of the neighboring peaks in the MS indicates the repeating unit of ($SiOMe_2$). The identity of the attached Na^+ can give a reasonable ascription of all the

TABLE 1 | MALDI-TOF MS data of 30 cP hydroxyl silicone oil.

$[M + Na]^+$ *m/z*	Chemical formula	Intensity	$(M + Na)^+$ *m/z*	Chemical formula	Intensity
1,078	C28H86O15Si14Na	124	2,710	C72H218O37Si36Na	291
1,153	C30H92O16Si15Na	203	2,784	C74H224O38Si37Na	268
1,227	C32H98O17Si16Na	266	2,858	C76H230O39Si38Na	259
1,301	C34H104O18Si17Na	324	2,933	C78H236O40Si39Na	237
1,375	C36H110O19Si18Na	329	3,007	C80H242O41Si40Na	242
1,449	C38H116O20Si19Na	369	3,081	C82H248O42Si41Na	221
1,523	C40H122O21Si20Na	374	3,155	C84H254O43Si42Na	189
1,597	C42H128O22Si21Na	377	3,229	C86H260O44Si43Na	220
1,671	C44H134O23Si22Na	376	3,303	C88H266O45Si44Na	189
1745	C46H140O24Si23Na	399	3,377	C90H272O46Si45Na	167
1819	C48H146O25Si24Na	400	3,451	C92H278O47Si46Na	161
1894	C50H152O26Si25Na	400	3,526	C94H284O48Si47Na	151
1968	C52H158O27Si26Na	404	3,600	C96H290O49Si48Na	149
2043	C54H164O28Si27Na	407	3,674	C98H296O50Si49Na	129
2,117	C56H170O29Si28Na	394	3,748	C100H302O51Si50Na	148
2,191	C58H176O30Si29Na	406	3,822	C102H308O52Si51Na	129
2,265	C60H182O31Si30Na	389	3,896	C104H314O53Si52Na	130
2,339	C62H188O32Si31Na	383	3,970	C106H320O54Si53Na	130
2,414	C64H194O33Si32Na	351	4,045	C108H326O55Si54Na	99
2,488	C66H200O34Si33Na	351	4,119	C110H332O56Si55Na	122
2,562	C68H206O35Si34Na	338	4,193	C112H338O57Si56Na	111
2,636	C70H212O36Si35Na	299	4,267	C114H344O58Si57Na	95

TABLE 2 | M_n, M_w, and *PD* of silicone oils with different viscosities.

Sample/viscosity	M_n	M_w	*PD*	Si-OH%
30 cP	2,383	2,658	1.12	1.61
50 cP	3,185	3,924	1.23	1.38
100 cP	1,135	1,215	1.07	3.19
150 cP	1,151	1,201	1.04	2.90
200 cP	1,460	1,554	1.06	2.48

signal in the MS of the hydroxyl silicone oil, which agrees well with the fact that it tends to be ionized by the attachment with Na^+.

Thus, the number-average molecular weight (M_n), weight-average molecular weight (M_w), dispersity (*PD*), and hydroxyl content of silicone oils (Si-OH%) were calculated to be 2,276, 2,553, 1.12, and 1.68, respectively, according to the following formula:

$$M_n = \sum(n_i \times M_i)/\sum n_i,$$
$$M_w = \sum(n_i \times M_i^2)/\sum(n_i \times M_i),$$
$$PD = M_w/M_n,$$
$$OH\% = \sum((n_i/\sum n_i)/ \times 34/M_i) \times 100\%,$$

Here, n_i and M_i refer to the MS intensity and molecular weight of any component i of the oligomer.

50 cP hydroxyl silicone oil has the same mass gap (74 Da) of the neighboring peaks in the MS, but it shows a different mass distribution with a wider mass range (1,000–9,000 Da). As shown in **Table 2**, 50 cP hydroxyl silicone oil has a higher molecular weight, more dispersity, and less hydroxyl content.

As displayed in **Figure 7**, there are two series of peaks in the MS of 100, 150, and 200 cP silicone oils. The mass gap for the adjacent peaks is also 74 Da ($SiOMe_2$) in each series of MS peaks. The main series of equidistant peaks is 16 Da less in molecular weight than the corresponding minor series of equidistant peaks, indicating that ionization of hydroxyl silicone oil by the attachment with Na^+ results in the main one in the MALDI-TOF MS, and attachment with K^+ results in the minor one. K^+ originates from the residue catalyst (KOH) in the polymerization process. Also, the corresponding parameters of their main sequence peaks mass distribution are listed in **Table 2**.

Similarly, M_n, M_w, *PD*, and Si-OH% of several oligomeric hydroxyl silicone oils were also calculated and are summarized in **Table 2**. As can be seen, the hydroxyl silicone oils of 100 cP, 150 cP, and 200 cP have relatively higher viscosity than 30 cP and 50 cP, but they show much lower molecular weight (~1,000 Da vs. ~ 3,000 Da). Thus, molecular weight is not the deciding factor for the viscosity of the oligomeric hydroxyl silicone oil. The results indicate that the content of the silicon hydroxyl group, which results in the formation of an intermolecular hydrogen bond, exerts more influences on their viscosity (**Table 2**).

CONCLUSION

In this work, the hydroxyl silicone oils have been successfully characterized by MALDI-TOF MS. The effects of the addition of pyridine and cationic reagent into matrix on the characterization of silicone oil were investigated. The results showed that the addition of pyridine and NaAc was beneficial to MALDI-TOF

MS detection of hydroxyl silicone oils. The reduced baseline, the increased S/N, and a beautiful peak shape were obtained. Furthermore, the mixed crystal of matrix and 30 cP hydroxyl silicone oil was subjected to SEM and EDS analysis, and the results verified that addition with pyridine promotes the homogeneity of the crystal of DHB and silicone oil. Finally, several oligomeric hydroxyl silicone oils were characterized by MALDI-TOF MS, and the corresponding molecular weight and degree of polymerization were calculated, and the results indicated that the content of the silicon hydroxyl group, rather than the molecular weight, exerts obvious influences on their viscosity.

DATA AVAILABILITY STATEMENT

The original contributions presented in the study are included in the article/**Supplementary Materials**, further inquiries can be directed to the corresponding author KJ, jiangkezhi@hznu.edu.cn.

ETHICS STATEMENT

This research was based on characterizing silicon oils by MALDI-TOF MS with the modified matrix. No human or animal blood samples were used, and thus, ethics approval was not required as per institutional and national guidelines.

AUTHOR CONTRIBUTIONS

KJ and CG initiated the study, supervised the study, and discussed the results. XZ, YH, and KJ contributed to method development and performed the experiment. XZ, CL, and YW contributed to data acquisition and performed the analysis. KJ and YW contributed to analysis and interpretation of the data. XZ and KJ contributed to the drafting of the manuscript. All the authors have accepted responsibility for the entire content of this submitted manuscript and approved the submission.

FUNDING

The authors gratefully acknowledge the financial support from the Analysis and Detection Foundation of Science and Technology Department in Zhejiang Province, China (Grant Nos. LGC21B050009 and LGC19B050008).

SUPPLEMENTARY MATERIAL

The Supplementary Material for this article can be found online at: https://www.frontiersin.org/articles/10.3389/fchem.2021.755174/full#supplementary-material

REFERENCES

Aziz, T., Fan, H., Khan, F. U., Haroon, M., and Cheng, L. (2018). Modified Silicone Oil Types, Mechanical Properties and Applications. *Polym. Bull.* 76, 2129–2145. doi:10.1007/s00289-018-2471-2

Bauer, B. J., Byrd, H. C. M., and Guttman, C. M. (2002). Small Angle Neutron Scattering Measurements of Synthetic Polymer Dispersions in Matrix-Assisted Laser Desorption/ionization Matrixes. *Rapid Commun. Mass. Spectrom.* 16, 1494–1500. doi:10.1002/rcm.737

Chen, X., and Jiao, C. (2009). Synergistic Effects of Hydroxy Silicone Oil on Intumescent Flame Retardant Polypropylene System. *Fire Saf. J.* 44, 1010–1014. doi:10.1016/j.firesaf.2009.06.008

Chmelík, J., Planeta, J., Řehulka, P., and Chmelík, J. (2001). Determination of Molecular Mass Distribution of Silicone Oils by Supercritical Fluid Chromatography, Matrix-Assisted Laser Desorption Ionization Time-Of-Flight Mass Spectrometry and Their Off-Line Combination. *J. Mass. Spectrom.* 36, 760–770. doi:10.1002/jms.179

Hanton, S. D., and Liu, X. M. (2000). GPC Separation of Polymer Samples for MALDI Analysis. *Anal. Chem.* 72, 4550–4554. doi:10.1021/ac000095n

Hanton, S. D. (2001). Mass Spectrometry of Polymers and Polymer Surfaces. *Chem. Rev.* 101, 527–570. doi:10.1021/cr9901081

Karas, M., and Hillenkamp, F. (1988). Laser Desorption Ionization of Proteins with Molecular Masses Exceeding 10,000 Daltons. *Anal. Chem.* 60, 2299–2301. doi:10.1021/ac00171a028

Li, Z., Liu, Q., Lu, X., Deng, C., Sun, N., and Yang, X. (2019). Magnetic Metal-Organic Framework Nanocomposites for Enrichment and Direct Detection of Environmental Pollutants by Negative-Ion Matrix-Assisted Laser Desorption/ionization Time-Of-Flight Mass Spectrometry. *Talanta* 194, 329–335. doi:10.1016/j.talanta.2018.10.058

Liu, J., Ronk, M., Fujimori, K., Lee, H., and Nashed-Samuel, Y. (2021). Analysis of Silicone Oil in Prefilled Syringes and Biopharmaceutical Drug Products Using High-Performance Liquid Chromatography. *AAPS PharmSciTech* 22, 75. doi:10.1208/s12249-021-01947-6

Mautjana, N. A., and Pasch, H. (2012). Matrix-Assisted Laser Desorption Ionization Mass Spectrometry of Synthetic Polymers. *Macromol. Symp.* 313-314, 157–161. doi:10.1002/masy.201250317

Mei, S. F., Gao, Y. X., Deng, Z. S., and Liu, J. (2014). Thermally Conductive and Highly Electrically Resistive Grease through Homogeneously Dispersing Liquid Metal Droplets inside Methyl Silicone Oil. *J. Electron. Packaging* 136. doi:10.1115/1.4026414

Montaudo, G., Montaudo, M. S., Puglisi, C., and Samperi, F. (1995). Characterization of Polymers by Matrix-Assisted Laser Desorption/ionization Time-Of-Flight Mass Spectrometry: Molecular Weight Estimates in Samples of Varying Polydispersity. *Rapid Commun. Mass. Spectrom.* 9, 453–460. doi:10.1002/rcm.1290090514

Pasch, H., and Ghahary, R. (2000). Analysis of Complex Polymers by MALDI-TOF Mass Spectrometry. *Macromol. Symp.* 152, 267–278. doi:10.1002/1521-3900(200003)152:1<267:aid-masy267>3.0.co;2-n

Peacock, P. M., and McEwen, C. N. (2004). Mass Spectrometry of Synthetic Polymers. *Anal. Chem.* 76, 3417–3428. doi:10.1021/ac040064i

Ren, F., Xu, Q., Zhou, Z., Xu, W., and Ma, H. (2019). Synthesis and Characterization of High Heat Resistant Hydroxyl Silicone Oil with Boron and Sulfoxide in Backbone. *Silicon* 12, 2203–2210. doi:10.1007/s12633-019-00313-3

Scrivens, J. H., and Jackson, A. T. (2000). Characterisation of Synthetic Polymer Systems. *Int. J. Mass Spectrom.* 200, 261–276. doi:10.1016/s1387-3806(00)00322-5

Semchyschyn, D. J., and Macdonald, P. M. (2000). Limits of Detection of Polydimethylsiloxane in29Si NMR Spectroscopy. *Magn. Reson. Med.* 43, 607–610. doi:10.1002/(sici)1522-2594(200004)43:4<607:aid-mrm17>3.0.co;2-i

Snovida, S. I., Rak-Banville, J. M., and Perreault, H. (2008). On the Use of DHB/aniline and DHB/N,N-dimethylaniline Matrices for Improved Detection of Carbohydrates: Automated Identification of Oligosaccharides and Quantitative Analysis of Sialylated Glycans by MALDI-TOF Mass Spectrometry. *J. Am. Soc. Mass. Spectrom.* 19, 1138–1146. doi:10.1016/j.jasms.2008.04.033

Tanaka, K., Waki, H., Ido, Y., Akita, S., Yoshida, Y., Yoshida, T., et al. (1988). Protein and Polymer Analyses up Tom/z 100 000 by Laser Ionization Time-Of-

Flight Mass Spectrometry. *Rapid Commun. Mass. Spectrom.* 2, 151–153. doi:10.1002/rcm.1290020802

Yalcin, T., Schriemer, D. C., and Li, L. (1997). Matrix-assisted Laser Desorption Ionization Time-Of-Flight Mass Spectrometry for the Analysis of Polydienes. *J. Am. Soc. Mass. Spectrom.* 8, 1220–1229. doi:10.1016/s1044-0305(97)00192-x

Zhang, Y., Liu, Z., Liu, Z., and Yao, L. (2020). Mechanical Properties of High-Ductility Cementitious Composites with Methyl Silicone Oil. *Mag. Concrete Res.* 72, 747–756. doi:10.1680/jmacr.18.00192

Conflict of Interest: The authors declare that the research was conducted in the absence of any commercial or financial relationships that could be construed as a potential conflict of interest.

Publisher's Note: All claims expressed in this article are solely those of the authors and do not necessarily represent those of their affiliated organizations, or those of the publisher, the editors, and the reviewers. Any product that may be evaluated in this article, or claim that may be made by its manufacturer, is not guaranteed or endorsed by the publisher.

frontiers in Chemistry

ORIGINAL RESEARCH
published: 15 December 2021
doi: 10.3389/fchem.2021.786283

Quantifying the Matrix Metalloproteinase 2 (MMP2) Spatially in Tissues by Probe via MALDI Imaging Mass Spectrometry

Daojiang Yu[1]†, Peng Lai[2]†, Tao Yan[1], Kai Fang[1], Lei Chen[1] and Shuyu Zhang[1,3]**

[1]The Second Affiliated Hospital of Chengdu Medical College, China National Nuclear Corporation 416 Hospital, Chengdu, China, [2]Department of Endocrinology, Xuzhou Center Hospital, Xuzhou, China, [3]Department of Oncology, The Affiliated Changzhou No. 2 People's Hospital of Nanjing Medical University, Changzhou, China

As a matrix metalloproteinase, the abnormal expression of MMP2 is associated with multiple biological processes, including tissue remodeling and cancer progression. Therefore, spatial analysis of MMP2 protein in tissues can be used as an important approach to evaluate the expression distribution of MMP2 in complex tissue environments, which will help the diagnosis and treatment of various diseases, including tissue or organ injuries. Moreover, this analysis will also help the evaluation of prognoses. However, MMP2 is difficult to be spatially determined by MALDI TOF mass spectrometry due to its large molecular weight (over 72 KD) and low content. Therefore, a new method should be developed to help this detection. Here, we have designed a specific MMP2 probe that closely binds to MMP2 protein in tissue. This probe has a Cl on Tyr at the terminal, which can provide two isotope peaks to help the accuracy quantitative of MMP2 protein. Based on this, we used the probe to determine the spatial expression of MMP2 in the tissues based on MALDI TOF mass spectrometry. This approach may help to study the influence of multifunctional proteases on the degree of malignancy *in vivo*.

Keywords: MMP2, MALDI-TOF/MS, spatial quantitative protein detection, tumor, tissue remodeling

OPEN ACCESS

Edited by:
Cheng Guo,
Zhejiang University, China

Reviewed by:
Samuel M Meier-Menches,
University of Vienna, Austria
Fei Fang,
Michigan State University, United States
Jie Tan,
Hunan University, China

***Correspondence:**
Daojiang Yu
ydj51087@163.com
Shuyu Zhang
zhang.shuyu@hotmail.com

†*These authors have contributed equally to this work*

Specialty section:
This article was submitted to Analytical Chemistry, a section of the journal Frontiers in Chemistry

Received: *30 September 2021*
Accepted: *25 November 2021*
Published: *15 December 2021*

Citation:
Yu D, Lai P, Yan T, Fang K, Chen L and Zhang S (2021) Quantifying the Matrix Metalloproteinase 2 (MMP2) Spatially in Tissues by Probe via MALDI Imaging Mass Spectrometry. Front. Chem. 9:786283. doi: 10.3389/fchem.2021.786283

INTRODUCTION

Matrix metalloproteinases (MMPs) are a superfamily of zinc-containing endopeptidases. MMPs play vital roles in the degradation of extracellular matrix components. They are also involved in various types of physical processes such as cell proliferation, migration, differentiation, apoptosis, and angiogenesis by interacting with certain cytokines and chemokine (Griselda et al., 2020). These processes occur to promote tissue or organ regeneration through actively remodeling. Moreover, the abnormal expression of MMPs would lead to serious diseases. For example, MMP2 can regulate tissue remodeling, a normal process in which old bone is broken down and new bone is created to replace it. At least eight mutations in the MMP2 gene have been documented to cause multicentric osteolysis, nodulosis, and arthropathy (MONA). In addition, MMP2 was also reported to be over expressed in several solid tumors, including gastric carcinoma, breast carcinoma, lung cancer, etc (Montalban-Arques and Scharl, 2019, Weng et al., 2019, Zhang D et al., 2019). Hence, it is of great importance to locate the expression MMP2 in complex tissues.

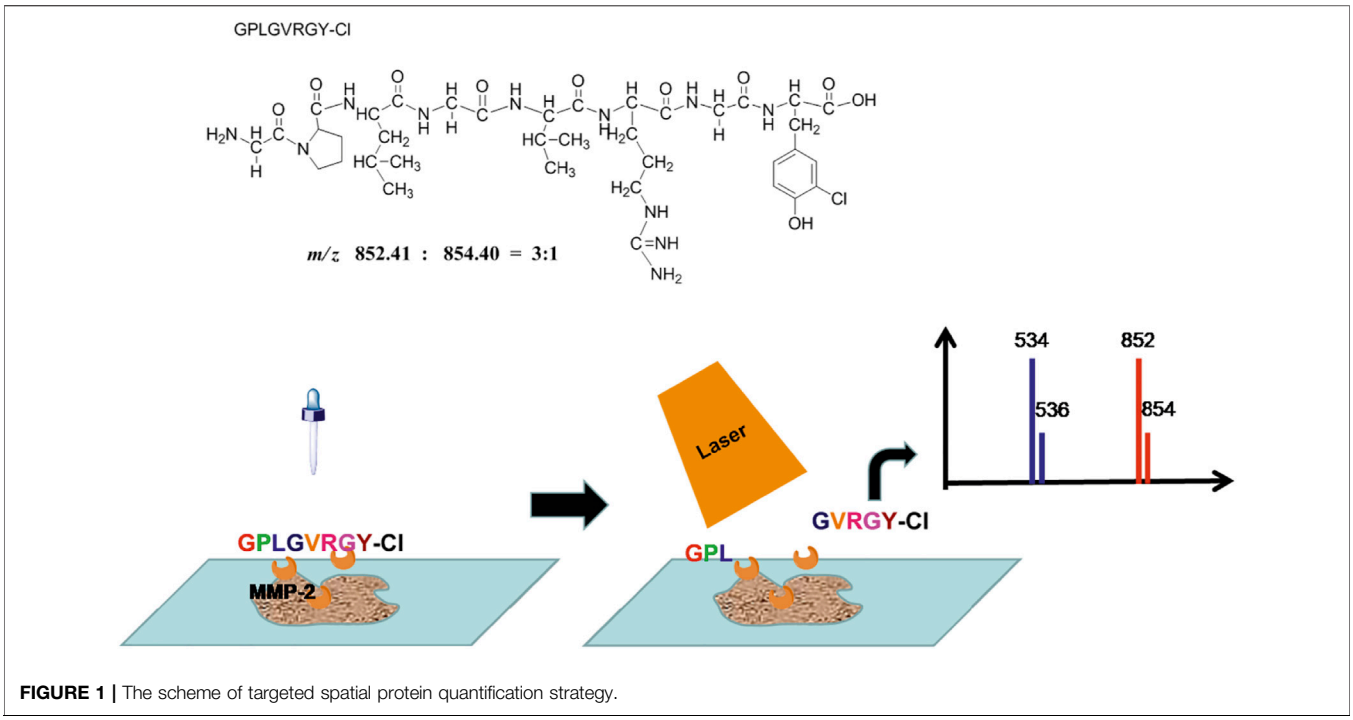

FIGURE 1 | The scheme of targeted spatial protein quantification strategy.

Matrix-assisted laser desorption/ionization mass spectrometry (MALDI MS) has become a powerful means of detection technology, which achieved more and more attention by clinical researchers (Barre et al., 2019; Balluff et al., 2021). Based on this method, even the spatial location of biomarkers in the organization can be provided by means of visualization (Shariatgorji et al., 2019). At present, this technique has successfully achieved the spatial analysis of small molecules, such as amino acids, lipids, nucleic bases, and partial macro-molecules, containing peptides and proteins (Moore et al., 2019; Boskamp and Soltwisch, 2020). However, it also has difficulty in the detection of proteins due to their large molecular weight and low content (Ryan et al., 2019). Although the MALDI technique is suitable for the detection of macromolecules, its sensitivity and resolution would decrease significantly when detecting proteins with a molecular weight greater than 20 KDa (Zhang et al., 2019b). The MMP2 protein has a molecular weight of 72 kDa, which would provide challenges for MALDI spatial detection.

Herein, we have developed a strategy for the MMP2 MALDI spatial protein quantification determination. A peptide probe was designed containing the MMP2 digestion sequence. This peptide also had a chlorine atom on Tyr at the peptide terminal, which could provide two isotopes to increase detection accuracy. This peptide probe can be digested by MMP2 into a fragment containing isotope, and the content of MMP2 can be obtained according to the proportion between fragment and original probe. Additionally, this method has been successfully applied to the MMP2 imaging detection in CRC tissues, which can provide help for the prognoses and clinical medication of patients.

MATERIALS AND METHODS

The peptide probe was synthesized by BANKPEPTIDE Biological Technology CO (Anhui, China), with the Cl in the benzene ring of tyrosine at the C terminal. O-carboxy cinnamic acid (CHCA) was used as the matrix for MALDI analysis and purchased from Merck (United States). Acetonitrile (ACN) was analytically pure and purchased from Sinopharm Technology CO (Shanghai, China).

A total of 20 couples of human cancer and tumor-adjacent tissues were collected from CRC patients in the form of frozen sections. These tissues are slices left from clinical biopsies. All samples were obtained with informed consent under a protocol approved by the Second Affiliated Hospital of Chengdu Medical College (No. E2021015). Patients' clinical information and pathological results were also recorded.

All tissues were sectioned at 10 μm thickness and -20 C using a Leica cryostat (Leica Microsystems, Wetzlar Germany) and traw mounted onto indium tin oxide (ITO)- coated glass slides (4–8 Ω resistance, Delta Technologies, United States) and stored at -80°C until analyzed.

For tissue targeted spatial protein quantification experiments, three layers of peptide prove (0.5 mg/ml prepared in 10% MeOH with 0.1% TFA) were sprayed onto the tissue sections. The investigation used 5 μg/ml of probe, so the incubation time was 15 min at room temperature. Then three layers of CHCA (10 mg/ml prepared in 80% ACN) were sprayed onto the tissue sections after incubation.

MALDI analysis was carried out by Bruker ultrafleXtreme MALDI TOF/TOF (Bruker Daltonik, Bremen, Germany) with

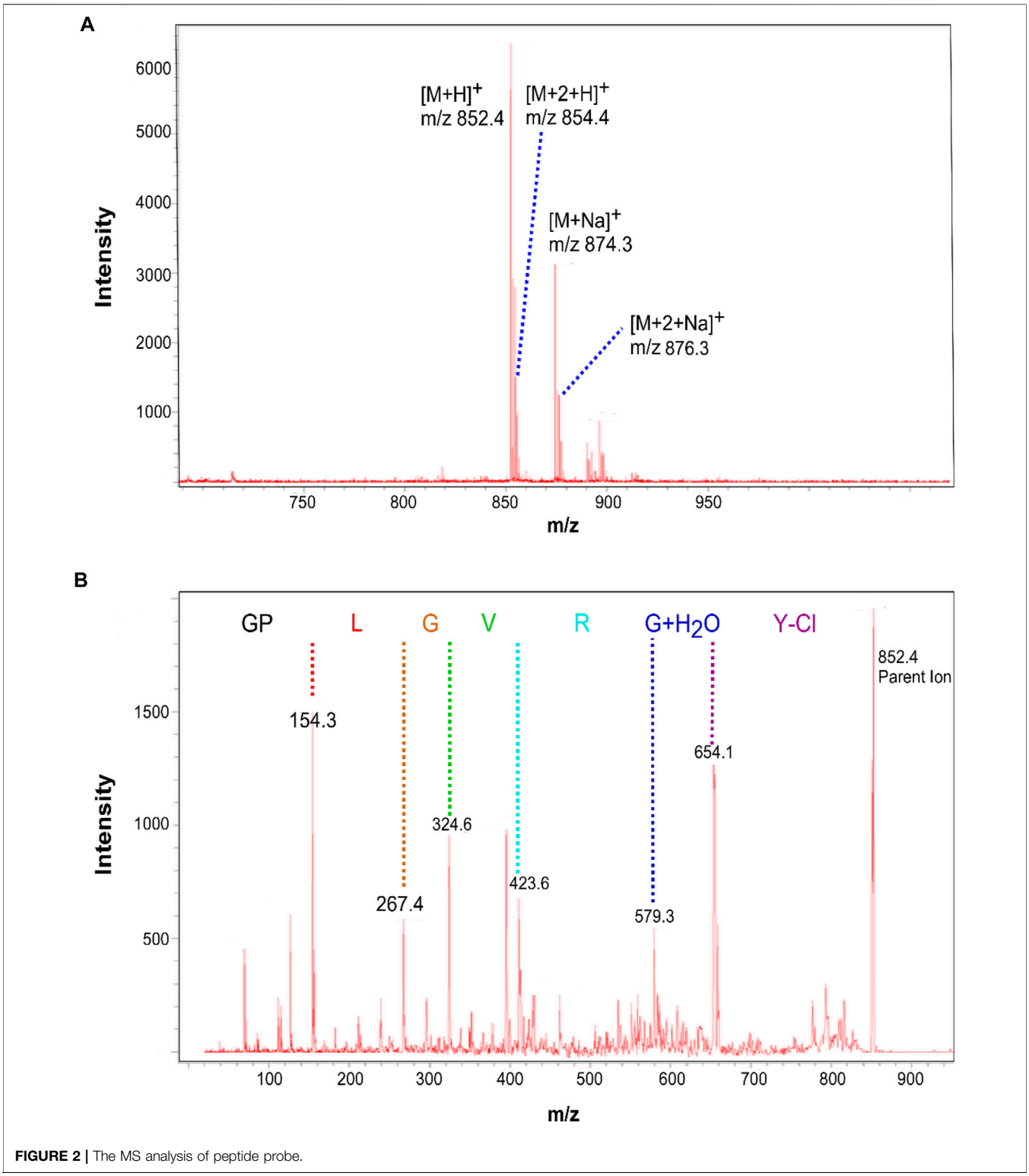

FIGURE 2 | The MS analysis of peptide probe.

a positive ion mode (delay: 150 ns; ion source one voltage: 20 kV; ion source two voltage: 18 kV; lens voltage: 6 kV). All spectra were shown baseline-subtracted, smoothed, and auto-scaled in the *Y*-direction, covering a range of 300–3,000 Da, with *X*-axis scale increments of 1Da.

RESULTS

The whole strategy of this method was shown in **Figure 1**. In our analysis strategy, a peptide probe was synthesized as the substrate of MMP2. For specific identification of this probe in MALDI mass

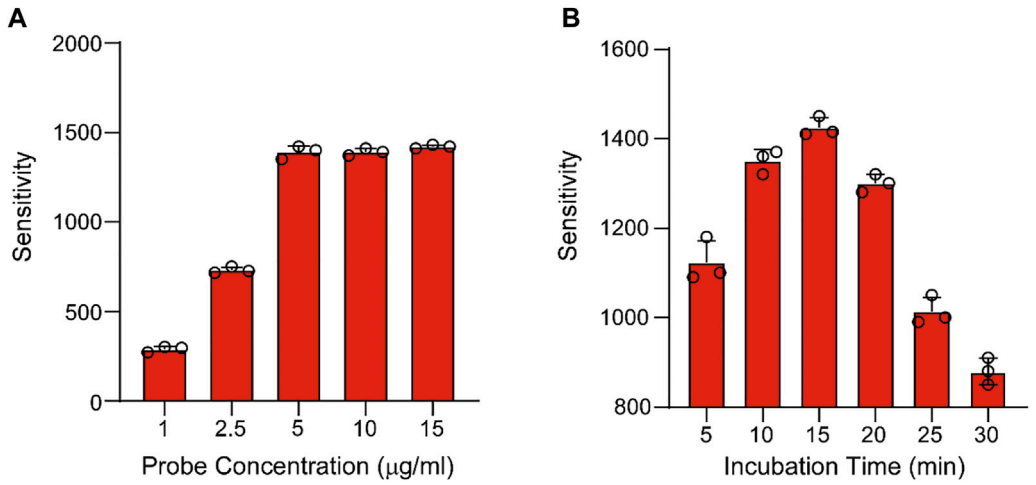

FIGURE 3 | The optimization of the amount **(A)** and incubation time **(B)** of probe.

TABLE 1 | clinicopathological features of patients with CRC included in this study.

Parameters	n = 20
Age (median, range, years)	62 (28–74)
Gender	
Male	12 (60%)
Female	8 (40%)
Infiltration depth	
T1 + T2	6 (30%)
T3 + T4	14 (70%)
Lymph node metastasis	
Yes	13 (65%)
No	7 (35%)
Distant metastasis	
Yes	4 (20%)
No	16 (80%)
AJCC TNM Stage	
I + II	6 (30%)
III + IV	14 (70%)

spectrometry, Cl was used binding to the tyrosine terminal, which provided a $[M+2]^+$ peak with abundance of 30%. Then the probe can be digested by MMP2 in the tissues and a couple of peaks were detected in MALDI MS (*m/z* 534 and 536 for enzyme-digested product, *m/z* 852 and 854 for peptide probe). Moreover, the ratio between 534 and 852 reflect the amount of peptide probe before and after enzymatic hydrolysis, which can further show the degree of enzymatic hydrolysis, indicating the concentration of MMP2. Thus, this ratio can be considered as the potential biomarker for the quantitative determination of MMP2.

In the experiment, the peptide probe was firstly identified by MALDI MS. From the result (**Figure 2**), $[M + H]^+$ (*m/z* 852) and $[M + Na]^+$ (*m/z* 874) peaks were found with the isotope peaks $[M+2 + H]^+$ (*m/z* 854) and $[M+2 + Na]^+$ (*m/z* 876), which indicated the probe was successfully synthesized. In addition, tandem mass result showed that the sequence accuracy of the peptide probe. Then, the digestion effect was investigated *in vitro*. The peptide was incubated by MMP2 enzyme and the digestion products were detected by MS. From the results, the probe was successfully digested by MMP2, with two products in sequence of GPL (*m/z* 335) and GVRGY-Cl (*m/z* 534).

After *in vitro* experiment, the peptide probe was applied into the *in vivo* experiment for colon cancer tissues. The concentration of probe and the incubation time were also optimized beforehand. The peptide probe was dissolved into 10% MeOH with 0.1% TFA and sprinkled onto the tissues. Then the tissues were put into the MALDI MS to detect the sensitivity of product peak. For probe concentration optimization, five types of concentration, including 1, 1.5, 5, 10, and 15 μg/ml were studied respectively. When the concentration of probe was over 5 μg/ml, the sensitivity of the product remained unchanged, indicating that the optimal concentration of probe was 5 μg/ml (**Figure 3A**). Next, the incubation time was also optimized. In this investigation, six incubation times, containing 5, 10, 15, 20, 25, and 30 min were compared, in which 15 min achieved the best sensitivity of product peak (**Figure 3B**). After method optimization, the method validation was also processed by tissue samples. From our results of probe detection in tissues, the LOD was 50 ng/ml and the LOQ was 150 ng/ml from tissue samples. The LOD and the LOQ were 10 ng/ml and 30 ng/ml from the blank slides. Moreover, the method validation showed the recovery was over 50%. Since we are testing a pair of peaks, there is almost no false-discovery.

Finally, MMP2 was reported to be over-expression in several solid tumors, including CRC, gastric carcinoma, breast carcinoma, and lung cancer, etc (Fouad et al., 2019; Ramezani et al., 2020). It has also been reported that MMP2 played a crutial role in tumor invasion and metastasis. For the further understanding its mechanism, the position of MMP2 in tumor tissues need to be determined (Zhang et al., 2019a). Thus, 20 sets of tissue samples from colon cancer patients were collected to prove the ability of our methods. As shown in **Table 1**, the

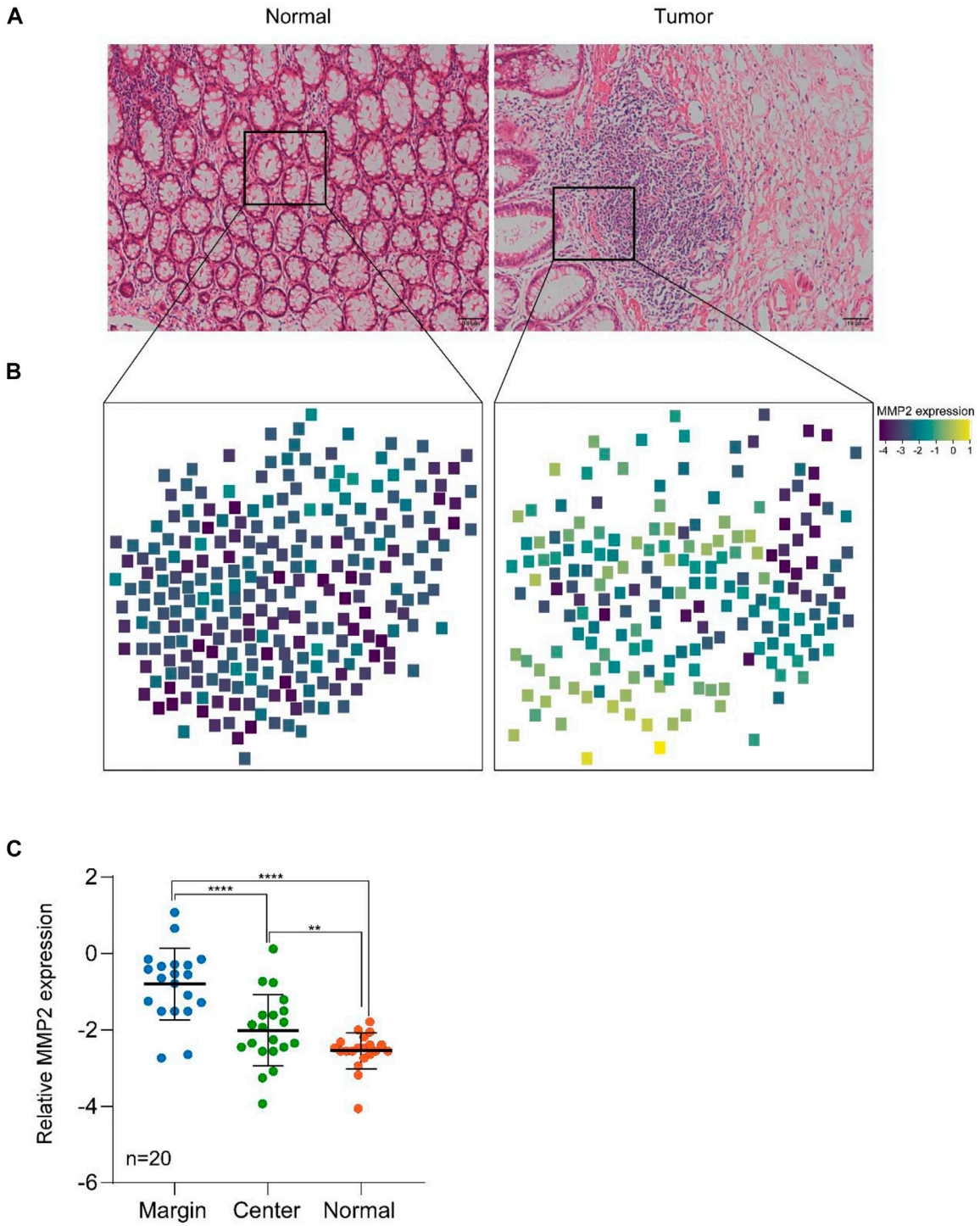

FIGURE 4 | The targeted spatial protein quantification of MMP2 in colon cancer and normal tissues. **(A)** H&E analysis of representative normal and tumor samples. **(B)** Spatial MMP2 expression in colon cancer and normal tissues. **(C)** MMP2 expression in different regions of tissues. **, $p < 0.01$, ****, $p < 0.0001$. p value was calculated using two-side student t test.

average age of the patients was 62 year-old, and there were 12 men and eight women. Most of the patients were in the deep infiltration depth but some of them had already reached lymph node metastasis or distant metastasis. What we investigated was whether the detected MMP2 expression had a relationship with the tumor invasion. We used a tissue targeted spatial protein quantification strategy based on MALDI TOF analysis for the study of the MMP2 over-expression location sites. In this

strategy, the peptide probe was firstly sprayed onto the tissues. The optimal amount and the incubation time have investigated above. Then HCCA was used as the matrix and sprayed on the tissues before MALDI analysis. For the detection, 300 points were randomly distributed on the tissue, and the ratio between probe fragments and probe were combined with the coordinates of each point as the indicator for MMP2 expression and location sites. The higher the ratio, the more complete the digestion, and the higher the expression of the MMP2. Finally, the ratio and the coordinates were statistically simulated to achieve the tissue distribution information for the expression of MMP2. In addition, this information will combine with the HE staining to obtain the final expression profile of MMP2.

As shown in **Figure 4**, the spatial expression of MMP2 in cancer tissue and normal tissue was successfully detected, which having a marked difference. The expression in cancer tissue was significantly higher than that in normal tissue. Additionally, in cancer tissue, the expression of MMP2 was also higher in cancer cells than in normal cells, which was consistent with the literature. Moreover, also in cancer tissues, the expression of MMP2 in marginal sites was significantly higher than that in central sites, indicating that the expression of MMP2 may be related to the tumor invasion. Finally, we counted the expression of MMP2 in 20 pairs tissues of colon cancer patients. The statistical results showed that the expression of MMP2 was higher in the marginal region than in the central region, which was consistent in all cancer tissues.

DISCUSSION

The infiltration and invasion of CRC had a complex mechanism, which involved multiple steps regulated by gene mutation, RNA expression, and protein modifications. Specially for tumor invasion, the cancer cells did not penetrate the basement membrane (BM) without the help of matrix metalloproteinases (MMPs) (Xu et al., 2019). Therefore, the MMPs can be considered as the important biomarkers to evaluate the tumor invasion (Ivancic et al., 2020, Koga et al., 2019, Kolenčík et al., 2020). MMPs are a series of zinc-containing endopeptidases, which mainly composed of MMP2 and MMP9 (Ceballos et al., 2019). They played a significant role in the degradation of extra-cellular matrix components (Wang et al., 2019; Zhou et al., 2019). Moreover, MMP2 was reported to be over-expressed in several solid tumors, including CRC, gastric carcinoma, breast carcinoma, lung cancer, etc (Fouad et al., 2019; Ramezani et al., 2020). It has also been reported that MMP2 played a crutial role in tumor invasion and metastasis. For the further understanding its mechanism, the position of MMP2 in tumor tissues need to be determined (Zhang et al., 2019b). In addition, if the high expression sites of MMP2 can be quickly detected, it can be applied in the rapid clinical pathology, providing guidance for clinical surgery.

In this study, we developed a strategy for the quantification of MMP2 at the spatial level via the MALDI method by using a peptide probe. Numerous differences were observed in different tissue regions, and the results showed that MMP2 was highly expressed in tumor margins compared to the central region. This clearly show the tumor invasiveness in a quantitative manner, which could be used as an important reference for tumor dissection surgery. It is worth noting that the intensity ratio between the cleaved product and the intact probe may not accurately reflect the ratio, since the efficiency of ionization of the two analytes is unknown. Therefore, this ratio should only be used with caution.

Furthermore, the probes coupled with the MALDI-TOF/MS method can be also used to quantify other proteins, such as the MMP family, the kinase family, and so on. Quantification of these proteins at spatial level is crucial for personalized medicine for tumors and other diseases. MMPs also play important roles in tissue remodeling, which means this method can also benefit patient with serious injuries.

CONCLUSION

In this work, we have developed a strategy for the MMP2 MALDI spatial protein quantification determination by using a peptide probe, and this method has been successfully applied into the detection of the expression and location sites of MMP2 in colon cancer and normal tissue. In addition, the expression of MMP2 was found to be higher in the margins of cancer tissues, which may be related to the tumor infiltration. This method could help the clinical evaluation of the prognosis for colon cancer patients.

DATA AVAILABILITY STATEMENT

The raw data supporting the conclusions of this article will be made available by the authors, without undue reservation.

ETHICS STATEMENT

The studies involving human participants were reviewed and approved by Second Affiliated Hospital of Chengdu Medical College. The patients/participants provided their written informed consent to participate in this study.

AUTHOR CONTRIBUTIONS

DY, PL, TY, KF, and SZ performed the experiments and participated in article writing. PL, TY, and LC collected the clinical samples. All authors contributed to the article and approved the submitted version.

FUNDING

This work is supported by the Natural Science Foundation of Sichuan Province (2020YJ0194), the Innovation Project of Chengdu (2021-YF05-01603-SN) and the Young Talent Program of the China National Nuclear Corporation.

REFERENCES

Balluff, B., Hopf, C., Porta Siegel, T., Grabsch, H. I., and Heeren, R. M. A. (2021). Batch Effects in MALDI Mass Spectrometry Imaging. *J. Am. Soc. Mass. Spectrom.* 32, 628–635. doi:10.1021/jasms.0c00393

Barré, F. P. Y., Paine, M. R. L., Flinders, B., Trevitt, A. J., Kelly, P. D., Ait-Belkacem, R., et al. (2019). Enhanced Sensitivity Using MALDI Imaging Coupled with Laser Postionization (MALDI-2) for Pharmaceutical Research. *Anal. Chem.* 91, 10840–10848. doi:10.1021/acs.analchem.9b02495

Boskamp, M. S., and Soltwisch, J. (2020). Charge Distribution between Different Classes of Glycerophospolipids in MALDI-MS Imaging. *Anal. Chem.* 92, 5222–5230. doi:10.1021/acs.analchem.9b05761

Ceballos, M. P., Rigalli, J. P., Ceré, L. I., Semeniuk, M., Catania, V. A., and Ruiz, M. L. (2019). ABC Transporters: Regulation and Association with Multidrug Resistance in Hepatocellular Carcinoma and Colorectal Carcinoma. *Curr. Med. Chem.* 26, 1224–1250. doi:10.2174/0929867325666180105103637

Fouad, H., Salem, H., Ellakwa, D. E. S., and Abdel-Hamid, M. (2019). MMP-2 and MMP-9 as Prognostic Markers for the Early Detection of Urinary Bladder Cancer. *J. Biochem. Mol. Toxicol.* 33, e22275. doi:10.1002/jbt.22275

Griselda, A., Idalia, G., Claudia, C., and Jesús, R. (2020). The Roles of Matrix Metalloproteinases and Their Inhibitors in Human Diseases. *Int. J. Mol. Sci.* 21 (24), 9739. doi:10.3390/ijms21249739

Ivancic, M. M., Megna, B. W., Sverchkov, Y., Craven, M., Reichelderfer, M., Pickhardt, P. J., et al. (2020). Noninvasive Detection of Colorectal Carcinomas Using Serum Protein Biomarkers. *J. Surg. Res.* 246, 160–169. doi:10.1016/j.jss.2019.08.004

Koga, Y., Hirahashi, M., Ohishi, Y., and Oda, Y. (2019). Clinicopathological Features and Phenotypic Classification of De Novo-Type Colorectal Carcinomas Differ from Those of Colorectal Carcinomas Derived from Flat Adenomas. *Pathol. Int.* 69, 331–340. doi:10.1111/pin.12803

Kolenčík, D., Shishido, S. N., Pitule, P., Mason, J., Hicks, J., and Kuhn, P. (2020). Liquid Biopsy in Colorectal Carcinoma: Clinical Applications and Challenges. *Cancers* 12, 1376. doi:10.3390/cancers12061376

Montalban-Arques, A., and Scharl, M. (2019). Intestinal Microbiota and Colorectal Carcinoma: Implications for Pathogenesis, Diagnosis, and Therapy. *EBioMedicine* 48, 648–655. doi:10.1016/j.ebiom.2019.09.050

Moore, L. M., Cho, S., and Thoren, K. L. (2019). MALDI-TOF Mass Spectrometry Distinguishes Daratumumab from M-Proteins. *Clinica Chim. Acta* 492, 91–94. doi:10.1016/j.cca.2019.02.017

Ramezani, P., Abnous, K., Taghdisi, S. M., Zahiri, M., Ramezani, M., and Alibolandi, M. (2020). Targeted MMP-2 Responsive Chimeric Polymersomes for Therapy against Colorectal Cancer. *Colloids Surf. B: Biointerfaces* 193, 111135. doi:10.1016/j.colsurfb.2020.111135

Ryan, D. J., Spraggins, J. M., and Caprioli, R. M. (2019). Protein Identification Strategies in MALDI Imaging Mass Spectrometry: A Brief Review. *Curr. Opin. Chem. Biol.* 48, 64–72. doi:10.1016/j.cbpa.2018.10.023

Shariatgorji, M., Nilsson, A., Fridjonsdottir, E., Vallianatou, T., Källback, P., Katan, L., et al. (2019). Comprehensive Mapping of Neurotransmitter Networks by MALDI-MS Imaging. *Nat. Methods* 16, 1021–1028. doi:10.1038/s41592-019-0551-3

Wang, Z., Wang, Y., Jia, X., Han, Q., Qian, Y., Li, Q., et al. (2019). MMP-2-Controlled Transforming Micelles for Heterogeneic Targeting and Programmable Cancer Therapy. *Theranostics* 9, 1728–1740. doi:10.7150/thno.30915

Weng, X., Chen, W., Hu, W., Xu, K., Qi, L., Chen, J., et al. (2019). PTPRB Promotes Metastasis of Colorectal Carcinoma via Inducing Epithelial-Mesenchymal Transition. *Cell Death Dis* 10, 352. doi:10.1038/s41419-019-1554-9

Xu, Y., Zhang, J., Liu, X., Huo, P., Zhang, Y., Chen, H., et al. (2019). MMP-2-Responsive Gelatin Nanoparticles for Synergistic Tumor Therapy. *Pharm. Develop. Technol.* 24, 1002–1013. doi:10.1080/10837450.2019.1621899

Zhang, D., Yang, Y., Qin, Q., Xu, J., Wang, B., Chen, J., et al. (2019). MALDI-TOF Characterization of Protein Expression Mutation during Morphological Changes of Bacteria under the Impact of Antibiotics. *Anal. Chem.* 91, 2352–2359. doi:10.1021/acs.analchem.8b05080

Zhang, H., Lu, Y., Wu, J., and Feng, J. (2019a). LINC00460 Hypomethylation Promotes Metastasis in Colorectal Carcinoma. *Front. Genet.* 10, 880. doi:10.3389/fgene.2019.00880

Zhang, H., Ma, Y., Wang, H., Xu, L., and Yu, Y. (2019b). MMP-2 Expression and Correlation with Pathology and MRI of Glioma. *Oncol. Lett.* 17, 1826–1832. doi:10.3892/ol.2018.9806

Zhou, W., Yu, X., Sun, S., Zhang, X., Yang, W., Zhang, J., et al. (2019). Increased Expression of MMP-2 and MMP-9 Indicates Poor Prognosis in Glioma Recurrence. *Biomed. Pharmacother.* 118, 109369. doi:10.1016/j.biopha.2019.109369

Conflict of Interest: The authors declare that the research was conducted in the absence of any commercial or financial relationships that could be construed as a potential conflict of interest.

frontiers in Chemistry

REVIEW
published: 16 December 2021
doi: 10.3389/fchem.2021.771801

Recent Advances in Combinations of TLC With MALDI and Other Desorption/Ionization Mass-Spectrometry Techniques

Roman Borisov[1,2]*, *Anastasiia Kanateva*[1] *and Dmitry Zhilyaev*[1,2]

[1]*A. V. Topchiev Institute of Petrochemical Synthesis, Russian Academy of Sciences, Moscow, Russia,* [2]*Peoples Friendship University of Russia (RUDN University), Moscow, Russia*

The combination of planar chromatography with desorption/ionization mass-spectrometry (MS) techniques provides chemists with unique tools for fast and simple separation of mixtures followed by the detection of analytes by the most powerful analytical method. Since its introduction in the early 1990s, thin-layer chromatography (TLC)/matrix-assisted mass spectrometry (MALDI) has been used for the analysis of a wide range of analytes, including natural and synthetic organic compounds. Nowadays, new desorption/ionization approaches have been developed and applied in conjunction with planar chromatography competing with MALDI. This review covers recent developments in the combination of TLC with various desorption/ionization MS methods which were made in recent several years.

Keywords: TLC, MALDI, ambient ionization mass spectrometry (AIMS), sorbents, derivatization

OPEN ACCESS

Edited by:
Lei Yue,
Hunan University, China

Reviewed by:
Václav Ranc,
Palacký University, Olomouc, Czechia
Xian Wang,
South-Central University for Nationalities, China

***Correspondence:**
Roman Borisov
borisov@ips.ac.ru

Specialty section:
This article was submitted to Analytical Chemistry, a section of the journal Frontiers in Chemistry

Received: *07 September 2021*
Accepted: *17 November 2021*
Published: *16 December 2021*

Citation:
Borisov R, Kanateva A and Zhilyaev D (2021) Recent Advances in Combinations of TLC With MALDI and Other Desorption/Ionization Mass-Spectrometry Techniques. Front. Chem. 9:771801. doi: 10.3389/fchem.2021.771801

INTRODUCTION

The conjugation of thin-layer chromatography (TLC) and mass spectrometry (MS) is one of the promising hybrid analytical methods. Despite the seeming simplicity, TLC with different detection systems is actively used in analytical and organic chemistry for the express separation of various mixtures and preliminary quantification, for example, for the analysis of oil and petroleum products (Cebolla et al., 2016; Speight, 2020; Makowska and Pellinen, 2021), monitoring the progress of organic reactions (Cagniant et al., 2001; Siebenhaller et al., 2018; Sahaka et al., 2021), separation of dyes and inks (Barker et al., 2017; Mohammad et al., 2017; Sharma and Kumar, 2017; Miron-Merida et al., 2021), and monitoring target compounds in different media (Kumar et al., 2017; Qu et al., 2021).

The potential of TLC as a modern micro-scale separation method is based on a number of its convenient properties, such as large sample throughput and suitability for screening separations (Matheis et al., 2015). This method may also be used for preliminary testing of separation conditions for HPLC applications due to low-cost optimization of mobile phase composition and easy and fast change of the stationary phase. Sample preparation for TLC is also not such a rigorous step, as for other chromatographic methods due to the disposability of the TLC plates. One of the unique advantages of TLC is the possibility of long-term storage of the analytical information after the separation process, so the TLC plates with target compounds may be further conjugated to the other analytical methods, such as IR, FID, or MS detection. The main disadvantages of TLC are difficult quantification and rather limited possibilities of qualitative analysis with classical detection methods, especially while separating complex mixtures, and if the question of quantitative analysis remains open to this day, for example, Stanek et al., 2019 developed the TLC method for the express

qualification and quantification of phenolic compounds and abscisic acid in honey, and succeeded with ~10% relative error of the concentration of the target compound (depending on the substance) using densitometric detection; similar results were obtained by Hynstova et al. (2018) who performed the separation of carotenoids and chlorophylls in dietary supplements containing *Chlorella vulgaris* and *Spirulina platensis* using high-performance TLC (HPTLC) and many others; the qualitative determination of the target components in the composition of complex mixtures can be reliably performed using suitable detection systems, and one of the main analytical methods in this case is conjugation to MS. At the same time, MALDI, among all the MS methods, occurred to be one of the most suitable methods for direct conjugation to planar chromatographic methods, opening broad possibilities for the identification of components of complex "omics" mixtures, screening, especially for small molecules, and development of methodological approaches, including new stationary phases for TLC, which might be suitable for direct MS detection of the separated compounds. MERCK KGaA, for instance, produces the so-called MS grade TLC plates which possess some important advantages; these TLC plates are characterized by a very low MS background due to the control of MS-detectable impurities, and the stationary phase layer thickness has been decreased to 100 μm, which is twice lower than that of standard TLC plates, as it was found that layer thickness influences the efficiency of laser desorption from the plate surface (Hillenkamp and Peter-Katalinic, 2013; Griesinger et al., 2014). It also should be noted that though MALDI can also be combined with other separation techniques such as, for example, capillary electrophoresis and liquid chromatography, TLC appears to be more suitable for MALDI experiments because the plates can be directly introduced to the ion source without any additional interfaces.

The aim of the present article was to review the recent advances of the combined TLC-MALDI technique, including the dedicated stationary phases, matrixes, derivatization, and application of the method. The last part of the review is devoted to the conjugation of TLC and novel desorption/ionization mass-spectrometry techniques, such as DART, DESI, and some other non-commercial systems with significant potential.

THIN-LAYER CHROMATOGRAPHY/ MATRIX-ASSISTED MASS SPECTROMETRY

Sorbents

In 2002, monolithic thin-layer sorbents based on silica gel containing no additional binder were introduced into laboratory practice by Merck (Germany). Together with the minimal thickness of the stationary phase layer (1–50 μm) providing improved separation properties, these TLC plates were found to be suitable to the direct coupling to different MS detection systems due to covalent binding of the stationary phase and, as a result, the low bleeding level. However, together with the advantages, a decrease in the thickness of the sorption layer also resulted in the decrease in the resolution due to the small elution pathway. The solution of the problem was in increasing of the separation efficiency, so the UTLC and HPTLC plates were taken into consideration. Increase of the efficiency allowed the increase of the sensitivity of the method, reaching about a dozen pmol per sample using UV detection and a few pmol with MALDI-MS.

Zhang et al. (2011) suggested the slides for ultrathin-layer chromatography (UTLC) which were prepared *via* coating nonporous silica particles, chemically modified with polyacrylamide, as 15 mkm films, on glass or silicon. The authors used the model mixture of three proteins, namely, myoglobin, cytochrome c, and lysozyme, for testing the separation ability of the prepared sorbent, and have received the nearly baseline resolution realized by the hydrophilic interaction chromatography mechanism. The sorbent demonstrated the HETP value of about 3 mkm, giving the opportunity to develop the separation efficiency more than 3500 TP per plate. Zhang et al. also varied the silica particle diameter, and tested the 900-, 700-, and 350-nm particles. The typical SEM image of a UTLC slide with a coating with silica nanoparticles demonstrates the smooth particles with narrow size distribution and optimal layer arrangement.

As it was found, the decreasing particle diameter improved the resolution but slowed down the separation. The plates with the optimized properties were used combined with MALDI-MS for the analysis of the proteins. MALDI for each protein was carried out at the region which was previously marked by the fluorescently labeled proteins under a microscope, and the mass spectrum for the center of each spot was recorded. The mass spectrum in each case agreed with the expected molar mass for each protein. The signal-to-noise ratio had an acceptable value, confirming the possibility of utilization of the approach.

In 2013, Svec et al. (Lv et al., 2013) suggested organic polymeric monolithic sorbents based on poly (4-methylstyrene-co-chloromethyl-styrene-co-divinylbenzene).
The authors compared the different polymerization initiation approaches and have chosen the synthetic procedure based on the thermally initiated process. The photopolymerization was not suitable for aromatic monomers because the latter absorb light in the UV range, resulting in decreased efficiency of the process. F. Svec et al. demonstrated that monolithic thin layers with a small surface area were able to produce efficient separations of peptides and proteins together with their on-layer MALDI-TOF-MS. Separation and subsequent identification of the components of the mixture of (Met5) enkephalin, oxytocin, and melittin labeled with fluorescamine were performed by Svec et. al to demonstrate the plate efficiency. All three components were baseline-separated using 65% acetonitrile in 0.1% aqueous TFA solution as a mobile phase. The MALDI-TOF-MS spectra were obtained directly from the TLC plates based on the poly(4-methylstyrene-co-chloromethylstyrene-co-divinylbenzene) monolithic sorbent with layer thickness of 50 mkm from the analyte spots using cyano-4-hydroxycinnamic acid as a matrix. The authors found the MS spectra were characterized with a good signal-to-noise ratio, confirming the main point of the TLC-MALDI-MS

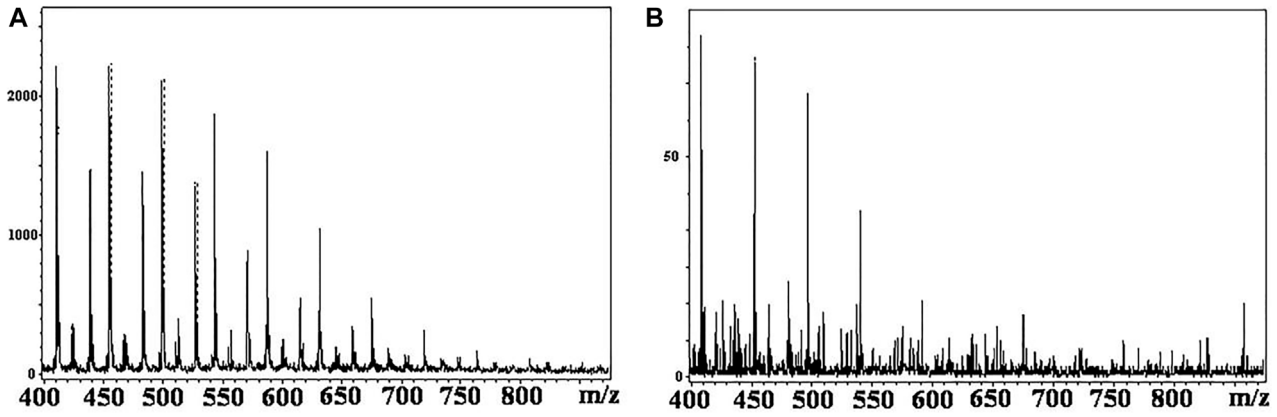

FIGURE 1 | MALDI-MS spectrum for the PEG sample (1 mg/ml) received directly from the monolithic TLC plate without additional matrix compounds. **(A)** 29% (w/w) GMA and **(B)** 14% (w/w) GMA. Figure reprinted with permission from Kucherenko et al. (2018). Copyright (2018) WILEY-VCH Verlag GmbH & Co. KGaA.

conjugation. The article also contained the results for eight different plates and double spotting of peptide mixtures, which demonstrated good repeatability and reproducibility of stationary phase properties.

In 2015, Hu et al. presented a TLC-ESI-MS method for direct analysis of raw samples. The main idea for the conjugation of TLC and MS methods was in the fact that the TLC plate could serve as a medium for absorbing interfering substances, allowing the detection of target compounds with reduced matrix effects. The authors have adapted the conventional TLC plates with an aluminum base coated with silica gel stationary phase particles. The suggested mode of separation of the target compounds and interfering substances allowed the decrease of sample pretreatment. The described procedure was efficient in the direct analysis of samples with salts and detergents, and rapid detection and quantitation of the target analyte in raw biological fluids were possible.

However, the main difficulties for this combination are the application of the MALDI-MS matrix onto the TLC plate and subsequent ionization. Kucherenko et al. suggested TLC plates with an organic polymer monolithic layer to work out the problem (Kucherenko et al., 2018; 2019). The chemical nature of monolithic polymers provides an opportunity to incorporate into the polymeric layer the functional groups which could play a role of "matrix," that is, to absorb and to redistribute the energy of laser pulse to ensure the soft ionization of the target compounds. At the same time, these functional groups will be covalently bonded to the polymer layer and will not result in a matrix cloud in the low molecular mass area of the mass spectra. Organic monolithic sorbents also have a highly developed surface area, allowing high-efficient separations due to the small size of the monolith domain structures. In the study by Kucherenko et al. (2018), the authors have developed the monolithic layers prepared by the copolymerization of ethylene dimethacrylate and glycidyl methacrylate, and deposited onto the surface of glass, and silicon plates were investigated as thin-layer chromatography separating media in hyphenated thin-layer chromatography–matrix-assisted laser desorption/ionization mass-spectrometry analysis. Varying compositions of the polymerization mixture and polymerization condition layers of different porosities and MALDI-MS compatibility were synthesized. The compatibility with MALDI-MS was tested using PEG, and it was demonstrated that layers prepared without glycidyl methacrylate are not compatible with MALDI-MS and do not allow obtaining any mass spectra. The best results were achieved with layers containing 19–29% glycidyl methacrylate. These layers allow mass spectra measurement without additional deposition of matrix compounds, supplying mass spectra almost "clean" in a low molar mass range (**Figure 1**).

Matrixes

One of the important distinctions of MALDI-MS from other soft ionization methods is the key role of the matrix in the ionization process. There are a large number of matrix compounds suitable for the analysis of low molecular weight analytes (Calvano et al., 2018; Kobylis et al., 2021). However, recently, some new matrixes have been proposed for TLC/MALDI. Thus, Mernie et al. (2019) described a very promising approach allowing direct TLC/MS profiling of oligosaccharides. The method is based on using magnetic nanoparticles functionalized with the traditional matrix compound-2,5-dihydroxybenzoic acid (DHB). The nanoparticles were dispersed in an ion liquid and applied on the TLC plate using a spinning device (**Figure 2**). Desorption/ionization of oligosaccharides in such conditions proceeds simultaneously with their fragmentation, forming characteristic ions. The use of this composite matrix also causes increasing of peak intensities of analytes' sodiated adducts and fragment ions.

Another example of the application of the inorganic matrix was proposed in the study by Fougère et al. (2018). The authors used core-shell silica-coated iron oxide magnetic nanoparticles as the matrix for the detection of flavonoid compounds by TLC/MALDI. The nanoparticle dispersion in ethanol was applied directly on the spots of interest, and MALDI mass spectra both in positive and negative modes were registered. The approach allowed the detection of anthocyanins in red wine,

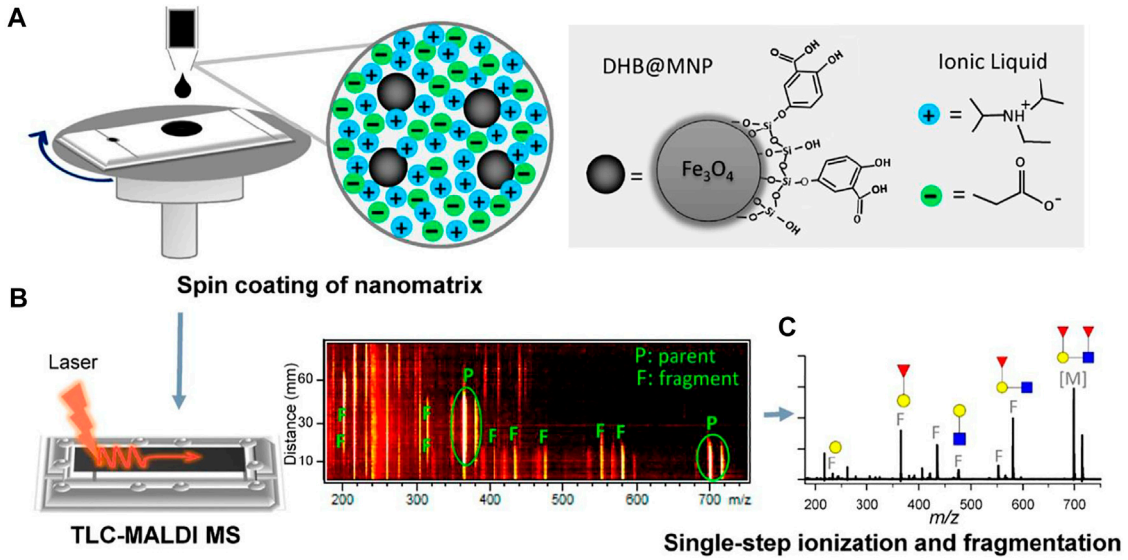

FIGURE 2 | Analytical workflow of DHB@MNP-assisted TLC-MALDI-MS using a saccharide mixture as a model (Mernie et al., 2019). **(A)** Saccharide mixture was separated on a C18-modified TLC plate, and the DHB@MNP nanomatrix was deposited on the TLC surface by spin-coating with the ionic liquid. **(B)** Automated scanning of the entire TLC separation lane was performed to obtain TOF-MS spectra at different migration distances. **(C)** Finally, on-spot structural elucidation of the saccharides was performed based on the parent and fragment ions generated from DHB@MNP-assisted fragmentation in single TOF-MS. Figure reprinted with permission from Mernie et al. (2019). Copyright (2019) the American Chemical Society (ACS).

glycosylated derivatives of quercetin in apple juice, and polyphenols in rose flower extract.

It is important to note, however, that the use of solutions of matrixes can cause secondary chromatographic processes on TLC plates and, hence, analyte spot blurring. This problem can be overcome by using solvent-free matrixes such as graphite-assisted laser desorption/ionization (GALDI) (Han et al., 2011). The sample preparation process in this case looks very simple and convenient because the matrix can be applied on TLC plates by denoting spots with a simple pencil lead. A large-scale test of this approach made on a number of synthetic organic compounds confirmed its utility (Borisov et al., 2014). However, the authors underlined that TLC/GALDI requires rather energies of the laser.

Composite glycerol/graphite/aromatic acid matrices were also proposed to avoid spot blurring and enhance desorption/ionization of the analytes (Esparza et al., 2016). Mixtures of traditional matrixes and graphite were dispersed in glycerin and applied on spots using a brush. The authors supposed that glycerol allows preventing secondary chromatographic processes and increasing analyte concentration on the surface of TLC plates. These factors increased the signals of analytes and reproducibility of mass spectra (**Figure 3**).

Dopants also sometimes play a very important role in ionization processes (Ali et al., 2017). In case of the previously mentioned GALDI-MS, sodium and potassium cations found in pencil lead take part in the formation of adducts of molecules. But, Y. Dong et al. found out that the concentration of alkali ions causing the formation of the corresponding adduct is higher on the surface of TLC plates (Dong et al., 2017). So, if the sorbent layer is scratched, the intensities of its peaks decrease, reducing the reproducibility of the results.

Derivatization

Planar chromatography is one of the first analytical methods where derivatization procedures were applied mainly for spot visualization (Zarzycki, 2015). Derivatization is also widely used in MALDI-MS and MALDI imaging for enhancing desorption/ionization efficiencies of the analytes (Zaikin and Halket, 2009; Zaikin and Borisov, 2021). However, chemical modification procedures are much less popular in case of TLC/MALDI. Nevertheless, such approaches look rather promising for the analysis of non- or low-polar analytes by this method. Thus, for example, a previously developed procedure for fixed-charge derivatization of alcohols (Borisov et al., 2014) was used for TLC/MALDI (Esparza et al., 2018). The derivatization agents, including 3-bromopropionyl chloride and pyridine, were applied directly on the elution zones of the analytes on the developed TLC plates. MALDI mass spectra registered from the plates contained intense peaks of the corresponding derivatives (**Figure 4**).

A similar approach was used for TLC/MALDI analysis of primary amines (Borisov et al., 2019). In this case, tris(2,6-dimethoxyphenyl)methilium hexafluorophosphate was used for the derivatization to yield cyclic acridine–like fixed-charge derivatives. The modification of analytes also causes change in the color of the spots. The latter is very useful to avoid using additional procedures to determine analyte elusion zones. The same derivatization agent was involved in the development of a method for analysis of aminoacids (Esparza et al., 2020). The derivatives of α-aminoacids underwent elimination of carbon dioxide under laser irradiation, but the formed ions produced intense peaks in the registered MALDI mass spectra. The proposed approach

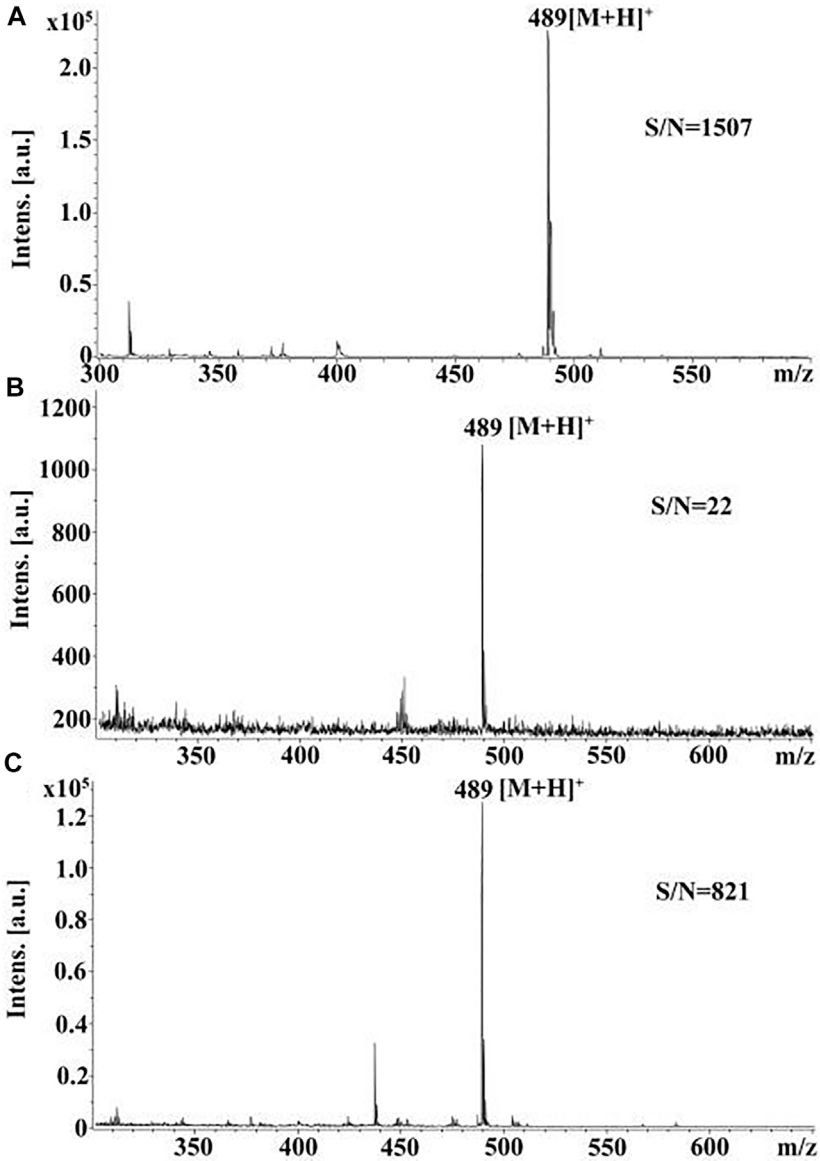

FIGURE 3 | MALDI mass spectra of vardenafil registered from **(A)** steel MALDI target using AT as the matrix, **(B)** TLC plate after elution and using AT as the matrix, and **(C)** TLC plate after elution using the composite matrix (AT-glycerol-graphite). Figure reprinted with permission from Esparza et al. (2016). Copyright (2016) Elsevier B. V.

was successfully applied for the analysis of dietary supplements (**Figure 5**).

Applications

The unique opportunities of the TLC/MALDI systems result in wide utilization of this method in the analytics of complex organic mixtures. One of the areas of interest in current analytical chemistry is lipid analysis. Cebolla et al. (2021) have recently presented a review on HPTLC contribution to lipid analysis in complex matrices during the period 2010–2021, when hyphenation of TLC to MS methods had experienced significant growth. Authors demonstrated that HPTLC separation of lipids on classes allowed the subsequent analysis by MALDI-TOF, resolving the difficulties in the analysis of acidic glycerophospholipid species due to ion suppression by phosphatidylcholine species. MALDI also allows structural identification of untargeted lipids which are ionized from the surface by continuous scanning along the plate track. In a similar way in which MS imaging allows the recording of mass spectra from the slices of biological tissues, MALDI may be used for screening the distribution of the lipids and other organic compounds on the HPTLC plate. Although most HPTLC-MALDI studies are performed with UV lasers using a matrix, other alternatives are also presented in the literature. In the study by Taki (2015), glycosphingolipids were separated on the HPTLC plate and then transferred to a plastic membrane which was fixed

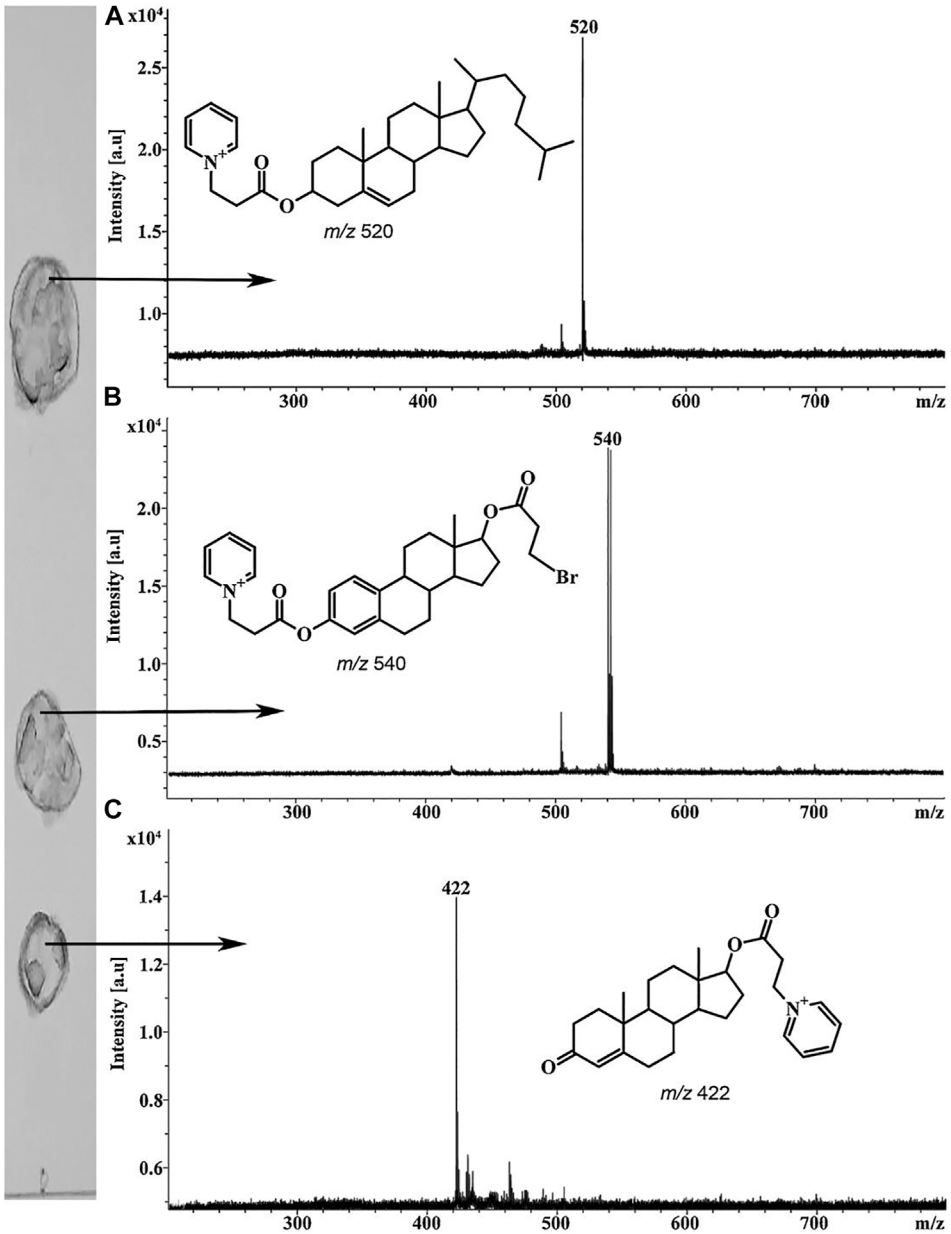

FIGURE 4 | MALDI mass spectra of steroid alcohols derivatized on the TLC plate cholesterol **(A)**, β-estradiol **(B)**, positions of bromopropionyl and pyridiniumpropionyl groups may vary and testosterone **(C)**. Figure reprinted with permission from Esparza et al. (2018). Copyright (2018) Elsevier B. V.

on a MALDI adapter (blotting process). Direct HPTLC/LDI without the matrix was realized using an IR laser by Leopold et al. (2018). This method allowed ablating more material per laser pulse on the order of a few micrometers in depth regarding UV lasers, improving sensitivity of the process, which is important taking into consideration the TLC plate thickness.

Ferey et al. (2017) have reported the utilization of TLC/MALDI-TOF-MS for the screening of invertase substrates in complex matrices. BfrA, a specific β-D-fructofuranosidase from *Leishmania major*, was chosen by the authors as a model enzyme to screen biological activity in plant extracts due to its capacity to hydrolyze specific carbohydrates. The first part of the approach was in differential analysis by TLC densitometry to determine the zones in the plant extract between the blank and enzymatic reaction. Zones of interest were then subsequently investigated *via* TLC/MALDI-TOF-MS for the identification of bioactive molecules. The development of the method demanded the solution of different analytical problems, such as separation of isomers (glucose and fructose), elimination of the high-matrix effect, and the analysis of polar molecules with low molar masses (sugars), which is a challenging problem itself while interacting about MALDI. However, the method occurred to be feasible for

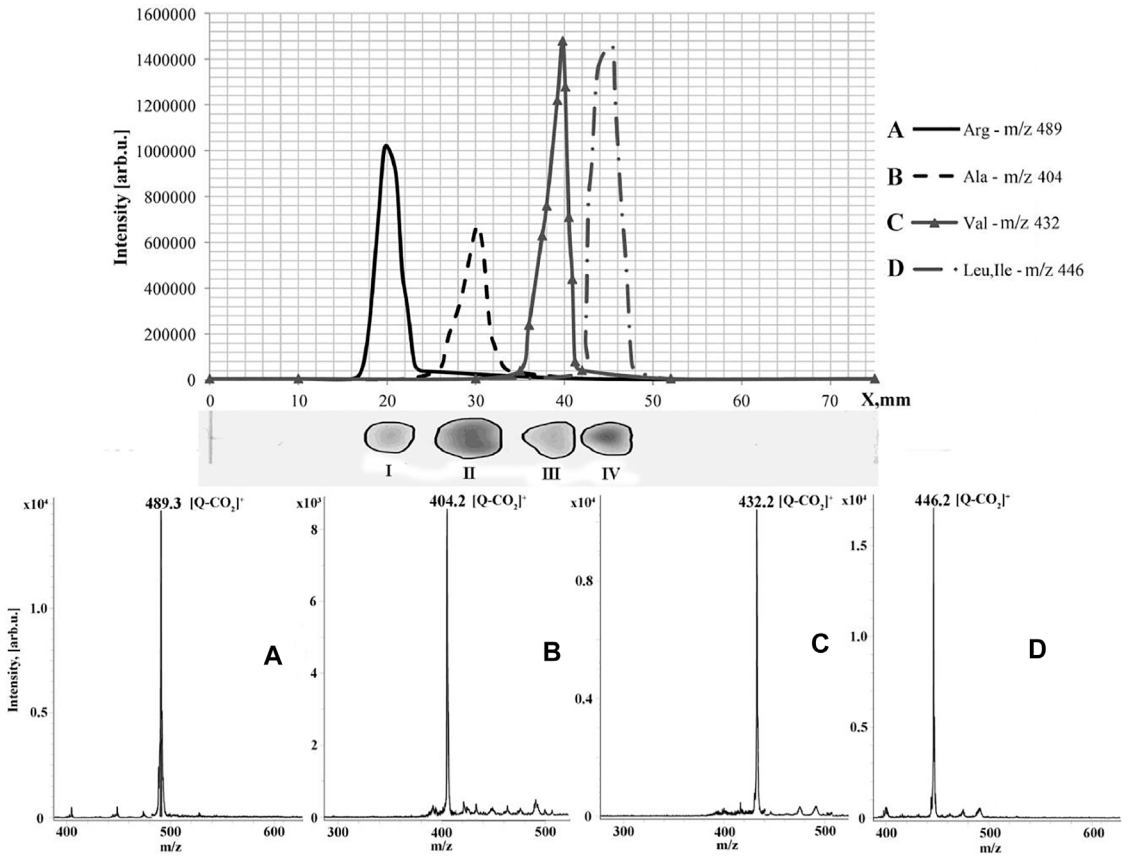

FIGURE 5 | Graphic and real thin-layer chromatograms (top two images) of dietary supplement and recorded MALDI mass spectra of TDPMH derivatives of the detected amino acids (bottom images). Figure reprinted with permission from Esparza et al. (2020). Copyright (2020) Elsevier B. V.

the analysis of bioactive molecules in complex mixtures containing interfering compounds (e.g., proteins and salts).

TLC/MALDI is widely used for the analysis of lipids (Engel and Schiller, 2021). Thus, Kouzel et al., (2017 have investigated the TLC-IR-MALDI-MS as an analytical tool for the detection and structural characterization of glyco and phospholipids directly from the TLC plate. The authors have coupled a pulsed IR-MALDI laser to a hybrid Synapt G2-S mass spectrometer and used the suggested ion source configuration for TLC-IR-MALDI-MS imaging of neutral glycosphingolipids, obtained from human colon epithelial HCT-8 cells. The aim of the article was the detection of the two glycosphingolipids, namely, globotriaosylceramide and globotetraosylceramide, which are the main receptors for Shiga toxins produced by enterohemorrhagic *Escherichia coli*. The direct TLC-IR-MALDI-MS analysis allowed the successful visualization of the chromatographic separation of the various lipo forms of globotriaosylceramide and globotetraosylceramide. The developed method allowed the fast and reliable overview of the glycosphingolipid composition of the investigated cell line of high medical relevance. This possibility may also be useful in glycolipidomic studies of complex biological matrices; for example, for globotriaosylceramide imaging, Kouzel et al. (2017) detected a higher extent of heterogeneity in lipo forms than that up to this point, analyzing monohexosyl and dihexosylceramide species. According to the structures of the biosynthesis precursor glycosphingolipids, namely, glucosylceramide and lactosylceramide, globotriaosylceramide species with sphingosine and fatty acid variations were identified by authors at m/z 1158.78 (d18:1, C24:0), m/z 1156.74 (d18:1, C24:1), m/z 1130.74 (d18:1, C22:0), and m/z 1046.66 (d18:1, C16:0). It is worth noting that the C24:0 fatty acid- and C24:1 fatty acid-carrying globotriaosylceramide species, differing only in the double bond in the acyl chain, were not separated on the chromatographic step due to their identical chromatographic properties in the utilized conditions. However, these compounds together formed a chromatographic zone which was definitely separated from the spots on the TLC plate containing globotriaosylceramide with C22:0 and C16:0 acyls. The additional MS data allowed to suggest that the colon epithelial cells synthesize globotriaosylceramide species with dihydroxylated sphinganine (d18:0), detected at m/z 1048.66 (d18:0, C16:0), and trihydroxylated sphinganine (t18:0) at m/z 1064.66 (t18:0, C16:0).

Torretta et al. (2016) have used HPTLC-MALDI-MS for the investigation of sphingolipid and glycosphingolipid profiles in the muscle, brain, and serum for creating a database of molecules for preclinical and clinical investigations. Based on the properties of

the studied tissues and fluids, the specific protocols for lipid extraction were used by the authors to maximize the HPTLC-MALDI-MS analytical throughput both for lipids extracted in the organic and aqueous phases. The received result allowed the authors to develop the database of specie-specific molecules, which may contribute to preclinical and clinical studies. The performed study indicated that alkaline hydrolysis was necessary for the detection of low-abundant species in serum and muscle tissues. The high hydrophobicity of ceramide was overcome by the development of the HPTLC plate in a specific eluent [chloroform/methanol 50:3.5 (v/v)], resulting in increased number and intensity of low-abundant ceramide species.

Kroslakova et al. (2016) have reported on the direct coupling of HPTLC with MALDI-TOF-MS for qualitative detection of flavonoids on phytochemical fingerprints. It is known that TLC fingerprints of plant raw materials and extracts for various applications usually focus on phenol acids and flavonoids. The TLC/MALDI-TOF-MS method has been applied by the authors for the development of fingerprints of flavonoids. The authors have demonstrated the feasibility of direct coupling of HPTLC with UV-MALDI-TOF-MS for the determination of the molecular mass of the flavonol glycoside, that is, rutin, and flavone glycoside, that is, luteolin-7-O-glucoside, and the corresponding aglycones, that is, quercetin and luteolin. After the primary TLC separation on the MS-grade plates, the developed chromatogram was treated with 2,5-dihydroxybenzoic acid as a MALDI matrix, dried, and scanned by UV-MALDI-TOF-MS. All the studied compounds were detected in MALDI-TOF mass spectra. This is particularly important for the coeluted compounds—aglycones luteolin and quercetin, which could not have been distinguished by the densitometric HPTLC method. The authors have demonstrated the potential of MALDI-TOF-MS for the analysis of low molar mass fingerprints of flavonoids directly from their HPTLC chromatogram.

THIN-LAYER CHROMATOGRAPHY AND NOVEL DESORPTION/IONIZATION MASS-SPECTROMETRY TECHNIQUES

Though MALDI-MS is the most used approach for direct detection of analytes from TLC plates, there also several desorption/ionization methods which are also capable of such analyses. Thus, even in the 1980s, it was shown that fast atom bombardment (Chang et al., 1984) and secondary ion mass spectrometry (Kushi and Handa, 1985) can be conjugated with planar chromatography. The development of ambient ionization methods, such as "direct analysis in real-time" (DART) and desorption electrospray ionization (DESI), makes it possible to ionize molecules from TLC plates with minimum sample preparation (Morlock and Schwack, 2010). On the one hand, such approaches look more promising than TLC/MALDI because they do not require any matrix, making the developed methods more reproducible and easy to use. On the other hand, laser-based vacuum systems such as MALDI guarantee high spatial resolution and minimum side-ionization processes.

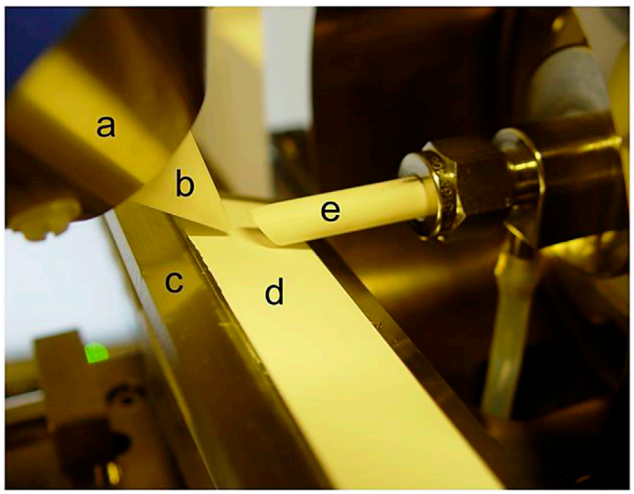

FIGURE 6 | DART ion source with possibility to change the gas flow angle for desorption/ionization of analytes from TLC plates. Reprinted with permission from Häbe and Morlock (2015). Copyright © 2015 John Wiley & Sons, Ltd.

The first study demonstrating the power of the combination of TLC and ambient ionization MS was published shortly after the presentation of DESI (Van Berkel et al., 2005). The method is based on spraying of the TLC surface with ultrasmall solvent droplets at velocities higher than 100 m/s, causing desorption of the ionized molecules of the analytes. The latter are transferred to the interface of the MS and detected (Manikandan, et al., 2016). The main drawback of this method is the dependence of the size of desorption spots on TLC plates on solvent flow rates (Bagatela, et al., 2015). Low flow rates lead to decreasing desorption of analytes and low intensities of corresponding ions, whereas high flow rates produce large spots causing diffusion of analytes across TLC plates, decreasing spatial resolution, and co-ionization of compounds with close R_f. Nevertheless, the approach was used, for example, to develop methods for detecting components of thermochromic inks for forensic purposes (Khatami et al., 2017). A very interesting combination of TLC/DESI with ion mobility spectroscopy/mass spectrometry (IMS/MS) was described by Claude et al. (2020). In this case, IMS was necessary to resolve co-eluting isomers of ecdysteroids, but, in fact, the proposed multidimensional separation system can be used for the analysis of very complex mixtures of various origins.

DART mass spectrometry operates using Penning ionization principles: excited atoms of gas (mainly helium) interact with molecules of ambient air components producing secondary ions, which desorb/ionize compounds from the surface of the analyzed object (Rondeau, 2017). This ionization mechanism is more preferable for TLC than DESI because using gas streams avoids diffusion of analytes (Morlock and Ueda, 2007). Moreover, rather high temperature of gas enhances desorption of analytes from plates, although some thermal decompositions of labile compounds can occur. The method can also be combined with online derivatization to enhance the ionization efficiencies of the analytes (Borisov et al., 2019).

TABLE 1 | Home-built interfaces for TLC/MS systems.

Desorption/ionization principle	Objects/analytes	Results	References
Laser desorption–low-temperature plasma (LD-LTP)	Tea, coffee beans, and soluble coffee extracts	Quantitative analysis of compounds in complex matrices, possibility of a low-cost laser system used in combination with an activated carbon matrix	Garcia-Rojas et al. (2020)
Low-temperature plasma (LTP)	Pharmaceuticals and biologically active compounds	Desorption/ionization efficiencies depend on the nature of solvents and analytes; LODs are compared to other approaches	Gong et al. (2020)
Laser desorption– low-temperature plasma (LD-LTP)	Pharmaceuticals and biologically active compounds	High spatial resolution and possibility to decrease LODs by increasing laser spot size	Gong et al. (2020)
Desorption atmospheric pressure photoionization (DAPPI)	Human lipids and plant oils	Detection of fatty acid diols and glycerol esters, cholesterol and its derivatives, and squalene	Rejsek et al. (2016)
Desorption atmospheric pressure chemical ionization (DAPCI)	Amino acids and drugs	Detection of amino acid and pharmaceutical compounds, linear signal	Winter et al. (2015)
Desorption atmospheric pressure chemical ionization (DAPCI)	Hop acids	Semi-quantitative determination of α- and β-acid ratio	Winter et al. (2017)
Sawtooth TLC-ESI/MS	Dyes	Detection of dyes using a very simple experimental design	Cheng et al. (2019)
Flowing atmospheric pressure afterglow (FAPA)	Pyrazole derivatives, alkaloids, steroids, and drugs	LODs comparable with other ambient methods achieved using a simple laser pointer for ablation, quantitative results	Ceglowski et al. (2015) Kuhlmann et al. (2019)
Electrostatic spray ionization (ESTASI)	Dyes and drugs	Detection of all tested compounds, low LODs	Zhong et al. (2015)
Electrostatic field–induced spray ionization (EFISI)	Herbal extracts	Detection of alkaloids, flavonoids, phenoic acids, lignans, coumarins, anthraquinones, monoterpenoids, sesquiterpenoids, diterpenoids, and triterpenoids	Zhang et al. (2019) Zhang et al. (2020)
Desorption/ionization induced by neutral clusters (DINeC)	Oligopeptides and extracts from yolk of a chicken egg	Extremely soft ionization technique allowing desorption ionization without any fragmentation	Heep et al. (2019)
Diode laser thermal vaporization–inductively coupled plasma (DLTV-ICP)	Algae	Reproducible quantification of selenium in algae using a low-cost experiment design; the results are comparable to HPLC-ICP MS	Bednarik et al. (2018)

The first version of the commercial DART ion source was inconvenient for TLC analysis because the gas stream was directed to the orifice of the MS interface and the analysis required cutting of the plates. Though a special adapter increases the efficiency of desorption/ionization and reproducibility of the results was proposed by Ovcharov et al. (2017), the problem was completely overcome with the release of new generation of DART ion sources, allowing to change the gas flow angle (so-called reflection scanning) and having TLC holders (**Figure 6**). The sensitivity of TLC/DART can also be increased using shortened source caps (Häbe and Morlock, 2015). There are also approaches allowing the visualization of the gas impact region on plates using neon additives to helium (Chernetsova and Morlock, 2015) or substances changing their color upon heating (Chernetsova et al., 2011).

All abovementioned improvements have rapidly increased the popularity of TLC/DART, and now, it is the most common combination of ambient mass spectrometry with planar chromatography. Thus, this approach is often used for the characterization of plant extracts. For example, DART-MS coupled with the ion trap mass analyzer was used for express identification of alkaloids extracted from plants and separated by TLC (Chen, et al., 2018). The combination of TLC with derivatization, bioautography, and DART-MS was successfully applied by Bañuelos-Hernández et al. (2020) for the analysis of Mexican *Plectranthus amboinicus* (Lour.) essential oil. Comparison of HPTLC-UV/Vis chromatograms before and after derivatization using the anisaldehyde–sulfuric acid reagent and HPTLC-Vis-EDA autograms allowed determining bioactive compound zones, which then were subjected to analysis by DART with a high-resolution mass analyzer. A similar approach was used for bioanalytical profiling of sunflower leaves (Móricz et al., 2018).

TLC/DART analysis can also be used for quantitative analysis of various compounds. Eichner and Spangenberg (2019) have developed a method for separation and quantitative determination of caffeine, artemisinin, and equol. The latter was also an object of interest in the study by Peters and Spangenberg, (2019). The comparison of results achieved using TLC-UV and TLC/DART for the quantification of this substance in cattle manure extracts clearly shows that selectivity of mass spectrometry allows obtaining more exact results. The authors underline that in case of UV detection, corresponding peaks were significantly broader, causing more errors.

A very promising approach was developed by Chen et al. (2021). In this study, DART-MS was combined with a laser system, in which irradiation significantly increased desorption of analytes. A similar method has already been published, but the authors used an expensive multi-wavelength laser device (Zhang et al., 2012), whereas the mentioned approach is based on a low-cost and easy-to-install laser system. It also allowed decreasing the temperature of the gas stream, which is rather high for the TLC/DART experiment as usual. The proposed approach was validated using various synthetic compounds and applied for the analysis of natural herbal medicines.

There are also a significant number of other home-built systems allowing desorption/ionization of analytes from TLC plates. Their descriptions are summarized in **Table 1**. Although such systems are not commercially produced, they demonstrate great potential for further development and may

take an important place in TLC/MS analysis. Laser-based systems appear to be most promising because they allow achieving the highest spatial resolution, which is very important for the analysis of co-eluted analytes.

CONCLUSION

Reproducibility and high spatial resolution achieved by MALDI-MS are still keeping this method as the most widely used desorption/ionization technique for the detection of analytes from TLC plates. Further developments of this method, including new chromatographic sorbents and matrix compounds/mixtures, and novel sample preparation procedures guarantee its popularity for the analysis of various objects. Most notably, there are new studies introducing TLC/MALDI as a useful tool in new research fields such as, for example, petroleomics. However, the fast growing number of ambient ionization techniques offers a good alternative for MALDI. These methods allow developing cost-effective, robust, and express approaches for the detection of various classes of analytes from TLC plates. We believe that all these MS ionization approaches will keep one of the first chromatographic separation methods actual for a lot of purposes.

AUTHOR CONTRIBUTIONS

All authors listed have made a substantial, direct, and intellectual contribution to the study and approved it for publication.

FUNDING

The study was prepared with the financial support of the Grant of Russian Science Foundation No. 21-73-20032.

REFERENCES

Ali, A., Shahid, N., and Musharraf, S. G. (2017). Application of Dyes as Doping Agents in MALDI-MS Matrices for the Signal Enhancement of Proteins. *RSC Adv.* 7, 6598–6604. doi:10.1039/C6RA27156A

Bagatela, B. S., Lopes, A. P., Cabral, E. C., Perazzo, F. F., and Ifa, D. R. (2015). High-performance Thin-Layer Chromatography/desorption Electrospray Ionization Mass Spectrometry Imaging of the Crude Extract from the Peels of Citrus Aurantium L. (Rutaceae). *Rapid Commun. Mass. Spectrom.* 29, 1530–1534. doi:10.1002/rcm.7246

Bañuelos-Hernández, A. E., Azadniya, E., Ramírez Moreno, E., and Morlock, G. E. (2020). Bioprofiling of Mexican Plectranthus Amboinicus (Lour.) Essential Oil via Planar Chromatography-Effect-Directed Analysis Combined with Direct Analysis in Real Time High-Resolution Mass Spectrometry. *J. Liquid Chromatogr. Relat. Tech.* 43, 344–350. doi:10.1080/10826076.2020.1737542

Barker, J., Ramotowski, R., and Nwokoye, J. (2016). The Effect of Solvent Grade on Thin Layer Chromatographic Analysis of Writing Inks. *Forensic Sci. Int.* 266, 139–147. doi:10.1016/j.forsciint.2016.05.003

Beate Fuchs, K. M., Fuchs, B., Lemmnitzer, K., Süß, R., Griesinger, H., Minarik, S., et al. (2015). Combining TLC Separation with MS Detection - A Revival of TLC. *J. Glycomics Lipidomics* 05, 1–3. doi:10.4172/2153-0637.1000e125

Bednařík, A., Kuta, J., Vu, D. L., Ranglová, K., Hrouzek, P., Kanický, V., et al. (2018). Thin-layer Chromatography Combined with Diode Laser thermal Vaporization Inductively Coupled Plasma Mass Spectrometry for the Determination of Selenomethionine and Selenocysteine in Algae and Yeast. *J. Chromatogr. A* 1533, 199–207. doi:10.1016/j.chroma.2017.12.017

Borisov, R., Esparza, C., Polovkov, N., Topolyan, A., and Zaikin, V. (2019). An Approach to Analysis of Primary Amines by a Combination of Thin-layer Chromatography and Matrix-assisted Laser Desorption Ionization Mass Spectrometry in Conjunction with post-chromatographic Derivatization. *J. Sep. Sci.* 42, 3470–3478. doi:10.1002/jssc.201900644

Borisov, R. S., Esparza, C., Goriainov, S. V., and Zaikin, V. G. (2019). Suitable *In-Situ* Derivatization of Alcohols by Reaction with Basic Amines in Direct Analysis in Real Time Mass Spectrometry. *Talanta* 200, 31–40. doi:10.1016/j.talanta.2019.03.037

Borisov, R. S., Polovkov, N. Y., Zhilyaev, D. I., Esparza, C. A., and Zaikin, V. G. (2014). Combination of Graphite-Assisted Laser Desorption/ionization (GALDI) Mass Spectrometry with Thin Layer Chromatography. *J. Anal. Chem.* 69, 1351–1355. doi:10.1134/S1061934814140032

Borisov, R. S., Zhilyaev, D. I., Polovkov, N. Y., and Zaikin, V. G. (2014). Simple Approach to Derivatization of Alcohols and Phenols for the Analysis by Matrix(surface)-Assisted Laser Desorption/ionization Time-Of-Flight Mass Spectrometry. *Rapid Commun. Mass. Spectrom.* 28, 2231–2236. doi:10.1002/rcm.7008

Cagniant, D., Nosyrev, I., Cebolla, V., Vela, J., Membrado, L., and Gruber, R. (2001). Structural Modifications of Petroleum Asphaltenes by Reductive Alkylation Investigated by TLC-FID. *Fuel* 80, 107–115. doi:10.1016/S0016-2361(00)00041-7

Calvano, C. D., Monopoli, A., Cataldi, T. R. I., and Palmisano, F. (2018). MALDI Matrices for Low Molecular Weight Compounds: an Endless story? *Anal. Bioanal. Chem.* 410, 4015–4038. doi:10.1007/s00216-018-1014-x

Cebolla, V. L., Jarne, C., Vela, J., Garriga, R., Membrado, L., and Galbán, J. (2021). Scanning Densitometry and Mass Spectrometry for HPTLC Analysis of Lipids: The Last 10 Years. *J. Liquid Chromatogr. Relat. Tech.* 44, 148–170. doi:10.1080/10826076.2020.1866600

Cebolla, V. L., Lázaro, M. J., and Herod, A. A. (2016). Petroleum Products-Thin Layer (Planar) Chromatography☆. *Ref. Module Chem. Mol. Sci.Chem. Eng.* 25, 3690–3701. doi:10.1016/B978-0-12-409547-2.12669-1

Cegłowski, M., Smoluch, M., Reszke, E., Silberring, J., and Schroeder, G. (2015). Flowing Atmospheric Pressure Afterglow Combined with Laser Ablation for Direct Analysis of Compounds Separated by Thin-Layer Chromatography. *Anal. Bioanal. Chem.* 408, 815–823. doi:10.1007/s00216-015-9165-5

Chang, T. T., Lay, J. O., and Francel, R. J. (1984). Direct Analysis of Thin-Layer Chromatography Spots by Fast Atom Bombardment Mass Spectrometry. *Anal. Chem.* 56, 109–111. doi:10.1021/ac00265a030

Chen, Y., Li, L., Xu, R., Li, F., Gu, L., Liu, H., et al. (2021). Characterization of Natural Herbal Medicines by Thin-Layer Chromatography Combined with Laser Ablation-Assisted Direct Analysis in Real-Time Mass Spectrometry. *J. Chromatogr. A* 1654, 462461. doi:10.1016/j.chroma.2021.462461

Chen, Z., Wang, M., Yang, Y., Du, X., Zhang, Z., and Li, Y. (2018). Qualitative and Quantitative Analysis of Porana Sinensis Hemsl by UHPLC-Q-Exactive MS, TLC Autographic Method and DART-MS. *Phytochem. Anal.* 30, 311–319. doi:10.1002/pca.2814

Cheng, S.-C., Bhat, S. M., Lee, C.-W., and Shiea, J. (2019). Simple Interface for Scanning Chemical Compounds on Developed Thin Layer Chromatography Plates Using Electrospray Ionization Mass Spectrometry. *Analytica Chim. Acta* 1049, 1–9. doi:10.1016/j.aca.2018.10.042

Chernetsova, E. S., and Morlock, G. E. (2015). Aspects of Surface Scanning by Direct Analysis in Real Time Mass Spectrometry Employing Plasma Glow Visualization. *Rapid Commun. Mass. Spectrom.* 29, 1242–1252. doi:10.1002/rcm.7221

Chernetsova, E. S., Revelsky, A. I., and Morlock, G. E. (2011). Some New Features of Direct Analysis in Real Time Mass Spectrometry Utilizing the Desorption at an Angle Option. *Rapid Commun. Mass. Spectrom.* 25, 2275–2282. doi:10.1002/rcm.5112

Claude, E., Tower, M., Lafont, R., Wilson, I. D., and Plumb, R. S. (2020). High Performance Thin-Layer Chromatography of Plant Ecdysteroids Coupled with

Desorption Electrospray Ionisation-Ion Mobility-Time of Flight High Resolution Mass Spectrometry (HPTLC/DESI/IM/ToFMS). *Chromatographia* 83, 1029–1035. doi:10.1007/s10337-020-03917-9

Dong, Y., Ferrazza, R., Anesi, A., Guella, G., and Franceschi, P. (2017). TLC Surface Integrity Affects the Detection of Alkali Adduct Ions in TLC-MALDI Analysis. *Anal. Bioanal. Chem.* 409, 5661–5666. doi:10.1007/s00216-017-0501-9

Eichner, F., and Spangenberg, B. (2019). Optimized Determination of Caffeine, Equol, and Artemisinin by High-Performance Thin-Layer Chromatography-Direct Analysis in Real Time-Time of Flight-Mass Spectrometry. *JPC - J. Planar Chromatogr. - Mod. TLC* 32, 197–203. doi:10.1556/1006.2019.32.3.4

Engel, K. M., and Schiller, J. (2021). The Value of Coupling Thin-Layer Chromatography to Mass Spectrometry in Lipid Research - a Review. *J. Chromatogr. B* 1185, 123001. doi:10.1016/j.jchromb.2021.123001

Esparza, C., Borisov, R. S., Polovkov, N. Y., and Zaikin, V. G. (2018). Post-chromatographic Fixed-Charge Derivatization for the Analysis of Hydroxyl-Containing Compounds by a Combination of Thin-Layer Chromatography and Matrix-Assisted Laser Desorption/ionization Mass Spectrometry. *J. Chromatogr. A* 1560, 97–103. doi:10.1016/j.chroma.2018.05.025

Esparza, C., Borisov, R. S., Varlamov, A. V., and Zaikin, V. G. (2016). Composite Glycerol/graphite/aromatic Acid Matrices for Thin-Layer Chromatography/matrix-Assisted Laser Desorption/ionization Mass Spectrometry of Heterocyclic Compounds. *J. Chromatogr. A* 1470, 118–122. doi:10.1016/j.chroma.2016.09.075

Esparza, C., Polovkov, N. Y., Topolyan, A. P., Borisov, R. S., and Zaikin, V. G. (2020). Suitable Analysis of α-amino Acids by a Direct Combination of Thin-Layer Chromatography and Matrix-Assisted Laser Desorption/ionization Mass Spectrometry in Conjunction with post-chromatographic Fixed-Charge Derivatization. *J. Chromatogr. A* 1626, 461335. doi:10.1016/j.chroma.2020.461335

Ferey, J., Da Silva, D., Lafite, P., Daniellou, R., and Maunit, B. (2017). TLC-UV Hyphenated with MALDI-TOFMS for the Screening of Invertase Substrates in Plant Extracts. *Talanta* 170, 419–424. doi:10.1016/j.talanta.2017.04.040

Fougère, L., Da Silva, D., Destandau, E., and Elfakir, C. (2018). TLC-MALDI-TOF-MS-based Identification of Flavonoid Compounds Using an Inorganic Matrix. *Phytochem. Anal.* 30, 218–225. doi:10.1002/pca.2807

García-Rojas, N. S., Moreno-Pedraza, A., Rosas-Román, I., Ramírez-Chávez, E., Molina-Torres, J., and Winkler, R. (2020). Mass Spectrometry Imaging of Thin-Layer Chromatography Plates Using Laser Desorption/low-Temperature Plasma Ionisation. *Analyst* 145, 3885–3891. doi:10.1039/D0AN00446D

Gong, X., Zhang, D., Embile, I. B., She, Y., Shi, S., and Gamez, G. (2020). Low-Temperature Plasma Probe Mass Spectrometry for Analytes Separated on Thin-Layer Chromatography Plates: Direct vs Laser Assisted Desorption. *J. Am. Soc. Mass. Spectrom.* 31, 1981–1993. doi:10.1021/jasms.0c00246

Griesinger, H., Fuchs, B., Süß, R., Matheis, K., Schulz, M., and Schiller, J. (2014). Stationary Phase Thickness Determines the Quality of Thin-Layer Chromatography/matrix-Assisted Laser Desorption and Ionization Mass Spectra of Lipids. *Anal. Biochem.* 451, 45–47. doi:10.1016/j.ab.2014.02.002

Häbe, T. T., and Morlock, G. E. (2015). Improved Desorption/ionization and Ion Transmission in Surface Scanning by Direct Analysis in Real Time Mass Spectrometry. *Rapid Commun. Mass. Spectrom.* 30, 321–332. doi:10.1002/rcm.7434

Häbe, T. T., and Morlock, G. E. (2015). Quantitative Surface Scanning by Direct Analysis in Real Time Mass Spectrometry. *Rapid Commun. Mass. Spectrom.* 29, 474–484. doi:10.1002/rcm.7127

Heep, J., Tuchecker, P. H. K., Gebhardt, C. R., and Dürr, M. (2019). Combination of Thin-Layer Chromatography and Mass Spectrometry Using Cluster-Induced Desorption/Ionization. *ACS Omega* 4, 22426–22430. doi:10.1021/acsomega.9b03060

Hillenkamp, F., and Peter-Katalinic, J. (2013). *MALDI MS: A Practical Guide to Instrumentation, Methods and Applications*. Second Edition. Weinheim: Wiley-VCH Verlag GmbH & Co. KGaA. doi:10.1002/9783527335961

Hu, B., Xin, G.-z., So, P.-K., and Yao, Z.-P. (2015). Thin Layer Chromatography Coupled with Electrospray Ionization Mass Spectrometry for Direct Analysis of Raw Samples. *J. Chromatogr. A* 1415, 155–160. doi:10.1016/j.chroma.2015.08.055

Hynstova, V., Sterbova, D., Klejdus, B., Hedbavny, J., Huska, D., and Adam, V. (2018). Separation, Identification and Quantification of Carotenoids and Chlorophylls in Dietary Supplements Containing Chlorella Vulgaris and Spirulina Platensis Using High Performance Thin Layer Chromatography. *J. Pharm. Biomed. Anal.* 148, 108–118. doi:10.1016/j.jpba.2017.09.018

Khatami, A., Prova, S. S., Bagga, A. K., Yan Chi Ting, M., Brar, G., and Ifa, D. R. (2017). Detection and Imaging of Thermochromic Ink Compounds in Erasable Pens Using Desorption Electrospray Ionization Mass Spectrometry. *Rapid Commun. Mass. Spectrom.* 31, 983–990. doi:10.1002/rcm.7867

Kim, H.-H., Han, S.-P., Kim, J.-K., and Kim, Y.-J. (2011). Detection of Long Alkyl Esters of Succinic and Maleic Acid Using TLC-MALDI-MS. *Bull. Korean Chem. Soc.* 32, 915–920. doi:10.5012/BKCS.2011.32.3.915

Kobylis, P., Stepnowski, P., and Caban, M. (2021). Review of the Applicability of Ionic Liquid Matrices for the Quantification of Small Molecules by MALDI MS. *Microchemical J.* 164, 105983. doi:10.1016/j.microc.2021.105983

Kouzel, I. U., Soltwisch, J., Pohlentz, G., Schmitz, J. S., Karch, H., Dreisewerd, K., et al. (2017). Infrared MALDI Mass Spectrometry Imaging of TLC-Separated Glycosphingolipids with Emphasis on Shiga Toxin Receptors Isolated from Human colon Epithelial Cells. *Int. J. Mass Spectrom.* 416, 53–60. doi:10.1016/j.ijms.2016.11.008

Kroslakova, I., Pedrussio, S., and Wolfram, E. (2016). Direct Coupling of HPTLC with MALDI-TOF MS for Qualitative Detection of Flavonoids on Phytochemical Fingerprints. *Phytochem. Anal.* 27, 222–228. doi:10.1002/pca.2621

Kucherenko, E., Kanateva, A., Kurganov, A., Borisov, R., and Pirogov, A. (2018). Monolithic Thin-layer Chromatography Plates with Covalently Bonded Matrix for Hyphenation with Matrix-assisted Laser Desorption/ionization. *J. Sep. Sci.* 41, 4387–4393. doi:10.1002/jssc.201800679

Kucherenko, E., Kanateva, A., Pirogov, A., and Kurganov, A. (2019). Recent Advances in the Preparation of Adsorbent Layers for Thin-Layer Chromatography Combined with Matrix-Assisted Laser Desorption/ionization Mass-Spectrometric Detection. *J. Sep. Sci.* 42, 415–430. doi:10.1002/jssc.201800625

Kuhlmann, C., Heide, M., and Engelhard, C. (2019). Fast Screening and Quantitative Mass Spectral Imaging of Thin-Layer Chromatography Plates with Flowing Atmospheric-Pressure Afterglow High-Resolution Mass Spectrometry. *Anal. Bioanal. Chem.* 411, 6213–6225. doi:10.1007/s00216-019-02013-8

Kumar, M., Kuzhiumparambil, U., Ralph, P. J., and Contreras-Porcia, L. (2017). "Polyamines," in *Algal Green Chemistry*. Editors R. Rastogi, D. Madamwar, and A. Pandey (Amsterdam: Elsevier), 243–255. doi:10.1016/B978-0-444-63784-0.00012-6

Kushi, Y., and Handa, S. (1985). Direct Analysis of Lipids on Thin Layer Plates by Matrix-Assisted Secondary Ion Mass Spectrometry1. *J. Biochem.* 98, 265–268. doi:10.1093/oxfordjournals.jbchem.a135267

Leopold, J., Popkova, Y., Engel, K., and Schiller, J. (2018). Recent Developments of Useful MALDI Matrices for the Mass Spectrometric Characterization of Lipids. *Biomolecules* 8, 173–198. doi:10.3390/biom8040173

Lv, Y., Lin, Z., Tan, T., and Svec, F. (2013). Preparation of Porous Styrenics-Based Monolithic Layers for Thin Layer Chromatography Coupled with Matrix-Assisted Laser-Desorption/ionization Time-Of-Flight Mass Spectrometric Detection. *J. Chromatogr. A* 1316, 154–159. doi:10.1016/j.chroma.2013.09.089

Makowska, M., and Pellinen, T. (2021). Thin Layer Chromatography Performed in Stages to Identify the Presence of Aromatic like Fraction in Chosen Bitumen Modifiers. *J. Traffic Transportation Eng. (English Edition)* 8, 453–466. doi:10.1016/j.jtte.2019.09.008

Manikandan, M., Kazibwe, Z., Hasan, N., Deenadayalan, A., Gopal, J., Pradeep, T., et al. (2016). Biological Desorption Electrospray Ionization Mass Spectrometry (DESI MS) - Unequivocal Role of Crucial Ionization Factors, Solvent System and Substrates. *Trac Trends Anal. Chem.* 78, 109–119. doi:10.1016/j.trac.2016.02.013

Mernie, E. G., Tolesa, L. D., Lee, M.-J., Tseng, M.-C., and Chen, Y.-J. (2019). Direct Oligosaccharide Profiling Using Thin-Layer Chromatography Coupled with Ionic Liquid-Stabilized Nanomatrix-Assisted Laser Desorption-Ionization Mass Spectrometry. *Anal. Chem.* 91, 11544–11552. doi:10.1021/acs.analchem.9b01241

Mirón-Mérida, V. A., Wu, M., Gong, Y. Y., Guo, Y., Holmes, M., Ettelaie, R., et al. (2021). Mathematical Characterization of Ink Diffusion and Imbibition Processes in Chromatography Paper as a Potential Biosensing Platform. *Sensing Bio-Sensing Res.* 32, 100421. doi:10.1016/j.sbsr.2021.100421

Mohammad, A., Khan, M., Ullah, Q., and Mohammad, F. (2017). Effective Separation of Organic Dyes Using Ionic Liquids as green mobile Phase and Polyaniline-Modified Silica Gel Nanocomposite-Based Thin-Layer Chromatography. *J. Anal. Sci. Technol.* 8, 1–14. doi:10.1186/s40543-017-0127-8

Móricz, Á. M., Ott, P. G., Yüce, I., Darcsi, A., Béni, S., and Morlock, G. E. (2018). Effect-directed Analysis via Hyphenated High-Performance Thin-Layer Chromatography for Bioanalytical Profiling of sunflower Leaves. *J. Chromatogr. A* 1533, 213–220. doi:10.1016/j.chroma.2017.12.034

Morlock, G., and Schwack, W. (2010). Coupling of Planar Chromatography to Mass Spectrometry. *Trac Trends Anal. Chem.* 29, 1157–1171. doi:10.1016/j.trac.2010.07.010

Morlock, G., and Ueda, Y. (2007). New Coupling of Planar Chromatography with Direct Analysis in Real Time Mass Spectrometry. *J. Chromatogr. A* 1143, 243–251. doi:10.1016/j.chroma.2006.12.056

Ovcharov, M. V., Barsegyan, S. S., Kovaleva, S. A., Kulikova, L. N., and Borisov, R. S. (2017). New Approaches to the Application of DART Mass Spectrometry Coupled with Planar Chromatography for the Analysis of Mixtures of Organic Compounds. *J. Anal. Chem.* 72, 1446–1450. doi:10.1134/S106193481714009X

Peters, V., and Spangenberg, B. (2019). Equol Determination in Cattle Manure by HPTLC-DART-TOF-MS. *J. Liquid Chromatogr. Relat. Tech.* 42, 311–316. doi:10.1080/10826076.2019.1585616

Qu, J., Zhang, Z.-H., Zhang, H., Weng, Z.-T., and Wang, J.-Y. (2021). Diethyl Malonate-Based Turn-On Chemical Probe for Detecting Hydrazine and its Bio-Imaging and Environmental Applications with Large Stokes Shift. *Front. Chem.* 8, 4457–4463. doi:10.3389/fchem.2020.602125

Rejšek, J., Vrkoslav, V., Vaikkinen, A., Haapala, M., Kauppila, T. J., Kostiainen, R., et al. (2016). Thin-Layer Chromatography/Desorption Atmospheric Pressure Photoionization Orbitrap Mass Spectrometry of Lipids. *Anal. Chem.* 88, 12279–12286. doi:10.1021/acs.analchem.6b03465

Rondeau, D. (2017). "DART Mass Spectrometry: Principle and Ionization Facilities," in *Direct Analysis in Real Time Mass Spectrometry* (Weinheim: Wiley-VCH Verlag GmbH & Co. KGaA), 43–80. doi:10.1002/9783527803705.ch2

Sahaka, M., Amara, S., Lecomte, J., Rodier, J.-D., Lafont, D., Villeneuve, P., et al. (2021). Quantitative Monitoring of Galactolipid Hydrolysis by Pancreatic Lipase-Related Protein 2 Using Thin Layer Chromatography and Thymol-Sulfuric Acid Derivatization. *J. Chromatogr. B* 1173, 122674. doi:10.1016/j.jchromb.2021.122674

Sharma, V., and Kumar, R. (2017). Fourier Transform Infrared Spectroscopy and High Performance Thin Layer Chromatography for Characterization and Multivariate Discrimination of Blue Ballpoint Pen Ink for Forensic Applications. *Vibrational Spectrosc.* 92, 96–104. doi:10.1016/j.vibspec.2017.05.006

Siebenhaller, S., Gentes, J., Infantes, A., Muhle-Goll, C., Kirschhöfer, F., Brenner-Weiß, G., et al. (2018). Lipase-Catalyzed Synthesis of Sugar Esters in Honey and Agave Syrup. *Front. Chem.* 6, 1–9. doi:10.3389/fchem.2018.00024

Speight, J. (2020). *Shale Oil and Gas Production Processes*. Laramie, WY: CD&W Inc. doi:10.1016/B978-0-12-813315-6.00009-9

Stanek, N., Kafarski, P., and Jasicka-Misiak, I. (2019). Development of a High Performance Thin Layer Chromatography Method for the Rapid Qualification and Quantification of Phenolic Compounds and Abscisic Acid in Honeys. *J. Chromatogr. A* 1598, 209–215. doi:10.1016/j.chroma.2019.04.052

Taki, T. (2015). TLC-blot (Far-Eastern Blot) and its Application to Functional Lipidomics. *Methods Mol. Biol.* 1314, 219–241. doi:10.1007/978-1-4939-2718-0_24

Torretta, E., Fania, C., Vasso, M., and Gelfi, C. (2016). HPTLC-MALDI MS for (Glyco)sphingolipid Multiplexing in Tissues and Blood: A Promising Strategy for Biomarker Discovery and Clinical Applications. *Electrophoresis* 37, 2036–2049. doi:10.1002/elps.201600094

Van Berkel, G. J., Ford, M. J., and Deibel, M. A. (2005). Thin-Layer Chromatography and Mass Spectrometry Coupled Using Desorption Electrospray Ionization. *Anal. Chem.* 77, 1207–1215. doi:10.1021/ac048217p

Winter, G. T., Wilhide, J. A., and LaCourse, W. R. (2017). Analysis of Hop Acids by Thin-Layer Chromatography and the Molecular Ionization Desorption Analysis Source (MIDAS) for Mass Spectrometry. *Int. J. Mass Spectrom.* 422, 74–79. doi:10.1016/j.ijms.2017.08.013

Winter, G. T., Wilhide, J. A., and LaCourse, W. R. (2015). Molecular Ionization-Desorption Analysis Source (MIDAS) for Mass Spectrometry: Thin-Layer Chromatography. *J. Am. Soc. Mass. Spectrom.* 27, 352–358. doi:10.1007/s13361-015-1289-5

Zaikin, V. G., and Borisov, R. S. (2021). Options of the Main Derivatization Approaches for Analytical ESI and MALDI Mass Spectrometry. *Crit. Rev. Anal. Chem.* 2021, 1–81. doi:10.1080/10408347.2021.1873100

Zaikin, V., and Halket, J. (2009). *A Handbook of Derivatives for Mass Spectrometry*. Chichester: IM Publications.

Zarzycki, P. K. (2015). Staining and Derivatization Techniques for Visualization in Planar Chromatography. *Instrumental Thin-Layer Chromatogr.* 2015, 191–237. doi:10.1016/B978-0-12-417223-4.00008-X

Zhang, J., Zhou, Z., Yang, J., Zhang, W., Bai, Y., and Liu, H. (2012). Thin Layer Chromatography/Plasma Assisted Multiwavelength Laser Desorption Ionization Mass Spectrometry for Facile Separation and Selective Identification of Low Molecular Weight Compounds. *Anal. Chem.* 84, 1496–1503. doi:10.1021/ac202732y

Zhang, N., Wang, M., Li, Y., Zhou, M., Wu, T., and Cheng, Z. (2020). TLC-MS Identification of Alkaloids in Leonuri Herba and Leonuri Fructus Aided by a Newly Developed Universal Derivatisation Reagent Optimised by the Response Surface Method. *Phytochem. Anal.* 32, 242–251. doi:10.1002/pca.2970

Zhang, P., Zhang, L., Shi, J., Zhang, N., Li, Y., Wu, T., et al. (2019). TLC-electrostatic Field Induced spray Ionization-MS Analysis of Diverse Structural Skeletons and its Coupling with TLC Bioautography for Characterization of Lipase Inhibitory Components in American Ginseng. *J. Pharm. Biomed. Anal.* 174, 486–494. doi:10.1016/j.jpba.2019.06.019

Zhang, Z., Ratnayaka, S. N., and Wirth, M. J. (2011). Protein UTLC-MALDI-MS Using Thin Films of Submicrometer Silica Particles. *J. Chromatogr. A* 1218, 7196–7202. doi:10.1016/j.chroma.2011.07.098

Zhong, X., Qiao, L., Liu, B., and Girault, H. H. (2015). Ambient *In Situ* Analysis and Imaging of Both Hydrophilic and Hydrophobic Thin Layer Chromatography Plates by Electrostatic spray Ionization Mass Spectrometry. *RSC Adv.* 5, 75395–75402. doi:10.1039/C5RA10977A

Conflict of Interest: The authors declare that the research was conducted in the absence of any commercial or financial relationships that could be construed as a potential conflict of interest.

Publisher's Note: All claims expressed in this article are solely those of the authors and do not necessarily represent those of their affiliated organizations, or those of the publisher, the editors, and the reviewers. Any product that may be evaluated in this article, or claim that may be made by its manufacturer, is not guaranteed or endorsed by the publisher.

frontiers in Chemistry

ORIGINAL RESEARCH
published: 14 January 2022
doi: 10.3389/fchem.2021.785848

MALDI-TOF MS Based Bacterial Antibiotics Resistance Finger Print for Diabetic Pedopathy

Haojie Sun[1,2], Peng Lai[2], Wei Wu[3], Hao Heng[2], Shanwen Si[2], Yan Ye[2], Jiayi Li[2], Hehe Lyu[2], Caiyan Zou[2], Mengzhe Guo[4], Yu Wang[2], Houfa Geng[2]* and Jun Liang[1,2]**

[1]Medical College, Soochow University, Suzhou, China, [2]Xuzhou Central Hospital, Xuzhou Clinical School of Xuzhou Medical University, Xuzhou, China, [3]Affiliated Hospital of Xuzhou Medical University, Xuzhou, China, [4]Jiangsu Key Laboratory of New Drug Research and Clinical Pharmacy, Xuzhou Medical University, Xuzhou, China

Diabetes mellitus has become a major global health issue. Currently, the use of antibiotics remains the best foundational strategy in the control of diabetic foot infections. However, the lack of accurate identification of pathogens and the empirical use of antibiotics at early stages of infection represents a non-targeted treatment approach with a poor curative effect that may increase the of bacterial drug resistance. Therefore, the timely identification of drug resistant bacteria is the key to increasing the efficacy of treatments for diabetic foot infections. The traditional identification method is based on bacterial morphology, cell physiology, and biochemistry. Despite the simplicity and low costs associated with this method, it is time-consuming and has limited clinical value, which delays early diagnosis and treatment. In the recent years, MALDI-TOF MS has emerged as a promising new technology in the field of clinical microbial identification. In this study, we developed a strategy for the identification of drug resistance in the diagnosis of diabetic foot infections using a combination of macro-proteomics and MALDI MS analysis. The macro-proteomics result was utilized to determine the differential proteins in the resistance group and the corresponding peptide fragments were used as the finger print in a MALDI MS analysis. This strategy was successfully used in the research of drug resistance in patients with diabetic foot infections and achieved several biomarkers that could be used as a finger print for 4 different drugs, including ceftazidime, piperacillin, levofloxacin, and tetracycline. This method can quickly confirm the drug resistance of clinical diabetic foot infections, which can help aid in the early treatment of patients.

Keywords: MALDI TOF, macro-proteomics, drug resistance, diabetic foot, finger print

OPEN ACCESS

Edited by:
Kezhi Jiang,
Hangzhou Normal University, China

Reviewed by:
Haoyang Wang,
Shanghai Institute of Organic Chemistry, China
Guodong Cao,
Anhui Medical University, China

****Correspondence:***
Jun Liang
mwlj521@163.com
Houfa Geng
genghoufa@njmu.edu.cn
Yu Wang
wangyubh@163.com

Specialty section:
This article was submitted to Analytical Chemistry, a section of the journal Frontiers in Chemistry

Received: *29 September 2021*
Accepted: *27 December 2021*
Published: *14 January 2022*

Citation:
Sun H, Lai P, Wu W, Heng H, Si S, Ye Y, Li J, Lyu H, Zou C, Guo M, Wang Y, Geng H and Liang J (2022) MALDI-TOF MS Based Bacterial Antibiotics Resistance Finger Print for Diabetic Pedopathy. Front. Chem. 9:785848. doi: 10.3389/fchem.2021.785848

INTRODUCTION

Diabetes mellitus has become a major global health issue affecting approximately 9.3% of the population worldwide, and is expected to increase by 25% by 2030 (Sinclair et al., 2020). Approximately 30% of diabetic patients will develop diabetic pedopathy during their lifetime (Armstrong et al., 2017). Of all the complications of diabetes mellitus, diabetic pedopathy poses the most severe risks, and may result in a shortened life expectancy and a dramatic decline in the quality of life (Lavery et al., 2016). In the past few decades, diabetic pedopathy has ranked 10th among all diseases and is often a huge financial burden to the patients family as well as society as a whole (Lazzarini et al., 2018).

At present, antibiotics have been the foundational strategy used to control diabetic foot infections. Due to the lack of accurate identification of the pathogens, the empirical use of antibiotics at the early stages of infection represents a non-targeted treatment approach with a poor curative effect, and may result in bacterial drug resistance (Munita and Arias, 2016). The World Health Organization has recognized antibiotic resistance as one of the most important public health threats in the 21st century (World Health Organization, 2014). The ineffective use of antibiotics will hinder wound healing in patients with diabetic foot infections, and increase the length of stay in hospitals as well as hospital costs. Therefore, timely identification of bacteria and drug resistance is the key in the appropriate treatment of diabetic foot infections (Caruso et al., 2021).

Enterobacterales and *Staphylococcus aureus* are the most common pathogens identified in diabetic pedopathy (Ramirez et al., 2018; Alexi et al., 2021). They play a crucial role in MDR organisms, and their broad antibiotics resistance has increasingly attracted more attention from healthcare associated workers worldwide. Especially concerning is the resistance to cephalosporin and penicillin antibiotics, which may lead to life-threatening issues in the treatment of diabetes-related infections (Weinstein et al., 2019). Over the last decade, the resistance of Enterobacterales to cephalosporin has dramatically increased worldwide. The underlying resistance mechanisms are complex and difficult to be identify. Additionally, carbapenem-hydrolyzing enzymes produced by bacterium are also of great concern (Mao et al., 2017). For example, Klebsiella pneumonia, which has the characteristics of easy-spreading and extensive-contaminating, could have a detrimental effect in its surroundings, such as healthcare settings (Tascini et al., 2015). *S aureus* has primarily exhibits penicillin-resistance. Due to the horizontal transfer and natural selection of genes that encode for a mutant penicillin-binding protein (Masters et al., 2020), this bacteria has a low affinity to penicillin molecules, which underlies the penicillin-resistance.

Bacterial identification is a crucial component of clinical practice. The traditional method is based on the assessment of bacterial morphology, cell physiology, and biochemistry (Sun et al., 2021). While the simplicity of this method and low costs make it an attractive option, it is time-consuming and has limited clinical value due to its low positive rate (Jasson et al., 2010; Oberhettinger et al., 2020). This results in diagnostic and treatment delays.

In recent years, MALDI-TOF MS has emerged as a promising new technology in the field of clinical microbial identification. It is fast, stable, accurate, sensitive, and has a high resolution (Tan et al., 2012; Scott et al., 2016). Its expanded research application in clinical microorganisms has involved many fields, such as bacterial identification, drug resistance analysis, virulence, and epidemiology (Kostrzewa, 2018). Its potential for the rapid detection of bacterial drug resistance has made it especially attractive to many scholars. It falls within the mass range by giving the protein that is resistant to bacteria, and then analyzes the drug resistance of bacteria by looking for characteristic spectral peaks. This study explores its use in detecting bacterial drug resistance in diabetic foot infections and provides a basis for rapid clinical antibiotic selection.

We have developed a MALDI mass spectrometry (MS) fingerprint analysis to be used in the diagnosis of antibiotic resistance in patients with diabetic foot infections (**Figure 1**). First, the bacteria from the affected tissue of patients were cultured and the species were identified. The bacterial cultures were then tested for drug resistance and divided into either a drug-resistant or drug-sensitive group. Next, the bacterial macro-proteomics analysis was introduced to identify the differential proteins between these two groups. Finally, the fragments of the identified differential proteins were compared using the MALDI analysis to identify the drug-resistance finger print. This study could aid in the establishment of a rapid drug resistance MALDI identification method to be used for the clinical the determination of treatments for diabetic foot infections.

EXPERIMENTAL

Patient Characteristics

The subjects of the study included type 2 diabetic foot patients hospitalized in the Department of Endocrine and Metabolic Diseases of the Xuzhou Central Hospital from June 2021 to August 2021. The main inclusion criteria were: age was within the range of 18–80 years old, and Wagner 3–4. Exclusion criteria: no standing debridement, immunosuppressants had been used within 3 months prior to admission, and the use of antibiotics in the 4 weeks prior to admission. The diagnosis of diabetes mellitus is based on the 1999 WHO diabetes mellitus diagnostic criteria. The diagnosis of diabetic foot is based on the International Diabetes Foot working group (IWGDF) guide (Lipsky et al., 2020). This study was designed and implemented according to the declaration of Helsinki. All patients and their families were informed and agreed to participate in the study, which was approved by the hospital ethics committee of Xuzhou central hospital.

Specimen Collection

After flushing the wound with sterile saline, a well-trained diabetic podiatrist took the deep necrotic tissue of the wound to avoid superficial tissue contamination, which could cause inaccurate results. A total of 16 necrotic tissue specimens were collected and divided into two parts under sterile conditions: one part was used for conventional microbial culture and the other was used for MALDI TOF MS analysis.

Bacterial Inactivation and Protein Extraction

Bacterial inactivation was performed before MS analysis. The bacterial colonies after 72 h incubation were resuspended in 200 µl of pure water. The concentration of bacteria was chosen to be 5×10^6 CFU/ml. Then 600 µl of methanol (MeOH) was added to obtain a final 75% MeOH. This mixture was incubated for 15 min and then centrifuged at 12,000 rom for 10 min to obtain a bacterial pellet. The supernatant was removed and the bacterial pellet was resuspended in 100% acetonitrile (ACN) with 0.1% formic acid. The mixture was passed through the secondary

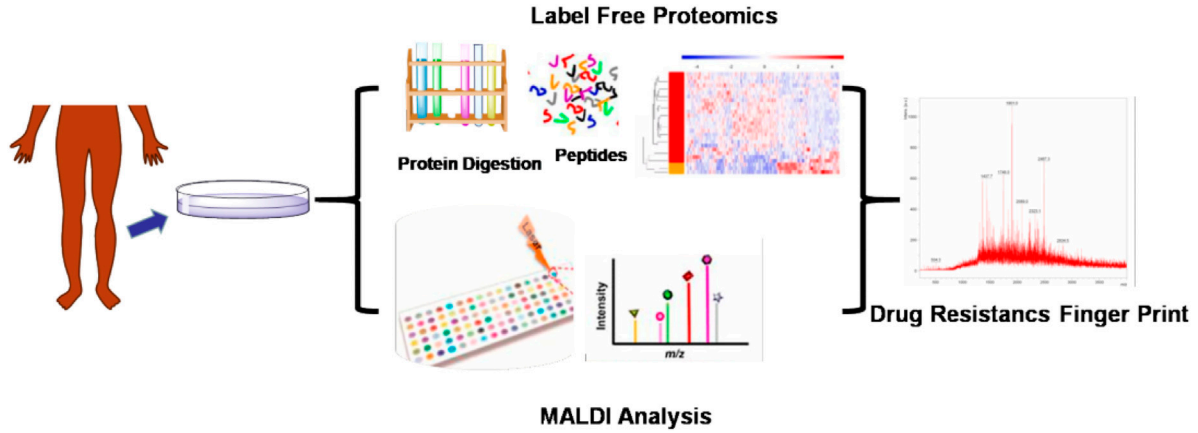

FIGURE 1 | The strategy of the drug resistance finger print research for diabetic foot.

centrifugation (also 12,000 rpm for 10 min) and the bacterial proteins were extracted.

MALDI TOF MS Method

MALDI TOF MS analysis was performed by a Bruker ultrafle Xtreme MALDI TOF/TOF mass spectrometry (Bruker Daltonics, France). α-cyano-4- hydroxycinnamic acid (HCCA) was used as the matrix and was dissolved into ACN. The extracted proteins were dissolved into water and 1 μl of protein solution was mixed with 1 μl of matrix. The mixture was dripped on a reusable polished steel target and left to dry. The ion mode was positive ion mode with delay: 150 ns; ion source 1 voltage: 20 kV; ion source 2 voltage: 18 kV; lens voltage: 6 kV. All spectra were shown baseline-subtracted, smoothed, and auto-scaled in the *Y*-direction, covering a range of 300–3,000 Da.

Label Free Macro-Proteomics Analysis

100 μg of protein was reduced with 5 m Mdithiothreitol (DTT) for 1 h at 37°C and subsequently alkylated with 10 mM iodoacetamide for 45 min at RT (room temperature) in the dark. Samples were diluted 1:3 with 50 mM Tris-HCl (pH 8.0) and subjected to proteolytic digestion with trypsin (Promega) at a 1:50 enzyme-to-substrate ratio and incubated overnight at RT. The digested samples were then acidified with 50% trifluoroacetic acid (TFA, Sigma) to a pH value of approximately 2.0. Tryptic peptides were desalted on reversed-phase C18 SPE columns and dried using a Speed-Vac.

Peptides (0.8 μg) were separated on an Easy nLC 1200 UHPLC system (Thermo Scientific) on an in-house packed 20 cm × 75 mm diameter C18 column. The column the flow rate was 0.200 μL/min with 0.1% formic acid and 2% acetonitrilein water (A) and 0.1% formic acid, 90% acetonitrile (B). The peptides were separated with a 6–30% B gradient in 84 min and analyzed using the Thermo Velos mass spectrometer (Thermo Scientific). Parameters were as follows: MS1: resolution—60,000, mass range 350–1800 m/z, MS2: resolution −=50,000, high-energy collision dissociation activation energy (HCD) was 37 eV, isolation width (m/z) was 0.7, AGC Target was 2.0 e5, Max IT was 10^5 ms.

Data Statistics

Experiments were repeated at least three times with consistent results. Data are presented as the Mean ± SEM (standard error of the mean) or Mean ± SD (standard deviation). Differences between groups were determined using a two-tailed Mann-Whitney U test or two-tailed Student's *t*-test. Pearson correlation coefficients (r) were calculated to evaluate correlation and statistical significance was assessed by a two-tailed *t*-test. The results of western blot analysis are the representative images of at least three independent experiments. For boxplots, the center line represents the median, the box limits show the upper and lower quartiles, and the outliers are represented as individual data points.

RESULTS

A total of 16 samples from patients with diabetic foot infections were collected and used to create bacterial cultures. 5 Gram-positive strains and 11 Gram-negative strains were successfully cultivated. Under the authentication of MALDI MS, the Gram-positive strains consisted of *staphylococcus aureus* and the Gram-negative strains consisted of bacillus (**Figure 2**). The bacterial cultures were then processed to determine drug-resistance. Both the *staphylococcus aureus* and bacillus were tested using 2 types of drug resistance experiments. In the case for bacillus, ceftazidime and piperacillin were chosen as the test drugs, and levofloxacin and tetracycline were chosen for *staphylococcus aureus*. The proteins in these bacterial cultures were then extracted and passed through the macro-proteomics and MALDI analysis.

For the bacillus, a total 1,500 proteins were detected by the macro-proteomics analysis. Additionally, there were over 500 identical proteins among them. The samples were then divided into two groups according to the drug resistance test results. As shown in **Supplementary Table S1**, there are five bacillus samples in the ceftazidime resistance group and six bacillus samples in the other group. Moreover, PCA analyses were carried out for these two groups according to the identical proteins. As shown in

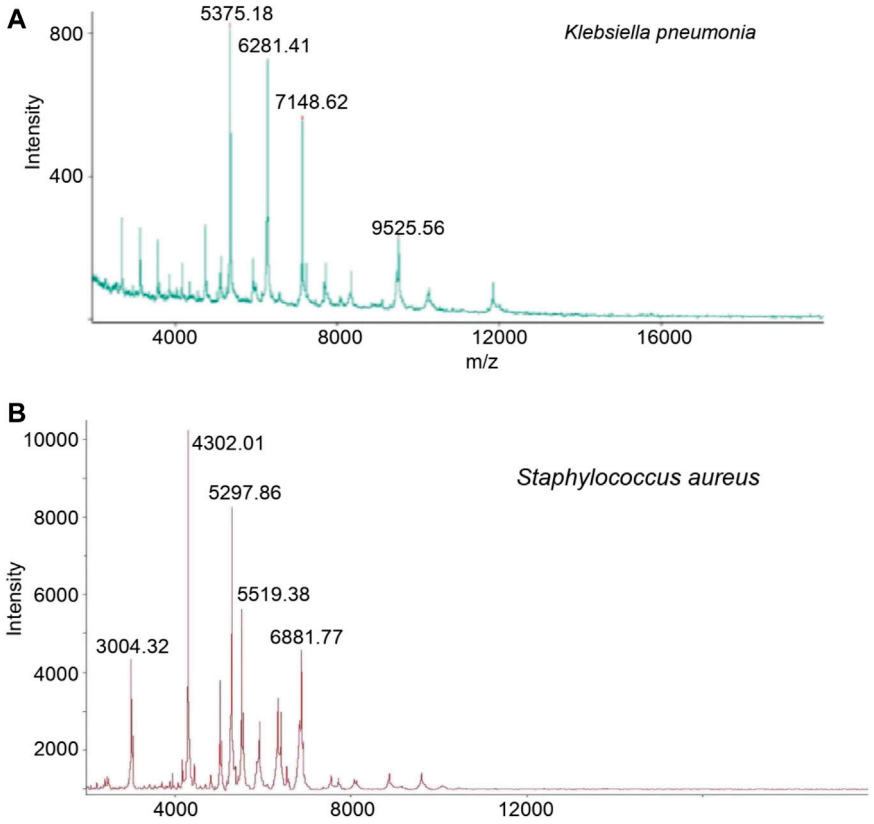

FIGURE 2 | The identification of *Klebsiella pneumonia* **(A)** and *Staphylococcus aureus* **(B)** based on MALDI TOF analysis after bacterial cultured.

Figure 3, these two groups can be well distinguished, with the Q^2 over 0.8. A total of 10 differential proteins ($p < 0.05$ in *t*-test) were obtained, including fumC, fmt, rpsT, proX, fisH, nuoC, proC, tyrS, ribC, and bfr. Additionally, the digested peptides fragments were found in the database, and were compared with the MALDI TOF analysis. Finally, three peptides were consistently obtained in both results (**Figures 3C,D**, **Supplementary Figure S1**), including the peptides from nuoC with a sequence of EALEWGTTGAGLR (m/z 1,360.7), from fisH with a sequence of ESTAYHEAGHAIIGR (m/z 1,611.8), and from tyrS with a sequence of LAEEIIYGPEHVSTGASNDIK (m/z 2243.1). These three peaks of peptides can be considered the finger print for the resistance of bacillus to ceftazidime.

The samples were also divided into two groups according to piperacillin resistance. As shown in **Supplementary Table S1**, there are six bacillus samples in the piperacillin resistance group and five bacillus samples in the other group. The PCA analyses were carried out for these two groups according to the identical proteins. As shown in **Figure 4**, these two groups can be well distinguished, with the Q^2 over 0.8. A total of 14 differential proteins ($p < 0.05$ in *t*-test) were obtained, including ybjP, rpmI, rof, rim, acnA, lolA, engB, hisS, bglX, cpxR, phoP, trxA, ompA, and bfr. Additionally, the digested peptides fragments were found in the database, which were compared with the MALDI TOF analysis. Finally, three peptides were obtained consistently in both results (**Figures 4C,D**, **Supplementary Figure S2**), including the peptides from acnA with a sequence of SDTYGWQEDSTYIR (m/z 1720.8), from ompA with a sequence of ATLKPEGQAALDQLYSQLSNLDPK (m/z 2600.4), and from rpmI with a sequence of GDLGLVIACLPYA (m/z 1,361.7). These three peaks of peptides can be considered as the finger print for the resistance of bacillus to piperacillin..

For the *staphylococcus aureus*, a total 1,000 proteins were detected by macro-proteomics analysis. In addition, there are over 200 identical proteins among them. The samples were divided into two groups according to the two other drug resistance test results. As shown in **Supplementary Table S2**, there are two *staphylococcus aureus* samples in levofloxacin resistance group and three *staphylococcus aureus* samples in the sensitive group. Moreover, the PCA analysis were carried out for these two groups according to the identical proteins. As shown in **Figure 5**, these two groups can be well distinguished with the Q^2 over 0.8. But only 3 differential proteins ($p < 0.05$ in *t*-test) were obtained, including rpsS, rplV, and rpsQ. Additionally, the digested peptides fragments were found in the database, which were compared with the MALDI TOF analysis. Finally, three peptides were obtained consistently in both results (**Figures 5C,D**, **Supplementary Figure S3**), including the peptides from rpsS with the sequence QHVPVFVTDRMVGHK (m/z 1722.9), from rplV with the sequence VLESAIANARHNDGADIDDLKVTK (m/z 2538.3),

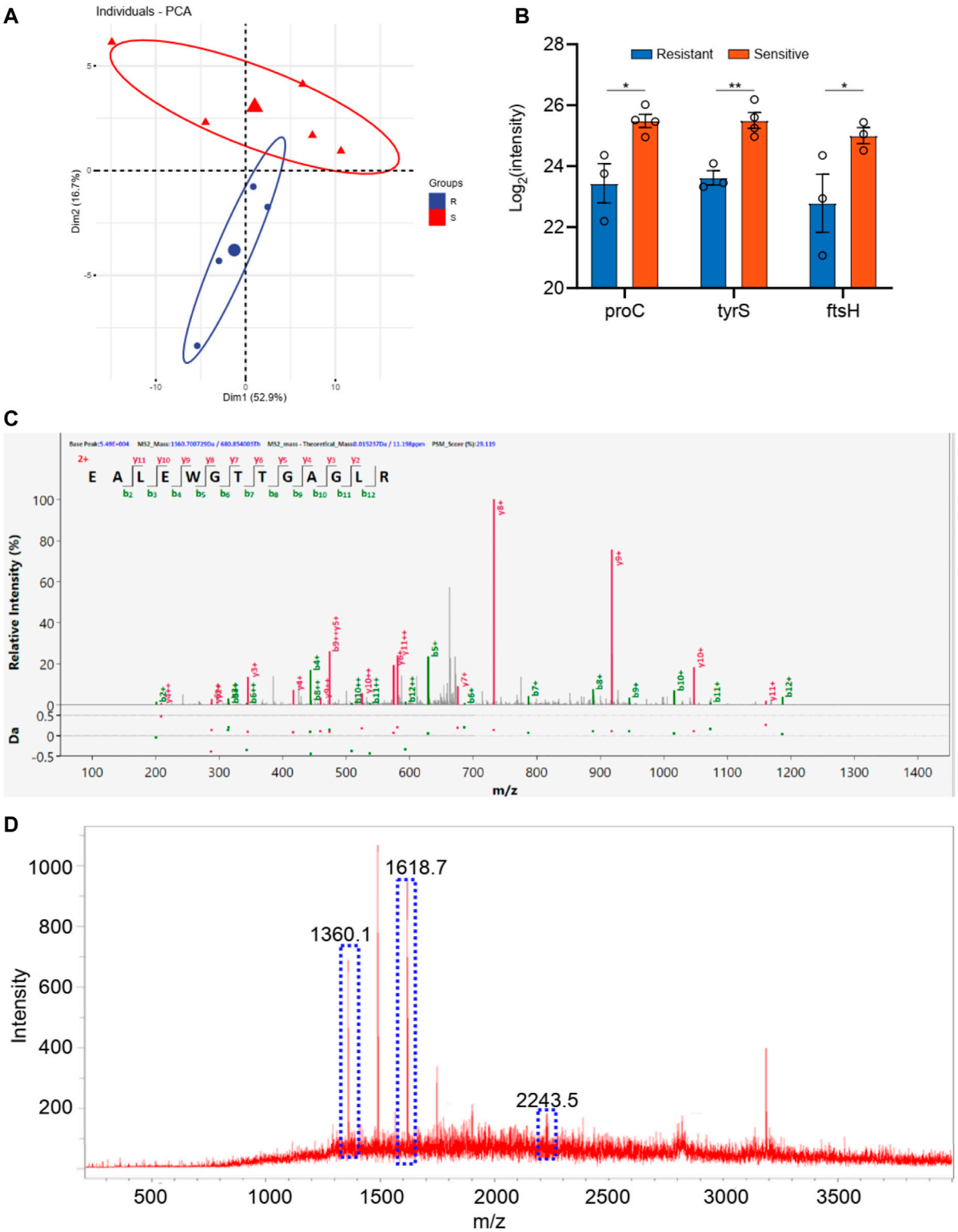

FIGURE 3 | (A) The PCA analysis of drug resistance of ceftazidime for *Klebsiella pneumonia*; **(B)** The differential proteins between drug resistance group and drug sensitive group; **(C)** The corresponding differential peptides and **(D)** the finger print in MALDI TOF.

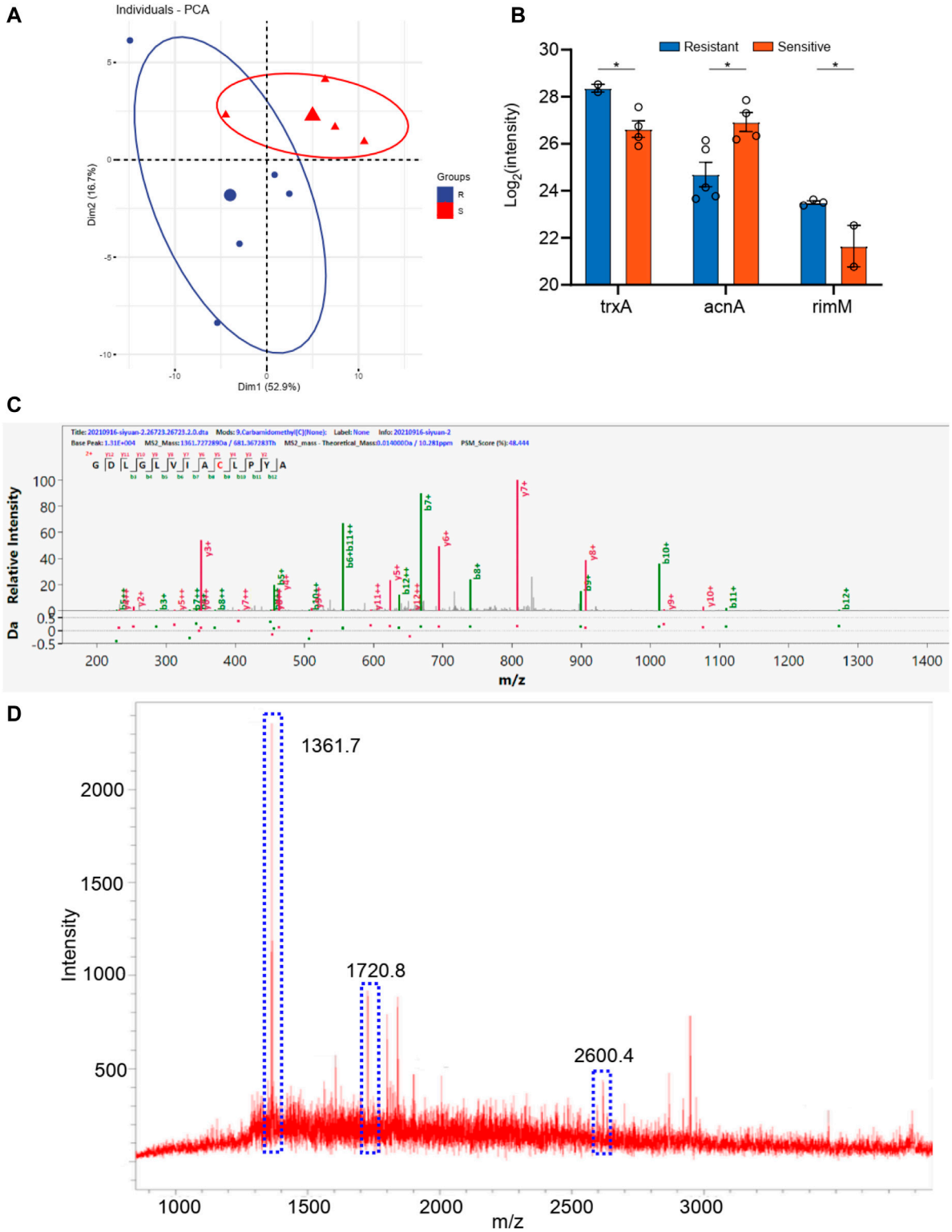

FIGURE 4 | (A) The PCA analysis of drug resistance of piperacillin for *Klebsiella pneumonia*; **(B)** The differential proteins between drug resistance group and drug sensitive group; **(C)** The corresponding differential peptides and **(D)** the finger print in MALDI TOF.

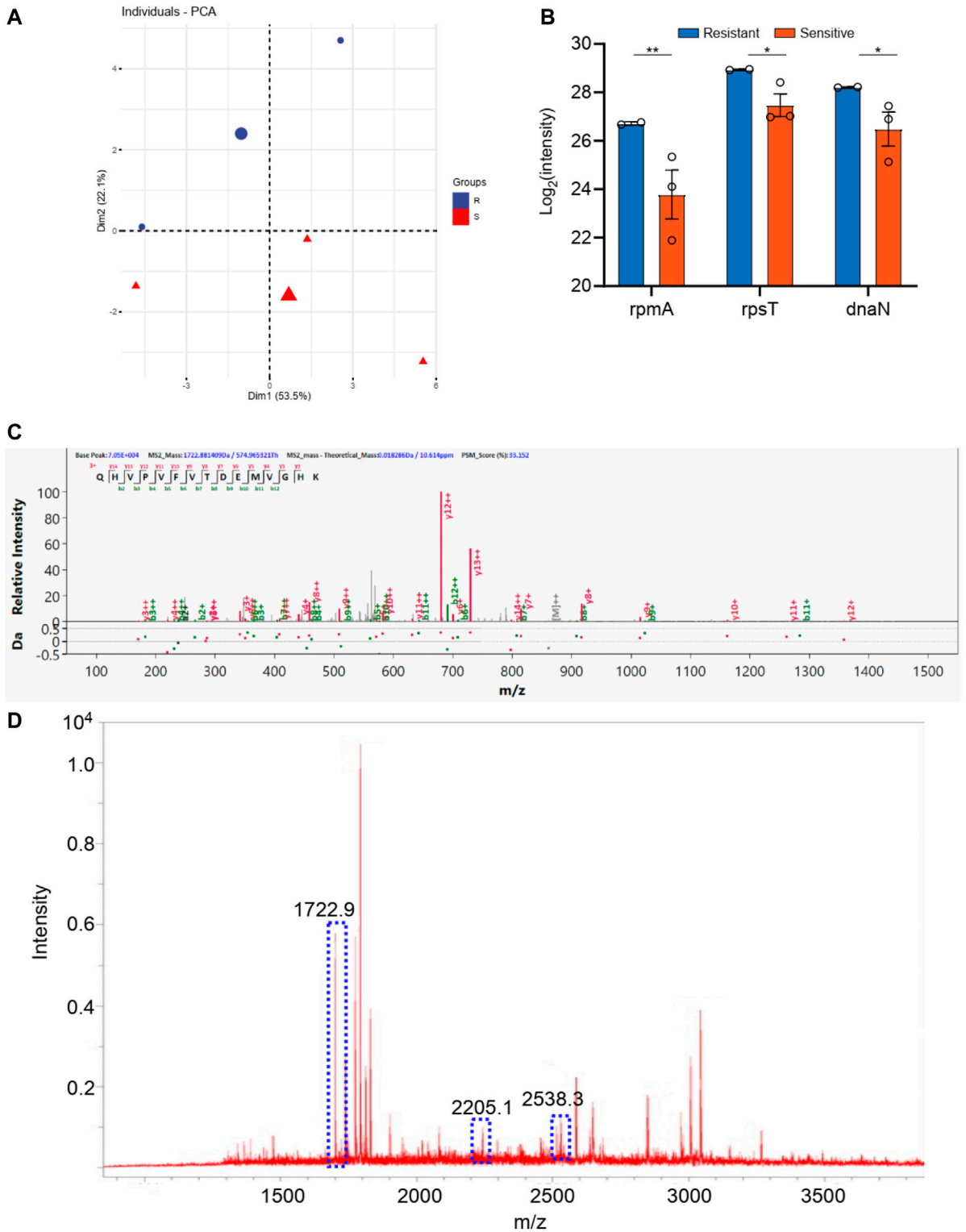

FIGURE 5 | (A) The PCA analysis of drug resistance of levofloxacin for *Staphylococcus aureus*; **(B)** The differential proteins between drug resistance group and drug sensitive group; **(C)** The corresponding differential peptides and **(D)** the finger print in MALDI TOF.

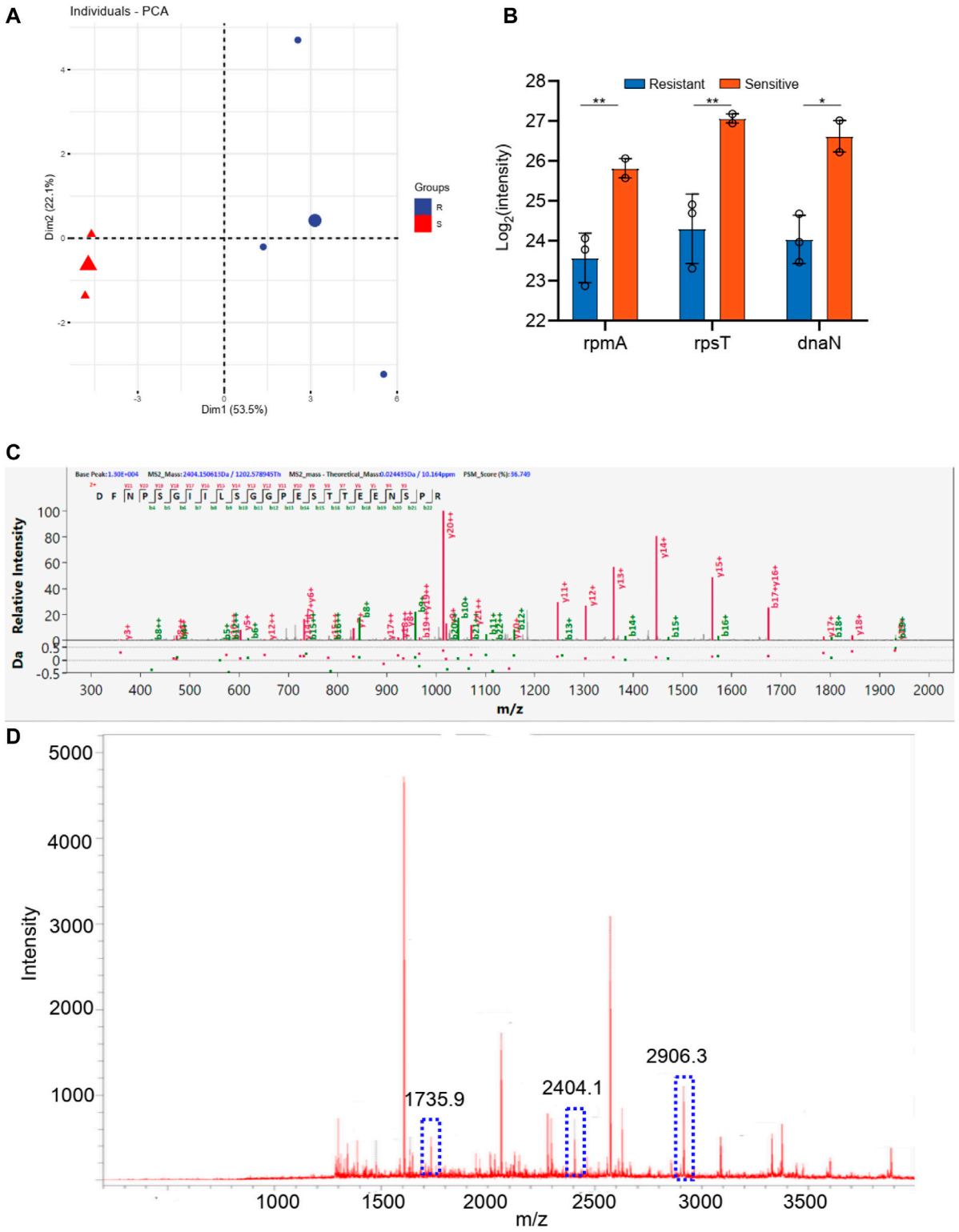

FIGURE 6 | (A) The PCA analysis of drug resistance of tetracycline for *Staphylococcus aureus*; **(B)** The differential proteins between drug resistance group and drug sensitive group; **(C)** The corresponding differential peptides and **(D)** the finger print in MALDI TOF.

and from rpsQ with the sequence LHVHDENNECGIGDVVEIR (m/z 2205.1). These three peaks of peptides can be considered as the finger print for the levofloxacin resistance of *staphylococcus aureus*.

The *staphylococcus aureus* samples were also divided into two groups according to the tetracycline resistance results. As shown in **Supplementary Table S2**, there are three *staphylococcus aureus* samples in levofloxacin resistance group and two *staphylococcus aureus* samples in the sensitive group. As shown in **Figure 6**, these two groups can be well distinguished with the Q^2 over 0.8. And 10 differential proteins ($p < 0.05$ in *t*-test) were obtained, including rpmA, rpsT, dnaN, guaA, proS, alaS, frr, adk, groS, and rplE. Additionally, the digested peptides fragments were found in the database, which were compared with the MALDI TOF analysis. Finally, three peptides were obtained consistently in both results (**Figures 6C,D**, **Supplementary Figure S4**), including the peptides from rplE with the sequence AKLHDYYKDEVVKK (m/z 1735.9), from guaA with the sequence DFNPSGIILSGGPESTTEENSPR (m/z 2404.2), and from proS with the sequence DAYSFHTSQESLQETYDAMYAAYSK (m/z 2906.3). These three peaks of peptides can be considered as the finger print for the tetracycline resistance of *staphylococcus aureus*.

In addition, we added 12 bacterial samples from diabetic podiatry to validate our method, including 7 samples of ceftazidime resistance of bacillus, and 5 samples of levofloxacin resistance of *staphylococcus aureus*. We examined whether there were characteristic peaks of resistance in these samples. It is worth noting that these samples were all tested blind, that is, the tester did not know whether the samples were drug-resistant bacteria samples before the test. The detection results showed that at least one characteristic peak of drug resistance could be detected in these drug resistant bacteria samples, indicating that the method developed by us has good accuracy (**Supplementary Table S3**, and **Supplementary Figure S4, S5**).

DISCUSSION

Recent studies have suggested that the microbiota in diabetic foot infections are diverse, which is typically beyond the identification capabilities of the traditional culture method. Although molecular-based methods, such as qPCR and mNGS, can effectively identify the bacterial species, they are difficult to routinely carry out in clinical practice and also have several inherent biases (Malone et al., 2017; Sadeghpour Heravi et al., 2019). Overall, there is still no simple and specific method to identify the antibiotics resistance of bacteria.

Using bacterial cultures made from diabetic pedopathy patients, we further conducted the MALDI TOF analysis. Consistent with previous studies (Złoch et al., 2021), our study found both Gram-positive and Gram-negative bacterium. A total of 5 strains of Gram-positive bacteria and 11 strains of Gram-negative bacteria were used for further MALDI detection and analysis, which authenticated that the Gram-positive strains consisted of *staphylococcus aureus* and the Gram-negative strains consisted of bacillus. Subsequently, a macro-proteomics analysis was carried out to detect the proteins associated with antibiotic resistance. As a result, a total of 1,500 proteins and 1,000 proteins were detected in the bacillus and *staphylococcus aureus* by macro-proteomics analysis, respectively. Combined with the results of bacterial culture, MALDI TOF, and proteomics, we found a series of differentially expressed proteins. According to the antibiotics resistance, subgroup analyses have confirmed the presence of a finger print of the different bacterium. The peaks of the nuoC, fisH, and tyrS peptides can be considered as the finger print for the resistance of bacillus to ceftazidime resistance. The peaks of the acnA, ompA, and rpmI peptides can be considered as the finger print for the resistance of bacillus to ceftazidime. The peaks of the rpsS, rplV, and rpsQ peptides can be considered as the finger print for the resistance of *staphylococcus aureus* to levofloxacin resistance. The peaks of the rplE, guaA, and proS peptides can be considered as the finger print for the resistance of *staphylococcus aureus* to tetracycline.

An appropriate antibiotic strategy is well known to be essential in the management of diabetic foot infections. However, the prompt identification of antibiotic resistance is the cornerstone of anti-infection therapy. The bacterial resistance fingerprint identified by this study can guide modifications to clinical antibiotic regimens in the earliest period, which may enhance infection control and wound healing of diabetic pedopathy, shorten the length of hospital stays, and reduce overall costs. Based on the convenience and accuracy of the new method in the identification of a bacteria finger print, as well as results from a previous study (Asghari et al., 2021), has confirmed that MALDI TOF could be widely used in clinic and guide decision-making regarding the use of antibiotics.

CONCLUSION

In this work, we have developed a strategy for the identification of drug resistance in the diagnosis of diabetic foot. Macro-proteomics and MALDI MS analysis were combined in this strategy. From the macro-proteomics result, the differential proteins which in the resistance group were obtained and the correspondence peptide fragments were used as the finger print in MALDI MS analysis. Then this strategy was successfully used in the drug resistance research in diabetic foot patients and achieved several biomarkers as finger print for 4 drugs, including ceftazidime, piperacillin, levofloxacin, and tetracycline. This method can quickly confirm the drug resistance of diabetic foot in clinical, which can help the treatment of patients as early as possible.

DATA AVAILABILITY STATEMENT

The original contributions presented in the study are included in the article/**Supplementary Material**, further inquiries can be directed to the corresponding authors.

ETHICS STATEMENT

The studies involving human participants were reviewed and approved by Xuzhou Central Hospital. The patients/participants provided their written informed consent to participate in this study.

AUTHOR CONTRIBUTIONS

HS, PL, and WW were contributed in sample collection, experimental operations, and data analysis, which can be considered as the co-first authors. HH, SS, YW, and CZ, YY, JL, HL were contributed into data analysis and improving paragraphs. MG, HG, and JuL were contributed in experimental design.

FUNDING

This work was supported by National Natural Science Foundation of China, 81870540; Jiangsu provincial primary talents program, ZBRCC2016022; Postdoctoral study of Department of human resources and social security, Jiangsu Province, China, (2017) No. 279; Science and Education Project for Young medical talents, Jiangsu Province, China, No. QNRC2016388; Xuzhou Primary Research & Development projects, KC21231; Xuzhou Primary Research & Development projects, KC21274.

SUPPLEMENTARY MATERIAL

The Supplementary Material for this article can be found online at: https://www.frontiersin.org/articles/10.3389/fchem.2021.785848/full#supplementary-material

REFERENCES

Armstrong, D. G., Boulton, A. J. M., and Bus, S. A. (2017). Diabetic Foot Ulcers and Their Recurrence. *N. Engl. J. Med.* 376 (24), 2367–2375. doi:10.1056/nejmra1615439

Asghari, E., Kiel, A., Kaltschmidt, B. P., Wortmann, M., Schmidt, N., Hüsgen, B., et al. (2021). Identification of Microorganisms from Several Surfaces by MALDI-TOF MS: *P. aeruginosa* Is Leading in Biofilm Formation. *Microorganisms* 9 (5), 992. doi:10.3390/microorganisms9050992

Caruso, P., Maiorino, M. I., Macera, M., Signoriello, G., Castellano, L., Scappaticcio, L., et al. (2021). Antibiotic Resistance in Diabetic Foot Infection: How it Changed with COVID-19 Pandemic in a Tertiary Care center. *Diabetes Res. Clin. Pract.* 175, 108797. doi:10.1016/j.diabres.2021.108797

Jasson, V., Jacxsens, L., Luning, P., Rajkovic, A., and Uyttendaele, M. (2010). Alternative Microbial Methods: An Overview and Selection Criteria. *Food Microbiol.* 27 (6), 710–730. doi:10.1016/j.fm.2010.04.008

Kostrzewa, M. (2018). Application of the MALDI Biotyper to Clinical Microbiology: Progress and Potential. *Expert Rev. Proteomics* 15 (3), 193–202. doi:10.1080/14789450.2018.1438193

Lavery, L. A., Davis, K. E., Berriman, S. J., Braun, L., Nichols, A., Kim, P. J., et al. (2016). WHS Guidelines Update: Diabetic Foot Ulcer Treatment Guidelines. *Wound Rep. Reg.* 24 (1), 112–126. doi:10.1111/wrr.12391

Lazzarini, P. A., Pacella, R. E., Armstrong, D. G., and van Netten, J. J. (2018). Diabetes-related Lower-Extremity Complications Are a Leading Cause of the Global burden of Disability. *Diabet. Med.* 35, 1297–1299. doi:10.1111/dme.13680

Lienard, A., Hosny, M., Jneid, J., Schuldiner, S., Cellier, N., Sotto, A., et al. (2021). *Escherichia coli* Isolated from Diabetic Foot Osteomyelitis: Clonal Diversity, Resistance Profile, Virulence Potential, and Genome Adaptation. *Microorganisms* 9 (2), 380. doi:10.3390/microorganisms9020380

Lipsky, B. A., Senneville, É., Abbas, Z. G., Aragón-Sánchez, J., Diggle, M., Embil, J. M., et al. (2020). Guidelines on the Diagnosis and Treatment of Foot Infection in Persons with Diabetes (IWGDF 2019 Update). *Diabetes Metab. Res. Rev.* 36, e3280. doi:10.1002/dmrr.3280

Malone, M., Johani, K., Jensen, S. O., Gosbell, I. B., Dickson, H. G., Hu, H., et al. (2017). Next Generation DNA Sequencing of Tissues from Infected Diabetic Foot Ulcers. *EBioMedicine* 21, 142–149. doi:10.1016/j.ebiom.2017.06.026

Mao, W., Xia, L., and Xie, H. (2017). Detection of Carbapenemase-Producing Organisms with a Carbapenem-Based Fluorogenic Probe. *Angew. Chem. Int. Ed.* 56 (16), 4468–4472. doi:10.1002/anie.201612495

Masters, E. A., de Mesy Bentley, K. L., Gill, A. L., Hao, S. P., Galloway, C. A., Salminen, A. T., et al. (2020). Identification of Penicillin Binding Protein 4 (PBP4) as a Critical Factor for *Staphylococcus aureus* Bone Invasion during Osteomyelitis in Mice. *Plos Pathog.* 16 (10), e1008988. doi:10.1371/journal.ppat.1008988

Munita, J. M., and Arias, C. A. (2016). Mechanisms of Antibiotic Resistance. *Microbiol. Spectr.* 4 (2), 1–24. doi:10.1128/microbiolspec.VMBF-0016-2015

Oberhettinger, P., Zieger, J., Autenrieth, I., Marschal, M., and Peter, S. (2020). Correction to: Evaluation of Two Rapid Molecular Test Systems to Establish an Algorithm for Fast Identification of Bacterial Pathogens from Positive Blood Cultures. *Eur. J. Clin. Microbiol. Infect. Dis.* 39 (10), 2003. doi:10.1007/s10096-020-04012-5

Ramirez, H. A., Pastar, I., Jozic, I., Stojadinovic, O., Stone, R. C., Ojeh, N., et al. (2018). *Staphylococcus aureus* Triggers Induction of miR-15B-5P to Diminish DNA Repair and Deregulate Inflammatory Response in Diabetic Foot Ulcers. *J. Invest. Dermatol.* 138 (5), 1187–1196. doi:10.1016/j.jid.2017.11.038

Sadeghpour Heravi, F., Zakrzewski, M., Vickery, K., G. Armstrong, D. D., and Hu, H. (2019). Bacterial Diversity of Diabetic Foot Ulcers: Current Status and Future Prospectives. *J. Clin. Med.* 8 (11), 1935. doi:10.3390/jcm8111935

Scott, J. S., Sterling, S. A., To, H., Seals, S. R., and Jones, A. E. (2016). Diagnostic Performance of Matrix-Assisted Laser Desorption Ionisation Time-Of-Flight Mass Spectrometry in Blood Bacterial Infections: a Systematic Review and Meta-Analysis. *Infect. Dis.* 48 (7), 530–536. doi:10.3109/23744235.2016.1165350

Sinclair, A., Saeedi, P., Kaundal, A., Karuranga, S., Malanda, B., and Williams, R. (2020). Diabetes and Global Ageing Among 65-99-Year-Old Adults: Findings from the International Diabetes Federation Diabetes Atlas, 9th Edition. *Diabetes Res. Clin. Pract.* 162, 108078. doi:10.1016/j.diabres.2020.108078

Sun, J., Shi, H., Xue, Y., Cheng, W., Yu, M., Ding, C., et al. (2021). Releasing Bacteria from Functional Magnetic Beads Is Beneficial to MALDI-TOF MS Based Identification. *Talanta* 225, 121968. doi:10.1016/j.talanta.2020.121968

Tan, K. E., Ellis, B. C., Lee, R., Stamper, P. D., Zhang, S. X., and Carroll, K. C. (2012). Prospective Evaluation of a Matrix-Assisted Laser Desorption Ionization-Time of Flight Mass Spectrometry System in a Hospital Clinical Microbiology Laboratory for Identification of Bacteria and Yeasts: a Bench-By-Bench Study for Assessing the Impact on Time to Identification and Cost-Effectiveness. *J. Clin. Microbiol.* 50 (10), 3301–3308. doi:10.1128/JCM.01405-12

Tascini, C., Lipsky, B. A., Iacopi, E., Ripoli, A., Sbrana, F., Coppelli, A., et al. (2015). KPC-producing *Klebsiella pneumoniae* Rectal Colonization Is a Risk Factor for Mortality in Patients with Diabetic Foot Infections. *Clin. Microbiol. Infect.* 21 (8), e1. doi:10.1016/j.cmi.2015.04.010

Weinstein, E. J., Han, J. H., Lautenbach, E., Nachamkin, I., Garrigan, C., Bilker, W. B., et al. (2019). A Clinical Prediction Tool for Extended-Spectrum Cephalosporin Resistance in Community-Onset

Enterobacterales Urinary Tract Infection. *Open Forum Infect. Dis.* 6 (4), ofz164. doi:10.1093/ofid/ofz164

World Health Organization (2014). Antimicrobial Resistance: Global Report on Surveillance 2014. Available at: https://apps.who.int/mediacentre/news/releases/2014/amr-report/en/index.html (Accessed September 25, 2021).

Złoch, M., Maślak, E., Kupczyk, W., Jackowski, M., Pomastowski, P., and Buszewski, B. (2021). Culturomics Approach to Identify Diabetic Foot Infection Bacteria. *Int. J. Mol. Sci.* 22 (17), 9574. doi:10.3390/ijms22179574

Conflict of Interest: The authors declare that the research was conducted in the absence of any commercial or financial relationships that could be construed as a potential conflict of interest.

Publisher's Note: All claims expressed in this article are solely those of the authors and do not necessarily represent those of their affiliated organizations, or those of the publisher, the editors, and the reviewers. Any product that may be evaluated in this article, or claim that may be made by its manufacturer, is not guaranteed or endorsed by the publisher.

frontiers in Chemistry

REVIEW
published: 03 February 2022
doi: 10.3389/fchem.2021.782432

Advances in MALDI Mass Spectrometry Imaging Single Cell and Tissues

Xiaoping Zhu[1,2], *Tianyi Xu*[1,2], *Chen Peng*[2] *and Shihua Wu*[1,2]*

[1]*Joint Research Centre for Engineering Biology, Zhejiang University-University of Edinburgh Institute, Zhejiang University, Haining, China,* [2]*Research Center of Siyuan Natural Pharmacy and Biotoxicology, College of Life Sciences, Zhejiang University, Hangzhou, China*

Compared with conventional optical microscopy techniques, mass spectrometry imaging (MSI) or imaging mass spectrometry (IMS) is a powerful, label-free analytical technique, which can sensitively and simultaneously detect, quantify, and map hundreds of biomolecules, such as peptides, proteins, lipid, and other organic compounds in cells and tissues. So far, although several soft ionization techniques, such as desorption electrospray ionization (DESI) and secondary ion mass spectrometry (SIMS) have been used for imaging biomolecules, matrix-assisted laser desorption/ionization (MALDI) is still the most widespread MSI scanning method. Here, we aim to provide a comprehensive review of MALDI-MSI with an emphasis on its advances of the instrumentation, methods, application, and future directions in single cell and biological tissues.

Keywords: matrix-assisted laser desorption/ionization (MALDI), imaging mass spectrometry, single-cell metabolomics, proteomics, spatial distribution, tissue mapping

OPEN ACCESS

Edited by:
Lin Wang,
Chinese Academy of Medical Sciences and Peking Union Medical College, China

Reviewed by:
Xi Li,
Princeton University, United States
Yujue Wang,
The State University of New Jersey, United States

***Correspondence:**
Shihua Wu
drwushihua@zju.edu.cn
Shihua Wu
shihuawu@intl.zju.edu.cn

Specialty section:
This article was submitted to Analytical Chemistry, a section of the journal Frontiers in Chemistry

Received: *24 September 2021*
Accepted: *17 November 2021*
Published: *03 February 2022*

Citation:
Zhu X, Xu T, Peng C and Wu S (2022) Advances in MALDI Mass Spectrometry Imaging Single Cell and Tissues. Front. Chem. 9:782432. doi: 10.3389/fchem.2021.782432

1 INTRODUCTION

Mass spectrometry (MS) is a fundamental analytical technique for sensitive detection and identification of hundreds of inorganic elements and organic molecules in complex mixtures. Since 1912, J.J. Thomson found that isotopes of neon had masses 20 and 22 in a 10:1 ratio and explained its apparently anomalous atomic weight of 20.2. MS became more and more important for many life and science fields. A large number of MS methods and instruments, including ion sources, detectors, and analyzers have been developed (Wiseman et al., 2009). In the last three decades, with the advent of soft ionization techniques, such as electrospray ionization (ESI) (Fenn et al., 1989) and matrix-assisted laser desorption/ionization (MALDI) (Karas et al., 1987; Tanaka et al., 1987), it became possible to obtain mass spectra of proteins, DNA/RNA, carbohydrates, lipids, polymers, etc. In addition, with dramatic instrument improvements in unique capabilities of specificity, sensitivity, speed, sampling, and automated computer data acquisition/reduction, MS became an indispensable tool for the label-free detection of intact biomolecules in biological samples.

Meanwhile, the development of approaches for detecting, identifying, and mapping spatially the localization of molecules using mass spectrometry imaging (MSI, also named as imaging mass spectrometry) has extended these strengths of analytical MS to the cellular and subcellular scales and enabled detailed molecular mapping of hundreds of molecules in biological tissues (Unsihuay et al., 2021a). MSI can provide detailed maps of hundreds of molecules in complex samples with high sensitivity and subcellular spatial resolution. As shown in **Figures 1A,B** and **Table 1**, up to now, there are several MSI ionization methods, such as desorption electrospray ionization (DESI), matrix-assisted laser desorption/ionization (MALDI), and secondary ion

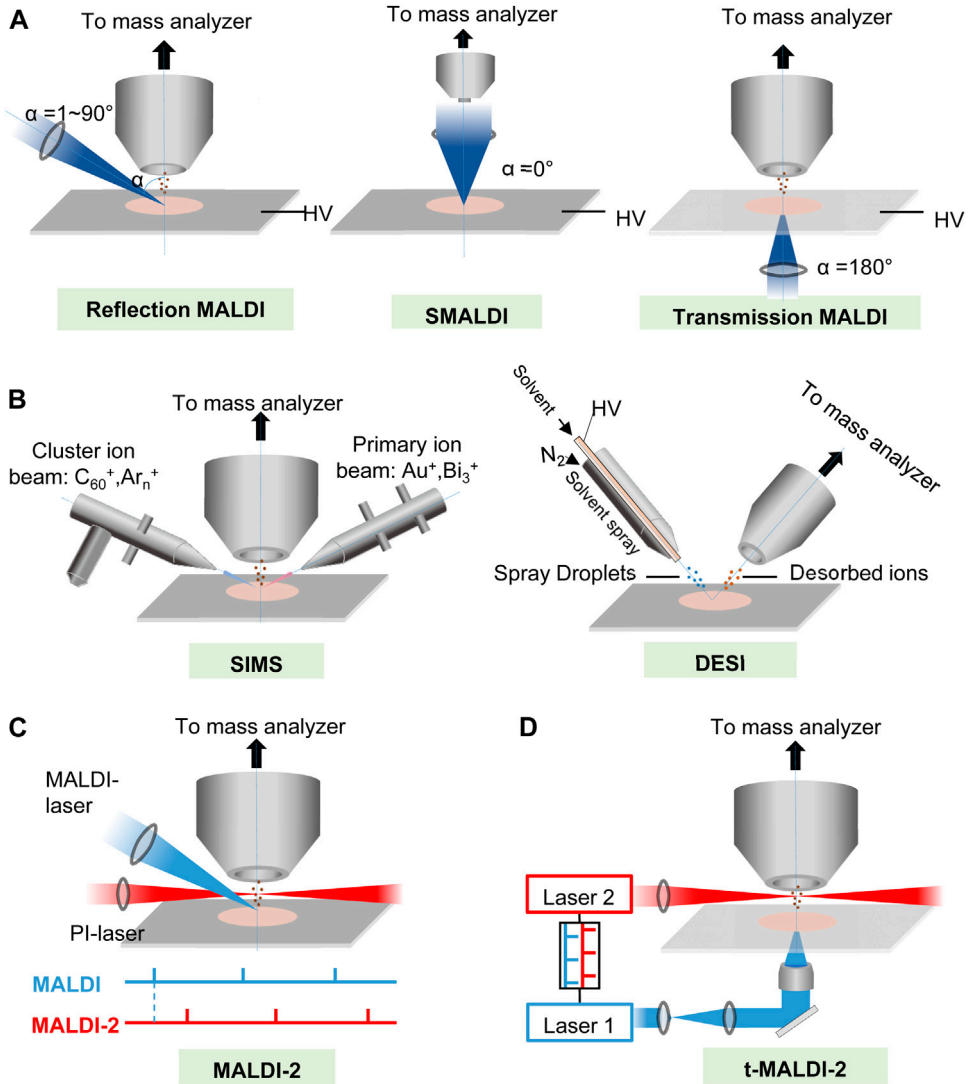

FIGURE 1 | The principles of **(A,B)** major MSI ionization methods and **(C,D)** two kinds of new post ionization (PI) laser enhanced new high-resolution MALDI ion sources. **(A)** Schematic of MALDI at several different laser angles (α). HV, high voltage. **(B)** Schematic of SIMS and DESI. **(C)** Schematic drawing of the modified MALDI ion source of the Synapt G2-S mass spectrometer. Primary MALDI and PI laser beams for more complete ionization and shielding aperture for increasing the cooling gas pressure in the region of ion generation. The lower panel illustrates the laser pulse triggering sequence. **(D)** Schematics of t-MALDI-2–MSI. An actively Q-switched Nd: YLF laser (laser 1, λ = 349 nm, M2 ~ 1.05) is focused onto a matrix-coated sample via a UV-transmitting ×50 objective in back-side illumination geometry. The Nd: YAG laser (laser 2 wavelength 2,266 nm) intersects the extended analyte matrix plume at a certain distance and a certain delay between the two laser pulses.

mass spectrometry (SIMS) (Gilmore et al., 2019; Schnackenberg et al., 2021). Similar to high-resolution MALDI ion sources, secondary ion mass spectrometry (SIMS, **Figure 1B**) ion beam technology has become a complementary mainstream method from the fringe of biological imaging due to significant developments in the primary ion beam technologies and mass spectrometers (Passarelli et al., 2017; Gilmore et al., 2019; Newell et al., 2020; Samfors and Fletcher, 2020; Sparvero et al., 2021; Van Nuffel et al., 2021). However, due to the ease of sample preparation, user-friendliness, speed, high sensitivity, and easy-to-interpret spectra, MALDI is still one of the most suitable MS ionization techniques for MSI in clinical laboratory (Norris and Caprioli, 2013a; Flatley et al., 2014; Schulz et al., 2019; Schnackenberg et al., 2021).

MALDI-MSI is a label-free, innovative, and emerging technique that produces two-dimensional (2D) ion density maps representing the distribution of an analyte(s) across a tissue section in relation to tissue histopathology. One main advantage of MALDI-MSI over other imaging modalities is its ability to determine the spatial distribution of hundreds of analytes within a single imaging run, without the need for a label or any prior knowledge (Schnackenberg et al., 2021). Furthermore, MALDI produces mainly singly charged ions, providing a less complex analyte ion profile than ESI where the

TABLE 1 | Differences between matrix-assisted laser desorption/ionization (MALDI), secondary ion mass spectrometry (SIMS), and desorption electrospray ionization (DESI) (Svatos, 2010; Yang et al., 2020).

	MALDI	SIMS	DESI
Beam source	Primary ion	Secondary ion	Primary ion
Ionization method	UV-laser	primary charged particles (Cs^+, SF_5^+, Au, and Sb clusters, C_{60}^+) eject and ionize material from surface	Modified ESI source spraying solvent using high-pressure gas flow on the sample surface
Sample preparation	Freezing microtome section and matrix application is needed	Freezing microtome section is needed, then directly analyzed	Directly analyzed
Matrix	Needed	None	None
Environment	Vacuum	Vacuum/low pressure	Atmosphere
Space resolution	10–100 μm	100 nm~1 μm	40–200 μm
Sample damaging level	High	Low	Low
Detected object	All kinds of biological samples, no limitation of molecular weight	Hydrophobic compounds with molecular weight not exceeding 1,000 Da	Compounds with molecular weight not exceeding 2,000 Da

occurrence of multiple charged ions from the same analyte tends to crowd the spectrum and renders interpretation difficult (Flatley et al., 2014). Over the last decade, MALDI-MS imaging has been used by researchers to explore areas of proteomics, lipidomics, and metabolomics in biological and clinical samples (Norris and Caprioli, 2013a; Chen et al., 2015; Cole and Clench, 2015; Rocha et al., 2017; Capitoli et al., 2019; Pareek et al., 2020; Schnackenberg et al., 2021). Histology-directed MS measurements provide unique insight into clinical questions for histology images and help to diagnose disease. MALDI-MS imaging, underpinning with enough specific molecular information, is poised to revolutionize the practice of anatomic pathology in the coming decade, and provide the next generation of diagnostic tests that will extend and improve the quality of life (Norris and Caprioli, 2013b). Although there are numbers of advances and applications in the versatile fields, in this review, we will highlight the recent key advances and application of MALDI-MSI with an emphasis on the instrumentation, methods, application, and future directions in single cell and biological tissues.

2 MATRIX-ASSISTED LASER DESORPTION/IONIZATION ION SOURCES AND MASS ANALYZER

The most basic MALDI process is to mix a concentrated matrix solution with an analyte solution and then dry it on a MALDI target plate to produce a matrix/analyte crystalline spot. Due to the high molar excess of the matrix, the matrix-dominated sample crystals absorb pulsed laser energy, leading to desorption and ionization of the matrix/analyte through the sample volume disintegration process (Cornett et al., 2007; Flatley et al., 2014). The information content of MS images is critically influenced by a combination of the 1) laser focusing optics/geometry, 2) precision of the sample positioning stage, 3) source pressure, 4) ion transfer, and 5) capabilities of the mass analyzer. (Roempp and Spengler, 2013; Gilmore et al., 2019). The ideal mass spherometer for MALDI-MSI would satisfy the "4S-criteia for performance" (speed, specificity, spatial resolution, and sensitivity). Each of these will impose limitations on the achievable lateral resolution and the information obtained from acquired mass spectra.

2.1 Classical Ion Sources

Historically, MALDI technology was first developed by Koichi Tanaka when he used the "metal fine powder and glycerol matrix" method for the same preparation (Tanaka et al., 1987). This method made a breakthrough of low molecular weight limit of laser desorption time-of-flight mass spectrometry (LD-TOF-MS). At that time, May 1987, the mass number that we had been able to measure had already exceeded 48,000 Da. Soon after this, the measured mass numbers were extended in the range of 72,000 to 100,000 Da (Tanaka et al., 1988). Almost at the same time as Tanaka, Karas and Hillenkamp also developed the MALDI method (Karas et al., 1987) to measure proteins with molecular masses exceeding 10,000 Da in 1987 (Karas and Hillenkamp, 1988). The novel soft ionization technique could introduce larger biomolecules such as proteins into the mass spectrometer (Flatley et al., 2014) and, thus, won dramatic applications and improvements. After 10 years, in 1997, MALDI was applied to biological imaging biological samples, e.g., human buccal mucosa cells and endogenous proteins (Caprioli et al., 1997). This group then went on to automate the MALDI-MSI process and demonstrated the application of the technique to imaging proteins and peptides in the mouse brain and glioblastoma sections. Soon, the application areas have rapidly expanded to include a large number of small molecules, e.g., small-molecule drugs, peptides, lipids, and neurotransmitters (Trim and Snel, 2016).

So far, there are several kinds of MALDI methods to generate ions. As shown in **Figure 1A**, according to the angle (α) of laser irradiation with respect to the sample surface normal and the pressure in the ion source, MALDI-MSI systems may be grouped into three major categories, transmission and reflection MALDI, and scanning microprobe matrix-assisted laser desorption/ionization (SMALDI) (Gilmore et al., 2019). For a classical transmission MALDI, the laser beam irradiates the sample at 180° relative to the analyzer axis; thus, the focused laser beam is required to penetrate the sample, and ions are ejected in the direction of laser propagation. The transmission geometry has been successfully employed for high lateral resolution lipid/metabolite MALDI-MSI with pixel resolutions down to 5 μm. While for the reflection of MALDI, the laser beam irradiates the matrix-covered sample surface with an angle between 0° and 90°

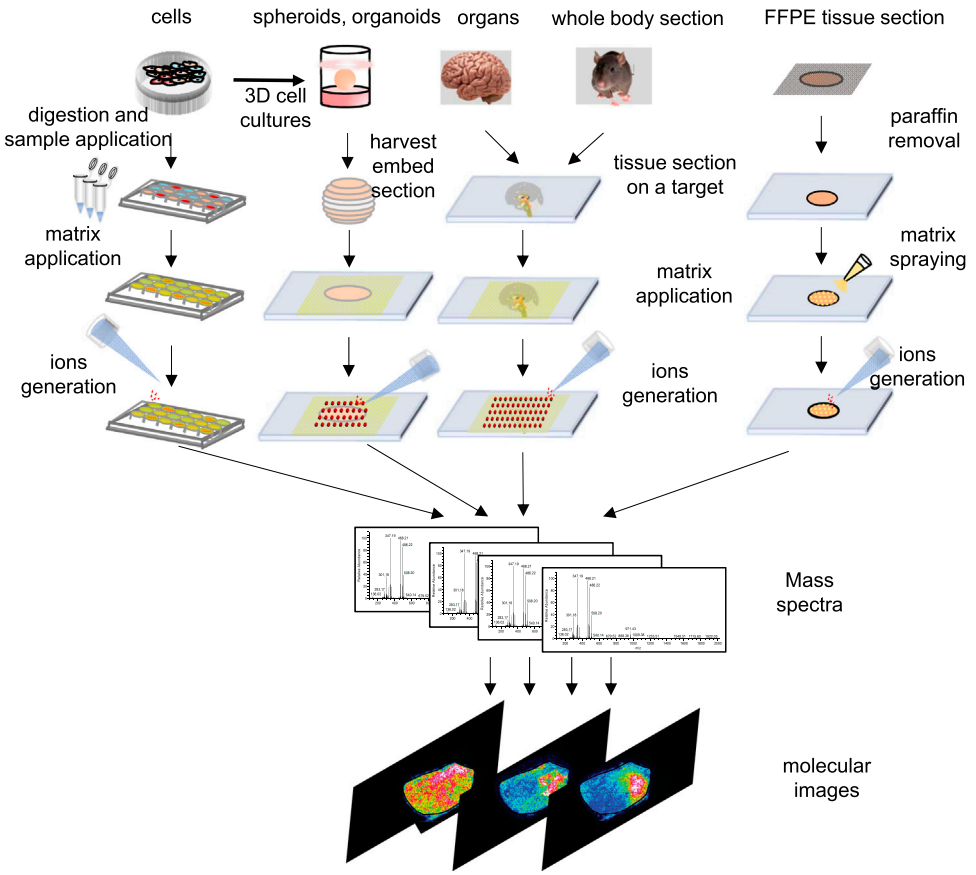

FIGURE 2 | Schematic outline of workflow of cells, spheroids, organ and tissue section, whole-body section and formalin-fix, paraffin-embedded (FFPE) tissue section for an MSI experiment in different samples.

regarding the analyzer inlet, which means ions are "reflected" from the sample surface, and sample perforation is not required. A previous study (Potocnik et al., 2015) indicated that using the rapifleX MALDI-TOF-MSI instrument to image lipid distributions in tissue sections, it was found that lateral resolutions were down to 10 µm. Scanning microprobe matrix-assisted laser desorption ionization (SMALDI) mass was invented by Spengler, B. and Hubert, M. in 2002 (Spengler and Hubert, 2002). It was further improved as atmospheric pressure scanning microprobe matrix-assisted laser desorption/ionization mass spectrometry (AP-SMALDI MS) for imaging (Vegvari et al., 2017; Bhandari et al., 2018; Bredehoeft et al., 2019; Kadesch et al., 2020; Mokosch et al., 2021; Mueller et al., 2021; Righetti et al., 2021), while atmospheric pressure MALDI ion sources AP-MALDI have also been developed for MSI (Guenther et al., 2011; Jackson et al., 2018; Keller et al., 2018) and achieved a lateral resolution at 1.4 µm (Kompauer et al., 2017).

2.2 New Post-Ionization Laser-Enhanced Ion Sources

As described above, MALDI-MSI can simultaneously record the lateral distribution of numerous biomolecules in tissue slices, but its sensitivity is restricted by limited ionization. Recently, Jens Soltwisch et al. (Soltwisch et al., 2015) introduced a wavelength-tunable PI laser strategy, called MALDI-2 (**Figure 1C**), that initiates secondary MALDI-like ionization processes in the gas phase. In MALDI-2, the beam of a pulsed ultraviolet (UV) laser intercepts the expanding particle plume in an N_2 cooling gas environment, which contrasts with previous photoionization studies where classical high-vacuum ion sources ($p \leq 10^{-6}$ mbar) were implemented. An effective diameter of ~5 µm of the primary laser beam was achieved by beam shaping and by mounting the focusing lens inside the MALDI ion source. In this way, the ion yields for numerous lipid classes, liposoluble vitamins, and saccharides could be increased, and imaged in animal and plant tissue with a 5-µm-wide laser spot, by up to two orders of magnitude. Critical parameters for initiation of the secondary ionization processes are pressure of the cooling gas in the ion source, laser wavelength, pulse energy, and delay between the two laser pulses. The technology could enable sensitive MALDI-MS imaging with a lateral resolution in the low micrometer range (Soltwisch et al., 2015; Soltwisch et al., 2020; Bien et al., 2021b).

The mechanisms underlying ionization by proton transfer in MALDI-2 possibly involve resonant two-photon ionization of the

matrix (m) by the PI laser (giving rise to $m^{+\bullet}$ ions and free e^-), succeeding collisions with neutral matrix molecules (leading to the generation of protonated or deprotonated matrix), and proton transfer to or from neutral analyte molecules (M) in subsequent collisions to yield the observed $[M + H]^+$ or $[M—H]^-$ products (Soltwisch et al., 2015). Thus, with the use of optimal PI laser conditions, increased ion signals were produced. With the idea, and with the use of laser-induced post-ionization transmission-mode MALDI ion sources (named t-MALDI-2, **Figure 1D**) and an Orbitrap mass analyzer to compose a t-MALDI-2 MSI system, M. Niehaus et al. (Niehaus et al., 2019) achieved a high a pixel size of 600 nm with brain tissue. The method could constitute a valuable new tool for research in cell biology and biomedicine.

2.3 Mass Analyzer

MALDI has been used in combination with TOF mass spectrometer for MALDI MSI, which could provide high spatial resolution (10 μm and better) and fast acquisition speed (e.g., provided by a 10-kHz laser), but they are less suitable for small molecules. Fourier Transform (FT) ion cyclotron resonance (ICR) or FT-orbitrap mass analyzer high resolving power and mass accuracy can provide high resolving power and mass accuracy, which are key for small molecule MSI and determinants of specificity. Currently, FT-ICR MS could provide the highest resolving power (>1,000,000 at *m/z* 200) capable of resolving isotopic fine structure. MALDI Orbitrap FT-MS also can provide high resolving power (>140,000) and lateral resolution. Some MALDI-QTOF instruments with intermediate resolving power combine MSI with ion mobility separation as a complementary separation technique that offers the potential to separation isometric molecules (Schulz et al., 2019).

3 GENERAL PROCESS OF MALDI-MSI

Principally, MALDI-MSI operation is a very simple and convenient process. As shown in **Figure 2**, the MSI sample preparation method includes sample collection, storage, sectioning, tissue pretreatment, matrix spraying, and so on, and is related to the type of sample and the nature of the object to be detected. Usually, a concentrated matrix solution is first mixed with the analyte solution and allowed to dry on a MALDI target plate (Flatley et al., 2014). After sufficient dry matrix coverage is achieved, the sample with high molar excess of the matrix is then recrystallized (Yang and Caprioli, 2011). The recrystallization allows analyte extraction from the sample surface in a controlled manner without a washing or spraying motion, leading to matrix/analyte desorption and ionization by a sample volume disintegration process (Yang and Caprioli, 2011). Sublimation and recrystallization offers the best spatial resolution in terms of crystal size, which allows the laser spot of the MALDI to define the spatial resolution of the experiment (Bouschen et al., 2010).

In the sample preparation process, even a slight movement in the analytes from their native positions is amplified. Thus, the main difficulty in the preparation of MALDI-MSI experimental tissue is that the chemical integrity of the targeted metabolites is not changed, and the true spatial distribution of the metabolites in the tissue is retained to minimize the displacement (Sturtevant et al., 2021). What is more, avoiding large volumes of matrix solvent is critical to maintaining optimal spatial resolution when performing MSI on small samples (Weaver and Hummon, 2013).

3.1 Sample Types and Pretreatment

MSI enables local molecular analysis at a broad range of length scales, from the subcellular level to whole body tissue sections, including organ tissue section, whole body section, spheroids in 3D cell cultures, and formalin-fixed and paraffin-embedded (FFPE) tissues, and their sample preparation processes are different.

3.1.1 Cell Sample

Cell samples from 2D monolayer cultures can also apply to MALDI-MSI. The sample preparation procedure is depicted in **Figure 2**. First, cells cultured in cell culture flasks are digested with trypsin. The cells are centrifuged, and the supernatant is discarded. The cell pellet is subsequently washed twice with PBS solution before re-suspended in PBS to obtain a cell suspension. Cell suspensions are deposited onto the MALDI target. After drying of the cell suspension liquid, the matrix is dropped onto the analyte and then used for MALDI-MSI (Chen et al., 2017).

Recently, Tanja Bien et al. demonstrated the pros and cons of the protocols with four model cell lines, cultured directly on indium tin oxide (ITO)-coated glass slides, and achieved the cultures at a pixel size of 2 μm by using transmission (t-) mode MALDI-2-MSI enabled on an Q Exactive plus Orbitrap mass spectrometer (Bien et al., 2021a). Cells were cultured directly on ITO-coated glass slides (70–100 Ω/sq, Merck) equipped with growth chambers. A total number of 2×104 cells in 0.5 ml of growth media were directly sown into each chamber of the slides and grown for 48 h to subconfluence. It should be noted that the direct growth on the ITO surface results in a slightly reduced adherence of the cells compared with the original glass slide of the chamber slide assembly.

3.1.2 Spheroid 3D Cell Cultures

Spheroids and organoids are three-dimensional (3D) cell models when cultured in suspension or nonadhesive environment, which is different from 2D monolayer cultures. Organoids are *in vitro* models of human development and disease study. They are often thought of as miniature versions of organs, and they often show very precise microscopic anatomical structures. Spheroids are 3D cultures composed of cellular polymers produced by a single cell type or a mixture of cells. Nowadays, 3D cell culture is widely used in screening environments for better assessment of drug safety and identifying potential cancer therapeutics (Lin and Chang, 2008; Hirschhaeuser et al., 2010).

In 2011, MALDI-MSI was combined with 3D cell culture to examine protein distribution for the first time, and it was found that cytochrome C and Histone H4 are the two predominant proteins in the 3D colon carcinoma cultures (Li and Hummon, 2011). Later, further studies of 3D cell culture about colon carcinoma (Liu et al., 2018c), human skin (Avery et al., 2011;

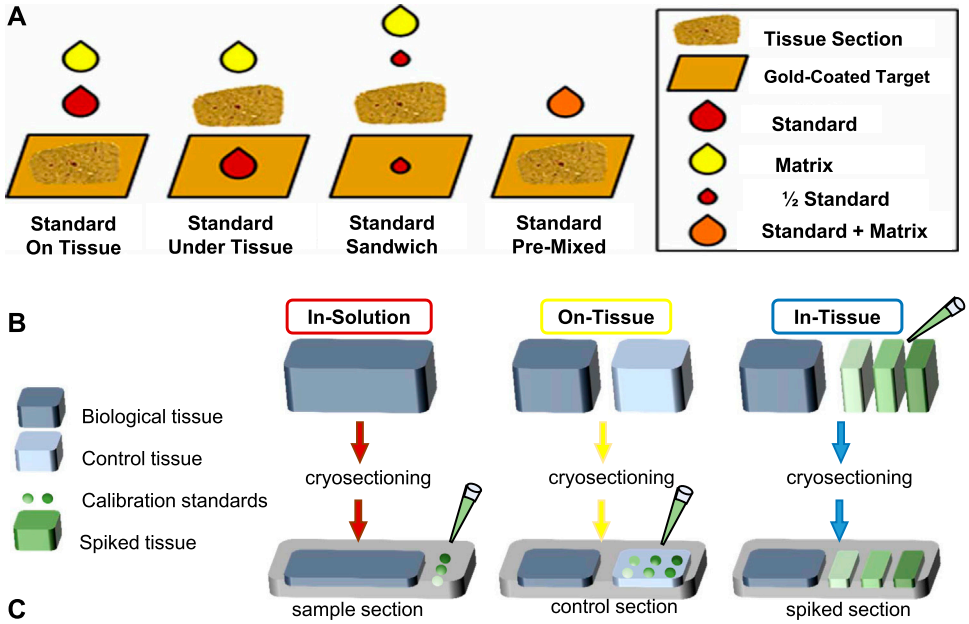

	In-Solution	On-Tissue	In-Tissue
Matrix effect	★	★★	★★★
Extraction efficiency	★	★★	★★★
Ease of execution	★★★	★★	★
Sample consumption	★★★	★★	★

FIGURE 3 | Representative standard applyed methods. **(A)** Four methods of applied internal standards for MSI (Chumbley et al., 2016). **(B, C)** Three common methods for calibration of standards applied. Modified from Porta et al. (2015) and Tobias and Hummon (2020). **(B)** The in-solution method is to directly spot the calibration standard on the indium tin oxide (ITO) slide. On the other hand, the on-tissue method places a control sample next to the sample section and spot calibration standards on the control section. In addition, the in-tissue method uses a tissue simulation model spiked with calibration standards of different concentrations, and the tissue simulation model is section and placed next to the sample portion. **(C)** A summary table of the characteristics of each method, where the asterisk indicates performance (low = 1 star, high = 3 stars).

Russo et al., 2018), blood–brain barrier (Bergmann et al., 2018), pancreatic cancer (Johnson et al., 2020), colorectal cancer (Liu et al., 2018b), and breast cancer (David et al., 2018) are combined with MALDI-MSI to analyze metabolites. Besides, Flint et al. characterized the metabolites, proteins, and metals of a novel aggregated spheroid model, termed "aggregoid," by DESI-MSI, and they demonstrated that absolute quantification of drugs is achievable in 3D tissue models (Flint et al., 2020). It is obvious that the combination of MSI and 3D cell culture has become a promising tool for early-stage drug analysis and disease analysis.

The basic workflow of 3D cell models used in MSI is depicted in **Figure 2**. Cells are seeded and incubated with a layer of agarose dissolved in cell culture media at the bottom of the inner plates to facilitate 3D spheroid and organoid formation. After 10–14 days, the spheroids grow to roughly 1 mm in diameter. The 3D cell models are then collected and embedded in gelatin for sectioning and subsequent MSI analysis (Weaver and Hummon, 2013). Details about sample preparation strategies for MSI of spheroid 3D culture models can be found in Wheatcraft et al. (2014) and sample preparation strategies for MSI of primary tumor organoids can be found in Johnson et al. (2020).

3.1.3 Organ Tissue Sections

Fresh frozen tissue slices (5–15 μm) collected from organs and whole body are the most common samples used in MALDI-MSI. Fresh frozen tissues, which are cut on a cryostat, are thaw mounted on a metal target or conductive glass slide. Excess lipids and salts can interfere with matrix crystallization and analyte ionization when analyzed protein, endogenous soluble ionization-suppressing compounds, and salts can interfere the detection of small molecules; therefore, sections are necessary to be washed by organic solvents (Lemaire et al., 2006; Schwamborn and Caprioli, 2010; Yang and Caprioli, 2011; Shariatgorji et al., 2012; Wheatcraft et al., 2014; Sun et al., 2019). The major process for the preparation of fresh frozen tissue sections for direct analysis by MALDI-MS is summarized in **Figure 2** (Schwartz et al., 2003; Goodwin, 2012).

Histologically, tissues are often stained for observation. Some histological stains, such as cresyl violet or methylene blue, are

TABLE 2 | Common matrices used for MALDI MSI targets (Tholey and Heinzle, 2006; Tobias and Hummon, 2020; Schnackenberg et al., 2021).

Matrix class	Matrix names	Targets
Classical organics	2,5-Dihydroxybenzoic acid (DHB)	Lipids, peptides, neuropeptides, drugs, small proteins
	α-Cyano-4-hydroxy cinnamic acid (CHCA/CCA)	Proteins, peptides, N-glycans, lipids
	Sinapinic acid (SA)	Proteins and peptides
	4-Chloro-α-cyanocinnamic acid (ClCCA)	Proteins and peptides
	2,5-Dihydroxyacetophenone (2,5-DHAP)	Phospholipids, proteins
	9-Aminoacridine (9-AA)	Free fatty acids, lipids
	1,5-Diaminonaphthalene (1,5-DAN)	Glycolipids, metabolites
	2-(2-Aminoethylamino)-5-nitropyridine	Phospholipids
	2-Mercaptobenzothiazole	Phospholipids
	4-Nitroaniline (PNA)	Phosphatidylethanolamine
	Norharmane	Bile acids, lipids
	Dithranol	Di-and triacylglycerols
	1,6-Diphenyl-1,3,5-hexatriene (DPH)	Free fatty acids
	1,8-Bis(dimethylamino) naphthalene (DMAN)	Free fatty acids
	N1,N4-Dihbenzylidenebene-1,4-diamine (DBDA)	Fatty acids
	Meso-tetratkis (pentafluorophenyl)-porphyrin	Free fatty acids
	2,4-Dihydroxyacetophenone (DHAP)	Glycoproteins
	2.4,6-Trihydroxyacetophenone (THAP)	Lipids
	Picolinic acid	Oligonucleotides
	Succinic acid	Oligonucleotides
Reactive matrices	2.4-Diphenyl-pyranylium tetrafluoroborate (DPP-TFB)	Small molecule amines, neurotransmitters
	2.4,6-Trimethyl-pyranylium tetrafluoroborate (TMP-TFB)	Dopamine
	p-N,N,N-Trimethy lammonioanilyl N-hydroxysuccinimidyl carbamate iodide (TAHS)	Steroids and catecholamine
	4-Hydroxy-3-methoxycinnamaldehyde (CA)	
	2,3,4,5-Tetrakis (31,4-dihydroxylphenyl)thiophene (DHPT)	
	2-Fluoro-1-methyl pyridinium (FMP) derivatives	Neurotransmitters
Inorganic nanomaterials	Metal based (e.g., gold, silver, titanium oxide)	Small molecules
	Silicon based (e.g., nanopost arrays, nanowires, nanopillars)	Small molecules
Room-temperature ionic liquids	DHB-Py, DHB-MI (1-methylimidazole), DHB-TBA, SA-TBA	Small molecules
	CCA-DEA (N,N-diethylaniline), CCA-ANI (Aniline)	Peptides
	SA-TBA, SA- Et_3N (triethylamine)	Proteins
	9-AA-NEDC	Lipids
	DHB-BuA (n-butylamine), CCA-MI, DHB-Py	Carbohydrates
	CCA-Py, CCA-MI, CCA-BuA	Phospholipids
	HPA (hydroxypicolinic acid)-DEA, CCA-ANI, CCA-MI	Oligonucleotides

compatible with subsequent MS analysis (Chaurand et al., 2004). However, other stains, such as hematoxylin and eosin (H&E), can interfere subsequent MS analysis; therefore, serial sections are obtained and stained to guide matrix deposition and laser ablation and to allow comparison of MS results with tissue histology (Schwamborn and Caprioli, 2010). Another solution is performing MS analysis first and staining after removing the matrix (Grey et al., 2009).

3.1.4 Formalin-Fixed and Paraffin-Embedded Tissues

In contrast to fresh frozen tissue, FFPE tissue specimens are the well-established processing methods employed in histological examination. They are prepared by immersing the sample in formalin to fixation, then removing the fixator and residual water in ethanol and using an organic solvent (such as xylene) to remove the ethanol, and finally embedding the sample in molten paraffin. Thus, FFPE samples have been through to be unusable for proteomic approaches because of protein cross-linking caused by formalin fixation for a long time (Becker et al., 2007). In 2007, the I. Fournier's group presented two methods for direct analysis of FFPE tissues by MALDI-MS (Lemaire et al., 2007), making it possible to get massive amounts of archived samples in the clinical pathology setting. In addition, the use of antigen retrieval techniques and *in situ* tryptic digestion has allowed the analysis of FFPE samples by MSI (Groseclose et al., 2008).

Recently, a MALDI-MSI protocol for tryptic peptides from FFPE tissues (Ly et al., 2019), which help to establish a standard operating procedure. High-mass-resolution MALDI-FT-ICR-MSI platform had also been used for the *in situ* analysis of metabolite content from the FFPE sample (Ly et al., 2016). Using this platform, an overlap of 72% of detected species was achieved in the mass range of m/z 50–1,000 in FFPE samples, compared with fresh frozen samples. Metabolites are found to be largely conserved in FFPE tissue samples, and thus, the data acquired with this protocol can be used in research and clinical practice, making full use to mining data in traditional FFPE tissue. Recent research applied MALDI-MS to FFPE tumor tissue sections and enabled cancer subtype classification, providing a promising complementary approach to current pathological technologies for precise digitized diagnosis of diseases (Möginger et al., 2020).

Nowadays, MSI is a powerful tool that has been used to detect biomarkers, such as peptides (Groseclose et al., 2008), proteins (Lemaire et al., 2007; Stauber et al., 2008; Araujo et al., 2014),

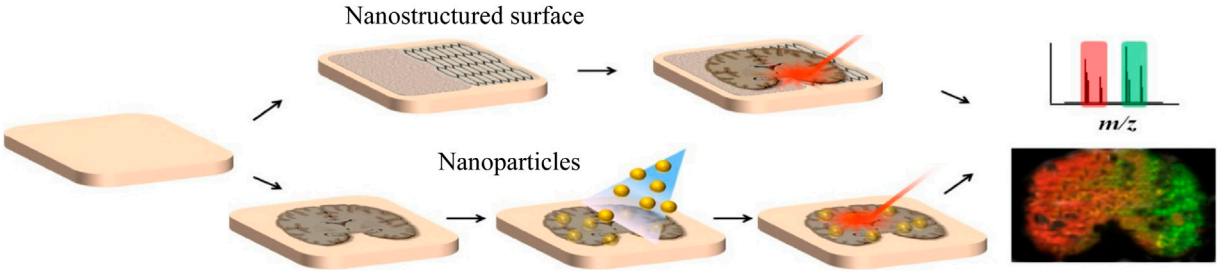

FIGURE 4 | LDI MSI with organic matrix-free systems harnessing nanostructured surfaces or nanoparticles (Kim et al., 2020).

lipids (Carter et al., 2011; Denti et al., 2020), metabolites (Djidja et al., 2017; Clift et al., 2021), and N-linked glycans (Bai et al., 1994; Eshghi et al., 2014; Gustafsson et al., 2015; Briggs et al., 2017) in FFPE tissues. Generally speaking, sample preparation of FFPE tissue applied in MALDI-MSI is slightly different from fresh frozen tissue (depicted in **Figure 2** with additional steps to remove the paraffin). Micro-digestion is needed before matrix spraying in case of protein analysis.

3.1.5 Whole-Body Sections

Whole-body autoradiography is a traditional technology carried out in animal tissues during the early stage of drug and metabolite distribution studies. However, there are a number of limitations about whole-body autoradiograph, especially the expensive synthesis of radiolabeled drugs and analyte specificity and identification.

MALDI-MSI has been shown to be more advantageous for imaging the distribution of drugs and metabolites in a whole-body section (Trim et al., 2008). In 2005, Rohner et al. performed MALDI-MSI and study the drug distribution in a whole-body mouse section for the first time (Rohner et al., 2005). Soon, whole body MALDI-MSI will be extended to detect proteins in a whole-body scale (Khatib-Shahidi et al., 2006). A typical MALDI-MSI process for whole-body tissue sections contained several steps. In brief, animals were deep frozen and embedded in precooled semiliquid gel of carboxymethylcellulose (CMC) and cut on a cryomicrotome. Then the sections were placed on a copper block and transferred to a desiccator with a membrane pump for section drying. The sections were mounted on metal plates using double-side adhesive tape and followed by matrix coating and MALDI-MSI. Considering the size of the sample, whole-body MALDI-MSI is usually used to study some small animals such as nematodes (Hameed et al., 2015), fruit flies (Khalil et al., 2017), and mice (Huber et al., 2018; Saigusa et al., 2019).

3.2 Standards Addition and Quantification

Absolute quantification is one of the key challenges in the MS analysis of complex mixtures. Aside from instrumental parameters, analyte recovery from tissue and ionization matrix effects are critical for quantitative MSI on tissue sections (Porta et al., 2015). Interactions between analyte and the tissue may result in different analyte recoveries. Besides, the absence of chromatographic separation enhances the effect of ionization competition and variation in ionization efficiencies (Stern et al., 2017), and the uniformity of matrix deposition can also affect ionization (Tobias and Hummon, 2020). Thus, isotopically labeled internal standards are used; specific preparation of calibration standard is critical for quantification in MALDI-MSI. There are generally four methods of applying internal standards on tissue for MSI depicted in **Figure 3A**, including standard on tissue, standard under tissue, standard sandwich, and standard premixed. However, depositing the standards on the tissue followed by the matrix was found to be the most accurate for quantitative MALDI-MSI (Chumbley et al., 2016; Unsihuay et al., 2021a).

In addition, calibration curve is needed for absolute quantification, so application of calibration standards before internal standard and matrix is needed to create the calibration curve. There are three strategies of calibration standards applied—*in-solution* strategy, *on-tissue* strategy, and *in-tissue* strategy to be developed for quantitative MSI. Their advantages are summarized in **Figures 3B,C**. Other details about the construction of calibration curves especially obtaining the analytical figures of merit in qMSI are shared by Tobias et al. (Tobias and Hummon, 2020).

3.3 Matrix Application

Coating matrix on the sample plate is a key step in MALDI-MSI analysis. It is possible that the matrix of MALDI puts considerable pressure on the spatial integrity of general biological samples, especially single-cell samples (Schober et al., 2012), which results in cellular components that may be broken and leaked. Fortunately, choosing a suitable matrix and suitable deposition method can avoid loss of analytes (Baker et al., 2017). In addition, the use of optimized matrix can promote the effective ionization of the target analyte and generate uniform and small eutectic, which is necessary for obtaining high spatial resolution images (Vallianatou et al., 2019). The ideal matrix generally has the following properties: strong electron absorption at the adopted laser wavelength, better vacuum stability, lower vapor pressure, and better miscibility with the analyte in the solid state (Calvano et al., 2018).

The choice of matrix can change the ionizable molecular weight and molecular species of the mass spectrometer. Up to now, there are numbers of matrices to be used for MALDI MS. **Table 2** selected some popular MALDI matrices including

organic small molecules, inorganic nanomaterials, reactive matrices (derivatization solutions), and ionic liquid matrix.

3.3.1 Common Matrix

Some matrices are popular due to their wide applicability, including α-cyano-4-hydroxycinnamic acid (CHCA) and 2,5-dihydroxybenzene. Formic acid (DHB) is used for peptides and metabolites (Tobias and Hummon, 2020). Different MALDI matrices have different sensitivities to different kinds of biomolecules. Perry et al. compared the intensity of various lipids in mouse liver tissue measured by the use of 9-aminoacridine (9AA), 5-chloro-2-mercaptobenzothiazole (CMBT), 1,5-diaminonaphthalene (DAN), and 2,5-dihydroxyacetophenone (DHA) and 2,5-dihydroxybenzoic acid (DHB), which provides a more reliable basis for the selection of MSI matrix (Perry et al., 2020). Liu et al. used n-phenyl-2-naphthylamine (PNA) with strong ultraviolet absorption and salt tolerance as a new type of matrix, which performed well in the analysis of a variety of small molecular metabolites including free fatty acids, amino acids, peptides, etc., then used for small-molecule imaging of rat middle cerebral artery occlusion (MCAO) brain tissue (Liu H. et al., 2018).

3.3.2 Reactive Matrices for Chemical Derivatization

As described above, matrices, such as DHB and CHCA, may enhance analytical sensitivity. But for some specific molecules, such as small molecules or compounds with low ionization efficiency or in low abundance, there is still no suitable matrix, and thus, they will not be detected by the conventional MSI workflow. The signal peaks generated by organic matrices can also greatly interfere with the analysis of small molecules in MSI. Chemical derivatization makes it possible to perform targeted mass spectrometry imaging of these molecules (Tobias and Hummon, 2020). Derivatization solutions or reactive matrix serve as chemical matrices for laser desorption/ionization, can also enhance the detection of target molecules that are low in abundance, or contain certain chemical moieties (such as double bonds in amines or lipid fatty acyl groups) by reacting with them (Waldchen et al., 2019).

The on-tissue chemical derivatization (OTCD), which is spray chemical derivatization first followed by matrix application (Harkin et al., 2021), has been used to improve ionization efficiency to effectively detect analytes directly from both fresh frozen tissue and FFPE tissue. Now OTCD has developed rapidly and used to detect many biological molecules, such as N-glycan (Nishikaze et al., 2013; Holst et al., 2016; Zhang et al., 2020; Saito et al., 2021), drugs (Barre et al., 2016), amines (Chacon et al., 2011; Manier et al., 2014), fatty acids (Wu et al., 2016; Wang et al., 2019; Iwama et al., 2021), amino acids (Toue et al., 2014; Esteve et al., 2016; Guo et al., 2020), poisons (Beasley et al., 2016), plant hormones (Enomoto et al., 2018), peptides (Franck et al., 2010), steroids (Guo et al., 2020; Angelini et al., 2021; Song et al., 2021), neurotransmitters (Ito and Hiramoto, 2019; Palanisamy et al., 2020; Shariatgorji et al., 2020), and so on. It is worth noting that the coating method of derivatization solution and matrix is also important because it affects not only the efficiency of OTCD but also the quality of imaging results.

If the derivatization solution also serves as a matrix (reactive matrix), then no additional step is required. Reactive matrix can also reduce the double interference of excessive chemical derivatization solution while reducing matrix effect. Recently, Shariatgorji et al. designed a reaction matrix based on fluoromethylpyridine that can promote covalent charge labeling of molecules containing phenolic hydroxyl groups and/or primary or secondary amine groups, including dopaminergic and serotonergic neurotransmitters (Shariatgorji et al., 2019). The matrix improves the detection limit of MALDI-MSI for low-abundance neurotransmitters and realizes the simultaneous imaging of neurotransmitters in the fine structure of the brain (Shariatgorji et al., 2019). Davison et al. used 2,4-diphenyl-pyran tetrafluoroborate (DPP-TFB) to react with monoamine neurotransmitters and directly measured the content in the brain tissue of mice by MSI (Davison et al., 2019). In addition, 2,4,6-trimethylpyridine tetrafluoroborate (TMP-TFB)-derived matrix MALDI-MS can image dopamine in mouse brains (Wang et al., 2021). Girard's T reagent and TAHS, respectively, enhanced the ionization efficiency of steroids and catecholamine (Takeo et al., 2019).

3.3.3 Organic Matrix-Free Inorganic Nanomaterials as Matrices

Inorganic materials can also be used in the application of small molecules in MALDI because they are not easily ionized, which will not interfere with analytes as traditional matrices. Recently, there is an increasing trend to use nano-structured surfaces and inorganic nanoparticles as substitutes for organic matrices and develop various organic-free MSI systems (**Figure 4**). For example, Rudd et al. used the desorption–ionization of porous silicon (DIOS) nanomaterials to study the changes in biodistribution during the reproductive cycle and found that muscle relaxation choline ester murexine and tyrosine sulfate colocalize in the lower branchial glands (Rudd et al., 2015). Carbon-based surfaces can also be used for matrix-free MSI. Kim et al. used graphene oxide (GO)/multiwalled carbon nanotube (MWCNT)-based films as a new matrix-free laser desorption/ionization platform with efficient analyte desorption/ionization, minimal fragmentation, high salt tolerance, excellent durability, and other advantages, suitable for tissue imaging mass spectrometry (Kim et al., 2011). Bien et al. cultured the cell line directly on indium tin oxide (ITO)-coated glass slides and used transmission (t-) mode MALDI-2-MSI to analyze the 2-μm pixel size culture, which can visualize the spatial distribution of dozens to hundreds of different biomolecules in tissue section and cell culture (Bien et al., 2021a). AuNPs and AgNPs are the most commonly studied and widely used nanoparticles in MSI, and they have the characteristics of easy adjustment of dimensional properties. McLaughlin et al. developed a neurotransmitter ionization method based on AuNPs, which sprayed AuNPs on tissue slices by air pressure and can perform mass spectrometry imaging of a variety of tissues and realized the localization of neurotransmitters in zebrafish embryos and neuroblastoma cells, with a horizontal spatial resolution of 5 μm (McLaughlin et al., 2020). Han et al. synthesized polydopamine (PDA)-encapsulated

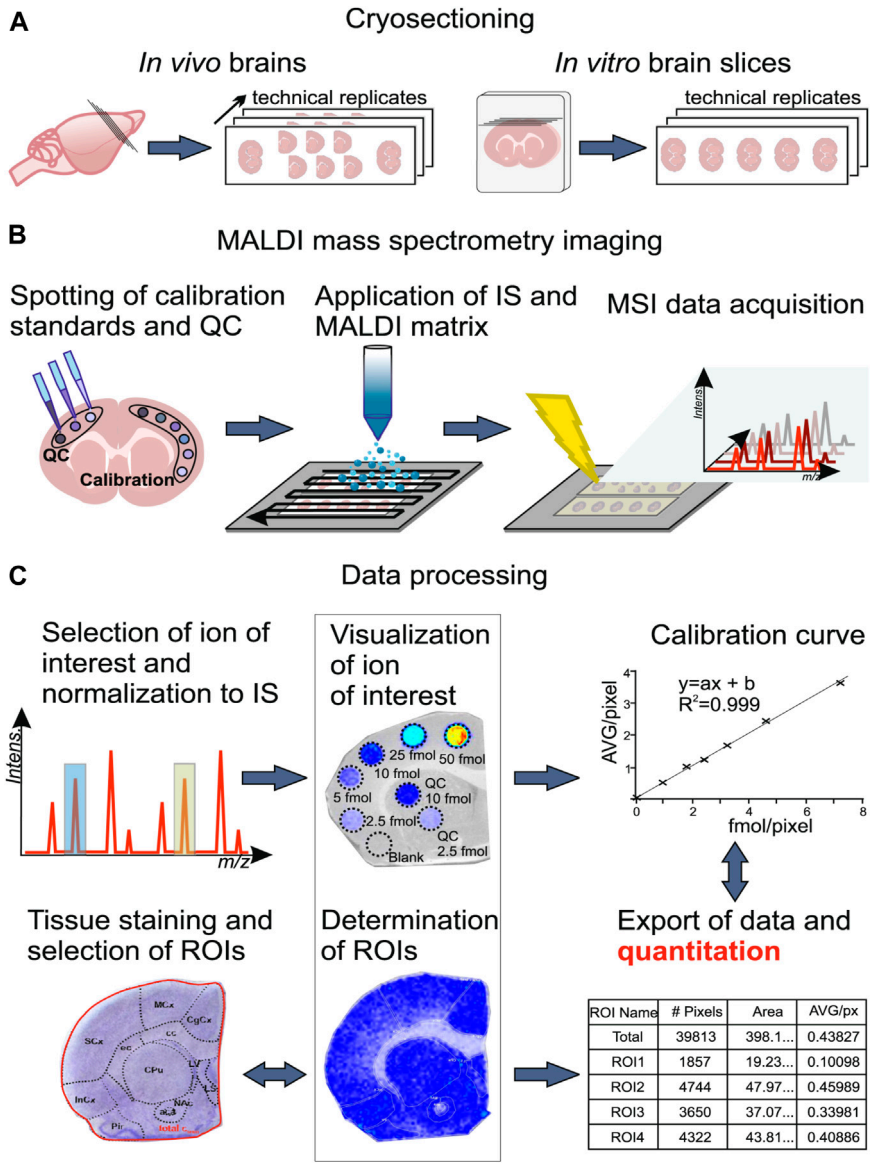

FIGURE 5 | Illustration of the workflow for assessing total brain drug concentrations using qMSI-uD (Luptakova et al., 2021).

AgNPs (AgNPs@PDA) as the matrix of MALDI MSI to analyze lipids in positive and negative ion mode, and controlled the signal of silver cluster ions by adjusting the thickness of the PDA layer (Han et al., 2019). It was found that with AgNPs@PDA as the matrix, the PC signal was greatly inhibited, while other lipids (including PE, HexCer, PS, PI, PIP, and ST) were, on the contrary, achieving the detection of 58 glycerophospholipids and 25 sphingomyelins in brain tissue slices.

3.3.4 Room-Temperature Ionic Liquid Matrix

During recent years, one kind of new green solvents, room-temperature ionic liquids (ILs), that remain liquid at room temperature have received much attention to replace current harsh organic solvents due to their distinct properties and characteristics compared with traditional solvents. Usually, ILs are composed of relatively bulky organic cations and relatively small inorganic anions and have a melting point below 100°C, and they are stable at temperatures below 250°C (Tholey and Heinzle, 2006). In addition, ILs have inherent properties, such as negligible vapor pressures, low volatility at room temperature, and high thermal stability, which, in turn, contribute to their recovery and reusability in separation and purification processes. So now ionic liquids have been widely applied in different research and industrial fields, such as chemistry, biology, catalysis, energy, and even environmental sciences (Hallett and Welton, 2011; Itoh, 2017; Ventura et al., 2017; Huang et al., 2019).

Due to their low vapor pressure, the ability to dissolve a wide range of substances, ionic liquids have been applied as matrix in

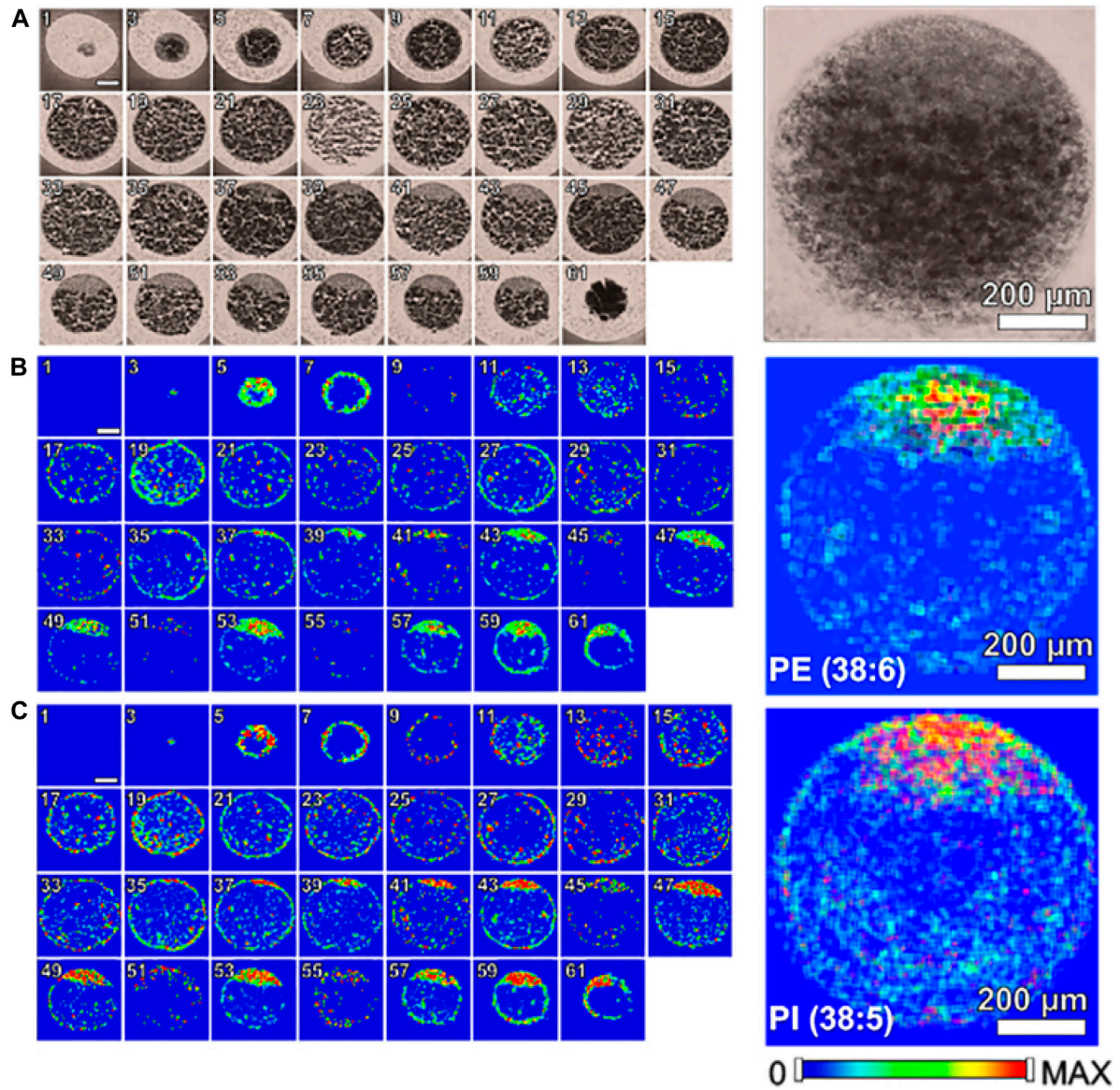

FIGURE 6 | Single cell molecular mapping Zenobi, 2013. Odd numbered optical images of fertilized zebrafish embryo at the one-cell stage, false color two-dimensional MALDI-MS images of PE (22:6_16:0) at *m/z* 762.509 and PI (18:0_20:5) at *m/z* 883.535, and projected images are shown on the right by overlaying all 2D images (Duenas et al., 2017a).

MALDI, called ionic liquid matrix (ILM). ILM is synthesized from conventional MALDI matrix compounds (such as DHB, CCA, and SA) and organic bases [such as pyridine (Py), tributylamine (TBA) and N, N-dimethylethylenediamine (DMED)]. One of the most striking advantages for applying ionic matrix in MALDI-MSI is that sample homogeneity can be achieved because the viscous liquid surface is highly homogeneous. Compared with solid matrices, ILM has good vacuum stability, good reproducibility, and high sensitivity (Armstrong et al., 2001). For example, the analysis of lipid can be enhanced by applying ILM in MALDI. Wang et al. used different ratios of 9-aminoacridine (9-AA) and N-(1-naphthyl) ethylenediamine dihydrochloride (NEDC), two matrices with orthogonal selectivity for the ionization of lipids (Wang et al., 2018). After mixing, the mouse brain lipid extract was analyzed, and the final detection range was enhanced.

3.3.5 New Spraying Method to Add Organic Matrix

Matrix application needs to be uniform, produce small crystal sizes, and appropriately extract analytes without introducing artifacts such as spatial delocalization. It is economical and easy to operate using a sieve and manual spraying with airbrushes (Yang et al., 2012). The first sublimation device for matrix deposition reported by Hankin et al. can produce a uniform layer of small crystals on the sample plate (Hankin

et al., 2007). This method is easy to control and has high repeatability, and can obtain high-quality mass spectrometry image. In addition, compared with the sublimation recrystallization method and sublimation only, the lipid ion signal intensity of the pneumatic matrix spraying method samples increased by 8 and 30 times on average in the experiment of Kompauer et al. (2017). Therefore, it is suggested to use pneumatic sprayers or sublimation devices to reduce errors.

3.4 Data Acquisition, Processing, and Visualization

After MALDI-MS analysis, MSI software is needed to control data acquisition, processing, and integration in order to generate ion imaging. There are many commercial and open-source software that can be used to process MSI data, such as Biomap (Stoeckli et al., 2002), FlexImaging, MALDI Imaging Team Imaging Computing System (MITICS), Datacube Explorer, ClinPro Tools (Ketterlinus et al., 2005), and so on. A comparison of several developed software for MSI was presented by Kamila Chughtai and Ron M.A. Heeren (Chughtai and Heeren, 2010). As the MSI data contains massive information including mass spectrometry information and spatial information, the resolution and spatial resolution have also been continuously improved with the development of MSI, which leads to large amounts of original imaging data, and it became increasingly difficult to process it.

The quality of MSI images can be improved by removing noise, correcting deviation of *m/z* peak, and normalization. The purpose of normalization is to reduce the signal difference between pixels that may be caused by disconformity matrix coating and ion suppression. Normalization based on total ion count (TIC) and vector norm normalization are currently the most commonly used methods. However, regarding potential biomarker distributions, other normalization algorithms may be needed to prevent producing misleading results (Deininger et al., 2011).

Data analysis considerations for 3D-MSI data analysis is very important after data normalization (Vos et al., 2021). Benchmark datasets for 3D MALDI-MSI provide high-quality 3D imaging datasets from different biological systems at several labs, which stimulates computational research in the field of computational 3D imaging MS (Oetjen et al., 2015). Nowadays, principal component analysis (PCA), hierarchical cluster analysis (HCA), and partial least square discriminate analysis (PLS-DA) are the most common multivariate statistical analysis methods used in MSI. These methods are successful in dimension reduction and feature extraction. The factor analysis method was studied, and it was proved to be able to simply and quantitatively extract the target sample markers (Chen et al., 2014).

3.5 Quantitative on-Tissue Matrix-Assisted Laser Desorption/Ionization-Mass Spectrometry Imaging Process

On-tissue quantitative determination of biomolecules or administrated drugs is very important for MSI analyses. For example, it is essential to determine the extent of drug transport across the region-specific blood–brain barrier (BBB) and discriminate the regional free (unbound) drug concentration at which the drug engages with its therapeutic target. Recently, a new method, qMSI for unbound drug determination (qMSI-uD), combining *in vivo* and *in vitro* neuropharmacokinetic studies with MSI, has been developed to assess the extent of unbound drug transport across the BBB and drug distribution in small anatomical regions (including subregions) in the brain (**Figure 5**). Using this method, direct imaging of three antipsychotic drugs (risperidone, clozapine, and olanzapine) with different BBB transport properties and regional distribution patterns was performed at 20-μm resolution. In addition, the method provides region-specific drug exposure data associated with drug response data, facilitating development of new drugs (Luptakova et al., 2021).

4 SINGLE-CELL IMAGING

Cells in multicellular organisms have different morphological and gene expression patterns. Cell phenotypic transition occurs during the development of the fertilized egg into different cell types, as well as under the physiological and pathological conditions of the differentiated cell. Heterogeneity among cells underlies individual variability in the activity of cellular networks and circuits (Goaillard et al., 2009). Due to the morphological, physiological, and pathological heterogeneity of cells, there is currently much interest in broad molecular profiling of a single cell. It is very important to study the biochemical and physiological characteristics of individual cells and their environment. Analysis of single cells can further our understanding of differential susceptibility to treatment of disease (Rubakhin et al., 2011). However, previous techniques have difficulties in capturing the information of cell phenotypic transition dynamics. Fortunately, live-cell imaging and analysis fill this gap (Wang et al., 2020). MSI can reveal the distribution of hundreds of compounds simultaneously in the cell and tissue sections down to single-cell level (Duenas and Lee, 2021).

It should be pointed that the size of the cell is small, and thus, a higher resolution is required. For human cells, the diameter of a cell ranges from 5 μm (sperm cell) to 150 μm (ovum) (Gillooly et al., 2015; Ginzberg et al., 2015) and, on average, about 10–20 μm. In some diseases, the average size of the affected cells will change, such as cancer cells, which are commonly larger than their respective normal cells, and usually, cells of different sizes are mixed. For example, cancer cells are often surrounded by smaller infiltrating lymphocytes (Stern et al., 2017). So, the needed minimum spatial resolution is determined by the smallest cell size or distance between cells (Scupakova et al., 2020). In initial MALDI single-cell imaging experiments, large frozen *A. californica* cells could be imaged at a 50-μm raster size, but for much smaller mammalian cells, MALDI-MSI needed to pursue higher resolutions (Lanni et al., 2012).

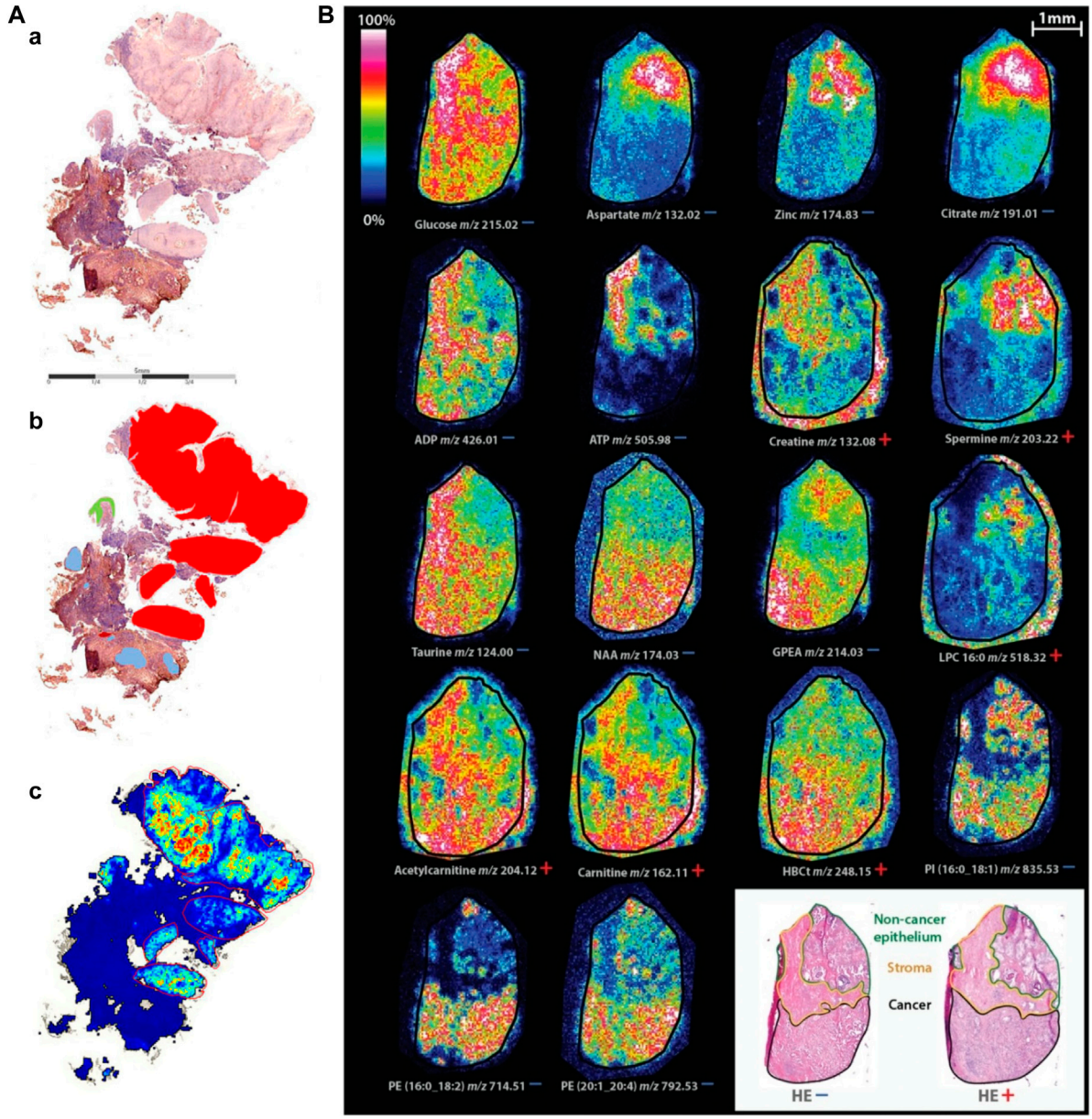

FIGURE 7 | Typical characterization of cancer and biomarker by MALDI-MSI. **(A)** Comparison of component analysis of MALDI-MSI measurements on FFPE sections with histopathological regions. One example of sample cohort is shown. (a) Hematoxylin and eosin-stained tissue section. (b) Annotated regions, red: squamous cell carcinoma, green: dysplastic epithelium, rest: nontumor region, containing connective tissue with inflammatory infiltration and glandular regions (blue). (c) Component that covers the tumor region; no spatial denoising was performed (Hoffmann et al., 2019). **(B)** Spatial distribution of identified masses in both ion modes on consecutive tissue sections (Andersen et al., 2021).

4.1 Single-Cell Metabolomics

Single-cell metabolomics provides insight into phenotypic variation between individual cells. Changes in metabolite concentrations and differences in lipid and protein profiles lead to unique metabolome profiles for individual cells (Scupakova et al., 2020). Metabolome molecular profiles can provide the most accurate information of cellular reaction networks, helping to understand the link between genotypes and phenotypes of individual cells. Existing microfluidics, micromanipulation, image analysis, and automation technologies have enabled high-throughput isolation of individual cells with minimal interference without affecting cell metabolism (Ali et al., 2019).

Up to now, single-cell MSI technology has been successfully used to obtain data from individual plant cells, which helps to reveal unprecedented insights on metabolic outcomes. It was commonly used to investigate the differential location and heterogeneity of secondary metabolites in plant tissues. For

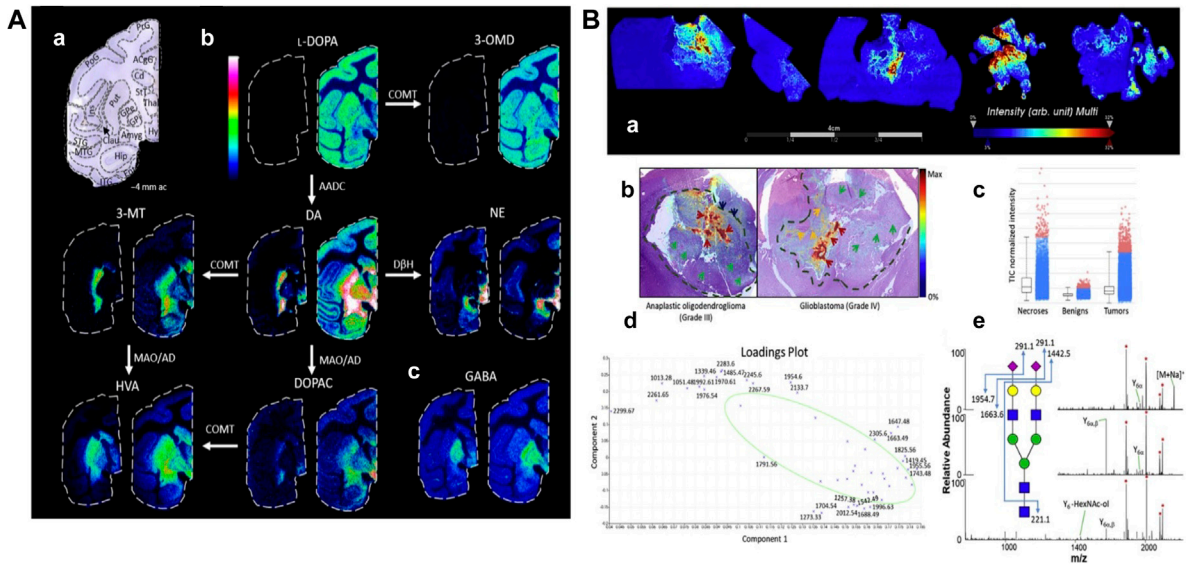

FIGURE 8 | Mapping typical molecular distributions of **(A)** neutrotransmitters, **(B)** N-glycoproteomes. **(A)** MALDI-MS images of neurotransmitters and metabolites in non-LID and LID. (a) Nissl-stained macaque brain tissue section at –4 mm ac with annotated brain regions. (b) Catecholaminergic metabolic pathway. (c) GABA (Fridjonsdottir et al., 2021). **(B)** Spatially resolved N-glycans by MALDI-MSI. (a) Summed ion images of Na^+ and K^+ adducts of $HexNAc_4$-Hex_5-$NeuAc_2$ on canine glioma biopsies. (b) Superposition of MALDI-MSI glycan images with H&E-stained adjacent sections. Arrows and dashed lines indicate regions annotated by the pathologist. (c–e) Normalized intensity of total ion signals, PCA analysis, and MS^n spectra of HexNAc4-Hex5-NeuAc2 (Malaker et al., 2021).

example, MALDI-MSI of maize leaves clearly indicated the distribution of two major anionic lipids in thylakoid membranes, which helps to reveal the genetically programmed and developmental modification of thylakoid membrane (Duenas et al., 2017b). High-resolution MS of individual lipid droplets from cotton seed tissues helps to understand the cellular context of lipid origin (Horn et al., 2012).

In addition, single-cell imaging can help to identify the colocalization of the distribution of individual molecular species, including particular lipids and proteins, and correlation with the morphological features of a tissue section, which also plays an important part in molecular pathology and cancer therapy. For instance, a single-cell MALDI-MSI approach revealed a decreased level of phosphatidylcholine (16:0/20:4) in multiple myeloma cells compared with plasma cells (Hossen et al., 2015). MSI is also a useful tool for testing chemotherapeutic drugs and drug combinations in cancer therapy, making it possible to monitor drug response in primary cancer spheroids (Mittal et al., 2019). The sensing ability of this method can be improved in single cancer cells and cancer stem cell analysis through nano-platform-mediated microwave digestion (Manikandan and Wu, 2016).

Recently, an open-source single-cell metabolomics method named SpaceM, which integrates light microscopy and MALDI-MSI has been developed for in situ detection of >100 metabolites from >1,000 individual cells per hour together with a fluorescence-based read out and retention of morphological spatial features based on fluorescence (Rappez et al., 2021). In addition, SpaceM can easily distinguish between cells in a state. SpaceM The SpaceM method includes following four steps. Firstly, cell segmentation of the microscopy images provide a broad panel of phenotypic information including fluorescence intensities and morphological individual cells. Next, MALDI-MSI is performed for untargeted detection of metabolisms. Then, MALDI pixel registration and single-cell intensity normalization are performed, which compensate for differences in cell sampling and filter out ambiguous ablation marks sampling multiple cells. Finally, SpaceM provides a matrix with a multiplex readout which comprises an untargeted metabolic profile, fluorescence intensities and spatio-morphological features, thus it integrates metabolism profile and phenotype.

4.2 Single-Cell Molecular Mapping

The regionalization of biological functions is a fundamental phenomenon of life, and this regionalization can be observed at different levels, ranging from organs to specific cells and even subcellular structures. At single-cell level, proteins and metabolites play a role in a specific time and space, which provides a specific chemical environment and interaction factor. Thus, understanding the subcellular localization is necessary to further study the biological process. However, there are several factors that hinder the development of single cell molecular mapping at subcellular level, such as the analyte delocalization caused by complex sample preparation process and, thus, hampering high spatial resolution, loss of molecular information due to the increase in spatial resolution, and the difficulties in handling processing, integration, and storage because of the increase in data size (Scupakova et al., 2020).

Recent advances in sample preparation, instrumentation and data processing have led the MALDI-MSI molecular mapping to approach subcellular level. An atmospheric pressure (AP) MALDI-MSI setup might achieve imaging of tissues and cells at a lateral resolution of 1.4 μm, a mass resolution greater than 100,000, and accuracy below 62 ppm (Kompauer et al., 2017).

Zebrafish, a small tropical aquarium fish native to Southeast Asia, have a unique combination of genetic and experimental embryologic advantages that make them as an ideal model vertebrate organism for studying and understanding developmental biology, drug discovery, and neurodegenerative diseases especially for early development. Recently, a study (Duenas et al., 2017a) applied high-spatial resolution MALDI-MSI to map and visualize the 3D chemical imaging of a single cell for spatial distribution of phospholipid classes, phosphatidylcholine (PC), phosphatidylethanolamines (PE), and so on, in newly fertilized individual zebrafish embryos. As shown in **Figure 6**, MALDI-MS images of PE (22:6_16:0) and PI (18:0_20:5) show that PE and PI are mostly absent or present minimally inside the yolk. In addition, to better understand how the metabolites may change when the zebrafish embryo develops, a number of embryos at different stages (1-, 2-, 4-, 8-, and 16-cell stage) were evaluated using high-spatial resolution 2D MALDI-MSI (Duenas et al., 2017a).

5 Two-Dimensional on-Tissue Mapping Molecular Distribution

Histopathological examination of tissues and cells provides clinically important and necessary insights. Visual inspection, which relies on stained tissue sections, is a classic pathological examination. The ability of MALDI-MSI to provide spatial location information is one of its great advantages. Now combining the analytical capabilities of MS with the benefits of microscopy to analyze molecular events occurring in specific cell types in tissues will take anatomic pathology a big step forward (Norris and Caprioli, 2013b).

5.1 Pathological Classification

Pathological classification of tumor cells is a difficult problem due to the similarities of different tumor (sub) types. Because assessment is usually performed manually, the results may be subject to human error. MALDI-MSI can determine the spatial distribution of multiple compounds (lipids, peptides, and proteins) in complex tissues in a single, label-free measurement. Especially in cancer research, spatial protein characterization of tissue and biomarker identification will lead to better diagnosis and individual predictive patterns of therapy response. Now, MALDI-MSI combined with machine learning has been used to classify various cancers including renal oncocytoma, clear cell renal cell carcinoma, and chromophobe renal cell carcinoma, and results showed that MSI correctly classified 87% of patients (Möginger et al., 2020). In addition, the major advantages of the method classifying cancer subtypes also simultaneously reveal the molecular features of cancer cells.

As shown in **Figure 7A**, although the heterogeneity of tumor tissue complicates diagnosis and individualized treatment, MALDI-MSI still can clearly discriminate tumor regions from nontumor regions by simultaneous detection and location of multiple protein markers (Hoffmann et al., 2019). A recent study indicated that MALDI-MSI could be used to directly detect excessive hormonal production from functional pituitary adenomas and generally classify pituitary adenomas by using statistical and machine learning analyses. The tissue characterization can be completed in fewer than 30 min and could, therefore, be applied for the near real-time detection and delineation of pituitary tumors for intraoperative surgical decision making (Calligaris et al., 2015). Therefore, clinical MALDI-MSI is helpful for the analysis of tumor tissue during surgery and can provide precise digitized diagnosis for intraoperative decision making.

5.2 Biomarker Discovery and Distribution

In general, for tumor diagnosis, biomarkers are used to distinguish between tumor cells and normal cells. MALDI-MSI can assist in the identification of lipid profile differences in breast cancer tissues, and it was found that phosphatidylcholine and triacylglycerol were the main compounds detected in cancer and normal areas as biomarkers. Very high intensity of the triacylglycerol ion signals were detected in the normal tissue region, whereas very strong ion signals of phosphatidylcholine were detected in the tumor tissue region (Cho et al., 2017). MALDI-MSI of normal and tumor areas can clearly see different lipid patterns, improving the accuracy of breast cancer diagnosis. Similar results were found in MALDI-TOF-MSI analysis of the lipid profile of prostate cancer, which showed that prostate cancer was related to the synthesis of fatty acids and lipid oxidation, while PC 16:0/16:1, PC 16:0/18:2, PC 18:0/22:5, PC 18:1/18:2, PC 18:1/20:0, PC 18:1/20:4, and SM d18:1/24:0 can be used as good biomarkers (Buszewska-Forajta et al., 2021). In addition, a form of medullary thyroid carcinoma (MTC) progresses from C-cell hyperplasia (CCH). The proteome changes in MTC and CCH tissues were analyzed by MALDI-MSI. The results showed that the trypsin profiles of MTC and CCH were significantly different, and there were four MTC markers available, K1C18 and three histones (H2A, H3C, and H4). Therefore, MALDI-MSI is a new proteomic tool that can be used to identify new molecular markers for diagnostic and prognostic significance (Smith et al., 2019).

As shown in **Figure 7B**, using MALDI-TOF-MSI, significant metabolic changes were found in relation to lipid metabolism and prostate secretory function between noncancer epithelium, stroma, and tumor. Elevated levels of metabolites associated with lipid metabolism in tumor include carnitine shuttle, which facilitates fatty acid oxidation, and metabolites of building blocks required for lipid synthesis. Levels of metabolites associated with prostate function, including citrate, aspartic acid, zinc, and spermine were higher in noncancer epithelium than in tumor. The stroma had higher levels of important energy metabolites (such as ADP, ATP, and glucose) and higher levels of the antioxidant taurine than the other. This study showed that specific tissue compartments of tumor have different metabolic profiles. Spatial metabolic profiling helps in precision therapy and potential biomarker discovery (Andersen et al., 2021).

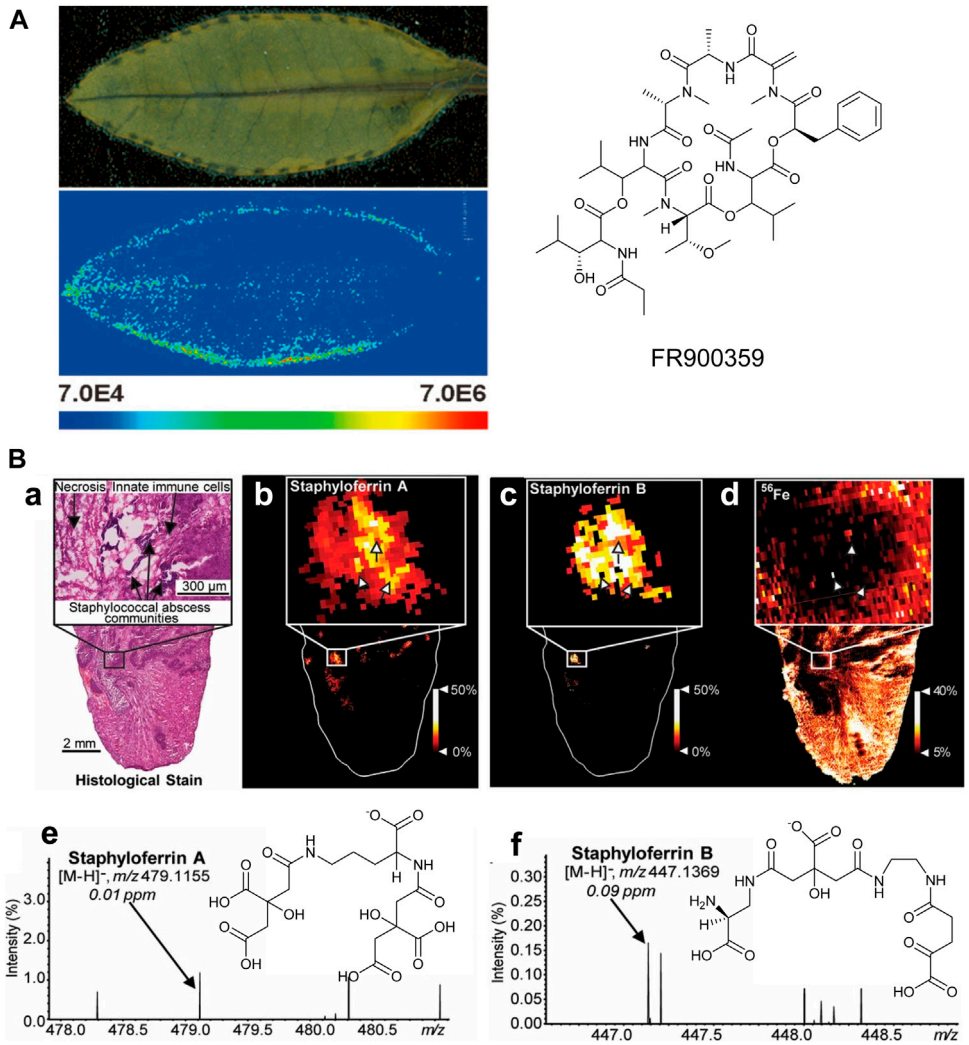

FIGURE 9 | (A) MALDI imaging mass spectrometry of an Ardisia crenata leaf (Cruesemann et al., 2018). **(B)** MALDI-IMS reveals siderophores staphyloferrin A (SA) and staphyloferrin B (SB) within the infectious environment. (a–d) The distributions of SA and SB with SACs. (e-f) The signals and the chemical structures of SA, $[M-H]^-$ and SB, $[M-H]^-$ (Perry et al., 2019).

Besides small-molecule biomarkers, such as lipids and phosphatidylcholine, there are some peptides and proteins to be found as diseases biomarkers. For example, a recent study (Balestrieri et al., 2021) indicated the signal intensity of galectin1 peptides in lung metastases compared with adjacent normal tissues and control lung. Moreover, the most intense peptide signals were found at the edges of metastases compared with adjacent normal lung tissues. MALDI-MSI can be applied to the application of proteomics methods in cancer research, especially in the spatial distribution of tumor cells.

Understanding the causes will facilitate targeted treatment and more appropriate allocation of medical resources. As for chronic kidney disease, there are two most common causes, diabetic nephropathy and hypertensive nephrosclerosis. Using MALDI-FTICR MS and nLC-ESI-MS/MS, it is speculated that four detected proteins with high signal intensity in the diabetic nephropathy tissue (PGRMC1, ANXA5, CO3, and LDHB) could be used as biomarkers to reliably distinguish the cause of CKD. Moreover, the signal intensity of PGRMC1 and CO3 increased in the late stage of the disease, which may be related to the progression (Smith et al., 2020).

5.3 Mapping Molecular Distribution

5.3.1 Imaging the Neurotransmitters

Acetylcholine (ACh) is an important neurotransmitter involved in neurodegenerative disorders. A study revealed age-related changes in acetylcholine levels in normal mice treated with the acetylcholinesterase inhibitor drug tacrine. Using MALDI-MSI, tacrine was found to significantly increase acetylcholine levels in most brain regions of mice. However, after administration, acetylcholine levels in

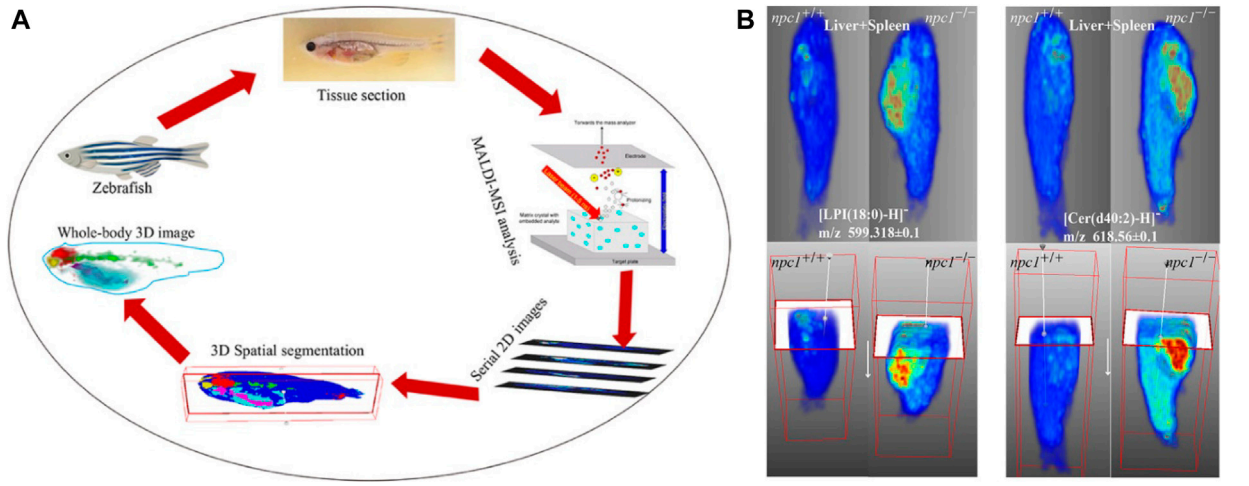

FIGURE 10 | Three dimensional (3D) reconstruction of zebrafish by MALDI-MSI (Liang et al., 2021). **(A)** The workflow of the 3D MALDI-MSI method. **(B)** Spatial distributions of Cer (d34:1) and Cer (d37:1) in fish brain.

retrosplenial cortex of 14-month-old animals were significantly lower than those of 12-week-old animals, suggesting that normal aging affects the reactivity of the cholinergic system. The distribution of tacrine and its hydroxylated metabolites in the brain was also observed, and the metabolite levels decreased significantly in 14-month-old mice. The results highlight the advantages of imaging techniques that can simultaneously investigate multiple molecular species and specific regions of drug target effects (Vallianatou et al., 2019).

L-DOPA therapy for Parkinson's disease often leads to dyskinesia. The distribution of L-DOPA and monoaminergic pathways in the brains (**Figure 8A**) of dyskinetic and nondyskinetic primates was mapped using MALDI-MSI. The levels of L-DOPA and its metabolite 3-O-methyldopa were increased in all measured brain regions of dyskinetic animals, and the levels of dopamine and metabolites were increased in all analyzed regions except the striatum. The level of dopamine was significantly correlated with the level of L-DOPA in extrastriatal regions. L-DOPA-induced dyskinesia is associated with whole-brain L-DOPA dysregulation. High dopamine abundance in extracranial regions may alter signal transduction throughout the brain, leading to various adverse effects of L-DOPA treatment (Fridjonsdottir et al., 2021).

5.3.2 Imaging N-Glycoproteomes

Aberrant glycosylation is a common feature of cancer. MALDI-MSI has been used to study changes in N-glycosylation in cancer, using a combination of MALDI N-glycan MSI and spatially resolved glycoproteomics. Thus, glycosylation imaging (**Figure 8B**) is directly linked to complete glycopeptide identification. This glycoproteomics technique identified more than 400 N-, O-, and S-glycopeptides from more than 30 proteins. The sialylated O-GalNAc structure was significantly increased in the tumor/necrotic area compared with the benign area, while S- and O-GlcNAc peptides were significantly decreased in the cancerous area. This experiment provides a unique way to understand the spatial variability of glycosylation changes in cancer (Malaker et al., 2021).

5.3.3 Imaging Host–Microbe Symbioses

Symbioses are widespread in nature. There are complex biochemical interactions between them which affect each other, and MALDI-MSI can help us further study about the relationship between host and microbe.

When a biological symbiosis is mutually beneficial, it is termed "mutualism." For example, obligatory plant–bacteria associations, as observed in the case of the nodulated *Ardisia crenata*, constitute fascinating ecological systems (Carlier et al., 2016). The cyclic depsipeptide FR900359, a strong and selective inhibitor of Gq proteins, is isolated from the tropical plant *Ardisia crenata* (Fujioka et al., 1988), but it is finally found to be produced from the symbiotic "Candidatus *Burkholderia crenata*," a bacterium that is mostly located in the nodules at the leaf margin of *A. crenata* (Carlier et al., 2016), which is consistent with recent MALDI-MSI results (**Figure 9A**). The small blue dots show the distribution of FR900359 (*m/z* 1,040.49), which corresponds to "Candidatus *Burkholderia crenata*" at the margin of *A. crenata* leaves, suggesting that FR900359 plays a novel mode of action for defense chemicals through Gq inhibition (Cruesemann et al., 2018).

There is a parasitic relationship between *Staphylococcus aureus* and vertebrate hosts. *Staphylococcus aureus* feeds on the nutrients of the host, which is another type of symbiotic relationship. Typically, the metalloproteins in the host isolate the very important metal elements in the body to prevent the absorption of microorganisms during infection. However, bacteria have also evolved metal acquisition strategies to combat nutritional immunity, such as the use of siderophores and small iron-scavenge molecules. Recent studies have used multimodal MALDI-MSI to image siderophores in infected tissues to visualize host–pathogen iron competition (Perry

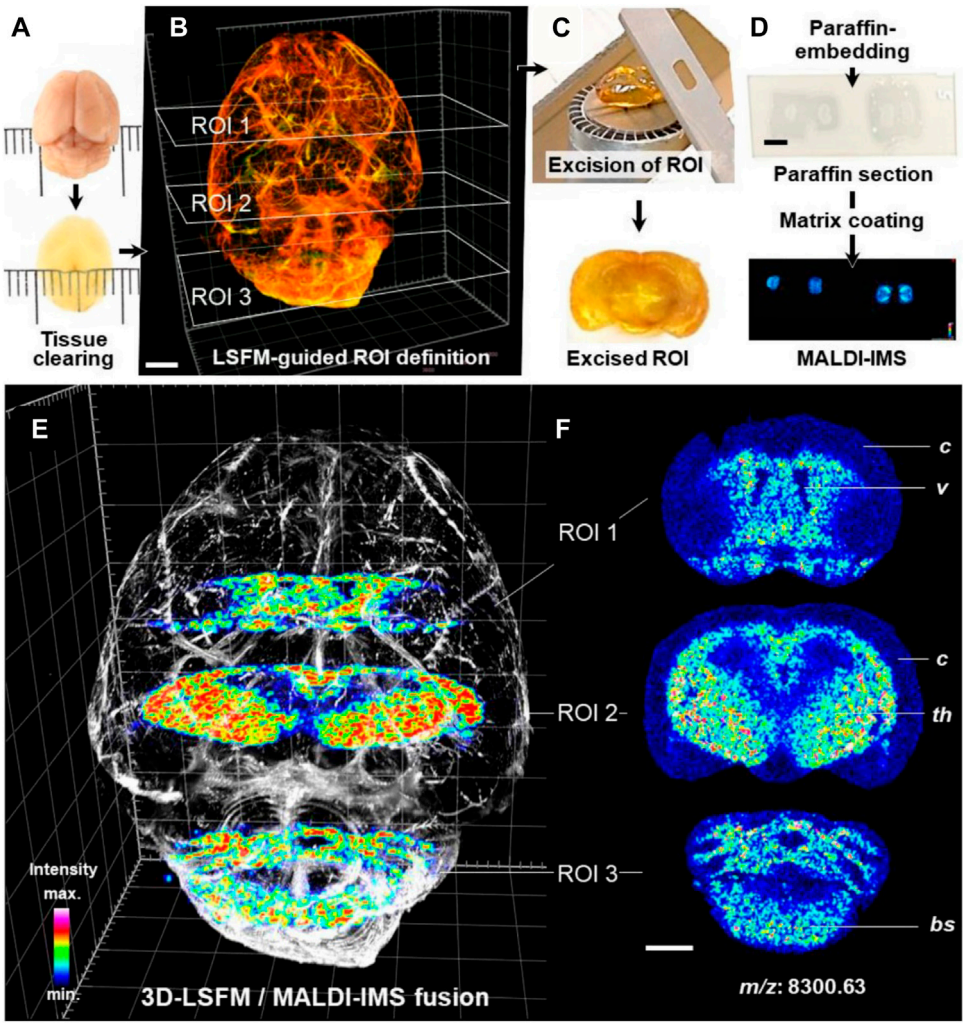

FIGURE 11 | 3D-LSFM-guided MALDI-MSI in an optically cleared mouse brain (Blutke et al., 2020). **(A–D)** Sequence of tissue-processing steps. **(E)** Fused image of the 3D-LSFM reconstruction of the cleared brain and MALDI-MS images of guanine nucleotide-binding protein subunit gamma-3 (GNG3, *m/z*: 8,300.63). **(F)** MALDI-MS images of GNG3. The spatial distribution of GNG3. Distinct brain structures are indicated for orientation: cerebral cortex (*c*), ventricles (*v*), thalamus (*th*), brain stem (*bs*).

et al., 2019). It can be observed that the heterogeneous distribution of *Staphylococcus aureus* siderophores across the infected lesions is observed, as shown in **Figure 9B**. These results suggest that each siderophore has a niche-specific role, rather than functional redundancy. Differential distributions of these siderophores may be explained by molecular heterogeneity within the abscess.

More recently, a spatial metabolomics pipeline (metaFISH) has been developed by combines fluorescence in situ hybridization (FISH) microscopy and high-resolution atmospheric-pressure MALDI-MSI in order to image host-microbe symbioses and its metabolic interactions and provide spatial assignment of host and symbiont metabolites. The metaFISH workflow consists of three steps. Firstly, mapping metabolites with high-resolution AP MALDI-MSI on cryosections and FISH after MSI on the same tissue section. Then, spectral preprocessing, image adjustment, cluster maps, phylotype assignment is needed to process correlative data. Finally, statistical analysis is performed using the fluorescence signals to bin metabolite groups. This method presented the spatial metabolome of a deep-sea mussel and its intracellular symbiotic bacteria, revealing the metabolic adaptability of epithelial cells to intracellular symbionts and metabolic phenotypic variation of the 16S rRNA phylotype of an individual symbiont, and making it possible to discover specialized metabolites from the host–microbe interface (Geier et al., 2020).

6 THREE-DIMENSIONAL SPATIAL IMAGING

Since biological processes take place in three-dimensional organisms, it is not surprising that 3D imaging has a

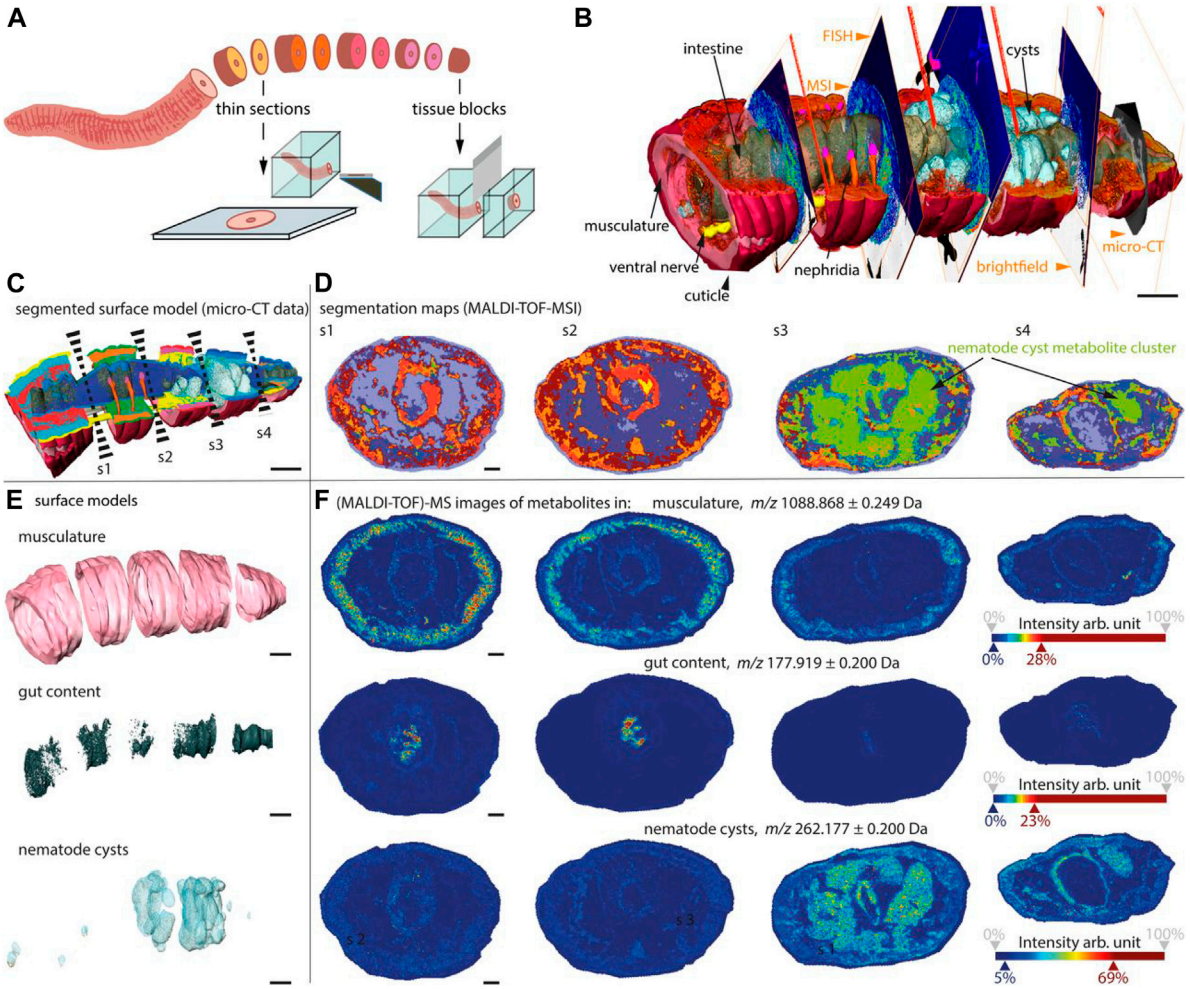

FIGURE 12 | CHEMHIST revealed organ-specific chemistry in the posterior segments of an earthworm (Geier et al., 2021).

noteworthy impact on different studies in life sciences. Recently, the use of MSI to image intact biomolecules has been extended to 3D analysis to determine the volumetric molecular distribution in tissue samples. The most common 3D MSI method includes collecting consecutive tissue sections of the samples, analyzing each section separately using traditional two-dimensional MSI, and then using computational methods to stack and reconstruct the final 3D MSI dataset from multiple two-dimensional MSI data.

6.1 Three-Dimensional Reconstruction of Spatial Distribution

A 3D MALDI-MSI method (**Figure 10**) was applied for whole-body analysis of zebrafish and was used to identify altered lipids and map their spatial distribution within zebrafish model Niemann–Pick disease type C1 (NPC1), a neurovisceral lipid storage disorder. The constructed 3D model of fish provided comprehensive information on the 3D distribution of lipids and allowed direct correlation between these lipids and fish organs. The results showed that compared with the wild type, some sphingolipids and phospholipids in the brain, spinal cord, intestines, and liver–spleen region of fish with NPC1 gene mutation had significant changes and showed different localization patterns. This 3D MALDI-MSI method can provide a global picture of lipid changes in different organs and functional systems (Liang et al., 2021).

To investigate the possible role of epididymis in the complex maturation of sperm, MALDI-MSI investigated the precise location of lipid metabolites in the rat epididymis, mainly detecting phosphatidylcholines, sphingolipids, glycerophosphates, triacylglycerols, plasmalogens, phosphatidylethanolamines, and lysophosphatidylcholines. During epididymal maturation, the number of sphingolipids and plasmalogens increased, while the proportion of triacylglycerols decreased from caput to cauda. Molecules belonging to the same family may have very different positions on the epididymis. A 3D model of the epididymis head was also reconstructed by 3D MALDI-MSI, which can be used to obtain localization information of specific analytes in the

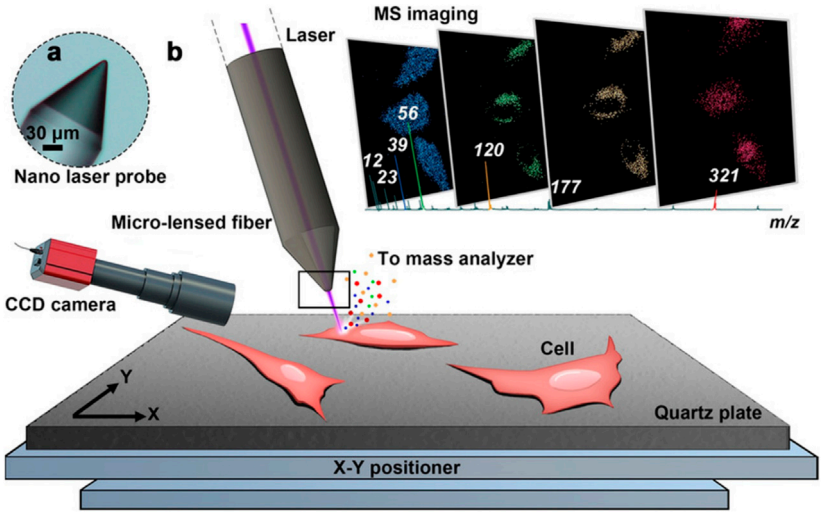

FIGURE 13 | Nano laser probe-based MSI system. **(A)** A microscope photograph of the tip of the nano laser probe (NLP). **(B)** Diagram of the ion source and MSI process (Meng et al., 2020).

entire tissue. This work opens a new perspective on the role of lipid metabolism in sperm maturation when it moves through the epididymis (Lagarrigue et al., 2020).

6.2 Three-Dimensional Mapping Together Light Sheet Fluorescence Microscopy

Light sheet fluorescence microscopy (LSFM) of optically cleared biological tissue samples has developed rapidly in the past decade and has become a powerful tool for 3D histomorphological analysis applied to various life sciences (Hillman et al., 2019; Ueda et al., 2020).

LSFM of cleared brain tissue samples could be combined with MALDI-MSI for protein detection and quantification (**Figure 11**). Fresh dissected murine brain tissue and archived FFPE human brain tissue were cleared. Regions of interest of tissue defined by LSFM were paraffin embedded and sectioned. The sections were then subjected to MALDI-TOF-MSI in mass ranges between 0.8 and 4 kDa (human) or 2.5–25 kDa (mouse) with a lateral resolution of 50 μm. The protein and peptide characteristics corresponding to the obtained MALDI-MSI spectra were determined by parallel LC-MS/MS analysis. MALDI-MSI will be of great value in combination with qualitative and quantitative morphological analysis of complex 3D tissue structures (Blutke et al., 2020).

6.3 Three-Dimensional Imaging Host–Microbe Interactions by Combining Mass Spectrometry Imaging and X-Ray Tomography

As is known to all, metabolites mediate most interkingdom symbioses. However, determining the metabolites of each member of the biological interaction remains a huge challenge. Recently, a chemo-histo-tomography (CHEMHIST) method (Geier et al., 2021) has been developed to link histological changes with metabolites by combining MSI and x-ray tomography (micro-CT) to correlate metabolite distribution with 3D histology of the same animal (**Figure 12**), down to submicrometer resolutions. This method is compatible with tissue-specific DNA sequencing and fluorescence *in situ* hybridization and can be used for taxonomic identification and localization of relevant microorganisms. These results revealed the physical and chemical interactions of an earthworm from its natural habitat with bacteria and parasitic nematodes in its tissues. Combined MSI and micro-CT, advances in chemical and structural *in situ* imaging will drive the study of metabolic interactions in symbiotic systems (Geier et al., 2021).

7 FUTURE DIRECTIONS

MALDI-MSI is now a promising tool for rapid and robust molecule-specific MS imaging of biological tissue sections at a broad range of length scales, ranging from the subcellular level to whole-body tissue sections. As the sample applied in MALDI-MSI varied, it is critical to standardize sample preparation, storage protocols, and data acquisition (Dihazi et al., 2013). Flatley et al. pointed out that many researches were of highly contradictory results and existing repeat mistakes for lack of standard operating protocols (SOPs) (Flatley et al., 2014).

Speed, specificity, spatial resolution, and sensitivity, the "4S-criteia for performance," is still suitable for further MALDI-MSI (Schulz et al., 2019). Improving the MSI resolution to single-cell level and even subcellular level will make it more suitable and useful for deeper biological discovery. It is for sure that MALDI reduces the disturbance to the cell. However, when it comes to single-cell level, the complexity of sample preparation of clinical samples may cause analyte delocalization. From an instrumental side, laser and detector technologies must be developed to meet the need of speed and accuracy in high-throughput analysis. Besides, advanced computational solutions must be developed to handle the

problems of large-scale data, processing, integration, and storage (Scupakova et al., 2020).

A significant challenge for most MSI is the failure to distinguish isomers, which may cause the misinterpretation of location and function of isomers, due to the lack of chromatography step. For example, fructose has been shown to contribute to the Warburg effect and cancer growth (Port et al., 2012; Nakagawa et al., 2020). However, it is difficult to image fructose using the ordinary MSI method due to the interference of its common isomer—glucose, which plays a minor role of energy source for cancer growth, different from fructose (Nakagawa et al., 2020). This limitation could be overcome by coupling MSI with approaches capable of resolving the isobaric molecules, such as tandem mass spectrometry (MS/MS) (Zhan et al., 2021), trapped ion mobility spectrometry (TIMS) (Sans et al., 2018; Spraggins et al., 2019). Recent efforts in coupling special reaction to tandem mass spectrometry imaging have succeeded in distinguish lipid isomers based on strategy for identifying C=C bond positions, such as on-tissue Paterno–Buchi reaction (Bednarik et al., 2018; Waldchen et al., 2019), ozone-induced dissociation (OzID) (Paine et al., 2018; Claes et al., 2021; Young et al., 2021), and online photochemical derivatization (Unsihuay et al., 2021b). There is also a strategy utilizing structure-specific derivatization methods to modify one of the isomers to separate isomers before sampling, which is rarely available.

MALDI and SIMS are important ionizations applied in subcellular-level MSI (Kallback et al., 2012). Compared with MALDI-MSI, SIMS-MSI can obtain higher spatial resolution images directly from biological tissue. Nowadays, nanoSIMS with a resolution of nm level has been applied in quantitation of subcellular protein (Vreja et al., 2015), lipid (Jiang et al., 2014), neurotransmitter (Lovric et al., 2017), drug (Jiang et al., 2017), and even DNA (Steinhauser et al., 2012) distribution in a single cell, but recent achievements in MALDI-MSI show that using MALDI as ionization can approach nm-level resolution. The use of t-MALDI-2 MSI system achieved a high pixel size of 600 nm with brain tissue (Niehaus et al., 2019). Besides, as shown in **Figure 13**, the resolution of recent nano laser probe-based MSI systems can be down to the nm level (subcellular level) by introducing desorption laser with a micro-lensed fiber, proving a great development in MALDI-MSI (Meng et al., 2020). Considering the lack of selectivity of samples of MALDI ionization (Susniak et al., 2020) and the ability to detect DNA (Kirpekar et al., 1999; Ehrich et al., 2005), we believe that MALDI will become more and more important in MSI.

8 GENERAL MARKS AND CONCLUSIONS

MSI is a powerful analytical technique that cannot only detect qualitatively and determine quantitatively hundreds and thousands of a large variety of natural and synthetic compounds, such as lipids, amino acids, metabolites, peptides, proteins, DNA, RNA, and even SARS-CoV-2 virus (Nachtigall et al., 2020), but also can map simultaneously spatial locations of these detected molecules. Therefore, there are increasing trends to apply MSI where required to know the relative abundance and spatial distribution of the molecules. Compared with other MSI techniques, such as SIMS and DESI, MALDI-MSI is a very simple, economic, and reliable technique. It does not need assisting solvents/gas jet or special ion beam, but only requires a suitable matrix on the sample plate and a pulsed laser beam for ionizing the targeted molecules. Laser desorption ionization together with assisted matrix made MALDI more practical, salt resistant, and sensible than other methods. In addition, the majority of ions ionized by MALDI are singly protonated; thus, the molecular weight could be common directly read, and less MS noises besides matrix signals have been detected. With the developments of organic matrix-free nano matrices such as GO, nano gold, titanium oxide and nanowires, and on-tissue or on-cell chemical derivation, MALDI-MSI will provide high sensitivity. Furthermore, MALDI ion resources can be easily coupled with high-resolution (resolving power) mass analyzers, such as TOF, FT-ICR, and Orbitrap, which provide high mass accuracy for MSI targets. During the recent years, with the developments of some new MALDI ion sources, such as atmosphere pressure AP-MALDI (Kompauer et al., 2017), AP-SMALDI (Vegvari et al., 2017; Bhandari et al., 2018; Bredehoeft et al., 2019; Kadesch et al., 2020; Mokosch et al., 2021; Mueller et al., 2021; Righetti et al., 2021), MALDI-2 (Soltwisch et al., 2015), transmission MALDI-2 (Niehaus et al., 2019), and nano laser probed-based laser desorption ionization (Meng et al., 2020), the lateral resolution of MALDI-MSI will possibly achieve nm or μm level for single cell and even subcellular scale imaging. Finally, the scanning speed of MALDI-MSI largely depends on the speed of MS detection, spectra recording and data processing. With the developments of MSI instruments and artificial intelligence for big data, the MALDI-MSI will achieve high-speed scanning and rapid analyses. Therefore, further high-resolution MALDI-MSI will be applied to wide fields from single cells, tissues, to 3D organisms for molecular understanding of life and other human-related fields.

AUTHOR CONTRIBUTIONS

SW conceptualized the study. XZ and TX developed the methodology. XZ, TX, CP, and SW wrote and prepared the original draft. SW, TX, XZ, and CP wrote, reviewed, and edited the manuscript. SW was in charge of the project administration and acquired the funding. All authors have read and agreed to the published version of the manuscript.

FUNDING

This research was supported by the Fundamental Research Funds for the Central Universities (2021QNA6001 and 2021FZZX003-02–12), Natural Science Foundation of Zhejiang Province, China (LY20B020011), and National Natural Science Foundation of China (21672188).

ACKNOWLEDGMENTS

The authors would like to thank the fund of the National Natural Science Foundation of China.

REFERENCES

Ali, A., Abouleila, Y., Shimizu, Y., Hiyama, E., Emara, S., Mashaghi, A., et al. (2019). Single-cell Metabolomics by Mass Spectrometry: Advances, Challenges, and Future Applications. *Trac-Trends Anal. Chem.* 120, 115436. doi:10.1016/j.trac.2019.02.033

Andersen, M. K., Hoiem, T. S., Claes, B. S. R., Balluff, B., Martin-Lorenzo, M., Richardsen, E., et al. (2021). Spatial Differentiation of Metabolism in Prostate Cancer Tissue by MALDI-TOF MSI. *Cancer Metab.* 9, 9. doi:10.1186/s40170-021-00242-z

Angelini, R., Yutuc, E., Wyatt, M. F., Newton, J., Yusuf, F. A., Griffiths, L., et al. (2021). Visualizing Cholesterol in the Brain by On-Tissue Derivatization and Quantitative Mass Spectrometry Imaging. *Anal. Chem.* 93, 4932–4943. doi:10.1021/acs.analchem.0c05399

Araújo, J. E., Oliveira, E., Otero-Glez, A., Santos Nores, J., Igrejas, G., Lodeiro, C., et al. (2014). A Comprehensive Factorial Design Study of Variables Affecting Protein Extraction from Formalin-Fixed Kidney Tissue Samples. *Talanta* 119, 90–97. doi:10.1016/j.talanta.2013.10.019

Armstrong, D. W., Zhang, L.-K., He, L., and Gross, M. L. (2001). Ionic Liquids as Matrixes for Matrix-Assisted Laser Desorption/ionization Mass Spectrometry. *Anal. Chem.* 73, 3679–3686. doi:10.1021/ac010259f

Avery, J. L., Mcewen, A., Flinders, B., Francese, S., and Clench, M. R. (2011). Matrix-assisted Laser Desorption Mass Spectrometry Imaging for the Examination of Imipramine Absorption by Straticell-Rhe-Epi/001 an Artificial Model of the Human Epidermis. *Xenobiotica* 41, 735–742. doi:10.3109/00498254.2011.573015

Bai, J., Liu, Y.-H., Cain, T. C., and Lubman, D. M. (1994). Matrix-assisted Laser Desorption/ionization Using an Active Perfluorosulfonated Ionomer Film Substrate. *Anal. Chem.* 66, 3423–3430. doi:10.1021/ac00092a020

Baker, T. C., Han, J., and Borchers, C. H. (2017). Recent Advancements in Matrix-Assisted Laser Desorption/ionization Mass Spectrometry Imaging. *Curr. Opin. Biotechnol.* 43, 62–69. doi:10.1016/j.copbio.2016.09.003

Balestrieri, K., Kew, K., Mcdaniel, M., Ramez, M., Pittman, H. K., Murray, G., et al. (2021). Proteomic Identification of Tumor- and Metastasis-Associated Galectin-1 in Claudin-Low Breast Cancer. *Biochim. Biophys. Acta-General Subjects* 1865, 129784. doi:10.1016/j.bbagen.2020.129784

Barré, F. P. Y., Flinders, B., Garcia, J. P., Jansen, I., Huizing, L. R. S., Porta, T., et al. (2016). Derivatization Strategies for the Detection of Triamcinolone Acetonide in Cartilage by Using Matrix-Assisted Laser Desorption/ionization Mass Spectrometry Imaging. *Anal. Chem.* 88, 12051–12059. doi:10.1021/acs.analchem.6b02491

Beasley, E., Francese, S., and Bassindale, T. (2016). Detection and Mapping of Cannabinoids in Single Hair Samples through Rapid Derivatization and Matrix-Assisted Laser Desorption Ionization Mass Spectrometry. *Anal. Chem.* 88, 10328–10334. doi:10.1021/acs.analchem.6b03551

Becker, K.-F., Schott, C., Hipp, S., Metzger, V., Porschewski, P., Beck, R., et al. (2007). Quantitative Protein Analysis from Formalin-Fixed Tissues: Implications for Translational Clinical Research and Nanoscale Molecular Diagnosis. *J. Pathol.* 211, 370–378. doi:10.1002/path.2107

Bednarik, A., Boelsker, S., Soltwisch, J., and Dreisewerd, K. (2018). An On-Tissue Paterno-Buchi Reaction for Localization of Carbon-Carbon Double Bonds in Phospholipids and Glycolipids by Matrix-Assisted Laser-Desorption-Ionization Mass-Spectrometry Imaging. *Angew. Chemie-International Edition* 57, 12092–12096.

Bergmann, S., Lawler, S. E., Qu, Y., Fadzen, C. M., Wolfe, J. M., Regan, M. S., et al. (2018). Blood-brain-barrier Organoids for Investigating the Permeability of Cns Therapeutics. *Nat. Protoc.* 13, 2827–2843. doi:10.1038/s41596-018-0066-x

Bhandari, D. R., Wang, Q., Li, B., Friedt, W., Römpp, A., Spengler, B., et al. (2018). Histology-guided High-Resolution AP-SMALDI Mass Spectrometry Imaging of Wheat-fusarium Graminearum Interaction at the Root-Shoot junction. *Plant Methods* 14, 103. doi:10.1186/s13007-018-0368-6

Bien, T., Bessler, S., Dreisewerd, K., and Soltwisch, J. (2021a). Transmission-mode MALDI Mass Spectrometry Imaging of Single Cells: Optimizing Sample Preparation Protocols. *Anal. Chem.* 93, 4513–4520. doi:10.1021/acs.analchem.0c04905

Bien, T., Hambleton, E. A., Dreisewerd, K., and Soltwisch, J. (2021b). Molecular Insights into Symbiosis-Mapping Sterols in a marine Flatworm-Algae-System Using High Spatial Resolution MALDI-2-MS Imaging with Ion Mobility Separation. *Anal. Bioanal. Chem.* 413, 2767–2777. doi:10.1007/s00216-020-03070-0

Blutke, A., Sun, N., Xu, Z., Buck, A., Harrison, L., Schriever, S. C., et al. (2020). Light Sheet Fluorescence Microscopy Guided MALDI-Imaging Mass Spectrometry of Cleared Tissue Samples. *Sci. Rep.* 10, 14461. doi:10.1038/s41598-020-71465-1

Bouschen, W., Schulz, O., Eikel, D., and Spengler, B. (2010). Matrix Vapor Deposition/recrystallization and Dedicated spray Preparation for High-Resolution Scanning Microprobe Matrix-Assisted Laser Desorption/ionization Imaging Mass Spectrometry (SMALDI-MS) of Tissue and Single Cells. *Rapid Commun. Mass. Spectrom.* 24, 355–364. doi:10.1002/rcm.4401

Bredehöft, J., Bhandari, D. R., Pflieger, F. J., Schulz, S., Kang, J. X., Layé, S., et al. (2019). Visualizing and Profiling Lipids in the Ovlt of Fat-1 and Wild Type Mouse Brains during Lps-Induced Systemic Inflammation Using AP-SMALDI MSI. *ACS Chem. Neurosci.* 10, 4394–4406. doi:10.1021/acschemneuro.9b00435

Briggs, M. T., Ho, Y. Y., Kaur, G., Oehler, M. K., Everest-Dass, A. V., Packer, N. H., et al. (2017). N- Glycan Matrix-assisted Laser Desorption/ionization Mass Spectrometry Imaging Protocol for Formalin-fixed Paraffin-embedded Tissues. *Rapid Commun. Mass. Spectrom.* 31, 825–841. doi:10.1002/rcm.7845

Buszewska-Forajta, M., Pomastowski, P., Monedeiro, F., Walczak-Skierska, J., Markuszewski, M., Matuszewski, M., et al. (2021). Lipidomics as a Diagnostic Tool for Prostate Cancer. *Cancers (Basel)* 13, 2000. doi:10.3390/cancers13092000

Calligaris, D., Feldman, D. R., Norton, I., Olubiyi, O., Changelian, A. N., Machaidze, R., et al. (2015). MALDI Mass Spectrometry Imaging Analysis of Pituitary Adenomas for Near-Real-Time Tumor Delineation. *Proc. Natl. Acad. Sci. USA* 112, 9978–9983. doi:10.1073/pnas.1423101112

Calvano, C. D., Monopoli, A., Cataldi, T. R. I., and Palmisano, F. (2018). MALDI Matrices for Low Molecular Weight Compounds: An Endless story? *Anal. Bioanal. Chem.* 410, 4015–4038. doi:10.1007/s00216-018-1014-x

Capitoli, G., Piga, I., Galimberti, S., Leni, D., Pincelli, A. I., Garancini, M., et al. (2019). MALDI-MSI as a Complementary Diagnostic Tool in Cytopathology: A Pilot Study for the Characterization of Thyroid Nodules. *Cancers (Basel)* 11, 1377. doi:10.3390/cancers11091377

Caprioli, R. M., Farmer, T. B., and Gile, J. (1997). Molecular Imaging of Biological Samples: Localization of Peptides and Proteins Using MALDI-TOF MS. *Anal. Chem.* 69, 4751–4760. doi:10.1021/ac970888i

Carlier, A., Fehr, L., Pinto-Carbó, M., Schäberle, T., Reher, R., Dessein, S., et al. (2016). The Genome Analysis of C Andidatus Burkholderia Crenata Reveals that Secondary Metabolism May Be a Key Function of the A Rdisia Crenata Leaf Nodule Symbiosis. *Environ. Microbiol.* 18, 2507–2522. doi:10.1111/1462-2920.13184

Carter, C. L., Mcleod, C. W., and Bunch, J. (2011). Imaging of Phospholipids in Formalin Fixed Rat Brain Sections by Matrix Assisted Laser Desorption/ionization Mass Spectrometry. *J. Am. Soc. Mass. Spectrom.* 22, 1991–1998. doi:10.1007/s13361-011-0227-4

Chacon, A., Zagol-Ikapitte, I., Amarnath, V., Reyzer, M. L., Oates, J. A., Caprioli, R. M., et al. (2011). On-tissue Chemical Derivatization of 3-methoxysalicylamine for MALDI-Imaging Mass Spectrometry. *J. Mass. Spectrom.* 46, 840–846. doi:10.1002/jms.1958

Chaurand, P., Schwartz, S. A., Billheimer, D., Xu, B. J., Crecelius, A., and Caprioli, R. M. (2004). Integrating Histology and Imaging Mass Spectrometry. *Anal. Chem.* 76, 1145–1155. doi:10.1021/ac0351264

Chen, S., Xiong, C., Liu, H., Wan, Q., Hou, J., He, Q., et al. (2015). Mass Spectrometry Imaging Reveals the Sub-organ Distribution of Carbon Nanomaterials. *Nat. Nanotech* 10, 176–182. doi:10.1038/nnano.2014.282

Chen, X., Wo, F., Chen, J., Tan, J., Wang, T., Liang, X., et al. (2017). Ratiometric Mass Spectrometry for Cell Identification and Quantitation Using Intracellular "Dual-Biomarkers". *Sci. Rep.* 7, 17432. doi:10.1038/s41598-017-17812-1

Chen, Y., Tang, F., Li, T.-G., He, J.-M., Abliz, Z., Liu, L.-T., et al. (2014). Application of Factor Analysis in Imaging Mass Spectrometric Data Analysis. *Chin. J. Anal. Chem.* 42, 1099–1103. doi:10.1016/s1872-2040(14)60757-x

Cho, Y.-T., Su, H., Chiang, Y.-Y., Shiea, J., Yuan, S.-S. F., Hung, W.-C., et al. (2017). Fine Needle Aspiration Combined with Matrix-Assisted Laser Desorption Ionization Time-Of-Flight/mass Spectrometry to Characterize Lipid Biomarkers for Diagnosing Accuracy of Breast Cancer. *Clin. Breast Cancer* 17, 373–381. doi:10.1016/j.clbc.2017.04.014

Chughtai, K., and Heeren, R. M. A. (2010). Mass Spectrometric Imaging for Biomedical Tissue Analysis. *Chem. Rev.* 110, 3237–3277. doi:10.1021/cr100012c

Chumbley, C. W., Reyzer, M. L., Allen, J. L., Marriner, G. A., Via, L. E., Barry, C. E., Iii, et al. (2016). Absolute Quantitative MALDI Imaging Mass Spectrometry: A Case of Rifampicin in Liver Tissues. *Anal. Chem.* 88, 2392–2398. doi:10.1021/acs.analchem.5b04409

Claes, B. S. R., Bowman, A. P., Poad, B. L. J., Young, R. S. E., Heeren, R. M. A., Blanksby, S. J., et al. (2021). Mass Spectrometry Imaging of Lipids with Isomer Resolution Using High-Pressure Ozone-Induced Dissociation. *Anal. Chem.* 93, 9826–9834. doi:10.1021/acs.analchem.1c01377

Clift, C. L., Drake, R. R., Mehta, A., and Angel, P. M. (2021). Multiplexed Imaging Mass Spectrometry of the Extracellular Matrix Using Serial Enzyme Digests from Formalin-Fixed Paraffin-Embedded Tissue Sections. *Anal. Bioanal. Chem.* 413, 2709–2719. doi:10.1007/s00216-020-03047-z

Cole, L. M., and Clench, M. R. (2015). Mass Spectrometry Imaging for the Proteomic Study of Clinical Tissue. *Prot. Clin. Appl.* 9, 335–341. doi:10.1002/prca.201400103

Cornett, D. S., Reyzer, M. L., Chaurand, P., and Caprioli, R. M. (2007). MALDI Imaging Mass Spectrometry: Molecular Snapshots of Biochemical Systems. *Nat. Methods* 4, 828–833. doi:10.1038/nmeth1094

Crüsemann, M., Reher, R., Schamari, I., Brachmann, A. O., Ohbayashi, T., Kuschak, M., et al. (2018). Heterologous Expression, Biosynthetic Studies, and Ecological Function of the Selective Gq-Signaling Inhibitor Fr900359. *Angew. Chem. Int. Ed. Engl.* 57, 836–840. doi:10.1002/anie.201707996

David, B. P., Dubrovskyi, O., Speltz, T. E., Wolff, J. J., Frasor, J., Sanchez, L. M., et al. (2018). Using Tumor Explants for Imaging Mass Spectrometry Visualization of Unlabeled Peptides and Small Molecules. *ACS Med. Chem. Lett.* 9, 768–772. doi:10.1021/acsmedchemlett.8b00091

Davison, A. S., Strittmatter, N., Sutherland, H., Hughes, A. T., Hughes, J., Bou-Gharios, G., et al. (2019). Correction to: Assessing the Effect of Nitisinone Induced Hypertyrosinaemia on Monoamine Neurotransmitters in Brain Tissue from a Murine Model of Alkaptonuria Using Mass Spectrometry Imaging. *Metabolomics* 15, 81. doi:10.1007/s11306-019-1540-3

Deininger, S.-O., Cornett, D. S., Paape, R., Becker, M., Pineau, C., Rauser, S., et al. (2011). Normalization in MALDI-TOF Imaging Datasets of Proteins: Practical Considerations. *Anal. Bioanal. Chem.* 401, 167–181. doi:10.1007/s00216-011-4929-z

Denti, V., Piga, I., Guarnerio, S., Clerici, F., Ivanova, M., Chinello, C., et al. (2020). Antigen Retrieval and its Effect on the MALDI-MSI of Lipids in Formalin-Fixed Paraffin-Embedded Tissue. *J. Am. Soc. Mass. Spectrom.* 31, 1619–1624. doi:10.1021/jasms.0c00208

Dihazi, H., Bohrer, R., Jahn, O., Lenz, C., Majcherczyk, A., Schmidt, B., et al. (2013). Mass Spectrometry Imaging: Linking Molecule Profiles to Tissue Spatial Distribution. *Expert Rev. Proteomics* 10, 17–20. doi:10.1586/epr.12.73

Djidja, M.-C., Claude, E., Scriven, P., Allen, D. W., Carolan, V. A., and Clench, M. R. (2017). Antigen Retrieval Prior to On-Tissue Digestion of Formalin-Fixed Paraffin-Embedded Tumour Tissue Sections Yields Oxidation of Proline Residues. *Biochim. Biophys. Acta (Bba) - Proteins Proteomics* 1865, 901–906. doi:10.1016/j.bbapap.2016.11.019

Dueñas, M. E., Essner, J. J., and Lee, Y. J. (2017a). 3d MALDI Mass Spectrometry Imaging of a Single Cell: Spatial Mapping of Lipids in the Embryonic Development of Zebrafish. *Sci. Rep.* 7, 14946. doi:10.1038/s41598-017-14949-x

Dueñas, M. E., Klein, A. T., Alexander, L. E., Yandeau-Nelson, M. D., Nikolau, B. J., and Lee, Y. J. (2017b). High Spatial Resolution Mass Spectrometry Imaging Reveals the Genetically Programmed, Developmental Modification of the Distribution of Thylakoid Membrane Lipids Among Individual Cells of maize Leaf. *Plant J.* 89, 825–838. doi:10.1111/tpj.13422

Dueñas, M. E., and Lee, Y. J. (2021). "Single-cell Metabolomics by Mass Spectrometry Imaging," in *Cancer Metabolomics: Methods and Applications*. Editor S. Hu (Basingstoke, United Kingdom: Springer Nature), 69–82. doi:10.1007/978-3-030-51652-9_5

Ehrich, M., Nelson, M. R., Stanssens, P., Zabeau, M., Liloglou, T., Xinarianos, G., et al. (2005). Quantitative High-Throughput Analysis of DNA Methylation Patterns by Base-specific Cleavage and Mass Spectrometry. *Proc. Natl. Acad. Sci.* 102, 15785–15790. doi:10.1073/pnas.0507816102

Enomoto, H., Sensu, T., Yumoto, E., Yokota, T., and Yamane, H. (2018). Derivatization for Detection of Abscisic Acid and 12-Oxo-Phytodienoic Acid Using Matrix-Assisted Laser Desorption/ionization Imaging Mass Spectrometry. *Rapid Commun. Mass. Spectrom.* 32, 1565–1572. doi:10.1002/rcm.8200

Esteve, C., Tolner, E. A., Shyti, R., Van Den Maagdenberg, A. M., and Mcdonnell, L. A. (2016). Mass Spectrometry Imaging of Amino Neurotransmitters: A Comparison of Derivatization Methods and Application in Mouse Brain Tissue. *Metabolomics* 12, 30. doi:10.1007/s11306-015-0926-0

Fenn, J. B., Mann, M., Meng, C. K., Wong, S. F., and Whitehouse, C. M. (1989). Electrospray Ionization for Mass Spectrometry of Large Biomolecules. *Science* 246, 64–71. doi:10.1126/science.2675315

Flatley, B., Malone, P., and Cramer, R. (2014). MALDI Mass Spectrometry in Prostate Cancer Biomarker Discovery. *Biochim. Biophys. Acta (Bba) - Proteins Proteomics* 1844, 940–949. doi:10.1016/j.bbapap.2013.06.015

Flint, L. E., Hamm, G., Ready, J. D., Ling, S., Duckett, C. J., Cross, N. A., et al. (2020). Characterization of an Aggregated Three-Dimensional Cell Culture Model by Multimodal Mass Spectrometry Imaging. *Anal. Chem.* 92, 12538–12547. doi:10.1021/acs.analchem.0c02389

Franck, J., Ayed, M. E., Wisztorski, M., Salzet, M., and Fournier, I. (2010). "On Tissue Protein Identification Improvement by N-Terminal Peptide Derivatization," in *Mass Spectrometry Imaging: Principles and Protocols*. Editors S. S. Rubakhin and J. V. Sweedler (Totowa, New Jersey: Humana Press), 323–338. doi:10.1007/978-1-60761-746-4_19

Fridjonsdottir, E., Shariatgorji, R., Nilsson, A., Vallianatou, T., Odell, L. R., Schembri, L. S., et al. (2021). Mass Spectrometry Imaging Identifies Abnormally Elevated Brain L-Dopa Levels and Extrastriatal Monoaminergic Dysregulation in L-Dopa-Induced Dyskinesia. *Sci. Adv.* 7, eabe5948. doi:10.1126/sciadv.abe5948

Fujioka, M., Koda, S., Morimoto, Y., and Biemann, K. (1988). Structure of FR900359, a Cyclic Depsipeptide from Ardisia Crenata Sims. *J. Org. Chem.* 53, 2820–2825. doi:10.1021/jo00247a030

Geier, B., Oetjen, J., Ruthensteiner, B., Polikarpov, M., Gruber-Vodicka, H. R., and Liebeke, M. (2021). Connecting Structure and Function from Organisms to Molecules in Small-Animal Symbioses through Chemo-Histo-Tomography. *Proc. Natl. Acad. Sci. United States America* 118, e2023773118. doi:10.1073/pnas.2023773118

Geier, B., Sogin, E. M., Michellod, D., Janda, M., Kompauer, M., Spengler, B., et al. (2020). Spatial Metabolomics of *In Situ* Host-Microbe Interactions at the Micrometre Scale. *Nat. Microbiol.* 5, 498–510. doi:10.1038/s41564-019-0664-6

Gillooly, J. F., Hein, A., and Damiani, R. (2015). Nuclear DNA Content Varies with Cell Size across Human Cell Types. *Cold Spring Harb Perspect. Biol.* 7, a019091. doi:10.1101/cshperspect.a019091

Gilmore, I. S., Heiles, S., and Pieterse, C. L. (2019). Metabolic Imaging at the Single-Cell Scale: Recent Advances in Mass Spectrometry Imaging. *Annu. Rev. Anal. Chem.* 12, 201–224. P.W. Bohn & J.E. Pemberton. doi:10.1146/annurev-anchem-061318-115516

Ginzberg, M. B., Kafri, R., and Kirschner, M. (2015). Cell Biology. On Being the Right (Cell) Size. *Science* 348, 1245075. doi:10.1126/science.1245075

Goaillard, J.-M., Taylor, A. L., Schulz, D. J., and Marder, E. (2009). Functional Consequences of Animal-To-Animal Variation in Circuit Parameters. *Nat. Neurosci.* 12, 1424–1430. doi:10.1038/nn.2404

Goodwin, R. J. A. (2012). Sample Preparation for Mass Spectrometry Imaging: Small Mistakes Can lead to Big Consequences. *J. Proteomics* 75, 4893–4911. doi:10.1016/j.jprot.2012.04.012

Grey, A. C., Chaurand, P., Caprioli, R. M., and Schey, K. L. (2009). MALDI Imaging Mass Spectrometry of Integral Membrane Proteins from Ocular Lens and Retinal Tissue. *J. Proteome Res.* 8, 3278–3283. doi:10.1021/pr800956y

Groseclose, M. R., Massion, P. P., Chaurand, P., and Caprioli, R. M. (2008). High-throughput Proteomic Analysis of Formalin-Fixed Paraffin-Embedded Tissue Microarrays Using MALDI Imaging Mass Spectrometry. *Proteomics* 8, 3715–3724. doi:10.1002/pmic.200800495

Guenther, S., Römpp, A., Kummer, W., and Spengler, B. (2011). AP-MALDI Imaging of Neuropeptides in Mouse Pituitary Gland with 5µm Spatial Resolution and High Mass Accuracy. *Int. J. Mass Spectrom.* 305, 228–237. doi:10.1016/j.ijms.2010.11.011

Guo, S., Tang, W., Hu, Y., Chen, Y., Gordon, A., Li, B., et al. (2020). Enhancement of On-Tissue Chemical Derivatization by Laser-Assisted Tissue Transfer for

MALDI MS Imaging. *Anal. Chem.* 92, 1431–1438. doi:10.1021/acs.analchem.9b04618

Gustafsson, O. J. R., Briggs, M. T., Condina, M. R., Winderbaum, L. J., Pelzing, M., Mccoll, S. R., et al. (2015). MALDI Imaging Mass Spectrometry of N-Linked Glycans on Formalin-Fixed Paraffin-Embedded Murine Kidney. *Anal. Bioanal. Chem.* 407, 2127–2139. doi:10.1007/s00216-014-8293-7

Hallett, J. P., and Welton, T. (2011). Room-temperature Ionic Liquids: Solvents for Synthesis and Catalysis. 2. *Chem. Rev.* 111, 3508–3576. doi:10.1021/cr1003248

Hameed, S., Ikegami, K., Sugiyama, E., Matsushita, S., Kimura, Y., Hayasaka, T., et al. (2015). Direct Profiling of the Phospholipid Composition of Adult caenorhabditis Elegans Using Whole-Body Imaging Mass Spectrometry. *Anal. Bioanal. Chem.* 407, 7589–7602. doi:10.1007/s00216-015-8932-7

Han, C., Li, S., Yue, Q., Li, N., Yang, H., and Zhao, Z. (2019). Polydopamine-capped Agnps as a Novel Matrix Overcoming the Ion Suppression of Phosphatidylcholine for MALDI MS Comprehensive Imaging of Glycerophospholipids and Sphingolipids in Impact-Induced Injured Brain. *Analyst* 144, 6304–6312. doi:10.1039/c9an01361j

Hankin, J. A., Barkley, R. M., and Murphy, R. C. (2007). Sublimation as a Method of Matrix Application for Mass Spectrometric Imaging. *J. Am. Soc. Mass. Spectrom.* 18, 1646–1652. doi:10.1016/j.jasms.2007.06.010

Harkin, C., Smith, K. W., Cruickshank, F. L., Logan Mackay, C., Flinders, B., Heeren, R. M. A., et al. (2021). On-tissue Chemical Derivatization in Mass Spectrometry Imaging. *Mass Spectrom. Rev.*Online ahead of print. doi:10.1002/mas.21680

Hillman, E. M. C., Voleti, V., Li, W., and Yu, H. (2019). Light-sheet Microscopy in Neuroscience. *Annu. Rev. Neurosci.* 42, 295–313. doi:10.1146/annurev-neuro-070918-050357

Hirschhaeuser, F., Menne, H., Dittfeld, C., West, J., Mueller-Klieser, W., and Kunz-Schughart, L. A. (2010). Multicellular Tumor Spheroids: An Underestimated Tool Is Catching up Again. *J. Biotechnol.* 148, 3–15. doi:10.1016/j.jbiotec.2010.01.012

Hoffmann, F., Umbreit, C., Krüger, T., Pelzel, D., Ernst, G., Kniemeyer, O., et al. (2019). Identification of Proteomic Markers in Head and Neck Cancer Using MALDI-MS Imaging, lc-MS/MS, and Immunohistochemistry. *Proteomics Clin. Appl.* 13, e1700173. doi:10.1002/prca.201700173

Holst, S., Heijs, B., De Haan, N., Van Zeijl, R. J. M., Briaire-De Bruijn, I. H., Van Pelt, G. W., et al. (2016). Linkage-specific *In Situ* Sialic Acid Derivatization for N-Glycan Mass Spectrometry Imaging of Formalin-Fixed Paraffin-Embedded Tissues. *Anal. Chem.* 88, 5904–5913. doi:10.1021/acs.analchem.6b00819

Horn, P. J., Korte, A. R., Neogi, P. B., Love, E., Fuchs, J., Strupat, K., et al. (2012). Spatial Mapping of Lipids at Cellular Resolution in Embryos of Cotton. *Plant Cell* 24, 622–636. doi:10.1105/tpc.111.094581

Hossen, M. A., Nagata, Y., Waki, M., Ide, Y., Takei, S., Fukano, H., et al. (2015). Decreased Level of Phosphatidylcholine (16:0/20:4) in Multiple Myeloma Cells Compared to Plasma Cells: A Single-Cell MALDI-Ims Approach. *Anal. Bioanal. Chem.* 407, 5273–5280. doi:10.1007/s00216-015-8741-z

Huang, J., Guo, X., Xu, T., Fan, L., Zhou, X., and Wu, S. (2019). Ionic Deep Eutectic Solvents for the Extraction and Separation of Natural Products. *J. Chromatogr. A* 1598, 1–19. doi:10.1016/j.chroma.2019.03.046

Huber, K., Khamehgir-Silz, P., Schramm, T., Gorshkov, V., Spengler, B., and Römpp, A. (2018). Approaching Cellular Resolution and Reliable Identification in Mass Spectrometry Imaging of Tryptic Peptides. *Anal. Bioanal. Chem.* 410, 5825–5837. doi:10.1007/s00216-018-1199-z

Ito, T., and Hiramoto, M. (2019). Use of Mtraq Derivatization Reagents on Tissues for Imaging Neurotransmitters by MALDI Imaging Mass Spectrometry: The Triple spray Method. *Anal. Bioanal. Chem.* 411, 6847–6856. doi:10.1007/s00216-019-02052-1

Itoh, T. (2017). Ionic Liquids as Tool to Improve Enzymatic Organic Synthesis. *Chem. Rev.* 117, 10567–10607. doi:10.1021/acs.chemrev.7b00158

Iwama, T., Kano, K., Saigusa, D., Ekroos, K., Van Echten-Deckert, G., Vogt, J., et al. (2021). Development of an On-Tissue Derivatization Method for MALDI Mass Spectrometry Imaging of Bioactive Lipids Containing Phosphate Monoester Using Phos-Tag. *Anal. Chem.* 93, 3867–3875. doi:10.1021/acs.analchem.0c04479

Jackson, S. N., Muller, L., Roux, A., Oktem, B., Moskovets, E., Doroshenko, V. M., et al. (2018). Ap-MALDI Mass Spectrometry Imaging of Gangliosides Using 2,6-dihydroxyacetophenone. *J. Am. Soc. Mass. Spectrom.* 29, 1463–1472. doi:10.1007/s13361-018-1928-8

Jiang, H., Goulbourne, C. N., Tatar, A., Turlo, K., Wu, D., Beigneux, A. P., et al. (2014). High-resolution Imaging of Dietary Lipids in Cells and Tissues by Nanosims Analysis. *J. Lipid Res.* 55, 2156–2166. doi:10.1194/jlr.m053363

Jiang, H., Passarelli, M. K., Munro, P. M. G., Kilburn, M. R., West, A., Dollery, C. T., et al. (2017). High-resolution Sub-cellular Imaging by Correlative Nanosims and Electron Microscopy of Amiodarone Internalisation by Lung Macrophages as Evidence for Drug-Induced Phospholipidosis. *Chem. Commun.* 53, 1506–1509. doi:10.1039/c6cc08549k

Johnson, J., Sharick, J. T., Skala, M. C., and Li, L. (2020). Sample Preparation Strategies for High-Throughput Mass Spectrometry Imaging of Primary Tumor Organoids. *J. Mass. Spectrom.* 55, e4452. doi:10.1002/jms.4452

Kadesch, P., Hollubarsch, T., Gerbig, S., Schneider, L., Silva, L. M. R., Hermosilla, C., et al. (2020). Intracellular Parasites Toxoplasma Gondii and Besnoitia Besnoiti, Unveiled in Single Host Cells Using AP-SMALDI MS Imaging. *J. Am. Soc. Mass. Spectrom.* 31, 1815–1824. doi:10.1021/jasms.0c00043

Källback, P., Shariatgorji, M., Nilsson, A., and Andrén, P. E. (2012). Novel Mass Spectrometry Imaging Software Assisting Labeled Normalization and Quantitation of Drugs and Neuropeptides Directly in Tissue Sections. *J. Proteomics* 75, 4941–4951. doi:10.1016/j.jprot.2012.07.034

Karas, M., Bachmann, D., Bahr, U., and Hillenkamp, F. (1987). Matrix-assisted Ultraviolet Laser Desorption of Non-volatile Compounds. *Int. J. Mass Spectrom. Ion Process.* 78, 53–68. doi:10.1016/0168-1176(87)87041-6

Karas, M., and Hillenkamp, F. (1988). Laser Desorption Ionization of Proteins with Molecular Masses Exceeding 10,000 Daltons. *Anal. Chem.* 60, 2299–2301. doi:10.1021/ac00171a028

Keller, C., Maeda, J., Jayaraman, D., Chakraborty, S., Sussman, M. R., Harris, J. M., et al. (2018). Comparison of Vacuum MALDI and Ap-MALDI Platforms for the Mass Spectrometry Imaging of Metabolites Involved in Salt Stress in Medicago Truncatula. *Front. Plant Sci.* 9, 1238. doi:10.3389/fpls.2018.01238

Ketterlinus, R., Hsieh, S. Y., Teng, S. H., Lee, H., and Pusch, W. (2005). Fishing for Biomarkers: Analyzing Mass Spectrometry Data with the New Clinprotools Software. *BioTechniques* 38, 37–40. doi:10.2144/05386su07

Khalil, S. M., Pretzel, J., Becker, K., and Spengler, B. (2017). High-resolution AP-SMALDI Mass Spectrometry Imaging of *Drosophila melanogaster*. *Int. J. Mass Spectrom.* 416, 1–19. doi:10.1016/j.ijms.2017.04.001

Khatib-Shahidi, S., Andersson, M., Herman, J. L., Gillespie, T. A., and Caprioli, R. M. (2006). Direct Molecular Analysis of Whole-Body Animal Tissue Sections by Imaging MALDI Mass Spectrometry. *Anal. Chem.* 78, 6448–6456. doi:10.1021/ac060788p

Kim, E., Kim, J., Choi, I., Lee, J., and Yeo, W.-S. (2020). Organic Matrix-free Imaging Mass Spectrometry. *BMB Rep.* 53, 349–356. doi:10.5483/bmbrep.2020.53.7.078

Kim, Y.-K., Na, H.-K., Kwack, S.-J., Ryoo, S.-R., Lee, Y., Hong, S., et al. (2011). Synergistic Effect of Graphene Oxide/mwcnt Films in Laser Desorption/ionization Mass Spectrometry of Small Molecules and Tissue Imaging. *Acs Nano* 5, 4550–4561. doi:10.1021/nn200245v

Kirpekar, F., Berkenkamp, S., and Hillenkamp, F. (1999). Detection of Double-Stranded DNA by Ir- and Uv-MALDI Mass Spectrometry. *Anal. Chem.* 71, 2334–2339. doi:10.1021/ac990018w

Kompauer, M., Heiles, S., and Spengler, B. (2017). Atmospheric Pressure MALDI Mass Spectrometry Imaging of Tissues and Cells at 1.4-μm Lateral Resolution. *Nat. Methods* 14, 90–96. doi:10.1038/nmeth.4071

Lagarrigue, M., Lavigne, R., Guével, B., Palmer, A., Rondel, K., Guillot, L., et al. (2020). Spatial Segmentation and Metabolite Annotation Involved in Sperm Maturation in the Rat Epididymis by MALDI Imaging Mass Spectrometry. *J. Mass. Spectrom.* 55, e4633. doi:10.1002/jms.4633

Lanni, E. J., Rubakhin, S. S., and Sweedler, J. V. (2012). Mass Spectrometry Imaging and Profiling of Single Cells. *J. Proteomics* 75, 5036–5051. doi:10.1016/j.jprot.2012.03.017

Lemaire, R., Desmons, A., Tabet, J. C., Day, R., Salzet, M., and Fournier, I. (2007). Direct Analysis and MALDI Imaging of Formalin-Fixed, Paraffin-Embedded Tissue Sections. *J. Proteome Res.* 6, 1295–1305. doi:10.1021/pr060549i

Lemaire, R., Wisztorski, M., Desmons, A., Tabet, J. C., Day, R., Salzet, M., et al. (2006). MALDI-MS Direct Tissue Analysis of Proteins: Improving Signal Sensitivity Using Organic Treatments. *Anal. Chem.* 78, 7145–7153. doi:10.1021/ac060565z

Li, H., and Hummon, A. B. (2011). Imaging Mass Spectrometry of Three-Dimensional Cell Culture Systems. *Anal. Chem.* 83, 8794–8801. doi:10.1021/ac202356g

Liang, X., Cao, S., Xie, P., Hu, X., Lin, Y., Liang, J., et al. (2021). Three-dimensional Imaging of Whole-Body Zebrafish Revealed Lipid Disorders Associated with Niemann-Pick Disease Type C1. *Anal. Chem.* 93, 8178–8187. doi:10.1021/acs.analchem.1c00196

Lin, R.-Z., and Chang, H.-Y. (2008). Recent Advances in Three-Dimensional Multicellular Spheroid Culture for Biomedical Research. *Biotechnol. J.* 3, 1172–1184. doi:10.1002/biot.200700228

Liu, H., Zhou, Y., Wang, J., Xiong, C., Xue, J., Zhan, L., et al. (2018a). N-phenyl-2-naphthylamine as a Novel MALDI Matrix for Analysis and *In Situ* Imaging of Small Molecules. *Anal. Chem.* 90, 729–736. doi:10.1021/acs.analchem.7b02710

Liu, X., Flinders, C., Mumenthaler, S. M., and Hummon, A. B. (2018b). MALDI Mass Spectrometry Imaging for Evaluation of Therapeutics in Colorectal Tumor Organoids. *J. Am. Soc. Mass. Spectrom.* 29, 516–526. doi:10.1007/s13361-017-1851-4

Liu, X., Lukowski, J. K., Flinders, C., Kim, S., Georgiadis, R. A., Mumenthaler, S. M., et al. (2018c). MALDI-MSI of Immunotherapy: Mapping the Egfr-Targeting Antibody Cetuximab in 3d colon-cancer Cell Cultures. *Anal. Chem.* 90, 14156–14164. doi:10.1021/acs.analchem.8b02151

Lovrić, J., Dunevall, J., Larsson, A., Ren, L., Andersson, S., Meibom, A., et al. (2017). Nano Secondary Ion Mass Spectrometry Imaging of Dopamine Distribution across Nanometer Vesicles. *Acs Nano* 11, 3446–3455. doi:10.1021/acsnano.6b07233

Luptakova, D., Vallianatou, T., Nilsson, A., Shariatgorji, R., Hammarlund-Udenaes, M., Loryan, I., et al. (2021). Neuropharmacokinetic Visualization of Regional and Subregional Unbound Antipsychotic Drug Transport across the Blood-Brain Barrier. *Mol. Psychiatry* Online ahead of print. doi:10.1038/s41380-021-01267-y

Ly, A., Longuespée, R., Casadonte, R., Wandernoth, P., Schwamborn, K., Bollwein, C., et al. (2019). Site-to-site Reproducibility and Spatial Resolution in MALDI-MSI of Peptides from Formalin-Fixed Paraffin-Embedded Samples. *Proteomics Clin. Appl.* 13, e1800029. doi:10.1002/prca.201800029

Ly, A., Buck, A., Balluff, B., Sun, N., Gorzolka, K., Feuchtinger, A., et al. (2016). High-mass-resolution MALDI Mass Spectrometry Imaging of Metabolites from Formalin-Fixed Paraffin-Embedded Tissue. *Nat. Protoc.* 11, 1428–1443. doi:10.1038/nprot.2016.081

Malaker, S. A., Quanico, J., Raffo-Romero, A., Kobeissy, F., Aboulouard, S., Tierny, D., et al. (2021). On-tissue Spatially Resolved Glycoproteomics Guided by N-Glycan Imaging Reveal Global Dysregulation of Canine Glioma Glycoproteomic Landscape. *Cel Chem. Biol.* Online ahead of print. doi:10.1016/j.chembiol.2021.05.007

Manier, M. L., Spraggins, J. M., Reyzer, M. L., Norris, J. L., and Caprioli, R. M. (2014). A Derivatization and Validation Strategy for Determining the Spatial Localization of Endogenous Amine Metabolites in Tissues Using MALDI Imaging Mass Spectrometry. *J. Mass. Spectrom.* 49, 665–673. doi:10.1002/jms.3411

Manikandan, M., and Wu, H.-F. (2016). Bio-mimicked Gold Nanoparticles with Complex Fetal Bovine Serum as Sensors for Single Cell MALDI MS of Cancer Cell and Cancer Stem Cell. *Sensors Actuators B: Chem.* 231, 154–165. doi:10.1016/j.snb.2016.02.060

Mclaughlin, N., Bielinski, T. M., Tressler, C. M., Barton, E., Glunde, K., and Stumpo, K. A. (2020). Pneumatically Sprayed Gold Nanoparticles for Mass Spectrometry Imaging of Neurotransmitters. *J. Am. Soc. Mass. Spectrom.* 31, 2452–2461. doi:10.1021/jasms.0c00156

Meng, Y., Cheng, X., Wang, T., Hang, W., Li, X., Nie, W., et al. (2020). Micro-Lensed Fiber Laser Desorption Mass Spectrometry Imaging Reveals Subcellular Distribution of Drugs within Single Cells. *Angew. Chem. Int. Ed.* 59, 17864–17871. doi:10.1002/anie.202002151

Mittal, P., Price, Z. K., Lokman, N. A., Ricciardelli, C., Oehler, M. K., Klingler-Hoffmann, M., et al. (2019). Matrix Assisted Laser Desorption/ionization Mass Spectrometry Imaging (MALDI MSI) for Monitoring of Drug Response in Primary Cancer Spheroids. *Proteomics* 19, e1900146. doi:10.1002/pmic.201900146

Möginger, U., Marcussen, N., and Jensen, O. N. (2020). Histo-molecular Differentiation of Renal Cancer Subtypes by Mass Spectrometry Imaging and Rapid Proteome Profiling of Formalin-Fixed Paraffin-Embedded Tumor Tissue Sections. *Oncotarget* 11, 3998–4015. doi:10.18632/oncotarget.27787

Mokosch, A. S., Gerbig, S., Grevelding, C. G., Haeberlein, S., and Spengler, B. (2021). High-resolution AP-SMALDI MSI as a Tool for Drug Imaging in Schistosoma Mansoni. *Anal. Bioanal. Chem.* 413, 2755–2766. doi:10.1007/s00216-021-03230-w

Mueller, M. A., Kompauer, M., Strupat, K., Heiles, S., and Spengler, B. (2021). Implementation of a High-Repetition-Rate Laser in an AP-SMALDI MSI System for Enhanced Measurement Performance. *J. Am. Soc. Mass Spectrom.* 32, 465–472.

Nachtigall, F. M., Pereira, A., Trofymchuk, O. S., and Santos, L. S. (2020). Detection of Sars-Cov-2 in Nasal Swabs Using MALDI-MS. *Nat. Biotechnol.* 38, 1168–1173. doi:10.1038/s41587-020-0644-7

Nakagawa, T., Lanaspa, M. A., San Millan, I., Fini, M., Rivard, C. J., Sanchez-Lozada, L. G., et al. (2020). Fructose Contributes to the Warburg Effect for Cancer Growth. *Cancer Metab.* 8, 16. doi:10.1186/s40170-020-00222-9

Newell, C. L., Vorng, J. L., Macrae, J. I., Gilmore, I. S., and Gould, A. P. (2020). Cryogenic OrbiSIMS Localizes Semi-Volatile Molecules in Biological Tissues. *Angew. Chem. Int. Ed.* 59, 18194–18200. doi:10.1002/anie.202006881

Niehaus, M., Soltwisch, J., Belov, M. E., and Dreisewerd, K. (2019). Transmission-mode MALDI-2 Mass Spectrometry Imaging of Cells and Tissues at Subcellular Resolution. *Nat. Methods* 16, 925–931. doi:10.1038/s41592-019-0536-2

Nishikaze, T., Okumura, H., Jinmei, H., and Amano, J. (2013). Advantages of Pyrene Derivatization to Site-specific Glycosylation Analysis on MALDI Mass Spectrometry. *Int. J. Mass Spectrom.* 333, 8–14. doi:10.1016/j.ijms.2012.08.006

Norris, J. L., and Caprioli, R. M. (2013a). Analysis of Tissue Specimens by Matrix-Assisted Laser Desorption/ionization Imaging Mass Spectrometry in Biological and Clinical Research. *Chem. Rev.* 113, 2309–2342. doi:10.1021/cr3004295

Norris, J. L., and Caprioli, R. M. (2013b). Imaging Mass Spectrometry: A New Tool for Pathology in a Molecular Age. *Prot. Clin. Appl.* 7, 733–738. doi:10.1002/prca.201300055

Oetjen, J., Veselkov, K., Watrous, J., Mckenzie, J. S., Becker, M., Hauberg-Lotte, L., et al. (2015). Benchmark Datasets for 3d MALDI- and DESI-Imaging Mass Spectrometry. *Gigascience* 4, 20. doi:10.1186/s13742-015-0059-4

Ogrinc Potočnik, N., Porta, T., Becker, M., Heeren, R. M., and Ellis, S. R. (2015). Use of Advantageous, Volatile Matrices Enabled by Next-Generation High-Speed Matrix-Assisted Laser Desorption/ionization Time-Of-Flight Imaging Employing a Scanning Laser Beam. *Rapid Commun. Mass. Spectrom.* 29, 2195–2203. doi:10.1002/rcm.7379

Paine, M. R. L., Poad, B. L. J., Eijkel, G. B., Marshall, D. L., Blanksby, S. J., Heeren, R. M. A., et al. (2018). Mass Spectrometry Imaging with Isomeric Resolution Enabled by Ozone-Induced Dissociation. *Angew. Chem. Int. Ed.* 57, 10530–10534. doi:10.1002/anie.201802937

Palanisamy, S., Huang, S., Zhao, H., Zhu, D., and Zhang, X. (2020). *In Situ* derivatization of au nanoclusters via aurophilic interactions of a triphenylphosphine gold(i) salt with neurotransmitters and their rapid MALDI-TOF-MS detection in mice brain tissue extracts. *J. Mater. Chem. B* 8, 38–44. doi:10.1039/c9tb01800j

Pareek, V., Tian, H., Winograd, N., and Benkovic, S. J. (2020). Metabolomics and Mass Spectrometry Imaging Reveal Channeled De Novo Purine Synthesis in Cells. *Science* 368, 283–290. doi:10.1126/science.aaz6465

Passarelli, M. K., Pirkl, A., Moellers, R., Grinfeld, D., Kollmer, F., Havelund, R., et al. (2017). The 3d Orbisims-label-free Metabolic Imaging with Subcellular Lateral Resolution and High Mass-Resolving Power. *Nat. Methods* 14, 1175–1183. doi:10.1038/nmeth.4504

Perry, W. J., Patterson, N. H., Prentice, B. M., Neumann, E. K., Caprioli, R. M., and Spraggins, J. M. (2020). Uncovering Matrix Effects on Lipid Analyses in MALDI Imaging Mass Spectrometry Experiments. *J. Mass. Spectrom.* 55, e4491. doi:10.1002/jms.4491

Perry, W. J., Spraggins, J. M., Sheldon, J. R., Grunenwald, C. M., Heinrichs, D. E., Cassat, J. E., et al. (2019). Staphylococcus Aureusexhibits Heterogeneous Siderophore Production within the Vertebrate Host. *Proc. Natl. Acad. Sci. USA* 116, 21980–21982. doi:10.1073/pnas.1913991116

Port, A. M., Ruth, M. R., and Istfan, N. W. (2012). Fructose Consumption and Cancer. *Curr. Opin. Endocrinol. Diabetes Obes.* 19, 367–374. doi:10.1097/med.0b013e328357f0cb

Porta, T., Lesur, A., Varesio, E., and Hopfgartner, G. (2015). Quantification in MALDI-MS Imaging: What Can We Learn from MALDI-Selected Reaction Monitoring and what Can We Expect for Imaging? *Anal. Bioanal. Chem.* 407, 2177–2187. doi:10.1007/s00216-014-8315-5

Rappez, L., Stadler, M., Triana, S., Gathungu, R. M., Ovchinnikova, K., Phapale, P., et al. (2021). Spacem Reveals Metabolic States of Single Cells. *Nat. Methods* 18, 799–805. doi:10.1038/s41592-021-01198-0

Righetti, L., Bhandari, D. R., Rolli, E., Tortorella, S., Bruni, R., Dall'Asta, C., et al. (2021). Unveiling the Spatial Distribution of Aflatoxin B1 and Plant Defense Metabolites in maize Using AP-SMALDI Mass Spectrometry Imaging. *Plant J.* 106, 185–199. doi:10.1111/tpj.15158

Rocha, B., Ruiz-Romero, C., and Blanco, F. J. (2017). Mass Spectrometry Imaging: A Novel Technology in Rheumatology. *Nat. Rev. Rheumatol.* 13, 52–63. doi:10.1038/nrrheum.2016.184

Roempp, A., and Spengler, B. (2013). Mass Spectrometry Imaging with High Resolution in Mass and Space. *Histochem. Cel Biol.* 139, 759–783.

Rohner, T. C., Staab, D., and Stoeckli, M. (2005). MALDI Mass Spectrometric Imaging of Biological Tissue Sections. *Mech. Ageing Develop.* 126, 177–185. doi:10.1016/j.mad.2004.09.032

Rubakhin, S. S., Romanova, E. V., Nemes, P., and Sweedler, J. V. (2011). Profiling Metabolites and Peptides in Single Cells. *Nat. Methods* 8, S20–S29. doi:10.1038/nmeth.1549

Rudd, D., Ronci, M., Johnston, M. R., Guinan, T., Voelcker, N. H., and Benkendorff, K. (2015). Mass Spectrometry Imaging Reveals New Biological Roles for Choline Esters and Tyrian Purple Precursors in Muricid Molluscs. *Sci. Rep.* 5, 13408. doi:10.1038/srep13408

Russo, C., Brickelbank, N., Duckett, C., Mellor, S., Rumbelow, S., and Clench, M. R. (2018). Quantitative Investigation of Terbinafine Hydrochloride Absorption into a Living Skin Equivalent Model by MALDI-MSI. *Anal. Chem.* 90, 10031–10038. doi:10.1021/acs.analchem.8b02648

Saigusa, D., Saito, R., Kawamoto, K., Uruno, A., Kano, K., Aoki, J., et al. (2019). Conductive Adhesive Film Expands the Utility of Matrix-Assisted Laser Desorption/ionization Mass Spectrometry Imaging. *Anal. Chem.* 91, 8979–8986. doi:10.1021/acs.analchem.9b01159

Saito, T., Watanabe, A., Nakano, M., and Matsuo, K. (2021). MALDI-TOF Mass Spectrometry Imaging for N-Glycans on Ffpe Tissue Sections of Mouse Nash Liver through Sialic Acid Benzylamidation. *Glycoconj J.* 38, 167–175. doi:10.1007/s10719-021-09984-w

Sämfors, S., and Fletcher, J. S. (2020). Lipid Diversity in Cells and Tissue Using Imaging SIMS. *Annu. Rev. Anal. Chem.* 13, 249–271. P.W. Bohn & J.E. Pemberton. doi:10.1146/annurev-anchem-091619-103512

Sans, M., Feider, C. L., and Eberlin, L. S. (2018). Advances in Mass Spectrometry Imaging Coupled to Ion Mobility Spectrometry for Enhanced Imaging of Biological Tissues. *Curr. Opin. Chem. Biol.* 42, 138–146. doi:10.1016/j.cbpa.2017.12.005

Schnackenberg, L. K., Thorn, D. A., Barnette, D., and Jones, E. E. (2021). MALDI Imaging Mass Spectrometry: An Emerging Tool in Neurology. *Metab. Brain Dis.* Online ahead of print. doi:10.1007/s11011-021-00797-2

Schober, Y., Guenther, S., Spengler, B., and Römpp, A. (2012). Single Cell Matrix-Assisted Laser Desorption/ionization Mass Spectrometry Imaging. *Anal. Chem.* 84, 6293–6297. doi:10.1021/ac301337h

Schulz, S., Becker, M., Groseclose, M. R., Schadt, S., and Hopf, C. (2019). Advanced MALDI Mass Spectrometry Imaging in Pharmaceutical Research and Drug Development. *Curr. Opin. Biotechnol.* 55, 51–59. doi:10.1016/j.copbio.2018.08.003

Schwamborn, K., and Caprioli, R. M. (2010). MALDI Imaging Mass Spectrometry - Painting Molecular Pictures. *Mol. Oncol.* 4, 529–538. doi:10.1016/j.molonc.2010.09.002

Schwartz, S. A., Reyzer, M. L., and Caprioli, R. M. (2003). Direct Tissue Analysis Using Matrix-Assisted Laser Desorption/ionization Mass Spectrometry: Practical Aspects of Sample Preparation. *J. Mass. Spectrom.* 38, 699–708. doi:10.1002/jms.505

Ščupáková, K., Balluff, B., Tressler, C., Adelaja, T., Heeren, R. M. A., Glunde, K., et al. (2020). Cellular Resolution in Clinical MALDI Mass Spectrometry Imaging: The Latest Advancements and Current Challenges. *Clin. Chem. Lab. Med.* 58, 914–929. doi:10.1515/cclm-2019-0858

Shariatgorji, M., Källback, P., Gustavsson, L., Schintu, N., Svenningsson, P., Goodwin, R. J. A., et al. (2012). Controlled-ph Tissue Cleanup Protocol for Signal Enhancement of Small Molecule Drugs Analyzed by MALDI-MS Imaging. *Anal. Chem.* 84, 4603–4607. doi:10.1021/ac203322q

Shariatgorji, M., Nilsson, A., Fridjonsdottir, E., Vallianatou, T., Källback, P., Katan, L., et al. (2019). Comprehensive Mapping of Neurotransmitter Networks by MALDI-MS Imaging. *Nat. Methods* 16, 1021–1028. doi:10.1038/s41592-019-0551-3

Shariatgorji, R., Nilsson, A., Strittmatter, N., Vallianatou, T., Zhang, X., Svenningsson, P., et al. (2020). Bromopyrylium Derivatization Facilitates Identification by Mass Spectrometry Imaging of Monoamine Neurotransmitters and Small Molecule Neuroactive Compounds. *J. Am. Soc. Mass. Spectrom.* 31, 2553–2557. doi:10.1021/jasms.0c00166

Smith, A., Galli, M., Piga, I., Denti, V., Stella, M., Chinello, C., et al. (2019). Molecular Signatures of Medullary Thyroid Carcinoma by Matrix-Assisted Laser Desorption/ionisation Mass Spectrometry Imaging. *J. Proteomics* 191, 114–123. doi:10.1016/j.jprot.2018.03.021

Smith, A., Iablokov, V., Mazza, M., Guarnerio, S., Denti, V., Ivanova, M., et al. (2020). Detecting Proteomic Indicators to Distinguish Diabetic Nephropathy from Hypertensive Nephrosclerosis by Integrating Matrix-Assisted Laser Desorption/ionization Mass Spectrometry Imaging with High-Mass Accuracy Mass Spectrometry. *Kidney Blood Press. Res.* 45, 233–248. doi:10.1159/000505187

Soltwisch, J., Heijs, B., Koch, A., Vens-Cappell, S., Höhndorf, J., and Dreisewerd, K. (2020). MALDI-2 on a Trapped Ion Mobility Quadrupole Time-Of-Flight Instrument for Rapid Mass Spectrometry Imaging and Ion Mobility Separation of Complex Lipid Profiles. *Anal. Chem.* 92, 8697–8703. doi:10.1021/acs.analchem.0c01747

Soltwisch, J., Kettling, H., Vens-Cappell, S., Wiegelmann, M., Müthing, J., and Dreisewerd, K. (2015). Mass Spectrometry Imaging with Laser-Induced Postionization. *Science* 348, 211–215. doi:10.1126/science.aaa1051

Song, Z., Gao, H., Xie, W., Sun, Q., Liang, K., and Li, Y. (2021). Quantitative MALDI-MS Assay of Steroid Hormones in Plasma Based on Hydroxylamine Derivatization. *Anal. Biochem.* 616, 114089. doi:10.1016/j.ab.2020.114089

Sparvero, L. J., Tian, H., Amoscato, A. A., Sun, W. Y., Anthonymuthu, T. S., Tyurina, Y. Y., et al. (2021). Direct Mapping of Phospholipid Ferroptotic Death Signals in Cells and Tissues by Gas Cluster Ion Beam Secondary Ion Mass Spectrometry (GCIB-SIMS). *Angew. Chem. Int. Ed.* 60, 11784–11788. doi:10.1002/anie.202102001

Spengler, B., and Hubert, M. (2002). Scanning Microprobe Matrix-Assisted Laser Desorption Ionization (SMALDI) Mass Spectrometry: Instrumentation for Sub-micrometer Resolved Ldi and MALDI Surface Analysis. *J. Am. Soc. Mass. Spectrom.* 13, 735–748. doi:10.1016/s1044-0305(02)00376-8

Spraggins, J. M., Djambazova, K. V., Rivera, E. S., Migas, L. G., Neumann, E. K., Fuetterer, A., et al. (2019). High-performance Molecular Imaging with MALDI Trapped Ion-Mobility Time-Of-Flight (Timstof) Mass Spectrometry. *Anal. Chem.* 91, 14552–14560. doi:10.1021/acs.analchem.9b03612

Stauber, J., Lemaire, R., Franck, J., Bonnel, D., Croix, D., Day, R., et al. (2008). MALDI Imaging of Formalin-Fixed Paraffin-Embedded Tissues: Application to Model Animals of Parkinson Disease for Biomarker Hunting. *J. Proteome Res.* 7, 969–978. doi:10.1021/pr070464x

Steinhauser, M. L., Bailey, A. P., Senyo, S. E., Guillermier, C., Perlstein, T. S., Gould, A. P., et al. (2012). Multi-isotope Imaging Mass Spectrometry Quantifies Stem Cell Division and Metabolism. *Nature* 481, 516–519. doi:10.1038/nature10734

Stern, A. D., Rahman, A. H., and Birtwistle, M. R. (2017). Cell Size Assays for Mass Cytometry. *Cytometry* 91, 14–24. doi:10.1002/cyto.a.23000

Stoeckli, M., Staab, D., Staufenbiel, M., Wiederhold, K.-H., and Signor, L. (2002). Molecular Imaging of Amyloid β Peptides in Mouse Brain Sections Using Mass Spectrometry. *Anal. Biochem.* 311, 33–39. doi:10.1016/s0003-2697(02)00386-x

Sturtevant, D., Aziz, M., Romsdahl, T. B., Corley, C. D., and Chapman, K. D. (2021). *In Situ* Localization of Plant Lipid Metabolites by Matrix-Assisted Laser Desorption/Ionization Mass Imaging (MALDI-MSI). *Methods Mol. Biol. (Clifton, N.J.)* 2295, 417–438. doi:10.1007/978-1-0716-1362-7_24

Sun, C., Li, Z., Ma, C., Zang, Q., Li, J., Liu, W., et al. (2019). Acetone Immersion Enhanced MALDI-MS Imaging of Small Molecule Metabolites in Biological Tissues. *J. Pharm. Biomed. Anal.* 176, 112797. doi:10.1016/j.jpba.2019.112797

Susniak, K., Krysa, M., Gieroba, B., Komaniecka, I., and Sroka-Bartnicka, A. (2020). Recent Developments of MALDI MSI Application in Plant Tissues Analysis. *Acta Biochim. Pol.* 67, 277–281. doi:10.18388/abp.2020_5394

Svatos, A. (2010). Mass Spectrometric Imaging of Small Molecules. *Trends Biotechnol.* 28, 425–434. doi:10.1016/j.tibtech.2010.05.005

Takeo, E., Sugiura, Y., Uemura, T., Nishimoto, K., Yasuda, M., Sugiyama, E., et al. (2019). Tandem Mass Spectrometry Imaging Reveals Distinct Accumulation Patterns of Steroid Structural Isomers in Human Adrenal Glands. *Anal. Chem.* 91, 8918–8925. doi:10.1021/acs.analchem.9b00619

Tanaka, K., Ido, Y., Akita, S., Yoshida, Y., and Yoshida, T. (1987). Detection of High Mass Molecules by Laser Desorption Time-Of-Flight Mass Spectrometry. *Proc. Second Japan-China Jt. Symp. Mass Spectrom.*, 185–187.

Tanaka, K., Waki, H., Ido, Y., Akita, S., Yoshida, Y., and Yoshida, T. (1988). Protein and Polymer Analyses up to m/z 100 000 by Laser Ionization Time-of-Flight Mass Spectrometry. *Rapid Communications in Mass Spectrometry* 2, 151–153. doi:10.1002/rcm.1290020802

Tholey, A., and Heinzle, E. (2006). Ionic (Liquid) Matrices for Matrix-Assisted Laser Desorption/ionization Mass Spectrometry-Applications and Perspectives. *Anal. Bioanal. Chem.* 386, 24–37. doi:10.1007/s00216-006-0600-5

Tobias, F., and Hummon, A. B. (2020). Considerations for MALDI-Based Quantitative Mass Spectrometry Imaging Studies. *J. Proteome Res.* 19, 3620–3630. doi:10.1021/acs.jproteome.0c00443

Toghi Eshghi, S., Yang, S., Wang, X., Shah, P., Li, X., and Zhang, H. (2014). Imaging of N-Linked Glycans from Formalin-Fixed Paraffin-Embedded Tissue Sections Using MALDI Mass Spectrometry. *ACS Chem. Biol.* 9, 2149–2156. doi:10.1021/cb500405h

Toue, S., Sugiura, Y., Kubo, A., Ohmura, M., Karakawa, S., Mizukoshi, T., et al. (2014). Microscopic Imaging Mass Spectrometry Assisted by On-Tissue Chemical Derivatization for Visualizing Multiple Amino Acids in Human colon Cancer Xenografts. *Proteomics* 14, 810–819. doi:10.1002/pmic.201300041

Trim, P. J., Henson, C. M., Avery, J. L., Mcewen, A., Snel, M. F., Claude, E., et al. (2008). Matrix-assisted Laser Desorption/ionization-Ion Mobility Separation-Mass Spectrometry Imaging of Vinblastine in Whole Body Tissue Sections. *Anal. Chem.* 80, 8628–8634. doi:10.1021/ac8015467

Trim, P. J., and Snel, M. F. (2016). Small Molecule MALDI MS Imaging: Current Technologies and Future Challenges. *Methods* 104, 127–141. doi:10.1016/j.ymeth.2016.01.011

Ueda, H. R., Ertürk, A., Chung, K., Gradinaru, V., Chédotal, A., Tomancak, P., et al. (2020). Tissue Clearing and its Applications in Neuroscience. *Nat. Rev. Neurosci.* 21, 61–79. doi:10.1038/s41583-019-0250-1

Unsihuay, D., Mesa Sanchez, D., and Laskin, J. (2021a). Quantitative Mass Spectrometry Imaging of Biological Systems. *Annu. Rev. Phys. Chem.* 72, 307–329. M.A. Johnson & T.J. Martinez. doi:10.1146/annurev-physchem-061020-053416

Unsihuay, D., Su, P., Hu, H., Qiu, J., Kuang, S., Li, Y., et al. (2021b). Imaging and Analysis of Isomeric Unsaturated Lipids through Online Photochemical Derivatization of Carbon-Carbon Double Bonds**. *Angew. Chem. Int. Ed.* 60, 7559–7563. doi:10.1002/anie.202016734

Vallianatou, T., Shariatgorji, M., Nilsson, A., Fridjonsdottir, E., Källback, P., Schintu, N., et al. (2019). Molecular Imaging Identifies Age-Related Attenuation of Acetylcholine in Retrosplenial Cortex in Response to Acetylcholinesterase Inhibition. *Neuropsychopharmacol.* 44, 2091–2098. doi:10.1038/s41386-019-0397-5

Van Nuffel, S., Ang, K. C., Lin, A. Y., and Cheng, K. C. (2021). Chemical Imaging of Retinal Pigment Epithelium in Frozen Sections of Zebrafish Larvae Using Tof-SIMS. *J. Am. Soc. Mass. Spectrom.* 32, 255–261. doi:10.1021/jasms.0c00300

Vegvari, A., Fehniger, T. E., Dahlback, M., Marko-Varga, G., and Strupat, K. (2017). *In Vivo* distribution of Tiotropium in a Rodent Model Utilizing AP-SMALDI Mass Spectrometry Imaging. *Cac* 13, 182–186. doi:10.2174/1573411012666160211235640

Ventura, S. P. M., E Silva, F. A., Quental, M. V., Mondal, D., Freire, M. G., and Coutinho, J. A. P. (2017). Ionic-liquid-mediated Extraction and Separation Processes for Bioactive Compounds: Past, Present, and Future Trends. *Chem. Rev.* 117, 6984–7052. doi:10.1021/acs.chemrev.6b00550

Vos, D. R. N., Ellis, S. R., Balluff, B., and Heeren, R. M. A. (2021). Experimental and Data Analysis Considerations for Three-Dimensional Mass Spectrometry Imaging in Biomedical Research. *Mol. Imaging Biol.* 23, 149–159. doi:10.1007/s11307-020-01541-5

Vreja, I. C., Kabatas, S., Saka, S. K., Kröhnert, K., Höschen, C., Opazo, F., et al. (2015). Secondary-ion Mass Spectrometry of Genetically Encoded Targets. *Angew. Chem. Int. Ed.* 54, 5784–5788. doi:10.1002/anie.201411692

Wäldchen, F., Spengler, B., and Heiles, S. (2019). Reactive Matrix-Assisted Laser Desorption/Ionization Mass Spectrometry Imaging Using an Intrinsically Photoreactive Paternò-Büchi Matrix for Double-Bond Localization in Isomeric Phospholipids. *J. Am. Chem. Soc.* 141, 11816–11820. doi:10.1021/jacs.9b05868

Wang, J., Wang, C., and Han, X. (2018). Enhanced Coverage of Lipid Analysis and Imaging by Matrix-Assisted Laser Desorption/ionization Mass Spectrometry via a Strategy with an Optimized Mixture of Matrices. *Analytica Chim. Acta* 1000, 155–162. doi:10.1016/j.aca.2017.09.046

Wang, S.-S., Wang, Y.-J., Zhang, J., Sun, T.-Q., and Guo, Y.-L. (2019). Derivatization Strategy for Simultaneous Molecular Imaging of Phospholipids and Low-Abundance Free Fatty Acids in Thyroid Cancer Tissue Sections. *Anal. Chem.* 91, 4070–4076. doi:10.1021/acs.analchem.8b05680

Wang, W., Douglas, D., Zhang, J., Kumari, S., Enuameh, M. S., Dai, Y., et al. (2020). Live-cell Imaging and Analysis Reveal Cell Phenotypic Transition Dynamics Inherently Missing in Snapshot Data. *Sci. Adv.* 6, eaba9319. doi:10.1126/sciadv.aba9319

Wang, Y., Tong, Q., Ma, S.-R., Zhao, Z.-X., Pan, L.-B., Cong, L., et al. (2021). Oral Berberine Improves Brain Dopa/dopamine Levels to Ameliorate Parkinson's Disease by Regulating Gut Microbiota. *Signal. Transduction Targeted Ther.* 6, 77. doi:10.1038/s41392-020-00456-5

Weaver, E. M., and Hummon, A. B. (2013). Imaging Mass Spectrometry: From Tissue Sections to Cell Cultures. *Adv. Drug Deliv. Rev.* 65, 1039–1055. doi:10.1016/j.addr.2013.03.006

Wheatcraft, D. R. A., Liu, X., and Hummon, A. B. (2014). Sample Preparation Strategies for Mass Spectrometry Imaging of 3d Cell Culture Models. *Jove-Journal Of Visualized Experiments,* 94, 52313. doi:10.3791/52313

Wiseman, J. M., Ifa, D. R., Zhu, Y., Kissinger, C. B., Manicke, N. E., Kissinger, P. T., et al. (2009). Mass Spectrometry across the Sciences Special Feature: Desorption Electrospray Ionization Mass Spectrometry: Imaging Drugs and Metabolites in Tissues (Vol 105, Pg 18120, 2008). *Proc. Natl. Acad. Sci. United States America* 106, 6022.

Wu, Q., Comi, T. J., Li, B., Rubakhin, S. S., and Sweedler, J. V. (2016). On-Tissue Derivatization via Electrospray Deposition for Matrix-Assisted Laser Desorption/Ionization Mass Spectrometry Imaging of Endogenous Fatty Acids in Rat Brain Tissues. *Anal. Chem.* 88, 5988–5995. doi:10.1021/acs.analchem.6b01021

Yang, J., and Caprioli, R. M. (2011). Matrix Sublimation/recrystallization for Imaging Proteins by Mass Spectrometry at High Spatial Resolution. *Anal. Chem.* 83, 5728–5734. doi:10.1021/ac200998a

Yang, J. Y., Phelan, V. V., Simkovsky, R., Watrous, J. D., Trial, R. M., Fleming, T. C., et al. (2012). Primer on agar-based Microbial Imaging Mass Spectrometry. *J. Bacteriol.* 194, 6023–6028. doi:10.1128/jb.00823-12

Yang, P. Y., Liu, Y. C., Zhao, H. Y., and Li, S. Y. (2020). Recent Progress in Mass Spectrometry Based Molecular Imaging. *Scientia Sinica(Vitae)* 50, 1237–1255.

Young, R. S. E., Claes, B. S. R., Bowman, A. P., Williams, E. D., Shepherd, B., Perren, A., et al. (2021). Isomer-resolved Imaging of Prostate Cancer Tissues Reveals Specific Lipid Unsaturation Profiles Associated with Lymphocytes and Abnormal Prostate Epithelia. *Front. Endocrinol. (Lausanne)* 12, 689600. doi:10.3389/fendo.2021.689600

Zenobi, R. (2013). Single-cell Metabolomics: Analytical and Biological Perspectives. *Science* 342, 1243259. doi:10.1126/science.1243259

Zhan, L., Huang, X., Xue, J., Liu, H., Xiong, C., Wang, J., et al. (2021). MALDI-TOF/TOF Tandem Mass Spectrometry Imaging Reveals Non-uniform Distribution of Disaccharide Isomers in Plant Tissues. *Food Chem.* 338, 127984. doi:10.1016/j.foodchem.2020.127984

Zhang, H., Shi, X., Vu, N. Q., Li, G., Li, Z., Shi, Y., et al. (2020). On-tissue Derivatization with girard's Reagent P Enhances N-Glycan Signals for Formalin-Fixed Paraffin-Embedded Tissue Sections in MALDI Mass Spectrometry Imaging. *Anal. Chem.* 92, 13361–13368. doi:10.1021/acs.analchem.0c02704

Conflict of Interest: The authors declare that the research was conducted in the absence of any commercial or financial relationships that could be construed as a potential conflict of interest.

Publisher's Note: All claims expressed in this article are solely those of the authors and do not necessarily represent those of their affiliated organizations, or those of the publisher, the editors, and the reviewers. Any product that may be evaluated in this article, or claim that may be made by its manufacturer, is not guaranteed or endorsed by the publisher.

frontiers in Chemistry

ORIGINAL RESEARCH
published: 03 March 2022
doi: 10.3389/fchem.2021.780626

Lipid Analysis of Fracture Hematoma With MALDI-MSI: Specific Lipids are Associated to Bone Fracture Healing Over Time

Rald V. M. Groven[1,2†], Sylvia P. Nauta[3,4†], Jane Gruisen[1,3], Britt S. R. Claes[3], Johannes Greven[5], Martijn van Griensven[2], Martijn Poeze[1,6], Ron M. A. Heeren[3], Tiffany Porta Siegel[3], Berta Cillero-Pastor[3] and Taco J. Blokhuis[1,6]*

[1]Division of Traumasurgery, Department of Surgery, Maastricht University Medical Center, Maastricht, Netherlands, [2]Department of Cell Biology-Inspired Tissue Engineering, MERLN Institute for Technology-Inspired Regenerative Medicine, Maastricht University, Maastricht, Netherlands, [3]Division of Imaging Mass Spectrometry, Maastricht MultiModal Molecular Imaging (M4i) Institute, Maastricht University, Maastricht, Netherlands, [4]Department of Orthopedic Surgery and Traumasurgery, Maastricht University Medical Center, Maastricht, Netherlands, [5]Department of Orthopaedics, Trauma and Reconstructive Surgery, University Hospital RWTH Aachen, Aachen, Germany, [6]NUTRIM, School for Nutrition and Translational Research in Metabolism, Maastricht University, Maastricht, Netherlands

Background: Fracture healing is a complex process, involving cell-cell interactions, various cytokines, and growth factors. Although fracture treatment improved over the last decades, a substantial part of all fractures shows delayed or absent healing. The fracture hematoma (fxh) is known to have a relevant role in this process, while the exact mechanisms by which it influences fracture healing are poorly understood. To improve strategies in fracture treatment, regulatory pathways in fracture healing need to be investigated. Lipids are important molecules in cellular signaling, inflammation, and metabolism, as well as key structural components of the cell. Analysis of the lipid spectrum in fxh may therefore reflect important events during the early healing phase. This study aims to develop a protocol for the determination of lipid signals over time, and the identification of lipids that contribute to these signals, with matrix-assisted laser desorption/ionization mass spectrometry imaging (MALDI-MSI) in fxh in healthy fracture healing.

Methods: Twelve fxh samples (6 porcine; 6 human) were surgically removed, snap frozen, sectioned, washed, and analyzed using MALDI-MSI in positive and negative ion mode at different time points after fracture (porcine: 72 h; human samples: range 1–19 days). A tissue preparation protocol for lipid analysis in fxh has been developed with both porcine and human fxh. Data were analyzed through principal component- and linear discriminant analyses.

Results: A protocol for the preparation of fxh sections was developed and optimized. Although hematoma is a heterogeneous tissue, the intra-variability within fxh was smaller than the inter-variability between fxh. Distinctive *m/z* values were detected that contributed to the separation of three different fxh age groups: early (1–3 days), middle (6–10 days), and late (12–19 days). Identification of the distinctive *m/z* values provided a panel of specific lipids that showed a time dependent expression within fxh.

OPEN ACCESS

Edited by:
Kezhi Jiang,
Hangzhou Normal University, China

Reviewed by:
Fei Fang,
Michigan State University, United States
Ling Lin,
Xiamen University Affiliated Cardiovascular Hospital, China
Xu Xu,
Shanghai Institute of Technology, China

***Correspondence:**
Berta Cillero-Pastor
b.cilleropastor@maastrichtuniversity.nl

†These authors have contributed equally to this work and share first authorship

Specialty section:
This article was submitted to Analytical Chemistry, a section of the journal Frontiers in Chemistry

Received: 21 September 2021
Accepted: 27 December 2021
Published: 03 March 2022

Citation:
Groven RVM, Nauta SP, Gruisen J, Claes BSR, Greven J, van Griensven M, Poeze M, Heeren RMA, Porta Siegel T, Cillero-Pastor B and Blokhuis TJ (2022) Lipid Analysis of Fracture Hematoma With MALDI-MSI: Specific Lipids are Associated to Bone Fracture Healing Over Time. Front. Chem. 9:780626. doi: 10.3389/fchem.2021.780626

Conclusion: This study shows that MALDI-MSI is a suitable analytical tool for lipid analysis in fxh and that lipid patterns within fxh are time-dependent. These lipid patterns within fxh may serve as a future diagnostic tool. These findings warrant further research into fxh analysis using MALDI-MSI and its possible clinical implications in fracture treatment.

Keywords: fracture hematoma, fracture healing, MALDI-MSI, sample preparation, lipids

INTRODUCTION

Fracture healing is a complex process in which a great variety of cells, signaling molecules, and cellular signaling pathways are involved (Claes et al., 2012). Although fracture treatment has advanced greatly over the past decades, a substantial portion of fractures still suffers from impaired healing in the form of delayed healing or non-union (Claes et al., 2012; Bastian et al., 2016a). Treatment of these complications often consists of multiple surgical interventions and, even if the interventions are successful, a long trajectory of rehabilitation (Volpin and Shtarker, 2014). Therefore, insights in fracture healing processes at an early stage may help to prevent or treat these complications (Dimitriou et al., 2005; Kolar et al., 2010; Wang et al., 2017).

The fracture healing process can be divided into three main phases: inflammation, bone repair, and bone remodeling (Bastian et al., 2016a). The first phase starts immediately after the fracture occurs, with the formation of the fracture hematoma (fxh). The fxh is considered to play a pivotal role in proper fracture healing, since it initiates the inflammatory response and creates a microenvironment to which a variety of cells is attracted by means of chemotaxis. Studies have shown that the removal or debridement of the fxh as well as an overshoot in the inflammatory response can induce adverse effects on fracture healing (Park et al., 2002; Claes et al., 2012; Bastian et al., 2016a; Loi et al., 2016; Schell et al., 2017). Cytokines and growth factors within the fxh facilitate the influx of inflammatory- and mesenchymal stem cells and regulate capillary growth, which is necessary to replace extracellular matrix with granulation tissue (Kolar et al., 2010; Claes et al., 2012; Schell et al., 2017). Therefore, the molecular environment in fxh changes based on this cellular trafficking (Kolar et al., 2010; Bastian et al., 2016b; Ghiasi et al., 2017).

During the following phases of fracture healing, the fxh acts as a basis for the formation of granulation tissue, also known as callus, which will gradually ossify as time progresses to bridge the fracture gap. Being an important initiator of the fracture healing cascade, investigating the molecular environment of the fxh at different time points after trauma could provide more insight into early fracture healing processes. Mass spectrometry offers potential advantages in understanding these dynamic molecular patterns and their regulatory effects on fracture healing as well as their possible complications.

Matrix-assisted laser desorption/ionization mass spectrometry imaging (MALDI-MSI) is a suitable imaging modality that allows for the untargeted, spatially resolved detection of a variety of molecules in tissue sections. The applicability of this technique to many research fields derives from its intrinsic property to detect a broad range of molecular classes, such as lipids or proteins, in a single experiment, without prior knowledge or hypothesis on the composition of a sample (Chughtai and Heeren, 2010).

A schematic overview of the MALDI-MSI workflow is depicted in **Figure 1**. A tissue section is covered with a matrix, which co-crystallizes with the analyte molecules. The matrix-analyte mixture absorbs the energy of the focused laser beam hitting the sample surface. This results in the local desorption and ionization of the analytes into the gas phase. The analysis of these ions with a mass spectrometer provides a mass spectrum, which depicts their mass-to-charge ratio (m/z). The analysis of mass spectra of multiple laser spots (or pixels) allows for the determination of the spatial distribution of certain molecules in the sample (Glish and Vachet, 2003; Murphy et al., 2009; Chughtai and Heeren, 2010; Watrous et al., 2011; Norris and Caprioli, 2013; Aichler and Walch, 2015). Histological staining of the same section after MSI enables the correlation of the detected molecules to a certain anatomical region within the sample.

To our knowledge, MALDI-MSI has not yet been reported for the analysis of fracture healing processes. Using MALDI-MSI to analyze fxh at different time points during the fracture healing process could help to understand changes in molecular patterns throughout different phases of fracture healing. Lipids are suitable target molecules for the examination of potential use and application of MALDI-MSI for fxh analysis since they are key molecules in cellular signaling, inflammation, and metabolism, as well as important structural components of the cell (Schwamborn and Caprioli, 2010; Li et al., 2014; Øyen et al., 2017; Chiurchiù et al., 2018; Matsumoto et al., 2019; Alekos et al., 2020; Kang et al., 2020).

In this study, we used MALDI-MSI to investigate the lipid signature and its spatial distribution in fxh samples taken at different time points between trauma and surgery. A sample preparation procedure was developed to improve lipid signal intensities. One of the key challenges in this sample preparation was the removal of blood from the fxh with a washing step, since it contains large quantities of heme. Heme is easily ionized and therefore negatively affects the ionization of lipids and other molecules, a process called ion suppression. The washing step should improve lipid signal intensities without delocalization. Furthermore, the intra-variability of the detected molecules within the fxh was evaluated to establish if differences in molecular patterns occur based on their specific location within the fxh. Thus, the aims of this study are to: 1) Develop a methodology for analysis of fxh with MALDI-MSI, 2) Investigate the intra-variability of the molecular profile within fxh, and 3) Identify fxh time-dependent molecular patterns between the fxh.

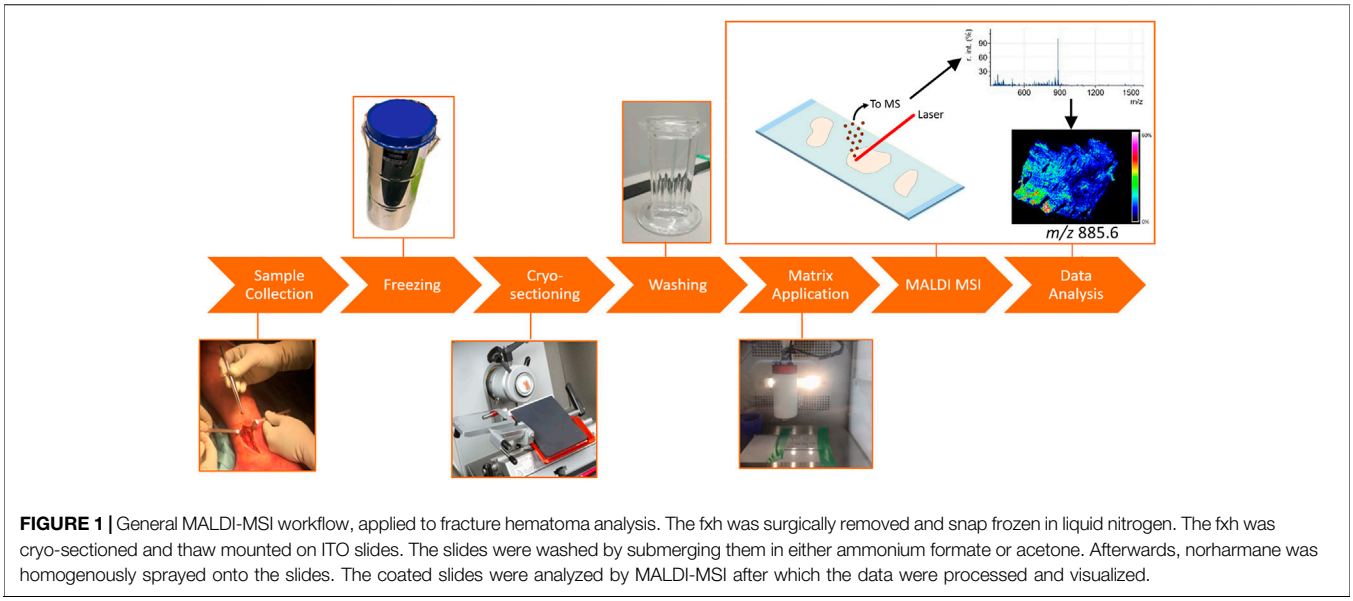

FIGURE 1 | General MALDI-MSI workflow, applied to fracture hematoma analysis. The fxh was surgically removed and snap frozen in liquid nitrogen. The fxh was cryo-sectioned and thaw mounted on ITO slides. The slides were washed by submerging them in either ammonium formate or acetone. Afterwards, norharmane was homogenously sprayed onto the slides. The coated slides were analyzed by MALDI-MSI after which the data were processed and visualized.

TABLE 1 | Overview of fxh tissues and ages used for the different objectives.

Objective	fxh tissue	fxh age
Tissue washing comparison	1 Human	3 days
	1 Porcine	3 days
Intra-hematoma variability	4 Porcine	3 days
Detection of molecular patterns	2 Human	2 days
	2 Human	9 days
	2 Human	19 days

MATERIALS AND METHODS

Materials

Ammonium formate, norharmane, Mayer's hematoxylin, and eosin were purchased from Sigma Aldrich (St. Louis, MO, USA). Acetone (HPLC grade), chloroform (HPLC grade), ethanol (HPLC grade), n-hexane (HPLC grade), methanol (ULC/MS-CC/SFC grade), and deionized water (ULC/MS-CC/SFC grade) were purchased from Biosolve B.V. (Valkenswaard, Netherlands).

Samples—Fracture Hematoma

Fxh were obtained from pigs for method development and investigation of the intra-variability. Fxh were obtained from humans for the method validation and the investigation of time-dependent molecular patterns. An overview of the fxh tissue and age used for the different objectives can be found in **Table 1**. The fxh age is defined as the number of days between the bone fracture and surgical intervention.

Porcine fxh

Porcine fxh were collected from closed tibia shaft fractures that were created during animal experiments, as previously published by Guo et al. (2020) In short, a multi-trauma model was used to study hematological and chemical profiles in a porcine model of severe multi-trauma over a time period of 72 h after trauma. During the experiments, all animals were kept sedated and fxh were harvested 72 h after fracture induction. All procedures were approved by the animal care and use office of the state of Nordrhein-Westfalen (approval number: LANUV AZ 81–02.04.2017.A412).

Human fxh

The human fxh were collected during open surgical reduction and internal fixation of metaphyseal long bone fractures. For the detection of molecular patterns, samples were gathered from male patients with metaphyseal bone fractures, without further known comorbidities, that showed uneventful fracture healing, with a mean age of 51 ± 20 years. Due to patient-specific reasons, fracture surgery was performed at different time points after trauma which enables harvesting of a range of fxh of different ages (2–19 days). The Medical Ethical Committee of the MUMC+ approved this study (approval number: MEC 16-4-251).

General Sample Preparation and MALDI-MSI Protocol

The workflow for the sample preparation and MALDI-MSI analysis of fxh can be described in six steps (**Figure 1**). H&E staining was performed after MALDI-MSI analysis. The general protocol was used for the different experiments with minor adaptions when specified.

Sample collection and freezing: The fxh were harvested and snap-frozen in aluminum containers dipped in liquid nitrogen to stop cellular biological processes (Goodwin, 2012). The fxh were stored at −80°C until further use. The containers were put on ice when transferring for a short period of time.

Cryo-sectioning: Indium tin oxide (ITO) slides were cleansed for 10 min each by sonicating them in n-hexane and ethanol consecutively. The fxh were cryo-sectioned at 12 µm using a Leica

CM1860 UV cryostat (Leica microsystems, B.V., Amsterdam, the Netherlands) between −22 and −24°C. The sectioned fxh were thaw mounted on ITO slides (Delta Technologies, Colorado, USA). Afterwards, the slides with fxh sections were dried with nitrogenous gas. The slides were stored at −80°C, until further use.

Washing: The ITO slides with tissues sections were submerged for a defined amount of time (15–120 s) in either ammonium formate or acetone. After submersion, the slides were dried by nitrogen gas. More details about this step can be found in the paragraph "Comparison of different tissue washing methods".

Matrix application: In this study, 7 mg/ml norharmane in 2:1 chloroform and methanol (v/v) was applied for the extraction of lipids. This matrix solution was sonicated for 15 minutes and applied to the slides using an HTX TM sprayer (HTX technologies, LC, North Carolina, USA). Ten layers of matrix were applied with a drying time of 30 s between each layer using a nozzle temperature of 30°C and a flow rate of 0.12 µL/min. The velocity was set at 1,200 mm/min with a track spacing of 3 mm.

MALDI-MSI: Experiments were performed with a RapifleX MALDI Tissuetyper mass analyzer system (Bruker, Bremen, Germany) in reflector mode. The data were acquired at a 50 µm by 50 µm raster size with 200 laser shots/pixel at a laser frequency of 10 kHz. Positive and negative ion mode spectra were acquired to analyze lipids over a mass range of *m/z* 340–1,200 and 340–1,600, respectively. The system was calibrated with red phosphorus before acquisition.

Data analysis: FlexImaging v4.1 (Bruker Daltonik GmbH, Bremen, Germany) was used to visualize the molecular distributions. SCiLS lab 2016b (SCiLS GmbH, Bremen, Germany) was used for data analysis and data conversion. Principal component analysis—linear discriminant analysis (PCA-LDA) was performed and visualized with an in-house-built ChemomeTricks toolbox for MATLAB (version 2014a, The MathWorks, Natick, USA) to compare different groups.

H&E staining: After the MSI analysis, the matrix was removed from the slides with 70% ethanol. The slides were hematoxylin-eosin (H&E) stained. The stained slides were scanned with a M8 Microscope and Scanner (PreciPoint, Freising, Germany) at ×20 magnification and co-registered with the MALDI-MSI distribution images.

Comparison of Different Tissue Washing Methods

Different tissue washing methods were compared to increase lipid signal intensities after washing of heme. In addition, the possible delocalization of molecules caused by the washing of the lipids was assessed. Slides with porcine or human fxh were submerged in ammonium formate (50 mM in water, pH 7) or acetone. In-between washing steps and at the end, slides were dried with a gentle flow of nitrogen gas. Unwashed samples served as a control. An overview of the different washing methods compared for negative and positive ion modes can be found in **Table 2**. The number of washing methods tested for positive ion mode was reduced based on the results in negative ion mode, as the longest washing methods resulted in reduced lipid intensity and increased lipid delocalization. Three technical replicates were acquired per washing method. The remaining tissue preparation protocol and analyses were as described above in the general methods.

Comparison of the washing methods was done based on the mean signal-to-noise (S/N) values of ten selected ion peaks and the heme peak (*m/z* value based on literature). In addition, the ratios of the intensity of selected *m/z* values over the heme ion intensity (M/H) were compared. The *m/z* values were selected based on the highest intensities (excluding isotopes) and to cover the mass range of *m/z* 650–950. The optimal washing method was selected based on the combination of high ratios, adequate blood removal, and minimal lipid delocalization.

Intra-variability of fxh

A comparison of the molecular profiles of the outside and center of the fxh was performed to study the heterogeneity of the samples. For this purpose, multiple slides were created with three consecutive sections of the outside and the center for four porcine fxh (see **Supplementary Figure S1**). The sections for the outside were sectioned as close to the border of the sample as possible after minimal trimming. The center of the fxh was determined based on visual observation of size and shape, as the center differs distinctively for each fracture hematoma due to their differences in size and shape. The remaining tissue preparation protocol and analyses were as described above in the general method.

Identify fxh Age-Dependent Molecular Patterns

One of the objectives was to compare the molecular profiles of human fxh of different fxh ages. The selected fxh ages were two, nine, and 19 days after bone fracture to represent different time points in the early stages of the fracture healing cascade. Per sample at least five technical replicates were acquired. The slides were used for acquisition in negative and positive ion mode. The remaining tissue preparation protocol and analyses were as described above in the general method.

The different fxh ages were compared in both negative and positive ion mode using PCA-LDA. This analysis defines discriminant functions (DFs) that maximize the variance between classes while minimizing the variance within classes. The DF-score plots show which groups can be separated using that DF while the scaled loadings plot provides the corresponding *m/z* values. The scaled loadings are a combination of the intensity of the *m/z* value and the extent to which the molecule contributes to the separation of classes across the specified discriminant function. The scaled loadings on the positive side contribute more to the class at the positive side of the DF score and vice versa.

Lipid Identification

Molecules of interest were determined based on the PCA-LDA analysis of human fxh of different fxh ages. These molecules of interest are identified based on the highest scaled loadings for the

TABLE 2 | Overview of the different washing methods that were applied to the fxh, including the polarity.

Washing solvent	Washing time	Negative ion mode	Positive ion mode
Ammonium formate	30 s	X	X
	15 s twice	X	X
	30 s twice	X	-
	15 s four times	X	-
Acetone	30 s twice	X	X
	30 s four times	X	-
No-wash (control)	-	X	X

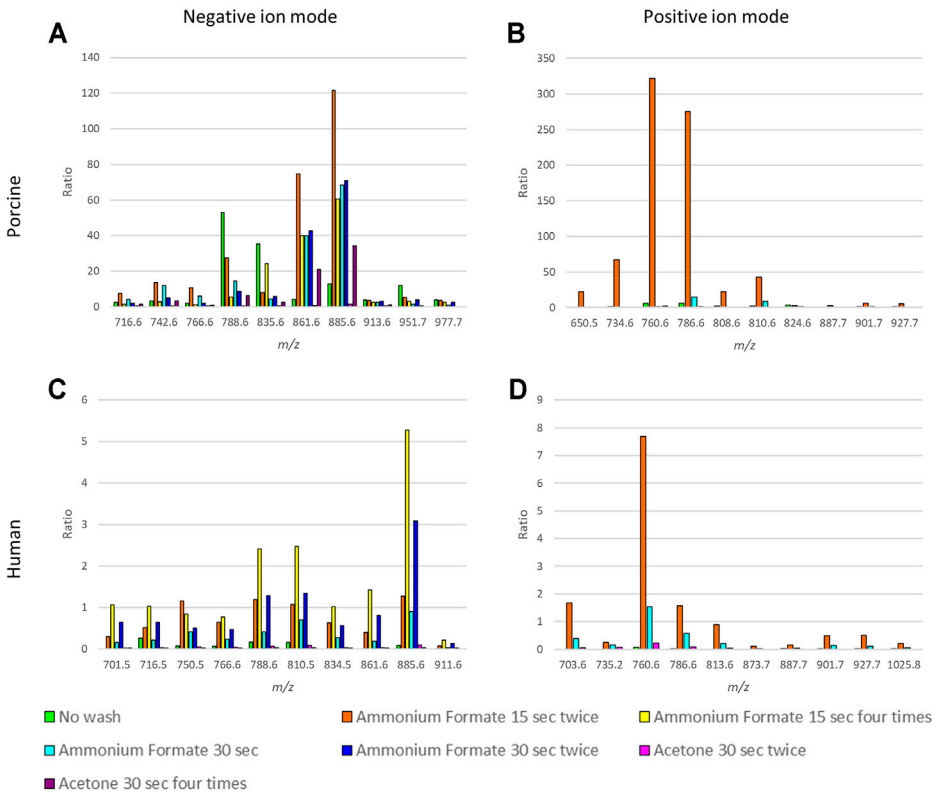

FIGURE 2 | Comparison of the ratios between heme and selected *m/z* values for different washing methods for negative and positive ion mode for porcine and human fracture hematoma. The ratios represent the ion intensities of selected *m/z* values over the heme ion intensity. The *m/z* values were selected based on the highest intensities (excluding isotopes) and to cover the mass range of lipids (*m/z* 650–950). **(A)** Ratios for 10 *m/z* values for the six washing methods and the control (no washing) for porcine fxh in negative ion mode. **(B)** Ratios for 10 *m/z* values for the three washing methods and the control (no washing) for porcine fxh in positive ion mode. **(C)** Ratios for 10 *m/z* values for the six washing methods and the control (no washing) for human fxh in negative ion mode. **(D)** Ratios for 10 *m/z* values for the three washing methods and the control (no washing) for human fxh in positive ion mode.

different classes. Background peaks, matrix clusters, and isotopes were removed from the lists of *m/z* values with high scaled loadings. The molecules were identified by MS/MS analysis using collision-induced dissociation (CID) to fragment molecules of interest. Data for lipid identification were acquired using a data-dependent acquisition (DDA)-imaging method, as described previously (Ellis et al., 2018). Shortly, MSI and MS/MS data were acquired on an Orbitrap Elite hybrid ion trap mass spectrometer (Thermo Fisher Scientific GmbH, Bremen, Germany) using a stage step size of 25 × 50 μm^2. MSI (MS^1) data of *m/z* 300–2000 were acquired at a nominal mass resolution of 240,000 (at *m/z* 400) using an injection time of 250 ms for both positive and negative ion mode. In parallel, the MS/MS data were acquired using the ion trap with an isolation window of 1 Da; a normalized collision energy of 30.0 (manufacturer units) with an activation q value of 0.17 in positive ion mode, and 38.0 and 0.25 in negative ion mode, respectively. Data analysis and lipid assignments were performed using Thermo Xcalibur (version 4.2, Thermo Fisher Scientific) and LipostarMSI (version 1.1.0b26, Molecular Horizon, Bettona, Italy) (Tortorella et al., 2020).

RESULTS

Comparing Different Tissue Washing Methods

Porcine fxh

The ratios between the mean intensities of selected *m/z* values and heme, as well as the S/N values of the selected *m/z* values of porcine fxh in both ion modes, were increased after washing the sections in either ammonium formate or acetone (**Figures 2A,B**, **Supplementary Table S1A,B**).

In negative ion mode, submerging the sections in ammonium formate for 15 seconds twice resulted in the highest ratios for most *m/z* values, as seen in **Figure 2A**. Washing the sections in acetone for 30 seconds twice enhanced the S/N value for heme compared to no wash, while for the other washing methods the heme S/N value decreased (**Supplementary Table S1A**). The highest S/N values for most of the selected *m/z* values were obtained with washing in ammonium formate for 30 seconds once or 15 seconds twice.

In positive ion mode, submerging the sections in ammonium formate for 15 seconds twice resulted in the highest ratios for most *m/z* values (**Figure 2B**). Only washing twice with ammonium formate for 15 seconds decreased the S/N value for heme compared to no wash (**Supplementary Table S1B**). For the other methods, the S/N value of heme increased. The highest S/N values for most of the selected *m/z* values were obtained with washing in ammonium formate for 30 seconds once or 15 seconds twice.

Human fxh

MSI results of human fxh also improved in both ion modes. The ratios between the mean intensities of selected *m/z* values and heme as well as the S/N values of the selected *m/z* values were increased after washing the sections in either ammonium formate or acetone, as for the porcine samples (**Figures 2C,D**, **Supplementary Table S1C,D**).

In negative ion mode, submerging the sections in ammonium formate for 15 seconds four times resulted in the highest ratios for most *m/z* values (**Figure 2C**). Washing the sections in ammonium formate for 30 seconds twice or 15 seconds four times resulted in a decreased S/N value of heme compared to unwashed controls, while the other washing methods resulted in an increased heme S/N value (**Supplementary Table S1C**). The highest S/N values for all the selected *m/z* values were obtained with washing in ammonium formate for 30 seconds once or 15 seconds twice, despite the S/N ratios being the highest for ammonium formate for 15 seconds four times.

In positive ion mode, submerging the sections in ammonium formate for 15 seconds twice resulted in the highest ratios for all of the *m/z* values (**Figure 2D**). All the washing methods resulted in an increased heme S/N value compared to no wash, but this increase was the smallest for an ammonium formate wash of 15 seconds twice (**Supplementary Table S1D**). The highest S/N values for all the selected *m/z* values were obtained with washing in ammonium formate for 30 seconds once or 15 seconds twice.

Delocalization

Figure 3 and **Supplementary Figure S2** show example images of MALDI-MSI distribution images for different washing methods for selected washing methods. The ammonium formate wash shows less delocalization than the acetone wash (**Figure 3** and **Supplementary Figure S2**). Almost no heme was present within the fxh tissue for the tissue washing method with ammonium formate, in contrast to washing with acetone (**Figure 3** and **Supplementary Figure S2**). Nevertheless, the intensity of heme is relatively high outside the tissue for the ammonium formate washing methods, which is attributed to the removal of the heme from the tissue with these methods. Increased delocalization was observed with increasing washing time, for example, the delocalization was larger for ammonium formate wash 15 s four times than for 15 s twice. In addition, it was observed that the delocalization for the selected *m/z* values was minimal and the highest intensities were present within the tissue for the ammonium formate wash.

Taking the above-mentioned results into account, the optimal fxh washing method is the ammonium formate wash for 15 s twice based on the increased intensity of the selected *m/z* values, the decreased heme intensity, and minimum delocalization of the molecules of interest. This washing method was further applied throughout this study.

Intra-Variability of fxh

Fxh is a very heterogeneous tissue due to the presence of different cell types, which affects the molecular profile as well. The molecular profiles of the outside and center of fxh are compared to examine the intra-variability of this profile throughout the fxh. This is important to prevent bias based on sampling location within a fxh.

Four porcine fxh were used to determine if the molecular profiles differed based on the sampling location within the fxh, which reflects the intra-variability of the fxh. **Figure 4A** shows that molecular profiles of the outside and center of fxh cannot be distinguished in negative ion mode, as the graphs for the outside and center section per sample mostly overlap. For positive ion mode, the same holds, although the intra-variability for sample 2 is bigger than for the other samples, as those graphs overlap less (see **Figure 4B**). The DF-2 scores (see **Supplementary Figure S3**) show the same trend for both negative and positive ion mode. In general, the results from the PCA-LDA analysis show that the inter-variability between samples is higher than the intra-variability within a sample.

Identify fxh Age-Dependent Molecular Patterns

Human fxh of different fxh ages (2, 9, and 19 days) were analyzed to compare the differences in molecular profiles at an early, middle, and late stage during fracture healing. Changes in the molecular profiles can help to improve the understanding of molecular changes during bone fracture healing.

Negative Ion Mode

In negative ion mode, DF-1 explains 1.47% of the total variance of the dataset and can be used to separate day 2 from day 19 (**Figure 5A**). **Figure 5C** shows the corresponding scaled loading plot. In the range from *m/z* 600 to 830, the peaks are more distinctive of day 2, while the peaks in the range *m/z* 830 to 1,000

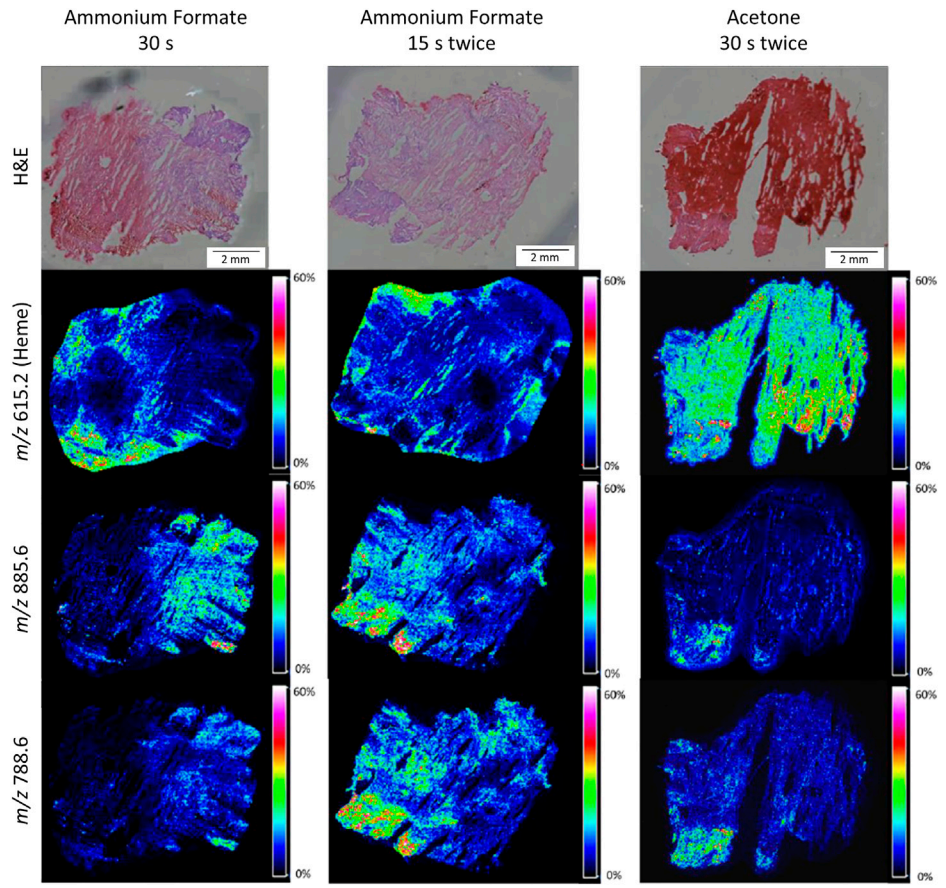

FIGURE 3 | H&E stained and MALDI-MSI distribution images for three different washing methods for human fxh. MALDI-MSI images are shown for the distribution of heme (*m/z* 615.2) and lipids with *m/z* values 885.6 and 788.6 in negative ion mode for the washing methods: ammonium formate for 30 s (left column), ammonium formate for 15 s twice (middle column), and acetone for 30 s twice (right column). All shown intensities are total ion current (TIC) normalized.

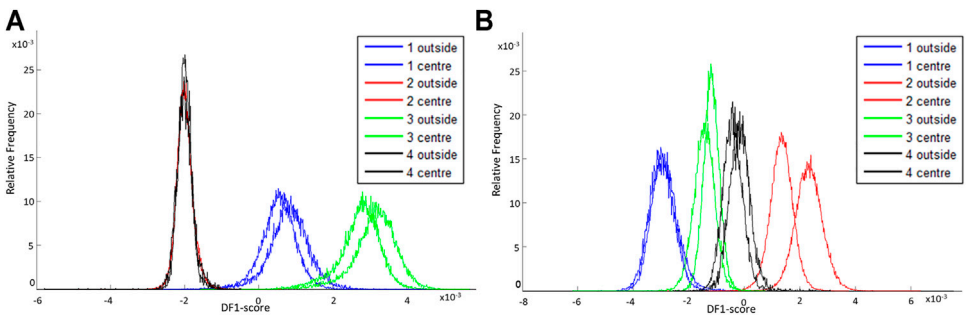

FIGURE 4 | DF-1 scores for comparison of the intra-variability of fracture hematoma for negative and positive ion mode. The DF-1 score explains the biggest variance in the data set as determined by a PCA-LDA of the mass spectra of the outside and center sections of different porcine fxh. **(A)** DF-1 score for the outside and center sections of four porcine fxh in negative ion mode. **(B)** DF-1 score for the outside and center sections of four porcine fxh in positive ion mode.

and some peaks in the mass range above that more distinctive of day 19. The results of the identification of the peaks with the highest scaled loadings can be found in **Table 3** (labeled with DF-1). For the separation between day 2 and day 19, certain phosphatidylinositols (PIs) and cardiolipins (CLs) are more characteristic of day 19, while a phosphatidylethanolamine (PE) is more characteristic of day 2. Phosphatidic acids (PAs) and phosphatidylserines (PSs) are present on both day 2 and 19, but the specific fatty acid chain composition and degree of saturation differ between both classes.

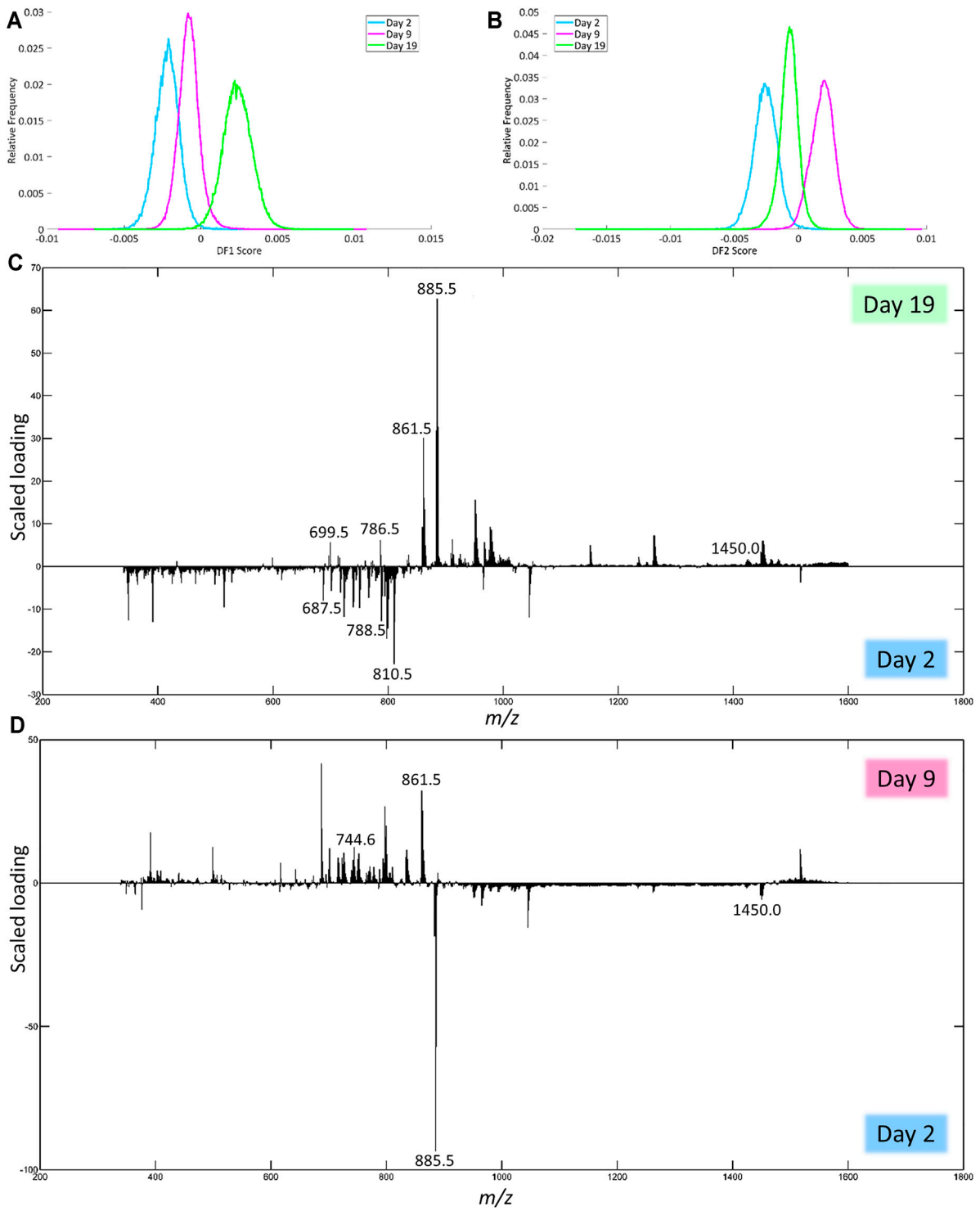

FIGURE 5 | Results of the PCA-LDA of the human fxh of different fxh age (2, 9, and 19 days) for negative ion mode. DF-scores and their corresponding scaled loading plots are shown. The scaled loading is a combination of the intensity of the *m/z* value with how much the molecule contributes to the separation of classes across the specified discriminant function. The positive side for the DF-score plot is related to the positive side of the scaled loading plots. This indicates that the *m/z* values at a certain side have a higher contribution in the class at that side. **(A)** DF-1 score representing the first discriminant function, which corresponds to the highest variance in the dataset. **(B)** The DF-2 score representing the second discriminant function. **(C)** Scaled loading plot of the full mass range for DF-1. **(D)** Scaled loading plot of the full mass range for DF-2.

TABLE 3 | Lipid assignments based on MS/MS data and high mass resolution experiments in negative ion mode. For each assignment, the *m/z* value obtained with the high mass resolution mass spectrometer (Orbitrap Elite), the lipid assignment, the detected ion, the ppm error, the condition to which the *m/z* value contributes, the DF, and the corresponding scaled loading are provided.

m/z value	Assignment	Ion	Δ ppm error	Condition	DF
687.54	SM 16:0_18:1; O2	$[M-CH3]^-$	0.5	Day 2	DF-1
699.50	PA 18:0_18:2 and PA 18:1_18:1	$[M-H]^-$	0.5	Day 19	DF-1
701.51	PA 18:0_18:1	$[M-H]^-$	0.5	Day 2	DF-1
				Day 9	DF-2
716.52	PE 16:0_18:1	$[M-H]^-$	0.7	Day 9	DF-2
723.50	PA 18:0_20:4	$[M-H]^-$	0.4	Day 2	DF-1
				Day 9	DF-2
742.54	PE 18:0_18:2 and PE 18:1_18:1	$[M-H]^-$	0.5	Day 9	DF-2
744.60	PE 18:0_18:1	$[M-H]^-$	0.6	Day 9	DF-2
766.54	PE 18:0_20:4	$[M-H]^-$	0.9	Day 2	DF-1
770.57	PE 18:0_20:2 and PE 18:1_20:1 and PE 18:2_20:0	$[M-H]^-$	1.8	Day 9	DF-2
786.53	PS 18:0_18:2 and PS 18:1_18:1	$[M-H]^-$	0.5	Day 19	DF-1
788.54	PS 18:0_18:1	$[M-H]^-$	0.6	Day 2	DF-1
				Day 9	DF-2
810.53	PS 18:0_20:4	$[M-H]^-$	0.5	Day 2	DF-1
				Day 9	DF-2
833.52	PI 16:0_18:2 and PI 16:1_18:1 and PI 16:2_18:0	$[M-H]^-$	0.6	Day 9	DF-2
835.53	PI 16:1_18:0 and PI 16:0_18:1	$[M-H]^-$	1.1	Day 19	DF-1
				Day 9	DF-2
859.53	PI 18:1_18:2	$[M-H]^-$	0.1	Day 19	DF-1
861.54	PI 18:0_18:2 and PI 18:1_18:1	$[M-H]^-$	0.6	Day 19	DF-1
				Day 9	DF-2
863.56	PI 18:0_18:1	$[M-H]^-$	0.8	Day 19	DF-1
				Day 9	DF-2
883.53	PI 18:1_20:4	$[M-H]^-$	0.8	Day 19	DF-1
				Day 2	DF-2
885.55	PI 18:0_20:4	$[M-H]^-$	0.8	Day 19	DF-1
				Day 2	DF-2
909.55	PI 18:0_22:6	$[M-H]^-$	0.9	Day 19	DF-1
911.56	PI 18:0_22:5 and PI 18:1_22:4	$[M-H]^-$	1.0	Day 19	DF-1
1447.96	CL 18:2_18:2_18:2_18:2	$[M-H]^-$	0.4	Day 19	DF-1
				Day 2	DF-2
1449.98	CL 18:1_18:2_18:2_18:2	$[M-H]^-$	1.0	Day 19	DF-1

DF-2 explains 2.39% of the total variance and can be used to separate day 2 from day 9 (**Figure 5B**). The corresponding scaled loading plot (**Figure 5D**) shows that most of the peaks in the mass range up to *m/z* 880 are more distinctive of day 9, while most peaks above this value are more distinctive of day 2 except for the peaks just above *m/z* 1,515, which correspond to day 9. The results of the identification of the peaks with the highest scaled loadings can be found in **Table 3** (labeled with DF-2). For the separation between days 2 and 9, certain PAs, PEs, and PSs are more characteristic of day 9, while certain CLs are more characteristic of day 2. PIs are present on both day 2 and 9, but the specific fatty acid chain composition and degree of saturation differ between both classes.

Positive Ion Mode

In positive ion mode, DF-1 explains 2.23% of the total variance of the dataset and can be used to separate day 2 from day 19 after trauma (**Figure 6A**). Based on the scaled loadings (**Figure 6C**), most of the peaks are more distinctive of day 2 up to *m/z* 925, except for a few peaks, most notably 3 clusters of peaks in the range of *m/z* 700 to 800. Most of the peaks above *m/z* 925 are more distinctive of day 19. The results of the identification of the peaks with the highest scaled loadings can be found in **Table 4** (labeled with DF-1). For the separation between day 2 and day 19, it seems that certain lysophosphatidylcholines (LPCs) have a higher presence on day 2. The main class of identified lipids is

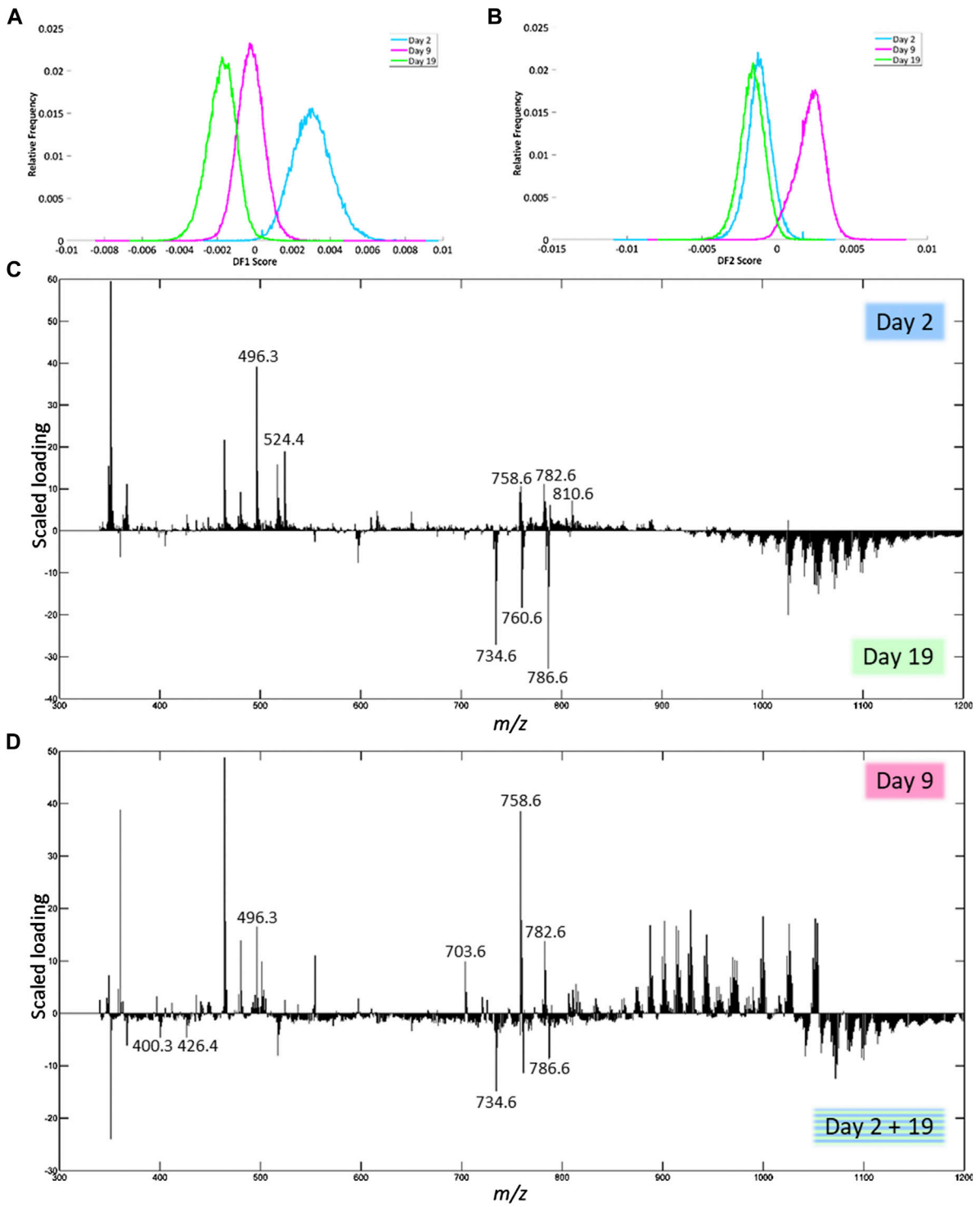

FIGURE 6 | Results of the PCA-LDA of the human fxh of different fxh age (2, 9, and 19 days) for positive ion mode. DF-scores and their corresponding scaled loading plots are shown. The scaled loading is a combination of the intensity of the *m/z* value with how much the molecule contributes to the separation of classes across the specified discriminant function. The positive side for the DF-score plot is related to the positive side of the scaled loading plots. This indicates that the *m/z* values at a certain side have a higher contribution in the class at that side. **(A)** DF-1 score representing the first discriminant function, which corresponds to the highest variance in the dataset. **(B)** The DF-2 score representing the second discriminant function. **(C)** Scaled loading plot of the full mass range for DF-1. **(D)** Scaled loading plot of the full mass range for DF-2.

TABLE 4 | Lipid assignments based on MS/MS and high mass resolution experiments in positive ion mode. For each assignment, the *m/z* value obtained with the high mass resolution mass spectrometer (Orbitrap Elite), the lipid assignment, the detected ion, the ppm error, the condition to which the *m/z* value contributes, the DF, and the corresponding scaled loading are provided.

m/z value	Assignment	Ion	Δ ppm error	Condition	DF
400.34	CAR 16:0	$[M + H]^+$	1.0	Day 2 + 19	DF-2
426.36	CAR 18:1	$[M + H]^+$	0.4	Day 2 + 19	DF-2
496.34	LPC 16:0	$[M + H]^+$	0.7	Day 2	DF-1
				Day 9	DF-2
524.37	LPC 18:0	$[M + H]^+$	1.5	Day 2	DF-1
703.57	SM 34:1; O2	$[M + H]^+$	0.4	Day 9	DF-2
734.57	PC 16:0_16:0	$[M + H]^+$	0.4	Day 19	DF-1
				Day 2 + 19	DF-2
758.57	PC 16:0_18:2	$[M + H]^+$	0.5	Day 2	DF-1
				Day 9	DF-2
760.58	PC 16:0_18:1	$[M + H]^+$	0.7	Day 19	DF-1
				Day 9	DF-2
768.59	PC O-36:4	$[M + H]^+$	0.7	Day 2	DF-1
782.57	PC 16:0_20:4	$[M + H]^+$	0.6	Day 2	DF-1
				Day 9	DF-2
784.58	PC 16:0_20:3 and PC 18:1_18:2	$[M + H]^+$	0.7	Day 19	DF-1
786.60	PC 18:0_18:2 and PC 18:1_18:1	$[M + H]^+$	0.7	Day 19	DF-1
				Day 2 + 19	DF-2
788.62	PC 18:0_18:1	$[M + H]^+$	1.4	Day 2	DF-1
810.60	PC 18:0_20:4	$[M + H]^+$	0.7	Day 2	DF-1

phosphatidylcholines (PCs), PCs are present in both the day 2 and day 19. However, the specific fatty acid chain composition and degree of saturation differ between day 2 and day 19.

DF-2 explains 2.79% of the total variance and can be used to separate day 9 from day 2 + 19 (**Figure 6B**). The corresponding scaled loading plot (**Figure 6D**) shows that clusters of peaks are more distinctive of day 9 or day 2 + 19. For the mass range up to *m/z* 850 and from *m/z* 1,020, most peaks are related to day 2 + 19, while for the mass range *m/z* 850 to 1,020 most peaks are related to day 9. The results of the identification of the peaks with the highest scaled loadings can be found in **Table 4** (labeled with DF-2). For the separation between day 9 and day 2 + 19, it seems that certain acylcarnitines (CARs) are more present at day 2 + 19, while an LPC and sphingomyelin (SM) are more present at day 9. Just as for DF-1, the main class of identified lipids is PCs, which are present on both day 9 and day 2 + 19. Again, the specific fatty acid chain composition and degree of saturation differ between day 9 and day 2 + 19.

DISCUSSION

In this study, the use of MALDI-MSI as a tool to examine the molecular events in fxh was explored. A methodology was developed for the analysis of fxh with MALDI-MSI with a focus on defining the optimal washing method. The intra-variability of the molecular profile in fxh was shown to be smaller than the inter-variability using this method. Lastly, fxh age-dependent lipid patterns within the fxh were identified. These age-dependent lipid patterns might be applied in predicting fracture healing outcome in the future.

Tissue Preparation

A two-step washing protocol with ammonium formate followed by an intermediary drying step is most effective in reducing the heme signal, minimizing lipid delocalization, and enhancing lipid signal intensities. Our results are in line with the study by Angel et al. (2012), which shows that longer washing times go hand in hand with increased lipid delocalization (Angel et al., 2012).

In general, most molecular intensities were enhanced after tissue washing with either ammonium formate or acetone, compared to no tissue washing at all. This result is in line with the study by Seeley et al. (2008), which also showed enhanced heme signal intensities after tissue washing with acetone as compared to not washing tissue sections (Seeley et al., 2008). In this study, acetone proved to be less effective, as acetone tissue washing resulted in a higher heme signal as compared to ammonium formate tissue washing or no washing. Additionally, more residual heme was located within the tissue after acetone wash in comparison to the ammonium formate wash.

Fracture Hematoma Intra-Variability

For the sample location of the fxh, it was shown that the intra-variability within a fxh was smaller than the inter-variability between fxh based on DF-1. No marked regions within the fxh could be identified that exhibit a specific function based on their spatial distribution. This is in line with expectations since the fxh is a very dynamic and diverse environment in which, depending on the phase of the fracture healing process, a great variety of cells is present (Kolar et al., 2010; Claes et al., 2012).

Comparison of Human fxh of Different fxh Age

Using MALDI-MSI, distinct lipid patterns were identified in fxh samples that were indicative of fxh age. Five lipid classes in negative ion mode and four lipid classes in positive ion mode showed to contribute most to differentiating the three age-based fxh groups. Herein, we focus on the lipid classes with the highest differentiating contribution.

Lipid Patterns in Negative Ion Mode

In negative ion mode, days 2 and 19 could predominantly be separated by the relatively higher presence of PIs and CLs on day 19 as compared to a higher presence of PEs on day 2 (**Table 3**).

PIs serve as precursors of signaling molecules within both the Inositol-3-phosphate/diaglycerol (IP3/DAG), as well as the phosphatidylinositol-3-Kinase/protein kinase B (PI3K/AKT) signaling pathway and assist in the effective regulation of angiogenesis (Davies et al., 2019). Regarding bone formation, another important aspect is the recruitment and release of calcium through the binding of IP3 to the endoplasmatic reticulum. Calcium release results in a positive feedback loop on the production of DAG, which is counteracted by diaglycerol kinase due to the conversion to PA, a key molecule in the mammalian target of rapamycin (mTOR) signaling pathway, as described below (Antal and Newton, 2013). Placing the above-mentioned functions of PIs into perspective, it can be expected that regulation of angiogenesis and calcium mobilization will be more present at day 19 as compared to day 2.

Furthermore, days 2 and 9 could be distinguished from each other by the increased presence of CLs on day 2 as compared to a higher presence of PAs, PSs, and PEs on day 9 (**Table 3**). PA, a metabolite of phosphatidylcholine, plays a role in the mTOR signaling pathway, which acts as a pivotal nutrient sensing mechanism and partakes in regulating cellular differentiation, survival, growth, and division. Within this pathway, PA proposedly serves as an indicator for the presence of its lipid precursor molecules within the cell since these are important for the before-mentioned processes (Foster, 2013). Additionally, PA has shown to be an important component in the induction of angiogenesis through activating the HIF-1α-VEGF pathway (Han et al., 2014). Lastly, PA enhances inflammation through mTOR signaling, both *in vitro* as well as *in vivo* (Lim et al., 2003; Lee et al., 2007). The higher presence of PA on day 9 as compared to day 2 is in line with physiological fracture healing due to its roles in the regulation of cell fate and angiogenesis, as well as a more widespread, regulated inflammatory response that would more likely take place around day 9 after fracture as compared to day 2.

PEs, like PCs, are important precursor molecules of phosphoethanolamine, which on its turn is catalyzed by phosphoethanolamine/phosphocholine phosphatase (PHOSPHO1) to serve as a donor of inorganic phosphate in the production of hydroxyapatite. Furthermore, they are involved in the glycine and serine metabolism, two key amino acids in the production of collagen (Roberts et al., 2004). Increased presence of PEs on day 9, combined with relatively large scaled loadings, matches its role in both collagen metabolism, as well as a phosphate donor for hydroxyapatite production.

Lipid Patterns in Positive Ion Mode

In positive ion mode, day 2 and day 19 were mostly distinguishable by the presence of specific PCs on days 2 or 19. Furthermore, a higher presence of LPCs was observed on day 2 as compared to day 19 (**Table 4**).

PCs are amongst the most abundant phospholipids in mammalian cell membranes and are known to play important roles in cellular metabolism and energetic state (van der Veen et al., 2017). They also regulate endochondral bone formation by promoting chondrocyte differentiation and cartilage matrix degradation in growth plates (Li et al., 2014). Furthermore, PCs play a role in the glycine and serine metabolism, which are key amino acids in collagen synthesis, and act as precursors of phosphocholines, important inorganic phosphate donors in the production of hydroxyapatite and thus influence bone mineralization (Roberts et al., 2004; Albaugh et al., 2017; de Paz-Lugo et al., 2018). A study by Øyen *et al.* (2017) showed that dietary supplementation of choline, an essential nutrient that is predominantly supplied as PC, was directly associated with increased bone mineral density (Øyen et al., 2017). Since PCs are the most abundant phospholipids within mammalian cell membranes, it was to be expected that their presence in fxh would be validated on both days 2 and 19. However, it has yet to be revealed what causes the shift in specific lipid isoforms amongst the different time points. Unfortunately, information about the presence of specific lipids throughout fracture healing is lacking. The shift in specific PCs might be due to certain osteogenic processes that can be expected to be more present during day 19 as compared to day 2.

LPCs are known to elicit a seemingly contradictory effect on osteoclasts by inhibiting their formation whilst enhancing their function. Besides, although predominantly investigated in valvular calcification, LPCs enhance cellular mineralization (Mebarek et al., 2013; Wiltz et al., 2014; Bouchareb et al., 2015). The dual (opposite) effect of LPCs on both osteoclast formation and function could contribute to adequate osteoclast turnover and functionality in the early fracture environment.

Furthermore, day 9 could be separated from day 2 + 19 due to the higher presence of certain long chain CARs on day 2 + 19, whilst SM and LPC were more characteristic of day 9 (**Table 4**).

SMs are important cellular signaling molecules that play a role in bone formation and apoptosis. A deficiency in the enzyme that converts SM to PC has been shown to impair bone and cartilage mineralization (Khavandgar and Murshed, 2015). Additionally, a

lack of SM due to the knockdown of sphingomyelin synthase 1 (SMS1) has been shown to impair bone development and case growth retardation due to the regulatory role of SMS1 in osteoblast development (Matsumoto et al., 2019). An increased presence of SM is, therefore, more likely to occur during day 9 after fracture since osteoblast development is initiated around that time (Bahney et al., 2019).

Limitations and future Research

This study showed that MALDI-MSI allows for the identification of a fxh age-dependent lipid signature. Still, a larger sample cohort is needed to validate these data. Especially the lipid signature in fxh of fractures that develop impaired healing would be of interest. Due to the limited sample size and the fact that all fractures in our cohort healed without adverse events, no conclusions in relation to clinical outcome can be drawn at this stage. Theoretically, the fracture location within a bone could influence the presence of lipids in the fracture hematoma. However, since all included fractures were located in the metaphyseal bone, we expect this influence to be minimal. Moreover, analysis of metabolites or proteins, being key players in bone healing- and formation, could further provide insights into the molecular mechanisms in fracture healing. Future research should therefore focus on validating the results of the present study in a larger cohort and developing a method for analyzing the protein signature of the fxh.

CONCLUSION

For the first time, our approach revealed the potential of MALDI-MSI as an analytical tool for the assessment of lipid patterns in fxh samples over time. An ammonium formate wash for 15 s twice was shown to adequately remove the heme from the porcine and human fxh and increase the overall molecular signal for negative and positive ion mode with minimum delocalization. The sample location within fxh is of less importance, as it was shown that the intra-variability within fxh was smaller than the inter-variability between fxh. Lastly, fxh age-dependent lipid patterns were identified, which showed to be involved in various processes that are important during fracture healing, such as angiogenesis, inflammation, cellular differentiation, mineralization, hydroxyapatite production, and collagen synthesis. Proper bone regeneration is in part dependent on the successful integration of the above-mentioned processes, and our results emphasize the important contributing role that lipids play. Assessment of specific molecular patterns within the fxh could provide insights into fracture healing processes and could potentially serve as a future source of theragnostic information on fracture healing.

DATA AVAILABILITY STATEMENT

The raw data supporting the conclusion of this article will be made available by the authors, without undue reservation.

ETHICS STATEMENT

The studies involving human participants were reviewed and approved by the Medical Ethical Committee of the MUMC+ (approval number: MEC 16-4-251). Written informed consent for participation was not required for this study in accordance with the national legislation and the institutional requirements. The animal study was reviewed and approved by the animal care and use office of the state of Nordrhein-Westfalen (approval number: LANUV AZ 81-02.04.2017.A412).

AUTHOR CONTRIBUTIONS

Sampling (pig + human): RG, JaG, JoG, and TB. Experimental design: SN, JaG, TPS, BC-P, and TB. Performing experiments: SN, JaG, and BC. Data analysis: RG, SN, JaG, and BC. Writing manuscript: RG and SN. Revising manuscript: RG, SN, BC, JoG, MvG, MP, RH, TPS, BC-P, and TB.

FUNDING

This research was part of the M4i research program and received financial support from the Dutch Province of Limburg under the LINK program.

SUPPLEMENTARY MATERIAL

The Supplementary Material for this article can be found online at: https://www.frontiersin.org/articles/10.3389/fchem.2021.780626/full#supplementary-material

REFERENCES

Aichler, M., and Walch, A. (2015). MALDI Imaging Mass Spectrometry: Current Frontiers and Perspectives in Pathology Research and Practice. *Lab. Invest.* 95 (4), 422–431. doi:10.1038/labinvest.2014.156

Albaugh, V. L., Mukherjee, K., and Barbul, A. (2017). Proline Precursors and Collagen Synthesis: Biochemical Challenges of Nutrient Supplementation and Wound Healing. *J. Nutr.* 147 (11), jn256404–7. doi:10.3945/jn.117.256404

Alekos, N. S., Moorer, M. C., and Riddle, R. C. (2020). Dual Effects of Lipid Metabolism on Osteoblast Function. *Front. Endocrinol.* 11, 578194. doi:10.3389/fendo.2020.578194

Angel, P. M., Spraggins, J. M., Baldwin, H. S., and Caprioli, R. (2012). Enhanced Sensitivity for High Spatial Resolution Lipid Analysis by Negative Ion Mode Matrix Assisted Laser Desorption Ionization Imaging Mass Spectrometry. *Anal. Chem.* 84 (3), 1557–1564. doi:10.1021/ac202383m

Antal, C. E., and Newton, A. C. (2013). Spatiotemporal Dynamics of Phosphorylation in Lipid Second Messenger Signaling. *Mol. Cel. Proteomics* 12 (12), 3498–3508. doi:10.1074/mcp.R113.029819

Bahney, C. S., Zondervan, R. L., Allison, P., Theologis, A., Ashley, J. W., Ahn, J., et al. (2019). Cellular Biology of Fracture Healing. *J. Orthop. Res.* 37 (1), 35–50. doi:10.1002/jor.24170

Bastian, O. W., Koenderman, L., Alblas, J., Leenen, L. P. H., and Blokhuis, T. J. (2016). Neutrophils Contribute to Fracture Healing by Synthesizing

Fibronectin + Extracellular Matrix Rapidly after Injury. *Clin. Immunol.* 164, 78–84. doi:10.1016/j.clim.2016.02.001

Bastian, O., Kuijer, A., Koenderman, L., Stellato, R. K., van Solinge, W. W., Leenen, L. P. H., et al. (2016). Impaired Bone Healing in Multitrauma Patients Is Associated with Altered Leukocyte Kinetics after Major Trauma. *Jir* 9, 69–78. doi:10.2147/JIR.S101064

Bouchareb, R., Mahmut, A., Nsaibia, M. J., Boulanger, M.-C., Dahou, A., Lépine, J.-L., et al. (2015). Autotaxin Derived from Lipoprotein(a) and Valve Interstitial Cells Promotes Inflammation and Mineralization of the Aortic Valve. *Circulation* 132 (8), 677–690. doi:10.1161/circulationaha.115.016757

Chiurchiù, V., Leuti, A., and Maccarrone, M. (2018). Bioactive Lipids and Chronic Inflammation: Managing the Fire Within. *Front. Immunol.* 9, 38. doi:10.3389/fimmu.2018.00038

Chughtai, K., and Heeren, R. M. A. (2010). Mass Spectrometric Imaging for Biomedical Tissue Analysis. *Chem. Rev.* 110 (5), 3237–3277. doi:10.1021/cr100012c

Claes, L., Recknagel, S., and Ignatius, A. (2012). Fracture Healing under Healthy and Inflammatory Conditions. *Nat. Rev. Rheumatol.* 8 (3), 133–143. doi:10.1038/nrrheum.2012.1

Davies, E. M., Gurung, R., Le, K. Q., and Mitchell, C. A. (2019). Effective Angiogenesis Requires Regulation of Phosphoinositide Signaling. *Adv. Biol. Regul.* 71, 69–78. doi:10.1016/j.jbior.2018.11.008

de Paz-Lugo, P., Lupiáñez, J. A., and Meléndez-Hevia, E. (2018). High glycine Concentration Increases Collagen Synthesis by Articular Chondrocytes *In Vitro*: Acute glycine Deficiency Could Be an Important Cause of Osteoarthritis. *Amino Acids* 50 (10), 1357–1365. doi:10.1007/s00726-018-2611-x

Dimitriou, R., Tsiridis, E., and Giannoudis, P. V. (2005). Current Concepts of Molecular Aspects of Bone Healing. *Injury* 36 (12), 1392–1404. doi:10.1016/j.injury.2005.07.019

Ellis, S. R., Paine, M. R. L., Eijkel, G. B., Pauling, J. K., Husen, P., Jervelund, M. W., et al. (2018). Automated, Parallel Mass Spectrometry Imaging and Structural Identification of Lipids. *Nat. Methods* 15 (7), 515–518. doi:10.1038/s41592-018-0010-6

Foster, D. A. (2013). Phosphatidic Acid and Lipid-Sensing by mTOR. *Trends Endocrinol. Metab.* 24 (6), 272–278. doi:10.1016/j.tem.2013.02.003

Ghiasi, M. S., Chen, J., Vaziri, A., Rodriguez, E. K., and Nazarian, A. (2017). Bone Fracture Healing in Mechanobiological Modeling: A Review of Principles and Methods. *Bone Rep.* 6, 87–100. doi:10.1016/j.bonr.2017.03.002

Glish, G. L., and Vachet, R. W. (2003). The Basics of Mass Spectrometry in the Twenty-First century. *Nat. Rev. Drug Discov.* 2 (2), 140–150. doi:10.1038/nrd1011

Goodwin, R. J. A. (2012). Sample Preparation for Mass Spectrometry Imaging: Small Mistakes Can lead to Big Consequences. *J. Proteomics* 75 (16), 4893–4911. doi:10.1016/j.jprot.2012.04.012

Guo, W., Bläsius, F. M., Greven, J., Luo, P., Wang, W., Lübke, C., et al. (2020). Hematological and Chemical Profiles in a Porcine Model of Severe Multiple Trauma. *Eur. Surg. Res.* 61 (2), 83–94. doi:10.1159/000510267

Han, S., Huh, J., Kim, W., Jeong, S., Min, D. S., and Jung, Y. (2014). Phospholipase D Activates HIF-1-VEGF Pathway via Phosphatidic Acid. *Exp. Mol. Med.* 46 (12), e126. doi:10.1038/emm.2014.86

Kang, J.-H., Ko, H.-M., Han, G.-D., Lee, S.-Y., Moon, J.-S., Kim, M.-S., et al. (2020). Dual Role of Phosphatidylserine and its Receptors in Osteoclastogenesis. *Cel. Death Dis.* 11 (7), 497. doi:10.1038/s41419-020-2712-9

Khavandgar, Z., and Murshed, M. (2015). Sphingolipid Metabolism and its Role in the Skeletal Tissues. *Cel. Mol. Life Sci.* 72 (5), 959–969. doi:10.1007/s00018-014-1778-x

Kolar, P., Schmidt-Bleek, K., Schell, H., Gaber, T., Toben, D., Schmidmaier, G., et al. (2010). The Early Fracture Hematoma and its Potential Role in Fracture Healing. *Tissue Eng. B: Rev.* 16 (4), 427–434. doi:10.1089/ten.TEB.2009.0687

Lee, J.-G., Lee, S.-H., Park, D.-W., Bae, Y.-S., Yun, S.-S., Kim, J.-R., et al. (2007). Phosphatidic Acid as a Regulator of Matrix Metalloproteinase-9 Expression via the TNF-α Signaling Pathway. *FEBS Lett.* 581 (4), 787–793. doi:10.1016/j.febslet.2007.01.048

Li, Z., Wu, G., Sher, R. B., Khavandgar, Z., Hermansson, M., Cox, G. A., et al. (2014). Choline Kinase Beta Is Required for normal Endochondral Bone Formation. *Biochim. Biophys. Acta (Bba) - Gen. Subj.* 1840 (7), 2112–2122. doi:10.1016/j.bbagen.2014.03.008

Lim, H.-K., Choi, Y.-A., Park, W., Lee, T., Ryu, S. H., Kim, S.-Y., et al. (2003). Phosphatidic Acid Regulates Systemic Inflammatory Responses by Modulating the Akt-Mammalian Target of Rapamycin-P70 S6 Kinase 1 Pathway. *J. Biol. Chem.* 278 (46), 45117–45127. doi:10.1074/jbc.M303789200

Loi, F., Córdova, L. A., Pajarinen, J., Lin, T.-h., Yao, Z., and Goodman, S. B. (2016). Inflammation, Fracture and Bone Repair. *Bone* 86, 119–130. doi:10.1016/j.bone.2016.02.020

Matsumoto, G., Hashizume, C., Watanabe, K., Taniguchi, M., and Okazaki, T. (2019). Deficiency of Sphingomyelin Synthase 1 but Not Sphingomyelin Synthase 2 Reduces Bone Formation Due to Impaired Osteoblast Differentiation. *Mol. Med.* 25 (1), 56. doi:10.1186/s10020-019-0123-0

Mebarek, S., Abousalham, A., Magne, D., Do, L., Bandorowicz-Pikula, J., Pikula, S., et al. (2013). Phospholipases of Mineralization Competent Cells and Matrix Vesicles: Roles in Physiological and Pathological Mineralizations. *Ijms* 14 (3), 5036–5129. doi:10.3390/ijms14035036

Murphy, R. C., Hankin, J. A., and Barkley, R. M. (2009). Imaging of Lipid Species by MALDI Mass Spectrometry. *J. Lipid Res.* 50 (Suppl. l), S317–S322. doi:10.1194/jlr.R800051-JLR200

Norris, J. L., and Caprioli, R. M. (2013). Analysis of Tissue Specimens by Matrix-Assisted Laser Desorption/ionization Imaging Mass Spectrometry in Biological and Clinical Research. *Chem. Rev.* 113 (4), 2309–2342. doi:10.1021/cr3004295

Øyen, J., Gjesdal, C. G., Karlsson, T., Svingen, G. F., Tell, G. S., Strand, E., et al. (2017). Dietary Choline Intake Is Directly Associated with Bone Mineral Density in the Hordaland Health Study. *J. Nutr.* 147 (4), 572–578. doi:10.3945/jn.116.243006

Park, S.-H., Silva, M., Bahk, W.-J., McKellop, H., and Lieberman, J. R. (2002). Effect of Repeated Irrigation and Debridement on Fracture Healing in an Animal Model. *J. Orthop. Res.* 20 (6), 1197–1204. doi:10.1016/s0736-0266(02)00072-4

Roberts, S. J., Stewart, A. J., Sadler, P. J., and Farquharson, C. (2004). Human PHOSPHO1 Exhibits High Specific Phosphoethanolamine and Phosphocholine Phosphatase Activities. *Biochem. J.* 382 (Pt 1), 59–65. doi:10.1042/bj20040511

Schell, H., Duda, G. N., Peters, A., Tsitsilonis, S., Johnson, K. A., and Schmidt-Bleek, K. (2017). The Haematoma and its Role in Bone Healing. *J. Exp. Ortop.* 4 (1), 5. doi:10.1186/s40634-017-0079-3

Schwamborn, K., and Caprioli, R. M. (2010). Molecular Imaging by Mass Spectrometry - Looking beyond Classical Histology. *Nat. Rev. Cancer* 10 (9), 639–646. doi:10.1038/nrc2917

Seeley, E. H., Oppenheimer, S. R., Mi, D., Chaurand, P., and Caprioli, R. M. (2008). Enhancement of Protein Sensitivity for MALDI Imaging Mass Spectrometry after Chemical Treatment of Tissue Sections. *J. Am. Soc. Mass. Spectrom.* 19 (8), 1069–1077. doi:10.1016/j.jasms.2008.03.016

Tortorella, S., Tiberi, P., Bowman, A. P., Claes, B. S. R., Ščupáková, K., Heeren, R. M. A., et al. (2020). LipostarMSI: Comprehensive, Vendor-Neutral Software for Visualization, Data Analysis, and Automated Molecular Identification in Mass Spectrometry Imaging. *J. Am. Soc. Mass. Spectrom.* 31 (1), 155–163. doi:10.1021/jasms.9b00034

van der Veen, J. N., Kennelly, J. P., Wan, S., Vance, J. E., Vance, D. E., and Jacobs, R. L. (2017). The Critical Role of Phosphatidylcholine and Phosphatidylethanolamine Metabolism in Health and Disease. *Biochim. Biophys. Acta (Bba) - Biomembr.* 1859 (9 Pt B), 1558–1572. doi:10.1016/j.bbamem.2017.04.006

Volpin, G., and Shtarker, Y. (2014). "Management of Delayed Union, Non-Union and Mal-union of Long Bone Fractures," in *European Surgical Orthopaedics and Traumatology*. Editor GE Bentley (Berlin: Springer). The EFORT Textbook.

Wang, X., Friis, T., Glatt, V., Crawford, R., and Xiao, Y. (2017). Structural Properties of Fracture Haematoma: Current Status and Future Clinical Implications. *J. Tissue Eng. Regen. Med.* 11 (10), 2864–2875. doi:10.1002/term.2190

Watrous, J. D., Alexandrov, T., and Dorrestein, P. C. (2011). The Evolving Field of Imaging Mass Spectrometry and its Impact on Future Biological Research. *J. Mass. Spectrom.* 46 (2), 209–222. doi:10.1002/jms.1876

Wiltz, D. C., Han, R. I., Wilson, R. L., Kumar, A., Morrisett, J. D., and Grande-Allen, K. J. (2014). Differential Aortic and Mitral Valve Interstitial Cell

Mineralization and the Induction of Mineralization by Lysophosphatidylcholine *In Vitro*. *Cardiovasc. Eng. Tech.* 5 (4), 371–383. doi:10.1007/s13239-014-0197-3

Conflict of Interest: The authors declare that the research was conducted in the absence of any commercial or financial relationships that could be construed as a potential conflict of interest.

Publisher's Note: All claims expressed in this article are solely those of the authors and do not necessarily represent those of their affiliated organizations, or those of the publisher, the editors and the reviewers. Any product that may be evaluated in this article, or claim that may be made by its manufacturer, is not guaranteed or endorsed by the publisher.

Advantages of publishing in Frontiers

OPEN ACCESS
Articles are free to read for greatest visibility and readership

FAST PUBLICATION
Around 90 days from submission to decision

HIGH QUALITY PEER-REVIEW
Rigorous, collaborative, and constructive peer-review

TRANSPARENT PEER-REVIEW
Editors and reviewers acknowledged by name on published articles

Frontiers
Avenue du Tribunal-Fédéral 34
1005 Lausanne | Switzerland

Visit us: www.frontiersin.org
Contact us: frontiersin.org/about/contact

REPRODUCIBILITY OF RESEARCH
Support open data and methods to enhance research reproducibility

DIGITAL PUBLISHING
Articles designed for optimal readership across devices

FOLLOW US
@frontiersin

IMPACT METRICS
Advanced article metrics track visibility across digital media

EXTENSIVE PROMOTION
Marketing and promotion of impactful research

LOOP RESEARCH NETWORK
Our network increases your article's readership